
All ETDs from UAB

UAB Theses & Dissertations

1998

Dynamic characterization of 2-aminopurine in oligonucleotides using fluorescence, magnetic resonance, and Raman spectroscopies.

Kervin Orlando Evans
University of Alabama at Birmingham

Follow this and additional works at: <https://digitalcommons.library.uab.edu/etd-collection>

Recommended Citation

Evans, Kervin Orlando, "Dynamic characterization of 2-aminopurine in oligonucleotides using fluorescence, magnetic resonance, and Raman spectroscopies." (1998). *All ETDs from UAB*. 6181.
<https://digitalcommons.library.uab.edu/etd-collection/6181>

This content has been accepted for inclusion by an authorized administrator of the UAB Digital Commons, and is provided as a free open access item. All inquiries regarding this item or the UAB Digital Commons should be directed to the [UAB Libraries Office of Scholarly Communication](#).

INFORMATION TO USERS

This manuscript has been reproduced from the microfilm master. UMI films the text directly from the original or copy submitted. Thus, some thesis and dissertation copies are in typewriter face, while others may be from any type of computer printer.

The quality of this reproduction is dependent upon the quality of the copy submitted. Broken or indistinct print, colored or poor quality illustrations and photographs, print bleedthrough, substandard margins, and improper alignment can adversely affect reproduction.

In the unlikely event that the author did not send UMI a complete manuscript and there are missing pages, these will be noted. Also, if unauthorized copyright material had to be removed, a note will indicate the deletion.

Oversize materials (e.g., maps, drawings, charts) are reproduced by sectioning the original, beginning at the upper left-hand corner and continuing from left to right in equal sections with small overlaps. Each original is also photographed in one exposure and is included in reduced form at the back of the book.

Photographs included in the original manuscript have been reproduced xerographically in this copy. Higher quality 6" x 9" black and white photographic prints are available for any photographs or illustrations appearing in this copy for an additional charge. Contact UMI directly to order.

UMI

A Bell & Howell Information Company
300 North Zeeb Road, Ann Arbor MI 48106-1346 USA
313/761-4700 800/521-0600

DYNAMIC CHARACTERIZATION OF 2-AMINOPURINE IN OLIGONUCLEOTIDES
USING FLUORESCENCE, MAGNETIC RESONANCE, AND RAMAN
SPECTROSCOPIES

by

KERVIN ORLANDO EVANS

A DISSERTATION

Submitted to the graduate faculty of The University of Alabama at Birmingham,
in partial fulfillment of the requirements for the degree of
Doctor of Philosophy

BIRMINGHAM, ALABAMA

1998

UMI Number: 9828544

**Copyright 1998 by
Evans, Kervin Orlando**

All rights reserved.

**UMI Microform 9828544
Copyright 1998, by UMI Company. All rights reserved.**

**This microform edition is protected against unauthorized
copying under Title 17, United States Code.**

UMI
300 North Zeeb Road
Ann Arbor, MI 48103

ABSTRACT OF DISSERTATION
GRADUATE SCHOOL, UNIVERSITY OF ALABAMA AT BIRMINGHAM

Degree Ph.D. Program Physics

Name of Candidate Kervin Orlando Evans

Committee Chair Thomas M. Nordlund

Title Dynamic Characterization of 2-Aminopurine in Oligonucleotides Using
Fluorescence, Magnetic Resonance, and Raman Spectroscopies

In two papers presented in this study, the dynamics of 2-aminopurine (2AP) as a free base, mononucleoside (2AP-dn or 2AP-rb), and in short oligonucleotides were characterized by its fluorescence, magnetic resonance, and Raman spectroscopic signatures. In the first paper, we have demonstrated that the fluorescence lifetime of 2AP as a free base and mononucleoside (2AP-dn) is single exponential (~ 12 and 11 ns, respectively). This implies a single excited state for both molecules. However, magnetic resonance measurements (2D-NOESY) indicate two conformations (*syn*- and *anti*-) in solution. Upon the attachment of another nucleoside (thymine) in the 3'-position of 2AP-dn, the fluorescence lifetime becomes triple exponential, implying three distinct excited states. This was the case for the oligonucleotides A-2AP-T, C-2AP-G, and G-2AP-C, also.

Because NMR showed only two different conformations of 2AP-dn, we characterized the three excited states as fully stacked, partially stacked, and unstacked. We found the enthalpy differences between these states to be in the range 1-10 kcal/mole, which is typical for stacked bases in oligonucleotides [Baker *et al.* (1978) *Biopolymers* 17, 1361-1372; Breslauer & Sturtevant (1977) *Biophysical Chemistry* 7, 205-209; Lee &

Tinoco (1977) *Biochemistry* 16, 5403-5414; Powell *et al.* (1972) *Biopolymers* 2, 235-250]. G-2AP-C was anomalous, with an enthalpy difference of 9.8 ± 2.4 kcal/mole. We proposed that this was caused by the NH_2 of 2AP hydrogen bonding to the O6 of guanine. However, stacking has a small effect on the fluorescence lifetime compared to that of adenine, which in conjunction with thymine (A-2AP-T) reduced the fluorescence lifetime to 7.4 ns. This agreed with another finding that adenine stacks the strongest with 2AP (Xu, D.-G. 1996, PhD dissertation).

In the second paper, we were able to demonstrate that the vibrational spectra of adenine and 2AP have distinctive differences in vibrational bands. We found that 2AP had bands at 445, 494, 1935, 2342, and 2361 cm^{-1} in its IR spectrum that adenine did not have. When we looked at 2AP-rb, we found distinguishing bands at 410, 436, 452, 575, 618, 895, 1274, 1700, 1782, 2341, 2360, 2725, 2764, 2891, 3191, 3225, and 3478 cm^{-1} . In the Raman spectra, we found 2AP to have distinguishing bands in the $420\text{-}500 \text{ cm}^{-1}$ and $1850\text{-}1945 \text{ cm}^{-1}$, and 2AP-rb at 492 and 855 cm^{-1} (862 for 2AP-rb in solution). We hope that one of these many distinguishing bands of 2AP can be used to independently monitor 2AP as it is incorporated into oligonucleotide sequences.

DEDICATION

This is dedicated to all of the people whom I have encountered in my life that have helped shape the person I am today: God, Almighty, without Whom none of this would have been possible; my father, Charles Earl Evans, who taught me by example to find a career that I loved so that I would enjoy going to work; my mother, Margaret Ann Evans, who stimulated my scientific curiosity by teaching me so many uses of mathematics and science; all of my teachers throughout the years who saw something in me to encourage; my wife, Mary Jo, who is my soul-mate; my brother, Kermit, who always looked up to me; my nieces and nephew (Kelitia, Keenya, Jasmine, Amber, and Clarence) whose curiosity inspired and challenged me; friends and family that took the time to answer my questions, support, and guide me. Thank you all!!!

ACKNOWLEDGMENTS

I express my sincerest thanks to my advisor, Dr. Thomas M. Nordlund, for the many lessons I learned under him. I thank my committee member Dr. Donald Muccio and Drs. Patricia Jackson, Anatoliy Kudryavstev, Luther W. Beegle, and Carmelo Rizzo of Vanderbilt University for their generous provision of facilities and assistance with spectroscopic measurements. My sincere thanks go to my committee members Drs. Edward Wills, Dan Urry, and John Young for their insight and guidance. My deepest appreciation and thanks go to Ms. Wanda Jordan and Drs. Terry Hickey and Joan Lorden for financial and mental support during my graduate studies. My dearest thanks go to my following friends: Dr. Da-Guang Xu for his wisdom and insight; Denise Brown, Neil Jenkins, and Patricia MacFarlane for the many racquetball games that diverted my frustrations and helped me keep my sanity.

TABLE OF CONTENTS

	<u>Page</u>
ABSTRACT.....	ii
DEDICATION.....	iv
ACKNOWLEDGMENTS.....	v
LIST OF TABLES	viii
LIST OF FIGURES.....	x
LIST OF ABBREVIATIONS	xiv
INTRODUCTION	1
PROJECT MOTIVATION.....	1
DNA and Its Molecular Structure.....	1
DNA-Protein Interactions	3
Detection and Monitoring of DNA Conformations.....	4
2-Aminopurine as Fluorescent Probe of DNA Conformation	5
BACKGROUND	7
Fluorescence Spectroscopy.....	8
Nuclear Magnetic Resonance	11
Raman Spectroscopy.....	12
Infrared Spectroscopy	13
DYNAMIC ANALYSIS OF THE MODIFIED DNA NUCLEOSIDE 2-AMINOPUR- INE IN SHORT OLIGONUCLEOTIDES USING TIME-RESOLVED FLUORES- CENCE AND NUCLEAR MAGNETIC RESONANCE SPECTROSCOPIES.....	23
FOURIER TRANSFORM-INFRARED, INFRARED, AND RAMAN COMPARA- TIVE STUDIES OF THE FLUORESCENT MODIFIED DNA BASE 2-AMINOPU- RINE AND ITS MONONUCLEOSIDES	84
GENERAL CONCLUSIONS	117

TABLE OF CONTENTS (continued)

	<u>Page</u>
GENERAL LIST OF REFERENCES.....	119
APPENDICES	
A TIME-RESOLVED FLUORESCENCE OF 2AP-T	123
B TIME-RESOLVED FLUORESCENCE OF A-2AP-T	132
C TIME-RESOLVED FLUORESCENCE OF G-2AP-C	141
D TIME-RESOLVED FLUORESCENCE OF C-2AP-G	150

LIST OF TABLES

<u>Table</u>	<u>Page</u>
DYNAMIC ANALYSIS OF THE MODIFIED DNA NUCLEOSIDE 2-AMINOPURINE IN SHORT OLIGONUCLEOTIDES USING TIME-RESOLVED FLUORESCENCE AND NUCLEAR MAGNETIC RESONANCE SPECTROSCOPES	
1	Chemical shift of the protons in 2AP, 2AP-rb, and 2AP-dn compared to those of 5'-AMP and 5'-dAMP. 31
2	Geminal and vicinal coupling constants of protons in 2AP-dn and 2AP-rb compared to those of 5'-AMP and 5'-dAMP. 32
3	Illustration of the corresponding reduced chi-squared values for the single-exponential lifetimes of 2AP in water and DMSO. 34
4	Single- and double-exponential lifetimes and reduced χ^2 for 2AP-dn in water. 35
5	Single- and double-exponential lifetimes and reduced χ^2 for 2AP-dn in DMSO. 36
6	Fluorescence decay parameters of 2AP-T and A-2AP-T oligonucleotides. 37
7	Fluorescence decay parameters of G-2AP-C and C-2AP-G oligonucleotides. 39
8	Comparison of average fluorescence lifetime of 2AP and the energy transfer from nearest neighboring base to 2AP. 48
FOURIER TRANSFORM-INFRARED, INFRARED, AND RAMAN COMPARATIVE STUDIES OF THE FLUORESCENT MODIFIED DNA BASE 2-AMINOPURINE AND ITS MONONUCLEOSIDES	
1	Raman and infrared absorption band assignments for crystalline adenine 200-1700 cm^{-1} 90
2	Raman and infrared absorption band assignments of crystalline 2AP 200-1800 cm^{-1} 92

LIST OF TABLES (continued)

<u>Table</u>	<u>Page</u>
3 Raman & Infrared Absorption Band Assignments of crystalline 2AP-rb.	95
4 Raman and Infrared Absorption Band Assignments of 2AP-rb 2000-3800 cm^{-1}	97
5 Comparison of IR and FT-IR bands of crystalline adenine, 2AP, and 2AP-rb.....	98
6 Raman band assignments for 2AP-dn and 2AP-rb in solution.	101

LIST OF FIGURES

<u>Figure</u>	<u>Page</u>
INTRODUCTION	
1 The structure of B-DNA.	14
2 The molecular structures of the DNA base pairs A-T and G-C. and the H-bonding between them.	15
3 The DNA base A and its analog 2AP.	16
4 Diagram showing the first two electronic energy levels and their vibrational energy levels, where S_0 and S_1 are the ground and first excited states, respectively.	17
5 Conventional set-up for a single-photon counting system.	18
6 Actual layout of single-photon counting system.	19
7 Double-cone precession of magnetic moments of protons in a static magnetic field.	20
8 Light scattering by a molecule.	21
9 Set-up for Raman spectroscopy measurements.	22
DYNAMIC ANALYSIS OF THE MODIFIED DNA NUCLEOSIDE 2-AMINO-PURINE IN SHORT OLIGONUCLEOTIDES USING TIME-RESOLVED FLUORESCENCE AND NUCLEAR MAGNETIC RESONANCE SPECTROSCOPES	
1 The structural difference between <i>syn</i> - and <i>anti</i> - conformations of 2AP-dn.	52
2 NMR spectra of a) 2AP, b) 2AP-dn, and c) 2AP-rb in D ₂ O.	53
3 Structural differences between adenine, A, and its fluorescence analog, 2AP.	54
4 2D-COSY spectrum of 2AP-dn at room temperature in D ₂ O.	55

LIST OF FIGURES (continued)

<u>Figure</u>	<u>Page</u>
5 2D-COSY spectrum of 2AP-rb at room temperature in DMSO-d6.	56
6 2D-NOESY spectrum of 2AP-dn at room temperature in DMSO-d6. 400 ms mixing time	57
7 Fluorescence decay curve of 2AP-dn in water (upper) at 22 °C.....	58
8 Fluorescence decay curve of 2AP-dn in DMSO (upper) at 22 °C.....	59
9 Fluorescence decay curve of 2AP-T (a) in water at 4 °C with (b) weighted residuals and (c) autocorrelation; (d) is the autocorrelation for a double- exponential fit.	60
10 Fluorescence decay curve of 2AP-T (a) in water at 18 °C with (b) weighted residuals and (c) autocorrelation.....	61
11 Fluorescence decay curve of 2AP-T (a) in water at 22 °C with (b) weighted residuals and (c) autocorrelation.....	62
12 Fluorescence decay curve of 2AP-T (a) in water at 42 °C with (b) weighted residuals and (c) autocorrelation.....	63
13 Fluorescence decay curve of A-2AP-T (a) in water at 4 °C with (b) weighted residuals and (c) autocorrelation (for triple-exponential fit); (d) autocorrelation for a double exponential fit.....	64
14 Fluorescence decay curve of A-2AP-T (a) in water at 18 °C with (b) weighted residuals and (c) autocorrelation.....	65
15 Fluorescence decay curve of A-2AP-T (a) in water at 22 °C with (b) weighted residuals and (c) autocorrelation.....	66
16 Fluorescence decay curve of A-2AP-T (a) in water at 42 °C with (b) weighted residuals and (c) autocorrelation.....	67
17 Fluorescence decay curve of G-2AP-C (a) in water at 4 °C with (b) weighted residuals and (c) autocorrelation (for triple-exponential fit); (d) autocorrelation for a double exponential fit.....	68
18 Fluorescence decay curve of G-2AP-C (a) in water at 18 °C with (b) weighted residuals and (c) autocorrelation.....	69

LIST OF FIGURES (continued)

<u>Figure</u>	<u>Page</u>
19 Fluorescence decay curve of G-2AP-C (a) in water at 22 °C with (b) weighted residuals and (c) autocorrelation.....	70
20 Fluorescence decay curve of G-2AP-C (a) in water at 38 °C with (b) weighted residuals and (c) autocorrelation.....	71
21 Fluorescence decay curve of C-2AP-G (a) in water at 4 °C with (b) weighted residuals and (c) autocorrelation (for a triple-exponential fit); (d) autocorrelation for a double exponential fit.....	72
22 Fluorescence decay curve of C-2AP-G (a) in water at 18 °C with (b) weighted residuals and (c) autocorrelation.....	73
23 Fluorescence decay curve of C-2AP-G (a) in water at 22 °C with (b) weighted residuals and (c) autocorrelation.....	74
24 Fluorescence decay curve of C-2AP-G (a) in water at 38 °C with (b) weighted residuals and (c) autocorrelation.....	75
25 Temperature dependence (4-42 °C) of the fluorescence decay (a) lifetimes and (b) corresponding amplitudes for 2AP-T.....	76
26 Temperature dependence (4-42 °C) of the fluorescence decay (a) lifetimes and (b) corresponding amplitudes for A-2AP-T.....	77
27 Temperature dependence (4-38 °C) of the fluorescence decay (a) lifetimes and (b) corresponding amplitudes for G-2AP-C.....	78
28 Temperature dependence (4-38 °C) of the fluorescence decay (a) lifetimes and (b) corresponding amplitudes for C-2AP-G.....	79
29 Van't Hoff analysis of fluorescence decay amplitude components for (a) 2AP-T and (b) A-2AP-T.....	80
30 Van't Hoff analysis of fluorescence decay amplitude components for (a) G-2AP-C and (b) C-2AP-G.....	81
31 The structure of the trinucleotide G-2AP-C, after energy minimization, showing possible H-bonding between -NH ₂ of 2AP and O6 of guanine.....	82

LIST OF FIGURES (continued)

<u>Figure</u>	<u>Page</u>
32 Van't Hoff plot analysis of A-2AP-T trinucleotide compared to the energy transfer efficiency of the CTGAA(2AP)TTCAG decamer.	83
FOURIER TRANSFORM-INFRARED, INFRARED, AND RAMAN COMPARATIVE STUDIES OF THE FLUORESCENT MODIFIED DNA BASE 2-AMINOPURINE AND ITS MONONUCLEOSIDES	
1 IR spectra of crystalline adenine (upper) and 2AP (lower)..	105
2 IR spectra of crystalline 2AP-rb.	106
3 FT-IR spectra of crystalline adenine and 2AP.	107
4 FT-IR spectra of crystalline adenosine and 2AP-rb.	108
5 Laser-Raman spectra ($188\text{-}2200\text{ cm}^{-1}$) of crystalline adenine (upper) and 2AP (lower) free bases.	109
6 Laser-Raman spectra ($2380\text{-}3800\text{ cm}^{-1}$) of crystalline adenine (upper) and 2AP (lower) free bases.	110
7 Laser-Raman spectra of crystalline 2AP-rb. $188\text{-}2200\text{ cm}^{-1}$ (upper) and $2300\text{-}3800\text{ cm}^{-1}$ (lower).	111
8 Molecular structure of 2AP used to assign vibrational modes.	112
9 Molecular structure of 2AP-rb.	113
10 Vertically polarized Raman spectra of 2AP-dn in solution, $200\text{-}2300\text{ cm}^{-1}$ (upper), $2400\text{-}3800\text{ cm}^{-1}$ (lower).	114
11 Vertically polarized Raman spectra of 2AP-rb in solution, $200\text{-}2300\text{ cm}^{-1}$ (upper), $2400\text{-}3800\text{ cm}^{-1}$ (lower).	115
12 Horizontally polarized Raman spectra of 2AP-rb in solution, $200\text{-}2300\text{ cm}^{-1}$ (upper), $2400\text{-}3800\text{ cm}^{-1}$ (lower).	116

LIST OF ABBREVIATIONS

DNA	Deoxyribonucleic acid
A	Adenine
G	Guanine
C	Cytosine
T	Thymine
C1'	Carbon in the 1'-position of a molecule
H-bonding	Hydrogen bonding
H-bonds	Hydrogen bonds
NMR	Nuclear magnetic resonance
2AP	2-Aminopurine
FT-IR	Fourier transform-infrared
S_0	Ground-singlet state of a molecule
S_1	First excited state of a molecule
R	ratio of molecules in the upper energy level vs. the lower level of the ground state
ΔE	difference in energy states
k	Boltzmann's constant
T	Kelvin temperature

LIST OF ABBREVIATIONS (continued)

γ	Radiative decay rate
k	Nonradiative decay rate
A_i	i -th pre-exponential factor of the fluorescence of a molecule
t	Time
$P(\lambda_{em}, t)$	Probability of a photon of wavelength λ_{em} being emitted at some time after excitation
τ_i	i -th fluorescence lifetime of a molecule
λ_{em}	Fluorescence emission wavelength
CW	Continuous wave
UV	Ultraviolet
λ_{em}	Wavelength
τ	Fluorescence lifetime
$F(t)$	Fluorescence intensity as a function of time
TAC	Time-amplitude converter
CFD	Constant-function-timing discriminator
ADC	Analog-to-digital converter
MCA	Multichannel analyzer
P	Angular momentum
μ	Nuclear magnetic moment
γ_m	Nuclear gyromagnetic ratio constant
I	Nuclear angular spin quantum number

LIST OF ABBREVIATIONS (continued)

B_0	Static magnetic field
ν_L	Larmor frequency
PMT	Photon multiplier detector
rf	Radio frequency
FID	Free-induction decay
$\partial\alpha / \partial Q$	Change in polarizability α as the normal mode of vibration Q changes
$\partial\mu_{dp} / \partial Q$	Change in dipole moment μ_{dp} as the normal mode of vibration Q changes
ΔH	Change in enthalpy, H
O6	Oxygen in the six-position of a molecule
DMSO	Dimethylsulfoxide
KCl	Potassium chloride
2D-NOESY	Two-dimensional nuclear-Overhauser-effect spectroscopy
TRIZMA	Tris[hydroxymethyl]aminomethane
EDTA	Ethylenediaminetetraacetic acid
ACS	American Chemical Society
DMT	Dimethoxytrityl
2AP-dn	2-Aminopurine-2'-deoxyribonucleoside
2AP-rb	2-Aminopurine ribonucleoside
^1H	Proton
D_2O	Deuterated water

LIST OF ABBREVIATIONS (continued)

pD	Negative value of the logarithm of the concentration of deuterium ions
COSY	Correlated spectroscopy
TMS	Tetramethylsilane
FWHM	Full-width-half-maximum
H6	Hydrogen in the six-position of a molecule
H1	Hydrogen in the one-position of a molecule
H8	Hydrogen in the eight-position of a molecule
H1'	Hydrogen in the 1'-position of a molecule
H2'	Hydrogen in the 2'-position of a molecule
5'-AMP	5'-Adenosine monophosphate
5'-dAMP	5'-Deoxyadenosine monophosphate
1D	One dimensional
J	Coupling constant
ΔH_{21}	Enthalpy difference between the states 1 and 2 of a molecule
ΔH_{32}	Enthalpy difference between the states 2 and 3 of a molecule
ΔH_{31}	Enthalpy difference between the states 1 and 3 of a molecule
US	Unstacked state
PS	Partially stacked state
FS	Fully stacked state

LIST OF ABBREVIATIONS (continued)

ΔH_1	Enthalpy difference for state 1 of a molecule
ΔH_2	Enthalpy difference for state 2 of a molecule
ΔH_3	Enthalpy difference for state 3 of a molecule
T	Temperature
CCD	Charged-coupled device
KBr	Potassium bromide
IR	Infrared

INTRODUCTION

PROJECT MOTIVATION

DNA and Its Molecular Structure

Deoxyribonucleic acid (DNA) is probably the most important molecule in any organism. It is DNA that is the storage facility of over a thousand genetic instructions. These instructions are encoded in the sequence of the deoxyribonucleotides and decoded by specific proteins that bind to the DNA through hydrogen bonds, ionic, and hydrophobic interactions between the amino acid side chains of the protein and the DNA bases. The protein then reads the sequence. It is because of this storage capacity that DNA has a dominant role in gene expression, suppression, and replication processes. Because DNA, during these processes, undergoes conformational changes that involve structural dynamics such as helix flexibility and base mobility, it is essential to study these DNA-protein interactions to be able to comprehend the initiation of the recognition process (Stryer, 1988). However, because of DNA's structural dynamics involved in these interactions, it is necessary to first examine the DNA's conformational structure and dynamics.

DNA is a lengthy polymer of deoxyribonucleotides that have three components: (1) a base, of which there are generally adenine (A), guanine (G), cytosine (C), or thymine (T), (2) a deoxyribose sugar, and (3) a phosphate. These components form individual nucleotides where the base is bonded by one of its nitrogens to the C1' (carbon

in the 1'-position) of the sugar molecule. The sugar molecule is in turn bonded to another sugar molecule by a phosphate group which connects the sugar's 3'-hydroxyl group to the 5'-hydroxyl of the next sugar. This connectivity is continued to form the long chains of nucleotides.

When physiological conditions are such that the water surrounding the DNA contains an alkali metal ion (i.e., Na^+), and relative humidity is 92%, the DNA is mostly in a form that Watson and Crick called B-DNA. This particular DNA form has two polynucleotide chains that are anti-parallel. These chains are coiled in a right-handed, helical manner around a common axis. The chains are held together by hydrogen bonding (H-bonding) between bases opposite one another (called complementary base pairing) and by stacking interactions between adjacent bases. The bases are located on the interior of the helix, with the phosphate and sugar groups on the exterior (Figure 1) forming the backbone. The bases' planes are almost perpendicular to the helical axis and the sugars' planes are nearly perpendicular to those of the bases. The helix diameter is ~ 20 Å with adjacent bases separated 3.4 Å along the axis, related by a 36° rotation. In the DNA's double helix, adenine is always paired with thymine (A-T) and guanine with cytosine (G-C), such that the bases opposite one another form a planar base pair (Figure 2) (Stryer, 1988; Voet & Voet, 1988).

However, the general B-form of DNA is not always maintained fully in solution. At times, this structure will undergo conformational changes. For instance, an increase in the ionic (salt) concentration of a solution of DNA can result in B-DNA converting into another form (Sarma, 1980). Another example occurs when a solution of DNA is heated above a characteristic temperature to cause the DNA to lose structural stability

because its H-bonds are broken. This in turn allows the bases to become exposed to the exterior environment of the helix until the helix finally becomes two separate strands of polynucleotides (denaturation). Denaturation may also occur to some degree when proteins bind to the DNA (Hogan & Austin, 1987; Voet & Voet, 1988).

DNA-Protein Interactions

As for DNA-protein interactions, one well-studied class is the restriction endonucleases and their nucleic acid recognition sequences. One of the simplest systems, Eco RI endonuclease and its recognition site, has been studied as a lone protein and as a DNA-protein complex in solution (Chan *et al.*, 1990; Kim *et al.*, 1990; McClarin *et al.*, 1986; Ramstein & Lavery, 1988; Robinson & Sligar, 1994). Eco RI is a protein that forms active dimers to recognize and cleave DNA at the specific duplex sequence 5'-d(CTGAAATTCAG)₂ (cleavage site is underlined). In crystalline form, the Eco RI-DNA complex has two B-DNA-like and two A-DNA-like units of three base pairs apiece, each separated by kinks.

Prior to binding, it is evident that the chemical and electronic structure of DNA plays a large part in recognition: in other words, base sequence is vital. Upon binding to DNA, recognition occurs through hydrogen bonds from the amino acids glutamate 144, arginines 145 and 200 to GAA of the DNA, and from amino acids 137-142 to TTC (Frederick *et al.*, 1984). Beyond this, molecular details of the structure of the complex are known after recognition and binding only.

Because the bases are on the interior of the helix, it is not quite clear how Eco RI is able to sense them (Hager *et al.*, 1990). It then becomes a question of how the protein

recognizes the specific base sequence. One possibility is that there is spontaneous opening and closing of base pairs. This would increase their exposure to the outside of the helix and, thus, to the protein (Chen *et al.*, 1991a; Gueron *et al.*, 1986; Kahn *et al.*, 1994; Nordlund *et al.*, 1989; Ramstein & Lavery, 1988; Tari & Secco, 1995). However, base motion would have to occur more quickly than the cleavage rate of Eco RI, 10 ms. In general, DNA can have base pair openings that occur in a few milliseconds or longer, as measured by nuclear magnetic resonance (NMR) (Chen *et al.*, 1991b; Lycksell *et al.*, 1987). In addition, base mobility for the Eco RI recognition sequence occurs up to several angstroms on a shorter time scale (Chan *et al.*, 1990; Chen *et al.*, 1991b; Lycksell *et al.*, 1987; Nordlund *et al.*, 1989; Westhof & Moras, 1987).

Detection and Monitoring of DNA Conformations

If base mobility in DNA allows or enhances the initiation of recognition by proteins, it then becomes ever more important to be able to detect DNA conformational changes in order to understand them. Monitoring these changes is possible through several techniques, of which the most widely used are optical absorption, fluorescence, infrared and Raman spectroscopy, NMR, and x-ray crystallography (Cantor & Schimmel, 1980). For example, circular dichroism and hypochromism are standard methods which are used to provide information of global conformation of DNA. That is to say that structural features like right-handed double-helix, single stranded, and random coiled are observable. Methods like NMR and x-ray crystallography can provide site-specific probing of DNA structure and interactions. Unfortunately, though, these two methods are unable to separate more than two states simultaneously.

Another limit of absorption, NMR, and x-ray crystallography is their time scale. For instance, absorption takes place in about 10^{-15} seconds where molecules and their environments are effectively static. As for NMR and x-ray, these methods cannot access changes on a time scale of 1 ms or faster. On the other hand, time-resolved fluorescence spectroscopy is more sensitive to environmental changes that generally occur in 10^{-9} to 10^{-8} seconds (Hager *et al.*, 1990). This makes fluorescence well suited for measuring structural changes, provided that a well-placed chromophore is within the DNA. Fluorescence has time resolution that is essentially unlimited, and sensitive detection and analysis methods have been developed to quantitate multiple states.

Unfortunately, the normal bases of DNA have fluorescence that decays in about 10^{-12} to 10^{-11} seconds. This is quite demanding on instrumentation sensitivity and response time (Ballini *et al.*, 1988; Georghiou *et al.*, 1985; Gueron *et al.*, 1974; Nordlund, 1988). Thus, it becomes necessary to use an extrinsic probe molecule or a chemically modified base which would give an increased fluorescence yield. Extrinsic probes, however, must always be used with care because of structural perturbations and because intrinsic DNA fluorescence is short-lived. Thus, a chemically modified base that has an increased yield, at the same time not significantly perturbing the DNA's structure, is a better choice.

2-Aminopurine as Fluorescent Probe of DNA Conformation

In our research, 2-aminopurine is such a molecule. This is an analog of the DNA base adenine (Figure 3) in which the amino group is moved from the 6 position to the 2 on the base-ring, creating a 1000-fold increase in the fluorescence (Georghiou *et al.*,

1985; Graslund *et al.*, 1987; Lycksell *et al.*, 1987; Millar & Sowers, 1990; Ward *et al.*, 1969). Also, the optical absorption and emission bands of 2-aminopurine (2AP) are clearly separated from those of normal bases (Rigler & Claesens, 1986; Ward *et al.*, 1969).

When incorporated into DNA in place of adenine, 2AP H-bonds to thymine (Bloom *et al.*, 1993; Lycksell *et al.*, 1987; Raney *et al.*, 1994). 2AP can also mispair with cytosine to create a disruption in the helical structure of the DNA (Ronen, 1979). 2AP incorporated into the recognition sequence of the Eco RI endonuclease d(CTGAATTCAG)_n produced a 9-fold reduction of binding to the sequence (McLaughlin *et al.*, 1987) without destroying the B-helical structure of the duplex; also, the cleavage rate of the duplex remains comparable to that of the unmodified sequence (McLaughlin *et al.*, 1987; Nordlund *et al.*, 1989).

Optically, we had shown that the emission spectrum of 2AP shifted to longer wavelengths as the solvent's dielectric constant increased, with the exception of dioxane. At the same time, we showed that the absorption and excitation spectra of 2AP also shifted to longer wavelengths as the solvent's dielectric constant increased. The exception was water, in which the spectra shifted to a shorter wavelength because of water and 2AP H-bonding together. The sensitivity of the excitation spectrum of 2AP in water is mirrored when it is incorporated into the decamer d[CTGA(2AP)TCAG]₂ as the decamer unfolds because of an increase in temperature (Evans *et al.*, 1992; Evans, 1996).

Further measurements on d[CTGA(2AP)TCAG]₂ had shown that its fluorescence can be described by multiple decay times. In contrast, 2AP free base has a fluorescence lifetime that is a single-exponential lifetime. Because each multiple decay time of 2AP's

fluorescence may be associated with a distinct excited state. 2AP must interconvert between them (Nordlund *et al.*, 1989). This suggests that base-pair opening fluctuations cause the highly nonexponential decay of the oligonucleotide's fluorescence. However, further detailed conformational states and the interconversion rates between them are, for the most part, unknown. Thus, the overall purpose of this research was to determine the conformations of 2AP nucleosides that are responsible for the multiple fluorescence decays.

As an approach to reaching my overall goal, my dissertation is centered on two papers. The first paper addresses a structural interpretation of the fluorescence of 2AP, free and incorporated into short oligonucleotides. This will be attempted by correlation of the fluorescence decay of 2AP with its nuclear magnetic resonance measurements. The second paper focuses on characterization of Raman, Fourier transform-infrared (FT-IR), and infrared spectroscopy signals of solid and aqueous samples of 2AP, as a free base and as its mononucleosides.

BACKGROUND

Fluorescence Spectroscopy

Fluorescence spectroscopy is a method that is quite sensitive to the environment of a chromophore. This makes fluorescence a potentially useful tool for monitoring DNA conformational changes using 2AP as the probe. Fluorescence is based on the ability of molecules to absorb a photon of one wavelength and emit a photon generally of a longer wavelength. This absorption and emission of light can be illustrated by a diagram showing the first two electronic energy levels of a molecule, the ground-singlet

state, S_0 , and the first excited state, S_1 (Figure 4). The energy spacing between the vibrational levels represented by the lines in each energy state is roughly 10 kcal/mole, which is much greater than thermal energies at room temperature and rotational level spacing, which are typically 1 kcal/mole (Cantor & Schimmel, 1980). Therefore, by statistical mechanics, the ratio of molecules, R , in the upper energy states to those in the lower one is described by the Boltzmann distribution.

$$R \propto e^{-\Delta E / kT} \quad (1)$$

This states that most of the molecules that undergo light absorption will be present in the lowest vibrational level of the ground state, S_0 , where ΔE is the energy difference between states, k is Boltzmann's constant, and T is the Kelvin temperature.

The Frank-Condon principle states that following absorption of a photon, a molecule is instantaneously ($\approx 10^{-15}$ s) excited to one of the vibrational levels in S_1 . Vibrational relaxation then occurs, in which the molecule rapidly ($\approx 10^{-12}$ s) relaxes to the lowest vibrational level of S_1 . From here, the molecule must release the remaining excess energy in the form of a photon; this process is called fluorescence emission (Figure 4). There is normally a shift to a longer wavelength in the emission process compared to the absorption (i.e., an energy loss called Stokes' shift) because of the vibrational relaxation. This occurs universally with chromophores in solution.

The amount of time the chromophore remains in its first excited state, S_1 , prior to returning to the ground state, S_0 , usually represents the average fluorescence lifetime of the chromophore. Upon excitation with an infinitely short pulse (δ -function), there are

initially N_0 chromophores in the excited state. The decay rate of this fluorescent lifetime is

$$\frac{dN(t)}{dt} = -(\gamma + k)N(t), \quad (2)$$

where $N(t)$ is the number of chromophores in the excited state at some time t following excitation; γ is the radiative decay rate; and k is the nonradiative decay rate. With $N(0) = N_0$, equation 2 then becomes $N(t) = N_0 e^{-t/\tau}$, where the excited state's lifetime is $\tau = (\gamma + k)^{-1}$. Because the fluorescence intensity, $F(t)$, is proportional to the number of molecules in this excited state, then the fluorescence also should have an exponential decay. However, these exponential decays are not always single. Thus, the fluorescence intensity may be written mathematically as the sum of exponentials:

$$F(t) = \sum_i A_i e^{-t/\tau_i}, \quad (3)$$

where A_i is the pre-exponential factor that represents the fractional contribution to the time-resolved decay of the component with a lifetime τ_i (Lakowicz, 1983, 1991).

To measure the time-resolved fluorescence, the single-photon counting system was used which determines the probability $P(\lambda_{em}, t)$ of a photon of wavelength λ_{em} being emitted at some time t after excitation. Generally, this fluorescence probability distribution can be constructed as follows: (1) A short pulse of light of an appropriate wavelength is used to create excited states of the molecule being studied; (2) this pulse of light produces a timing reference which starts a clock (the time-to-amplitude converter); (3) when a single-photon detector (a device that produces a useable output when a single photon is observed) observes a fluorescence photon generated by one of these excited

states, another signal is generated which stops the clock: (4) the time elapsed on the clock is recorded, and the clock is reset: (5) after steps 1-4 are repeated thousands of times, the recorded elapsed times are grouped into time intervals and plotted as the number of events in an interval as a function of elapsed time.

Experimentally, the fluorescence probability distribution is constructed as follows: The sample is repetitively excited by an argon-pumped, continuous wave (CW) mode-locked, cavity-dumped dye laser, which had the frequency doubled to ultraviolet (UV) light ($\lambda = 304$ nm). When a light pulse is fired, a reference signal (trigger T) is generated and goes to a level-crossing discriminator (PRA 1718). This reference signal then travels to the "START" input of the time-to-amplitude converter (TAC, PRA 1701), which begins to charge a capacitor. At the same time, the light pulse excites the sample, which subsequently fluoresces. The intensity of the excitation pulse has been adjusted such that at most one photon is detected by the detector (fast photomultiplier tube) for each exciting event. The signal generated by this photon is then sent to a constant-fraction timing discriminator (CFD), which in turn is delayed with respect to the START pulse. This delayed signal is sent to the "STOP" input of the TAC to stop charging the capacitor. The TAC then generates an output signal that has a voltage proportional to the difference in arrival times between the STOP and START signals. The pulse then goes to an analog-to-digital converter (ADC) input where the pulse's amplitude is translated into a number of clock cycles. The clock cycles are then stored as a count in memory locations of the multichannel analyzer (MCA) that correspond to each clock cycle. This data storage is continued until a histogram of the counts represents, to some precision,

the decay curve of the sample's fluorescence. Figure 5 illustrates a conventional single-photon counting system: figure 6 illustrates our actual system set-up.

Nuclear Magnetic Resonance

When it comes to tools for evaluating information about structural conformation of proteins and oligonucleotides, nuclear magnetic resonance (NMR) is an indispensable tool. NMR is based on the intrinsic angular momentum, \mathbf{P} , and magnetic moment, $\boldsymbol{\mu}$, of an atom's nucleus. Assuming that an atomic nucleus is spherical and spins, it has angular momentum. This spinning charge has associated with it a magnetic moment, $\boldsymbol{\mu}$. The angular momentum and $\boldsymbol{\mu}$ are related to one another by $\boldsymbol{\mu} = \gamma_m \mathbf{P}$, where γ_m is the gyromagnetic ratio constant that is nucleus dependent. Because angular momentum is quantized, an atom's magnetic moment then becomes $\mu = \sqrt{I(I+1)}\hbar$, I being the nuclear spin of half-integrals.

In the absence of a magnetic field, these magnetic moments are randomly oriented. However, when placed in a static magnetic field, \mathbf{B}_0 , a bulk magnetization is created along the z-axis: this is in the shape of a double cone for protons (Figure 7). The atom's angular momentum also obtains a particular orientation: one such that its component along the z-axis precesses about \mathbf{B}_0 . This precessional frequency (Larmor frequency) is described as

$$\nu_L = \frac{\gamma_m B_0}{2\pi} \quad (4)$$

For atoms with a nuclear spin of $1/2$, like protons, in a magnetic field, this double cone precession is due to the only two energy states possible,

$$E = \pm \frac{\hbar B_0}{2} \quad (5)$$

with more of the nuclei in the lower state. In order to observe a magnetic resonance signal, it is necessary to induce transitions between energy states. This is accomplished by a second magnetic field, \mathbf{B}_1 , being applied in the form of a pulsed, radio frequency (rf). This rf-pulse that tilts the z-component of the bulk magnetization out of its normal position, and slowly decays over time. This decay, called a free induction decay (FID), is what gives rise to a magnetic resonance signal. However, the signal from the FID is in the form of amplitude versus time. Because it is desirable to have the FID in the form of amplitude versus frequency, Fourier transforms are used to convert such (Bertini *et al.*, 1991; Friebolin, 1991; Macomber, 1988) signals into amplitude versus frequency.

Raman Spectroscopy

Raman spectroscopy is another spectral method used to monitor local conformation (Chan *et al.*, 1997; Spiro, 1987). It is based on the ability of a molecule to scatter light. Unlike in fluorescence, the incident light does not have enough energy to instigate a ground-to-excited state transition of the molecule. Instead, the incident light has enough energy to cause vibrational level transitions that are well below the first electronic state (called a virtual state). A small amount of the incident light is scattered in all directions, where additional frequencies are observed. The frequency of the scattered light can be less than that of the incident. This would result in a Stokes Raman band. If the frequency of the scattered light is the same as the incident, then a Rayleigh band is created: if the frequency is greater, then the band is an anti-Stokes Raman band

(Figure 8). Because the energy between the vibrational levels is greater than thermal energy at room temperature, Stokes Raman bands are primarily observed (Gardiner & Graves, 1989). Figure 9 shows the Raman spectroscopy set-up used.

Infrared Spectroscopy

When the incident light is in the infrared range, photons can excite vibrational levels of a molecule. Although infrared and Raman spectroscopies reveal relatively the same information, their mechanisms of origin are different. Whereas Raman intensities are proportional to the changing polarizability ($\partial\alpha/\partial Q$, where α is the polarizability and Q is the normal mode of vibration) of a molecule, infrared intensities are proportional to the changing dipole moment ($\partial\mu_{dp}/\partial Q$, where μ_{dp} is dipole moment of a molecule and Q is the normal mode of vibration) (Alpert *et al.*, 1970; Colthup *et al.*, 1964; Stewart, 1970).

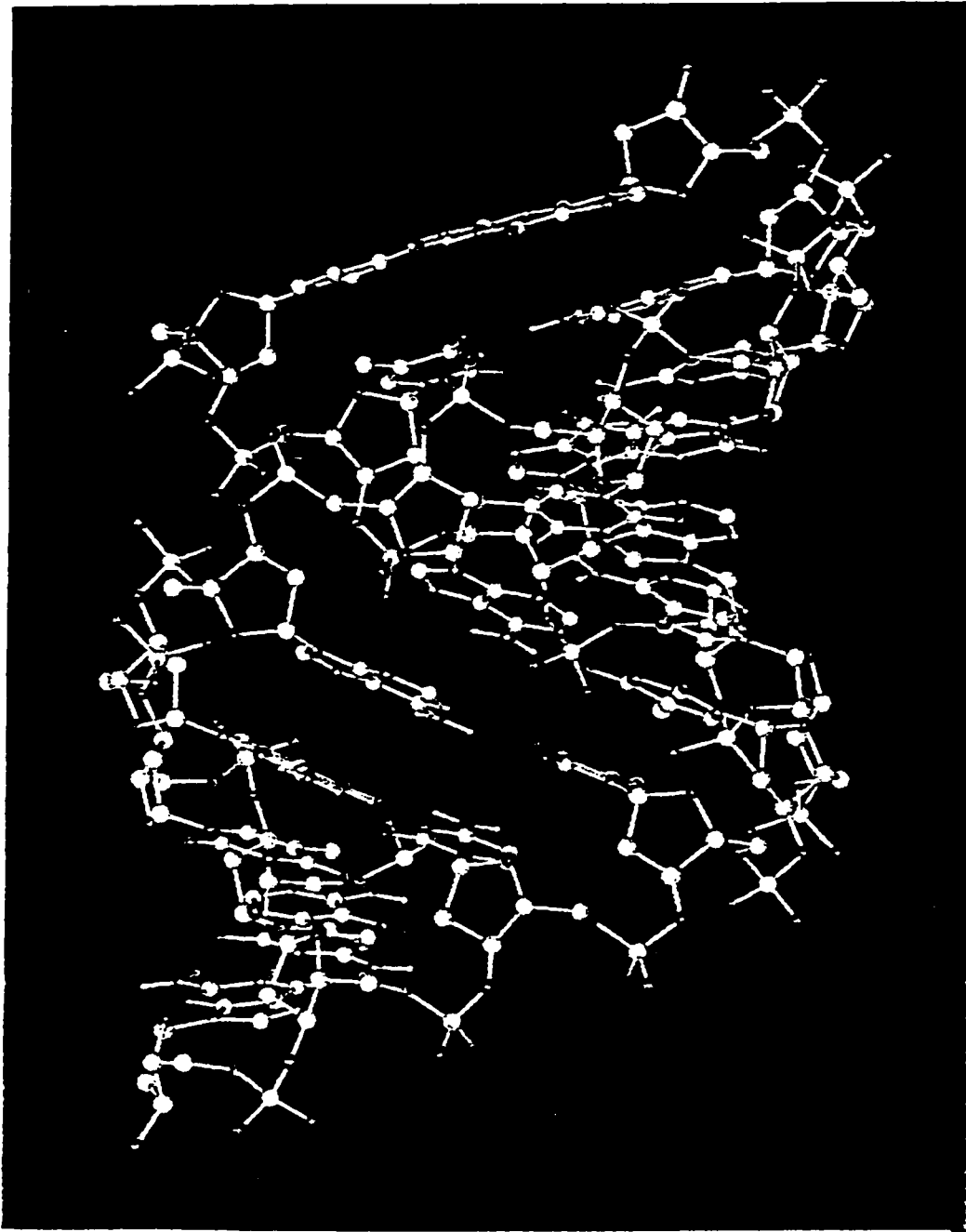


Figure 1: The structure of B-DNA.

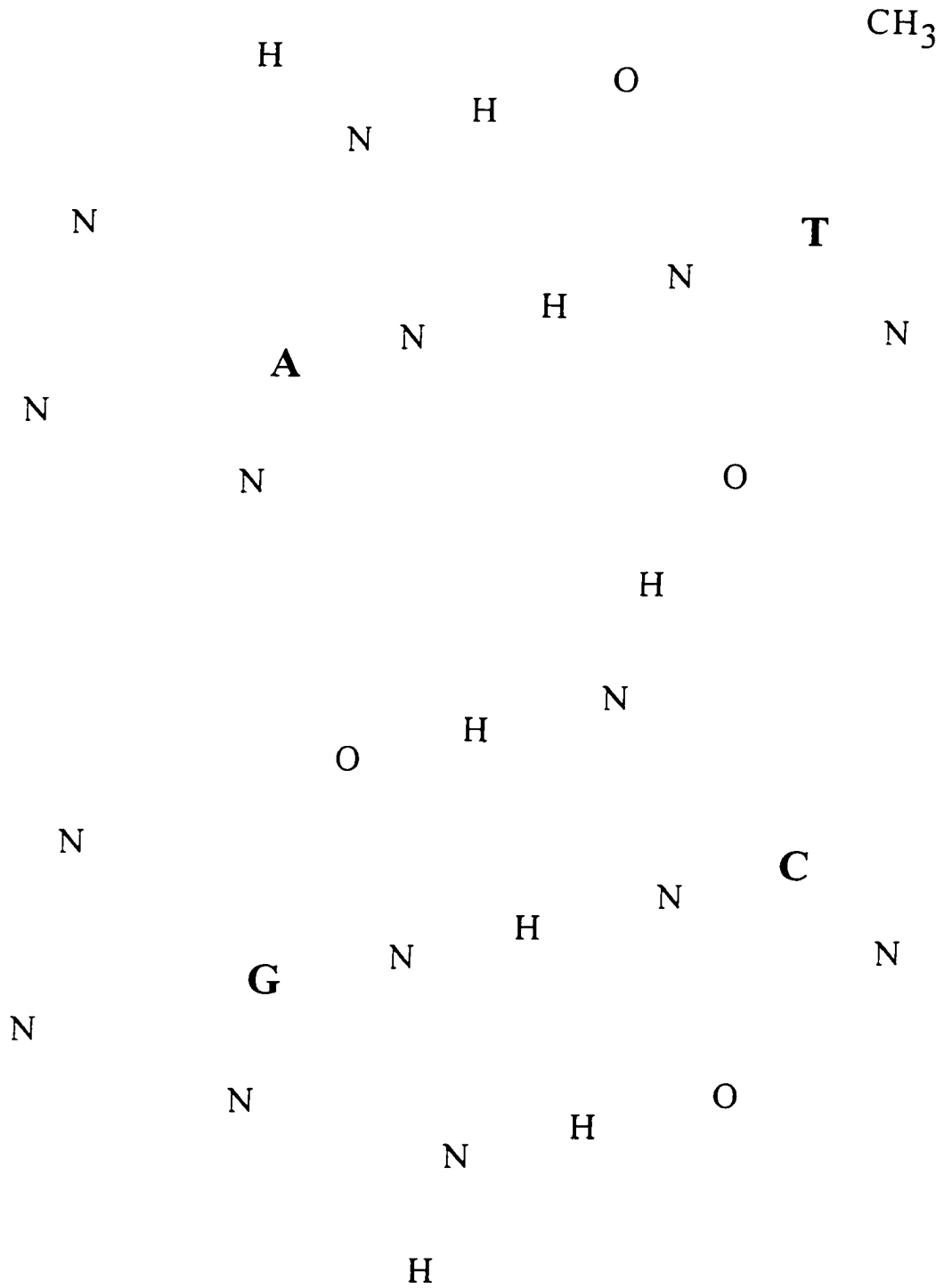


Figure 2: The molecular structures of the DNA base pairs A-T and G-C, and the H-bonding between them.

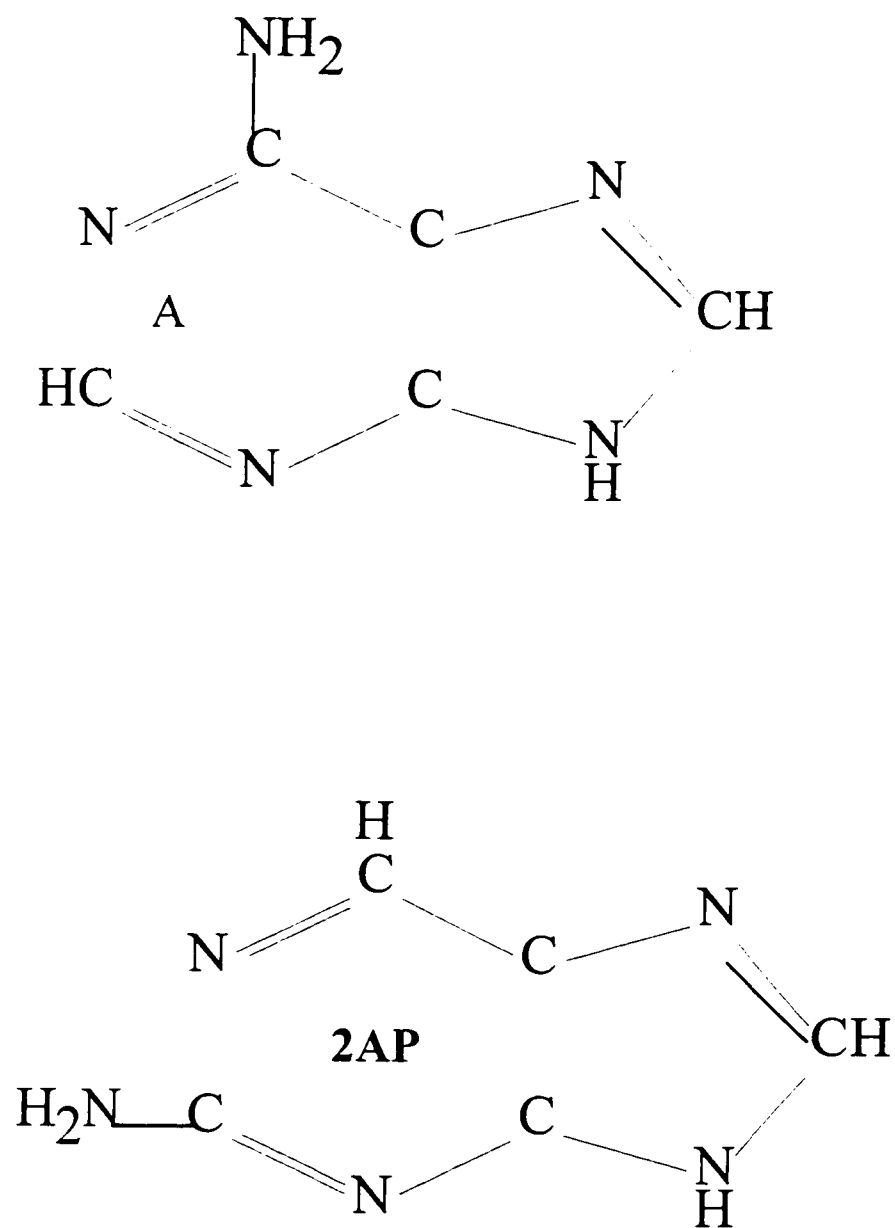


Figure 3: The DNA base A and its analog 2AP.

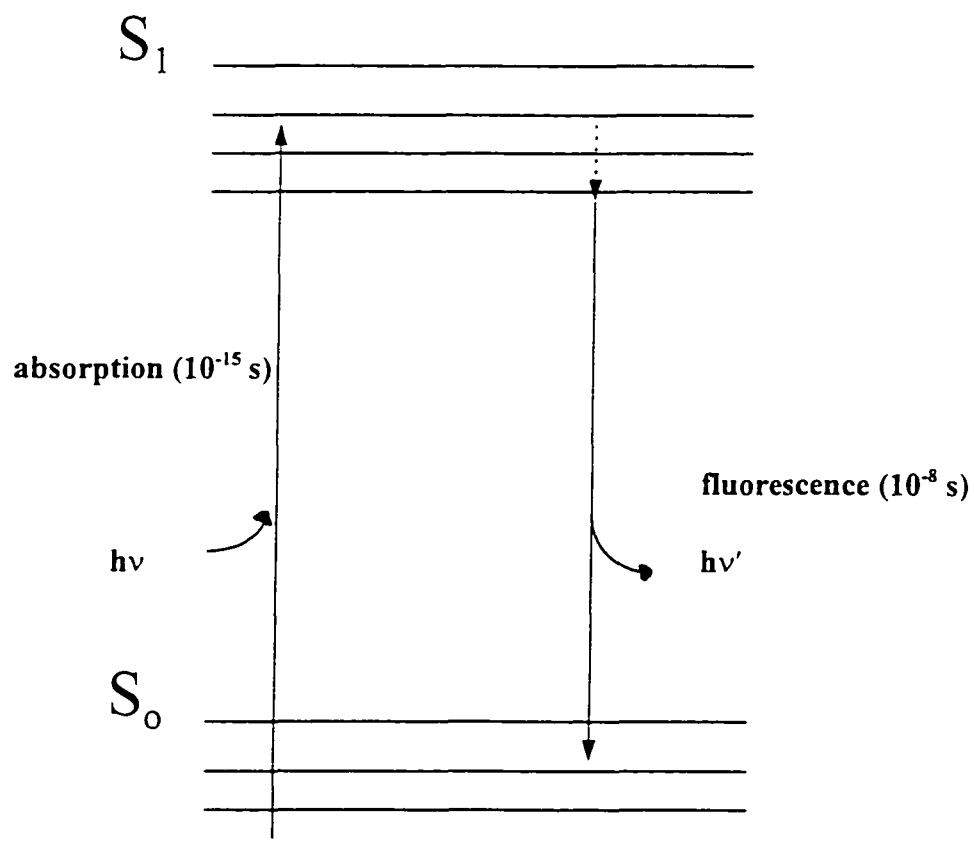


Figure 4: Diagram showing the first two electronic energy levels and their vibrational energy levels, where S_0 and S_1 are the ground and first excited states, respectively.

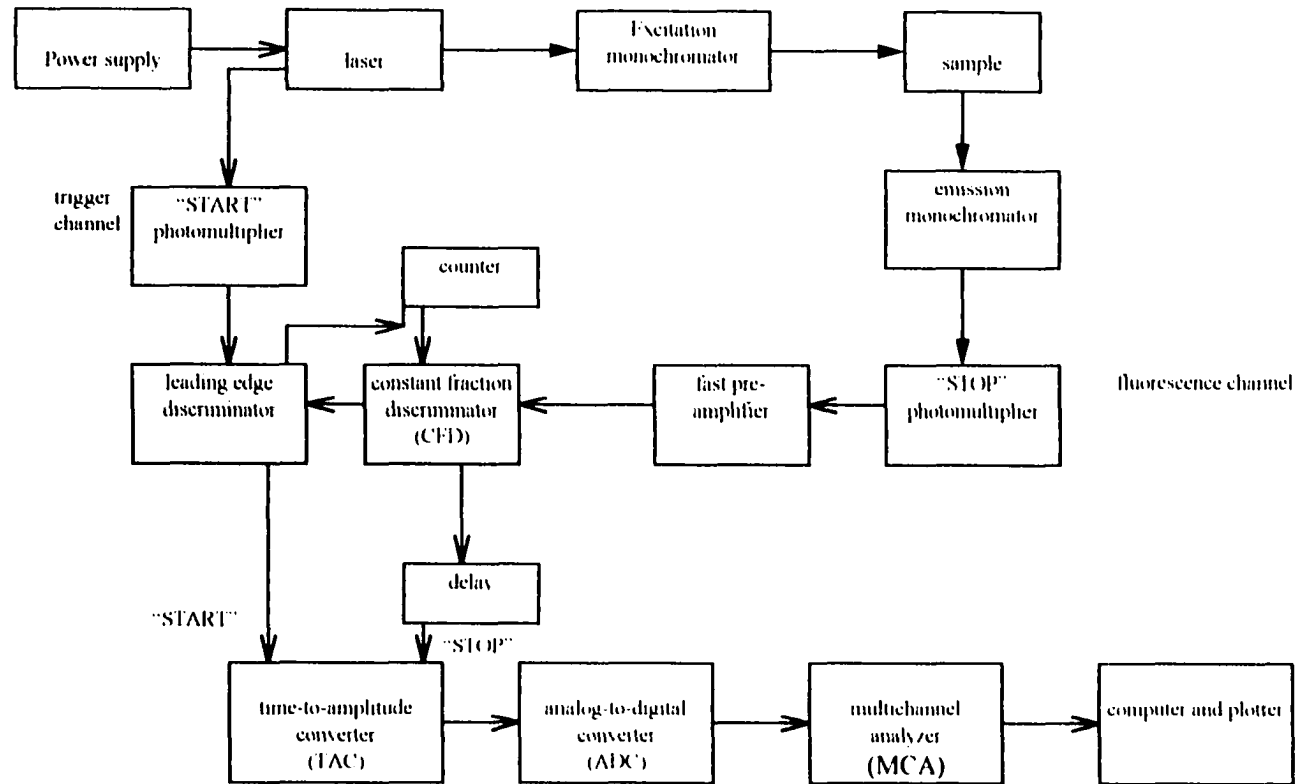


Figure 5: Conventional set-up for a single-photon counting system.

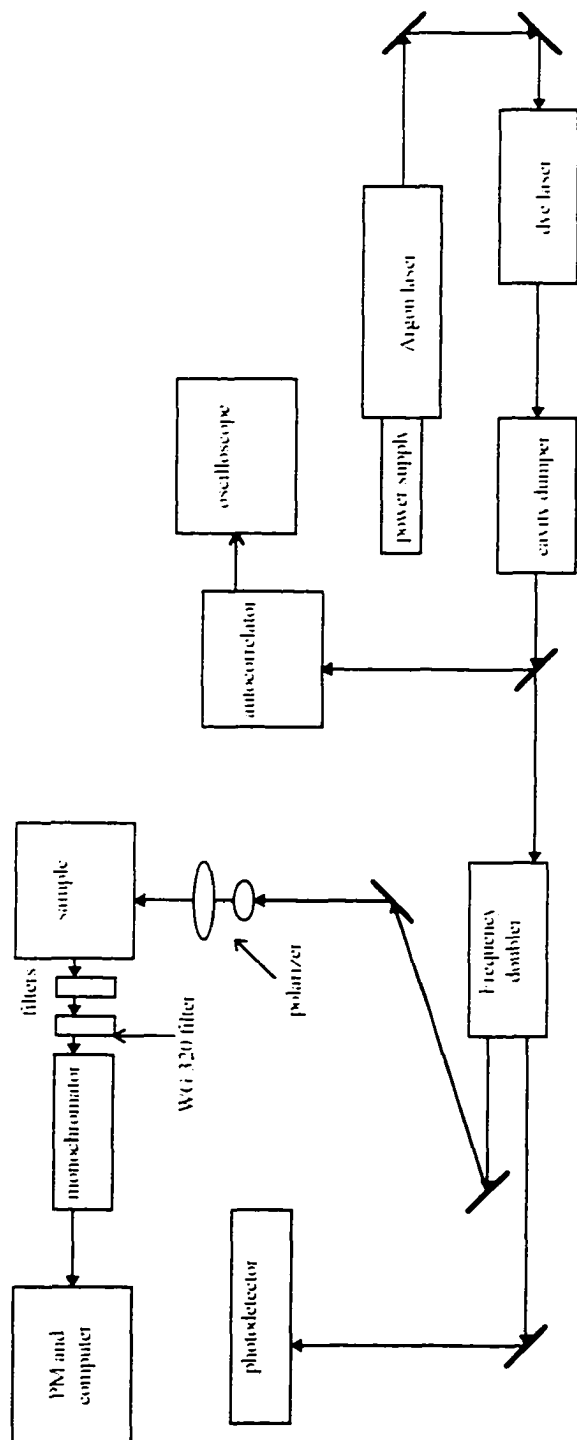


Figure 6: Actual layout of single-photon counting system.

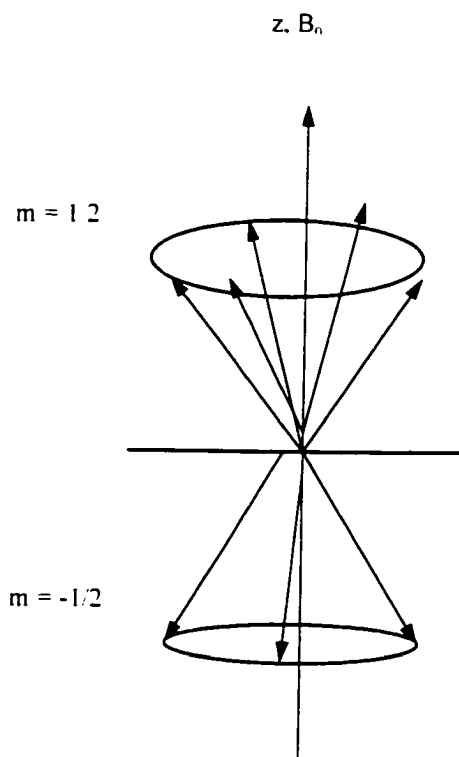


Figure 7: Double-cone precession of magnetic moments of protons in a static magnetic field.

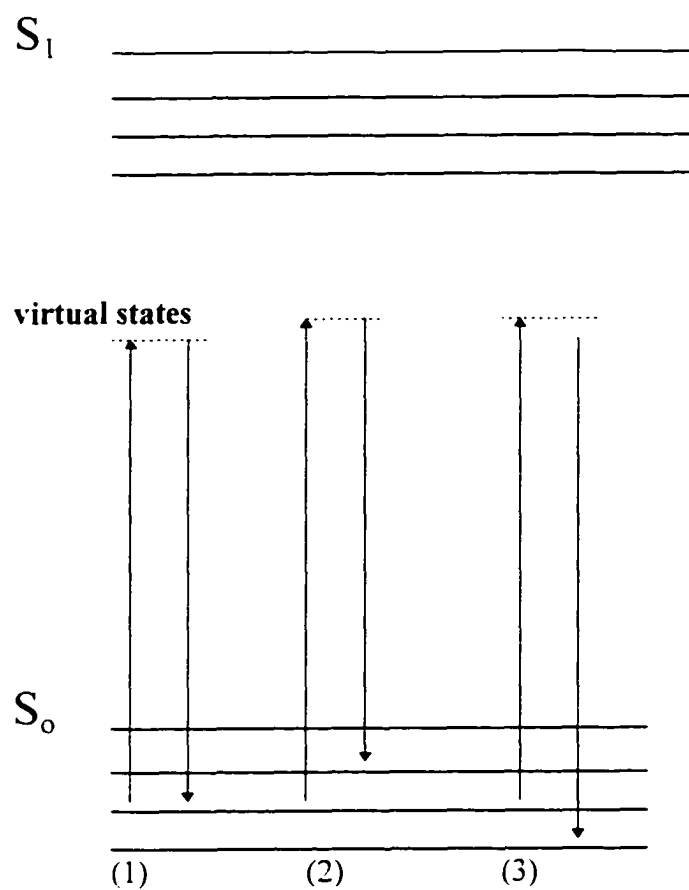


Figure 8: Light scattering by a molecule. (1) Rayleigh scattering, (2) Stokes Raman scattering, (3) anti-Stokes Raman scattering.

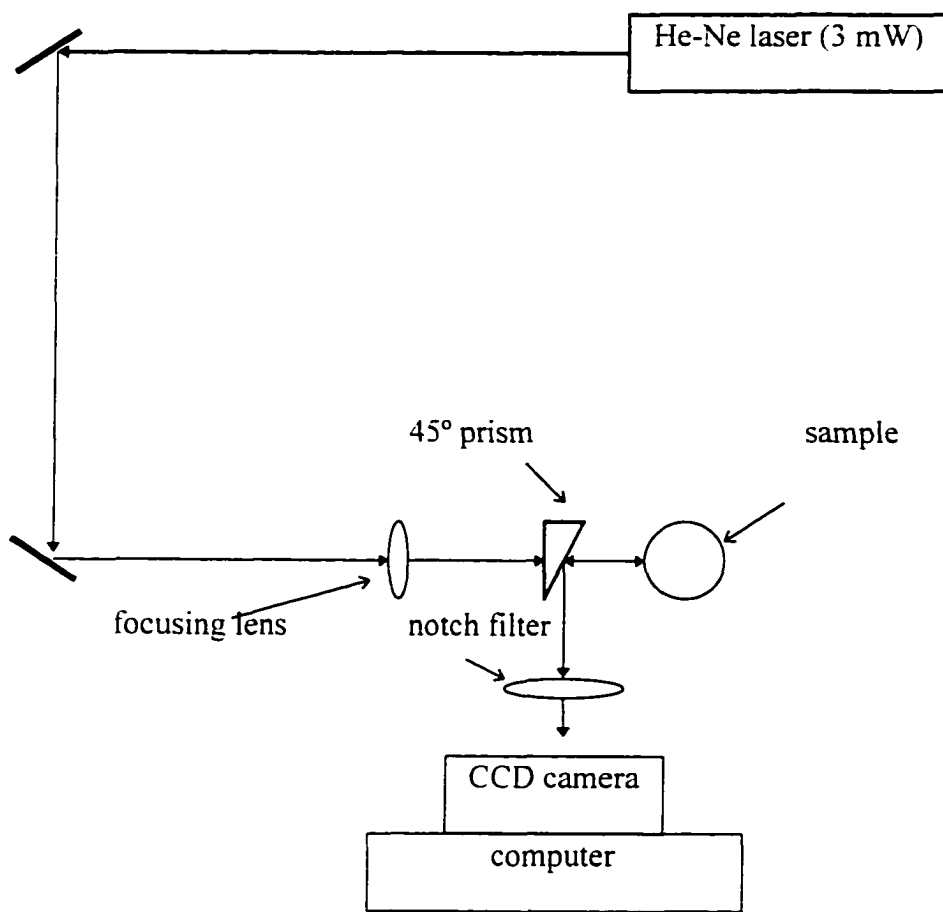


Figure 9: Set-up for Raman spectroscopy measurements.

DYNAMIC ANALYSIS OF THE MODIFIED DNA NUCLEOSIDE 2-AMINOPURINE
IN SHORT OLIGONUCLEOTIDES USING TIME-RESOLVED FLUORESCENCE
AND NUCLEAR MAGNETIC RESONANCE SPECTROSCOPIES

by

KERVIN O. EVANS, DA-GUANG XU, THOMAS M. NORDLUND

In preparation for *Journal of Fluorescence*

Format adapted for dissertation

ABSTRACT

In a continued effort to develop 2-aminopurine (2AP) as an optical probe of local conformational changes of DNA, we have been able to demonstrate that the *syn*- and *anti*- conformations of 2AP are not in themselves sufficient enough to exhibit a detectable multi-exponential fluorescence decay. Instead, we have shown that, in the least, a 3'-neighboring base interacting with 2AP does create a multi-exponential fluorescence decay (in particular, a triple-exponential decay) for 2AP. We classified the three states represented by these exponential components as being fully stacked (FS), partially stacked (PS), and unstacked (US). Using van't Hoff analysis, we calculated the enthalpies between these three states for a dinucleotide (2AP-T) and several trinucleotides (A-2AP-T, C-2AP-G, and G-2AP-C).

We found that the fluorescence lifetime of 2AP is quenched to 7.4 ns when adenine and thymine are the 5'- and 3'-neighbors, respectively, suggesting that adenine is a stronger quenching (thymine alone in the 3'-position only reduces the lifetime to 11.0 ns; 2AP as a free base has a 11.9 ns lifetime). We found G-2AP-C to have the largest enthalpic difference between fully stacked and unstacked states ($\Delta H = 9.4$ kcal/mole). Once again, an anomalous result was found when guanine is next to 2AP (Ujvari & Martin (1996) *Biochemistry* 35, 14574-14582; Xu (1996) PhD dissertation). We proposed that this is due to the $-NH_2$ of 2AP hydrogen bonding to O6 of guanine.

INTRODUCTION

Structural studies of DNA prior to and during binding to proteins are quite important in understanding how proteins recognize particular sequences of DNA. In addition to the chemical environment created by a particular sequence of base in DNA, it is believed that the opening and closing of the base pairs of DNA are vital for recognition (Chen & Prohofsky, 1994; Gueron *et al.*, 1986; Kahn *et al.*, 1994; Nordlund *et al.*, 1989; Ramstein & Lavery, 1988; Tari & Secco, 1995). These events would allow the protein full access to the bases of a recognition site. Therefore, in order to better understand the recognition process, it is important to monitor these local activities of DNA without interfering with the recognition process. This is easily accomplished by monitoring the fluorescence changes of a well-placed internal probe.

When considered as internal fluorescent probes, the normal DNA bases have a typical fluorescent lifetime of approximately 10^{-11} s (Ballini *et al.*, 1988; Georghiou *et al.*, 1985; Nordlund, 1988; Oraevsky *et al.*, 1981). This requires high instrument sensitivity or time resolution, which is not commonly available. Because of its increased fluorescence yield, 2-aminopurine (2AP, an analog of adenine), on the other hand, has been recognized as a adenine replacement that is a highly fluorescent probe for monitoring local DNA activities (Bloom *et al.*, 1993; Jia *et al.*, 1996; Nordlund *et al.*, 1989; Xu *et al.*, 1994).

During an earlier study, Nordlund *et al.*, 1989 showed that 2AP exhibited a multi-exponential fluorescence decay when incorporated in the decamer d[CTGA(2AP)TTCAG]₂. They attributed this fluorescence change (from a single exponential decay as a free mononucleoside to the multi-exponential of decamer) to 2AP

becoming more exposed to the external environment of the DNA: that is, H-bonds are broken such that the long lifetime is the fluorescence life of 2AP fully extended outside the helix, and the shortest lifetime is the fluorescence state of 2AP back inside the helix. This present study attempts to correlate actual structural conformations of the nucleoside (*syn*- and *anti*-; Figure 1) with fluorescence lifetimes. Our approach was to determine first if 2AP exhibited distinct fluorescence lifetimes for its individual conformations by measuring the lifetimes in water and DMSO. We included DMSO because of the following: (1) It is the solvent used in our 2D-NOESY NMR measurement, and (2) the ground state of molecule is lowered by a dielectric environment, which is quite different between water and DMSO. Such a dielectric change may be more favorable to one conformation over another. In our second approach, we wanted to determine how these lifetimes might change as the immediate base environment that 2AP experiences was gradually built, a nucleotide at a time. Thus, the oligonucleotides studied were at most three in length (di- and tri-nucleotides). In addition, others have shown 2AP in oligonucleotides to exhibit its most anomalous fluorescence excitation spectra when guanine is one of the immediate neighboring base (Ujvari & Martin, 1996; Xu, 1996). We have therefore included some trinucleotides that include guanine as the 3'- and 5'-neighboring base to determine how guanine may be affecting the fluorescence lifetime of 2AP.

EXPERIMENTAL PROCEDURE

Materials

2AP free base was purchased from Sigma Chemical Company and used without further purification. Also purchased were tris-[hydroxymethyl]aminomethane (TRIZMA-base, reagent grade, 99.9% pure) and ethylenediaminetetraacetic acid (EDTA, ACS reagent) from Sigma Chemical Company, and potassium chloride (KCl) crystals (ACS certified) from Fisher Scientific. The nucleoside 2-aminopurine-2'-deoxyribonucleoside (2AP-dn) was generously provided by Dr. George W. Koszalka, Burroughs Wellcome Co., Research Triangle Park, NC, and prepared and analyzed as previously described (Evans *et al.*, 1992). 2-aminopurine-CE phosphoramidate was purchased from Glen Research Corporation, Sterling, VA, for synthesizing the oligonucleotides.

The oligonucleotides containing 2AP were prepared using Applied Biosystems 392/394 automated DNA/RNA synthesizers (Perkin Elmer, Applied Biosystems Division, Foster, CA 94404) on a 0.2- or 1- μ M scale and a standard cycle. The standard cycle used the phosphoramidite method of oligonucleotide synthesis to add each nucleotide into a strand (Beaucage & Carthers, 1981). Each base was added by first detritylation to remove the acid-labile, dimethoxytrityl (DMT) protecting group of the phosphoramidite. This was then followed by coupling of the next base to the previously added one. Immediately afterward, capping by acetylation was done on the sequence to prevent any truncated sequences from propagating in subsequent coupling steps. Finally, the sequence was oxidated to eliminate the possibility of traces of water causing acetic anhydride to form acetic acid. The sequence was base deprotected in a bath that was ≥ 55 °C for 1 h after the sequence had been cleaved and phosphate deprotected. The full

sequence was then purified (overall yield ~95%) on a NAP-10 column and run on a Speed-VAC concentrator under a vacuum to dry. Purity was verified by using 2.5 ml oligomer solution to run gel (Acrylamide 40%) purification.

NMR Measurements

We measured the NMR spectra of the 2AP, 2AP-dn, and 2AP-rb at 20 °C with solvent suppression on a 400 MHz Bruker spectrometer. For initial proton chemical shift and coupling constants assignments, the 2AP free base and its mononucleosides were dissolved in deuterated water (D_2O) with sodium phosphate as the buffer to maintain a pD of 7.2. For the two-dimensional NMR (phase-sensitive correlated spectroscopy, or COSY, and nuclear Overhauser-effect spectroscopy or NOESY modes) spectra of the free base and mononucleosides, the solvent was degassed DMSO- d_6 (deuterated). Solution concentrations in all cases were approximately 30 mM. The parts per million (ppm) scale was referenced with DSS as the primary reference, and HDO (4.8 ppm) or DMSO (2.5 ppm) as a secondary reference.

Time-Resolved Measurements

For the 2AP, 2AP-dn and 2AP-rb, we used dimethyl sulfoxide (DMSO: reagent grade or better, Fisher Cert. ACS) and distilled, deionized water as the solvents. Solutions were made to 169 μ M stock concentrations and diluted to approximately 16.9 μ M for time-resolved measurements. We used distilled, de-ionized water for the solvent of the oligonucleotides. For the short oligonucleotides, a buffer consisting of 20 mM Tris-base, 0.1 M KCl, and 0.1 mM EDTA was used.

We checked concentrations of the oligonucleotides by measuring their absorption spectra on a Gilford Response II spectrophotometer with a 1 nm bandwidth. Data was stored digitally and transferred to a PC for analysis. We measured the time-resolved fluorescence on a PRA-2000 time-resolved photon counting system over a temperature range of 4–42 °C (Lakowicz, 1991). The temperature was controlled by a Brinkmann RM6 circulator. The time-resolved system was synchronously driven by a Spectra Physics series argon-pumped, CW mode-locked, cavity-dumped dye laser, which had the frequency doubled to UV light ($\lambda = 304$ nm). Response time was 300 ps full-width-half-maximum (FWHM). The fluorescence excitation was vertically polarized and collected by WG 320 and metal filters. Each data set collected had 2048 channels of data.

Fluorescence data were fit to sums of exponentials that were convoluted by a nonlinear least squares fitting program (Marquardt, 1963). The goodness of fit for each decay curve was determined by the reduced χ^2 value approaching 2 or less, the randomness of the weighted residuals and their autocorrelation functions about zero, and the Durbin-Watson (DW) parameter, which examines the correlation between the residual values in neighboring channels (for single-exponential, $DW \geq 1.65$; for double-exponentials, $DW \geq 1.75$; for triple exponentials, $DW \geq 1.85$) (Lampert *et al.*, 1983). The reduced χ^2 values were determined by

$$\chi^2 = \frac{1}{N - P} \sum_{i=1}^N \frac{(O_i - C_i)^2}{O_i} \quad (1)$$

where N is the number of observed (O_i) and calculated (C_i) data points (= 2048), and P is the number of parameters in the model. The weighted residuals and Durbin-Watson parameter were calculated as

$$WR_i = \frac{O_i - C_i}{O_i} \text{ and } DW = \frac{\sum_{i=1}^{n_1} (WR_i - WR_{i-1})^2}{\sum_{i=1}^{n_2} (WR_i)^2} \quad (2 \text{ and } 3)$$

respectively, where n_1 and n_2 are the first and last data points, respectively. However, we found the DW parameter less sensitive to the number of exponentials than the reduced χ^2 , weighted residuals, and autocorrelation.

RESULTS

Nuclear Magnetic Resonance Studies

One-dimensional ^1H spectra for 2AP, 2AP-rb, and 2AP-dn were straightforward and simple, as was expected (Figure 2). From this, the chemical shifts for each proton were assigned (Table 1) and compared to their adenine counterparts. Table 1 indicates the expected difference between adenine and 2AP, where the H6 assignment of adenine is replaced by the H2 of 2AP (as Figure 3 shows), whereas the proton assignments for the sugar ring are the same. Once the chemical shift assignments for 2AP-dn and 2AP-rb were confirmed by their 2D-COSY spectra (Figure 4 and 5) through the geminal and vicinal (two- and three-bond) coupling of protons, the coupling constants were determined (Table 2).

If multiple conformations of a nucleoside exist in solution, there should be through-space coupling between the H8 and H1' protons for the *syn* conformation, and between H8 and H2' for *anti* conformations (Patel *et al.*, 1982). Therefore, we measured 2D-NOESY spectrum of 2AP-dn (Figure 6), which confirmed the existence of both *syn*

Table 1. Chemical shift of the protons in 2AP, 2AP-rb, and 2AP-dn compared to those of 5'-AMP and 5'-dAMP.

	H-2	H-6	H-8	H-1'	H-2'	H-2''	H-3'	H-4'	H-5'	H-5''
2AP		8.54	8.13							
^a 2AP-rb		8.57	8.24	5.97	4.36		4.43	4.24	3.90	3.82
2AP-dn		8.54	8.22	6.36	2.83	2.51	4.64	4.14	3.82	3.76
^b 5'-AMP	8.12		8.35	6.00	4.61		4.36	4.25	4.00	3.98
^b 5'-dAMP	8.12		8.50	6.43	2.81	2.53	4.73	4.26	3.95	3.95

^a H-2' chemical shift determined from 1D-NMR spectrum in DMSO-d₆.

^b Chemical shifts taken from Davies and Danyluk (1974).

and *anti* conformations in solution (H8 at 8.22 ppm, H1' at 6.36 ppm, and H2' at 2.83 ppm; see Table 1).

Time-Resolved Fluorescence

With the *syn* and *anti* conformations of 2AP-dn established, we next wanted to discover whether if each conformation had its own distinct fluorescence lifetime. Time-resolved fluorescence decay curves for 2AP and 2AP-dn in water and DMSO were measured over a temperature range of 4–42 °C. 2AP showed a temperature-dependent, single-exponential fluorescence lifetime that gradually decreased from 11.9 ns to 11.4 ns in water, and from 5.2 to 4.2 ns in DMSO as the temperature was raised from 4 °C to 42 °C. Table 3 illustrates the single-exponential and reduced chi-squared values for the lifetimes.

Table 2. Geminal and vicinal coupling constants of protons in 2AP-dh and 2AP-rb compared to those of 5'-AMP and 5'-dAMP.

	$J(1',2')$	$J(1',2'')$	$J(2',3')$	$J(2'',3')$	$J(3',4')$	$J(4',5')$	$J(4',5'')$	$J(5',5'')$
2AP-rb	5.9		5.2		3.8	3.0	4.0	-12.8
2AP-dh	7.4	6.4	6.3	3.5		3.5	4.6	-12.5
"5'-AMP	5.8		5.1		3.7	4.8	5.3	-11.8
"5'-dAMP	7.3	6.2	6.1	3.4	3.0	3.7	3.7	

" Coupling constants taken from Davies and Danyluk (1974).

Figures 7 and 8 show the decay curves of 2AP-dn in water and DMSO, respectively, at 22 °C. Upon first glance, it would appear that two exponential functions would describe the fluorescence decay for 2AP-dn in water. However, the lifetimes are close enough to each other that a single exponential function may suffice to describe the decay curves. Tables 4 and 5 show the single- and double-exponential and reduced χ^2 values for the lifetime fits to the decay curves of 2AP-dn in water and DMSO, respectively. It is clear from comparing the parametric values of the two exponential fits that there is no significant difference between them. This would mean that a single-exponential function may describe the fluorescence just as well. Therefore, a double-exponential one is not justified.

With no clear fluorescence decay evidence of the conformations of 2AP-dn, we next wanted to see what a neighboring base would do to the fluorescence lifetime of 2AP-dn (in particular the immediate bases surrounding 2AP in GA[2AP]TTC). Thus, the short oligonucleotides 2AP-T and A-2AP-T were synthesized, and their fluorescence decays were measured. At the same time, others (Ujvari & Martin, 1996, Xu, 1996) have reported that the most anomalous effect on the fluorescence of 2AP occurs when G is one of the adjacent bases. Therefore, we included G-2AP-C and C-2AP-G to see what effect guanine has on the fluorescent lifetime of 2AP.

The fluorescence decay of these nucleotides is complex over the temperature range 4-42 °C, as Figures 9-12 (2ap-T), 13-16 (A-2ap-T), 17-20 (G-2ap-C), and 21-24 (C-2ap-G) show for four of these temperatures. Table 6 and 7 show the multi-exponential components for 2AP-dn with the attachment of another nucleotide in all cases.

Table 3. Illustration of the corresponding reduced chi-squared values for the single-exponential lifetimes of 2AP in water and DMSO.

T (°C)	lifetimes (ns)		reduced χ^2	
	<i>in water</i>	<i>in DMSO</i>	<i>in water</i>	<i>in DMSO</i>
4	11.89	5.25	1.28	1.93
6	11.90	5.47	1.34	1.22
8	11.83	5.44	1.55	2.22
10	11.79	5.36	1.16	1.46
14	11.73	5.21	1.16	3.45
18	11.70	5.04	1.32	1.62
22	11.60	5.00	1.16	1.67
26	11.58	4.68	1.31	1.80
30	11.51	4.47	1.15	1.75
34	11.47	4.43	1.25	1.91
38	11.42	4.36	1.12	1.77
42	11.38	4.24	1.38	1.67

Examination of the lifetime and amplitude components in tables 6 and 7 shows that the components are temperature dependent. In particular, Figure 25a clearly shows that the longest lifetime of 2AP-T is quite similar to that of free 2AP-dn (~11 ns), which agrees with others' finding that 2AP at the end of a strand of DNA acts similar to free 2AP (Ward, 1969). At the same time, Figure 25b shows that the middle amplitude component for 2AP-T dominates the fluorescence. Figure 26 shows that the lifetime for 2AP becomes more temperature-dependent in A-2AP-T with a decay time ≈ 7 ns; its amplitude component is the smallest and the amplitude component of the shortest

Table 4. Single- and double-exponential lifetimes and reduced χ^2 for 2AP-dn in water.

T (°C)	lifetime (ns)		reduced χ^2	
	single	double	single	double
4	11.83	11.32	1.31	1.16
		8.42		
6	10.57	11.83	1.22	1.28
		^a		
8	10.54	11.09	1.26	1.12
		8.61		
10	10.52	10.71	1.30	1.14
		7.32		
14	10.44	10.71	1.08	1.01
		8.27		
18	10.39	12.64	1.19	1.14
		9.91		
22	10.33	11.34	1.19	1.17
		9.75		
26	10.30	10.30	1.23	1.15
		^a		
30	10.18	10.57	1.47	1.47
		9.67		
34	10.09	10.88	1.98	1.29
		9.53		
38	10.00	10.85	1.64	1.55
		9.60		
42	9.93	10.65	1.14	1.13
		9.34		

^a Fitting program found only a single exponential.

Table 5. Single- and double-exponential lifetimes and reduced χ^2 for 2AP-dn in DMSO.

T (°C)	lifetime (ns)		reduced χ^2	
	single	double	single	double
4	5.46	5.52	1.06	1.68
		5.53		
6	5.52	6.09	1.15	1.29
		5.36		
8	5.54	5.54	1.09	1.44
		5.56		
10	5.49	5.90	1.17	1.17
		5.42		
14	5.34	6.40	1.03	1.05
		5.06		
18	5.14	5.19	1.32	1.10
		0.79		
22	5.01	5.58	1.27	1.13
		4.75		
26	4.67	4.72	1.448	1.27
		0.34		
30	4.56	4.58	1.43	1.36
		0.22		
34	4.48	4.54	1.27	1.16
		1.57		
38	4.13	4.18	1.65	1.44
		1.00		
42	4.09	4.18	1.50	1.21
		1.61		

Table 6. Fluorescence decay parameters of 2AP-T and A-2AP-T oligonucleotides.

T(°C)	2AP-T			A-2AP-T		
	lifetimes (ns)	amplitudes	reduced χ^2	lifetimes (ns)	amplitudes	reduced χ^2
4	11.05	0.11	1.11	7.04	0.11	1.16
	3.18	0.55		2.41	0.16	
	0.57	0.34		0.52	0.73	
6	11.05	0.10	1.04	7.42	0.10	1.13
	3.19	0.59		2.66	0.17	
	0.63	0.31		0.53	0.73	
8	10.87	0.10	1.07	7.04	0.12	1.21
	2.99	0.59		2.41	0.17	
	0.53	0.31		0.52	0.71	
10	10.97	0.09	1.00	6.77	0.11	1.18
	2.94	0.53		2.22	0.19	
	0.47	0.38		0.48	0.70	
12	10.36	0.09	1.28	6.96	0.11	1.29
	2.56	0.54		2.57	0.19	
	0.33	0.37		0.55	0.70	
18	10.46	0.11	1.03	6.86	0.09	1.21
	2.54	0.67		2.78	0.20	
	0.59	0.22		0.51	0.71	
22	10.96	0.10	1.03	6.10	0.12	1.08
	2.51	0.67		2.06	0.20	
	0.60	0.23		0.45	0.68	
26	10.96	0.08	1.11	6.23	0.10	1.07
	2.51	0.58		2.50	0.21	
	0.06	0.34		0.53	0.69	

Table 6. (continued)

T(°C)	2AP-T			A-2AP-T		
	lifetimes (ns)	amplitudes	reduced χ^2	lifetimes (ns)	amplitudes	reduced χ^2
30	10.36	0.08	1.10	5.48	0.10	1.13
	2.11	0.62		1.98	0.20	
	0.33	0.30		0.40	0.70	
34	10.66	0.09	1.01	5.77	0.09	1.18
	2.14	0.69		2.44	0.23	
	0.59	0.22		0.52	0.68	
38	10.48	0.07	1.34	5.78	0.06	1.09
	1.97	0.56		2.29	0.21	
	0.33	0.37		0.40	0.73	
42	10.34	0.08	0.99	5.46	0.08	1.20
	1.94	0.61		2.18	0.27	
	0.49	0.31		0.43	0.66	

lifetime being dominate. For 2AP in G-2AP-C, the longest lifetime component is about 6 ns with its corresponding amplitude component being the smallest: the corresponding amplitude for the shortest lifetime is dominant (Figure 28). In this case, it appears that the dominate lifetime and amplitude have the anomalous affect of increasing with increasing temperature (provided we ignore the data point at 38 °C because of its unusually high reduced χ^2 ; see Table 7). In C-2AP-G, the fluorescence decay components of 2AP become what seems only slightly temperature dependent, again with the corresponding amplitude to the shortest lifetime being dominant (Figure 28).

Table 7. Fluorescence decay parameters of G-2AP-C and C-2AP-G oligonucleotides.

T(°C)	G-2AP-C			C-2AP-G		
	lifetimes (ns)	amplitudes	reduced χ^2	lifetimes (ns)	amplitudes	reduced χ^2
4	6.52	0.14	1.29	8.69	0.09	1.20
	2.25	0.25		2.49	0.19	
	0.33	0.61		0.26	0.72	
6	7.26	0.09	1.16	9.35	0.06	1.26
	2.87	0.21		2.93	0.14	
	0.43	0.70		0.34	0.80	
8	7.92	0.07	1.48	10.10	0.06	1.33
	3.15	0.22		3.32	0.17	
	0.45	0.71		0.40	0.77	
10	7.36	0.08	1.64	9.74	0.06	1.35
	2.99	0.23		3.15	0.15	
	0.43	0.69		0.37	0.79	
12	7.79	0.06	1.85	9.14	0.07	1.36
	3.00	0.24		2.89	0.16	
	0.42	0.70		0.36	0.77	
14	7.75	0.06	1.30	9.35	0.05	1.05
	3.02	0.21		2.83	0.15	
	0.43	0.73		0.33	0.80	
18	8.35	0.05	1.88	9.20	0.06	1.20
	2.97	0.29		2.79	0.17	
	0.51	0.66		0.37	0.77	
22	7.19	0.03	1.13	9.64	0.04	1.16
	2.54	0.13		2.86	0.13	
	0.30	0.84		0.29	0.83	

Table 7. (continued)

T(°C)	G-2AP-C			C-2AP-G		
	lifetimes (ns)	amplitudes	reduced χ^2	lifetimes (ns)	amplitudes	reduced χ^2
26	8.47	0.03	1.26	9.41	0.04	1.09
	2.79	0.24		2.63	0.17	
	0.45	0.73		0.33	0.79	
30	8.12	0.03	1.27	9.55	0.04	1.25
	2.56	0.21		2.62	0.18	
	0.39	0.76		0.35	0.78	
34	9.34	0.02	1.24	9.28	0.03	1.15
	2.67	0.25		2.40	0.17	
	0.46	0.73		0.33	0.80	
38	6.73	0.02	2.44	9.39	0.04	1.11
	1.87	0.14		2.36	0.16	
	0.21	0.84		0.32	0.80	

Because each set of components for the fluorescence decay of 2AP represents distinct states in which 2AP exists and shows temperature dependence, we can describe the equilibrium between these states by the free energy equation:

$$K_{j,i} \equiv \frac{N_j}{N_i} = \exp\left(\frac{-\Delta G_{j,i}}{RT}\right), \quad (4)$$

where $K_{j,i}$ is the equilibrium constant between states j and i , N_j and N_i are the measurable quantities that represent each state, $\Delta G_{j,i}$ is the Gibbs free energy between the two states, R is the gas constant, and T is Kelvin temperature. If $K_{j,i}$ can be measured as a function of

temperature, then the enthalpy between states can be calculated by a van't Hoff analysis (Cantor & Schimmel, 1980), which is defined by

$$\Delta H = -R \frac{\partial(\ln K)}{\partial(T^{-1})} \quad (5)$$

which says that the enthalpy between states is determined by the changes in the natural logarithm of the equilibrium constant and the inverse of temperature. From the linearity of the *natural logarithm of K* versus T^{-1} , we can calculate ΔH for the states of 2AP in each oligonucleotide. Figure 29 shows that $\Delta H_{21} = 1.8 \pm 0.3$ kcal/mole, $\Delta H_{32} = -1.2 \pm 2.6$ kcal/mole, and $\Delta H_{31} = 0.6 \pm 2.6$ kcal/mole for 2AP-T, and $\Delta H_{21} = 3.7 \pm 1.0$ kcal/mole, $\Delta H_{32} = -1.8 \pm 0.8$ kcal/mole, and $\Delta H_{31} = 1.8 \pm 1.3$ kcal/mole for A-2AP-T. From Figure 30, we found for G-2AP-C and C-2AP-G that $\Delta H_{21} = 7.8 \pm 2.6$ and 4.3 ± 0.5 kcal/mole, respectively; and, $\Delta H_{32} = 2.1 \pm 2.1$ and 0.8 ± 2.1 kcal/mole, respectively; and, $\Delta H_{31} = 9.8 \pm 2.4$ and 5.1 ± 2.5 kcal/mole, respectively.

DISCUSSION

2AP Free Base

Over a temperature range of 4–42 °C 2AP had a single exponential fluorescent decay in water and DMSO, where DMSO clearly quenched the fluorescence of 2AP, as the lifetime goes from 11.9 ns (in water) to 5.8 ns (in DMSO). 2AP-dn followed this same trend: its single-exponential lifetime went from 11.8 ns in water to 5.5 ns in DMSO. It appears that a distinctive second lifetime is detectable around the freezing (and melting) point of DMSO (18 °C), which could be explained if frozen DMSO isolated 2AP-dn in one conformation, and the second one is detectable at the melting of

DMSO. However, careful examination of the weighted residuals and autocorrelation showed no significant difference between the single- and double-exponential fits. Therefore, a second lifetime component was not justified (Lakowicz, 1991). This, on the other hand, did not complement the NOESY NMR measurements that clearly showed the *syn* and *anti* conformations of 2AP-dn in DMSO (Figure 4).

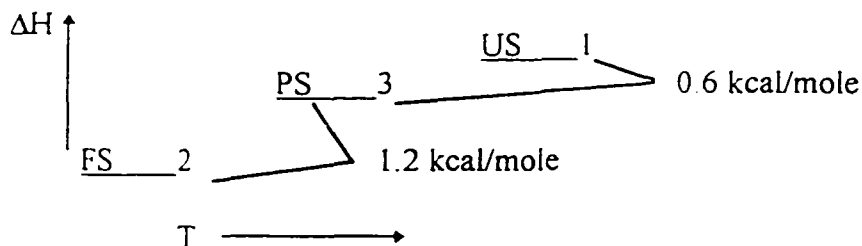
With the attachment of an adjacent base in the 3'-position (underlined) of 2AP-dn (2AP-T), the fluorescence went from one lifetime component to three, indicating three distinctive states of 2AP-dn. This was even the case when a second base (underlined) was attached in the 5'-position (A-2AP-T, G-2AP-C, or C-2AP-G). Presently, there is no evidence (spectroscopic or structural) of three conformations of mononucleosides, only two (Brahms *et al.*, 1992; Cho & Evans, 1991; Gramlich *et al.*, 1978; Guschlbauer, 1980; Plavec *et al.*, 1993; Stolarski *et al.*, 1980). Therefore, the *syn* and *anti* conformations do not adequately explain the three states clearly indicated by the fluorescence lifetimes. Thus, we presumed that stacking between neighboring bases was to be the dominant factor for the fluorescence quenching, and we classified the three states these lifetime components represent as the unstacked (US), partially stacked (PS), and fully stacked (FS) orientations that nucleotide strands (Allan & Reich, 1996; Cantor & Schimmel, 1980; Stryer, 1988) (in particular, 2AP) (Nordlund *et al.*, 1989; Wu *et al.*, 1990) can obtain.

2AP-T Dinucleotide

When thymine was attached to 2AP in the 3'-position, the fluorescence lifetime became a triple-exponential function, with the longest lifetime (11.0 ns) near that of 2AP

free base (11.9 ns). Therefore, we associated this lifetime component with the unstacked 2AP-dn. The 1.0 ns decrease in the fluorescence lifetime of 2AP-dn suggests that quenching is due to weak stacking interactions between 2AP-dn and thymine. This agrees with the conclusion that thymine and 2AP stack weakly (Xu, 1996).

Examination of the Van't Hoff plot of the states 1, 2, and 3 from Figure 29a (2AP-T) showed that the enthalpy differences are in the following order, $\Delta H_1 > \Delta H_3 > \Delta H_2$. This gave the following arrangement of the excited states (Diagram 1):

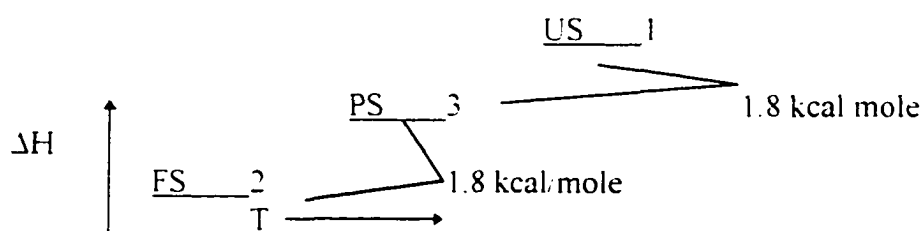


where the ordering is lowest enthalpy state to the highest bottom to top, with increasing temperature left to right. Because stacking interactions are most favorable at lowest temperature, we assigned ΔH_2 , in this case, as the FS-state of 2AP-dn; ΔH_3 is PS and ΔH_1 is the US. The ΔH between stacked and unstacked also suggests that stacking interactions between 2AP and thymine are weak. However, review of the populations of each state represented by the amplitude components did not show the expected increase in the US-state population with temperature. A possible explanation is that the transition from the FS- to PS-state is the primary transition. In other words, no matter how weak of a stacking interaction, 2AP-dn prefers to be stacked with its neighboring base (probably due mostly to the fact that this is an extremely short strand with high degree of flexibility for stacking). Other than that, there is no clear explanation of the lack of temperature-dependence of the amplitudes.

A-2AP-T Trinucleoside

With the addition of adenine as the 5'-neighboring base of 2AP, the fluorescence lifetime remained a triple exponential. However, the longest lived state lifetime decreased to 7.4 ns. This indicated a stronger stacking interaction between 2AP-dn and adenine, which too agrees with previous measurements (Xu, 1996). A second explanation would be that two neighboring bases (5'- and 3'-positions) together significantly quench the fluorescence of 2AP-dn. However, examination of the fluorescence lifetime of the other trinucleotide samples showed a lesser effect on the lifetimes. This seems to further emphasize that the A-2AP stacking interactions are stronger.

The Van't Hoff plot of Figure 29a showed the same enthalpy ordering as for 2AP-T. $\Delta H_1 > \Delta H_3 > \Delta H_2$. The difference being that the ΔH 's between the FS, PS, and US states are larger. The arrangement of enthalpies are as follow (Diagram 2):

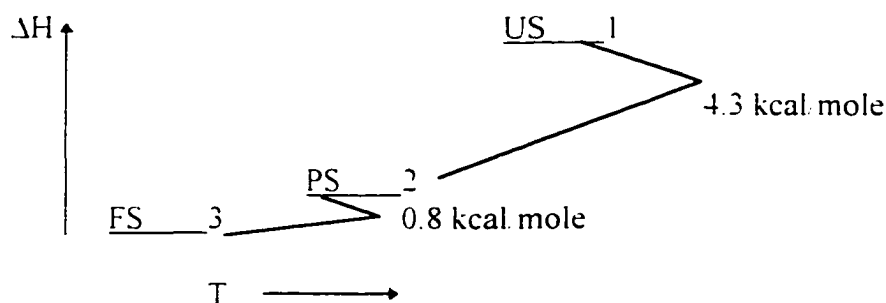


where the spacing between enthalpies are about equal. Again, the lowest enthalpy state was assigned to the fully stacked state. With A-2AP-T, a clearer temperature dependence of populations was exhibited by the amplitudes, with the PS state dominating. This may be explained by (1) the strong stacking interaction between adenine and 2AP, coupled with (2) the added presence of a second neighboring base. This combination may reduce

the freedom of 2AP to be unstacked, and increasing its chances of being stacked, fully or partially. Thus, an FS to PS transition would dominate.

C-2AP-G Trinucleotide

Once the 5'-and 3'-neighboring bases of 2AP-dn became cytosine and guanine, respectively, the lifetimes continued to be triple exponential. However, the longest lifetime was 10.1 ns. This implies that stacking between 2AP-dn, cytosine, and guanine is not as strong as when adenine and thymine are placed in those positions. The temperature dependence of the fluorescence decay parameters (lifetimes and amplitude) is the least of all samples. However, the ratio of the amplitude populations gave the following order of enthalpies between US, PS, and FS: $\Delta H_1 > \Delta H_2 > \Delta H_3$. This is illustrated by the following diagram of states (Diagram 3):

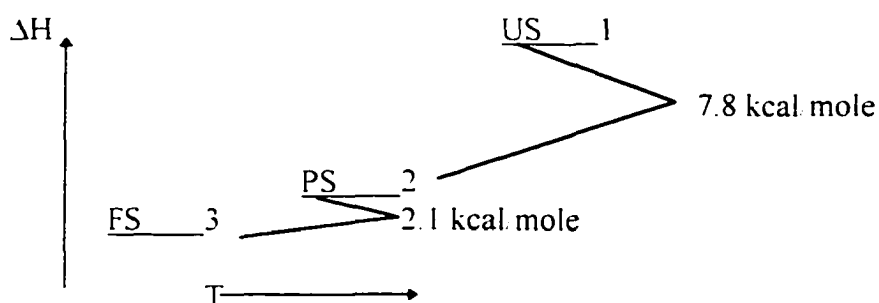


where the FS state is now identified by the third lifetime component, and PS state with the second. Also, with C-2AP-G, the transition from FS to PS states dominates in population. Although the stacking interactions of 2AP with cytosine and guanine were not as significant at quenching the lifetime of 2AP as adenine and thymine were, the dominance of the FS-to-PS transition could be simply explained by the continuous

movement of **all** bases. This alone would increase the possibility of stacking (fully and partially) interactions, be it between 2AP and one or both neighboring bases.

G-2AP-C Trinucleotide

The longest lifetime in this instance was 9.3 ns, which indicates stronger stacking than the previous case where guanine and cytosine were in the 3'- and 5'-positions, respectively; however, it was not as significant as that of A-2AP-T. The enthalpy differences are ordered also as those of C-2AP-G, as the diagram below shows (diagram 4):



where the FS and PS states dominate. In this case, the enthalpy difference between FS and US was almost 10 kcal/mole, twice that for C-2AP-G (≈ 5 kcal/mole). This anomaly seems to fit with the fact that the fluorescence of 2AP is anomalous (excitation wavelength shifts to approximately 301 nm) when guanine is next to it (Ujvari & Martin, 1996; Xu, 1996). Hydrogen bonding between water and 2AP is what causes the fluorescence excitation to shift to approximately 305 nm (Evans *et al.*, 1992). Keeping with this idea, it is possible that 2AP H-bonds to the O6 of guanine (Figure 31) to cause such anomalous effects on the fluorescence of 2AP. Although this H-bonding appears to possibly occur when guanine and cytosine positions are reversed ($5' \rightarrow 3'$, respectively) as

well, guanine in the 5'-position appears to be more influential on the change in enthalpies.

In addition, energy transfer has been established from adjacent bases to 2AP (Xu, 1996). And although this energy transfer is clearly to 2AP, it is reasonable to assume that energy can be transferred from 2AP to adjacent bases in a similar manner. This energy transfer from 2AP can reduce its fluorescence lifetime of a fluorophore. Therefore, a comparison of the average lifetime of 2AP in the samples to the energy transfer to 2AP would provide a hint of this energy transfer. However, such comparison illustrated no conclusive correlation (Table 8). On the other hand, the comparison did clearly show that fluorescence was quenched, more as the neighborhood environment increased around 2AP, but, no clear evidence of base dependency. However, Figure 32 does show that the same temperature dependence that governs energy transfer governs the change in fluorescence lifetime of 2AP, namely, stacking interactions.

Finally, enthalpy differences for the states of stacking interactions are additive such that ΔH of FS added to that of PS is equivalent to the ΔH of US (in all cases). This is an ideal condition between the states. However, the calculated errors for some of the enthalpy differences would preclude this condition. But examination of the following conditions suggests that this additive nature of the stacking states is not a mere coincidence. First, the parameters (amplitudes) that are plotted to calculate the differences in enthalpy were subject to a stringent statistical fitting criteria (reduced χ^2 is less than 2; weighted residuals and autocorrelations both were random about zero and less 0.14) that provides assurance that no more parameters were used than necessary. Second, these parameters were found well within error (usually $\leq 1\%$). These two facts

Table 8. Comparison of average fluorescence lifetime of 2AP and the energy transfer from nearest neighboring base to 2AP.

sample	average lifetime $\Sigma\alpha_i\tau_i$	relative yield %	energy transfer efficiency ^b	
			5'-base	3'-base
2ap	11.892	1.00	na	na
2ap-dn	11.830	0.995	na	na
2ap-T	3.101	0.261	na	17.0
A-2ap-T	1.476	0.124	57.2	17.0
C-2ap-G	1.465	0.123	23.5	32.4
G-2ap-C	1.694	0.142	32.4	23.5

^a Sample temperature was approximately 4 °C.

^b Energy transfer efficiency was taken and calculated from previously measured data (Xu, 1996).

together suggest that the additive nature of the ΔH 's is not a coincidence, but a product of the fits. Therefore, the errors associated with these ΔH 's are a bit less significant.

CONCLUSIONS

We have been able to study 2AP as a free purine base, a mononucleoside (2AP-dn), and as a component of four short oligonucleotides (2AP-T, A-2AP-T, C-2AP-G, and G-2AP-C). As a mononucleoside, 2AP-dn was shown, through NMR measurements, to exist in the *syn* and *anti* conformations in solution (DMSO). However, time-resolved fluorescence was able to detect only one excited state. But, once attached to a second nucleic acid base, 2AP exhibited a triple-exponential fluorescence. We associated these three components to 2AP as being FS, PS, and US, and illustrated that the enthalpy

differences between these states are within the 1-10 kcal mole measured enthalpy differences for other stacked nucleotides (Baker *et al.*, 1978; Breslauer & Sturtevant, 1977; Lee & Tinoco., 1977; Petersheim & Turner, 1983; Powell *et al.*, 1972). This also clearly illustrates that it is a nearest neighbor that causes the fluorescence of 2AP to go from single- to multi-exponential (Table 8).

In terms of nearest neighbor effect, we have shown that adenine has the strongest quenching effect on the fluorescence of 2AP. When the nearest neighbors (5'- and 3'-) are cytosine and guanine, the quenching effect is position dependent. Cytosine and guanine in the 3'- and 5'-positions, respectively, have the greater effect, where the stacking enthalpy differences are greatest. Through simulated molecular structures, this may be explained by the -NH₂ of 2AP hydrogen bonding to the O6 of guanine. This could also explain the most anomalous fluorescence excitation of 2AP when guanine is a nearest neighbor (Ujvari & Martin, 1996, Xu, 1996). All in all, the fluorescence of 2AP continues to provide highly useful information about the local conformations of base.

REFERENCES

- Allan, B. W., & Reich, N. O. (1996) *Biochemistry* 35, 14757-14762.
- Baker, B. M., Vanderkooi, J., & Kallenbach, N. R. (1978) *Biopolymers* 17, 1361-1372.
- Ballini, J.-P., Daniels, M., & Vigny, P. (1988) *European Biophysical Journal* 16, 131-142.
- Beaucage, S. L., & Carthers, M. H. (1981) *Tetrahedron Letters* 22, 1859-1862.
- Bloom, L. B., Otto, M. R., Beechem, J. M., & Goodman, M. F. (1993) *Biochemistry* 32, 11247-11258.
- Brahms, S., Fritsch, V., Brahms, J. G., & Westhof, E. (1992) *J. Mol. Biol.* 223, 455-476.

- Breslauer, K. J., & Sturtevant, J. M. (1977) *Biophysical Chemistry* 7, 205-209.
- Cantor, C. R., & Schimmel, P. R. (1980) in *Biophysical Chemistry, part III: The Behavior of Biological Macromolecules*, pp. 1077-8, 1130-3, W.H. Freeman and Company, San Francisco.
- Chen, Y. Z., & Prohofsky, E. W. (1994) *Biophysical Journal* 66, 820-826.
- Cho, B. P., & Evans, F. E. (1991) *Biochemical and Biophysical Research Communications* 180, 273-278.
- Davies, D. B., & Danyluk, S. S. (1974) *Biochemistry* 13, 4417-4434.
- Evans, K., Xu, D.-G., Kim, Y.-S., & Nordlund, T. M. (1992) *Journal of Fluorescence* 2, 209-216.
- Georghiou, S., Nordlund, T. M., & Saim, A. M. (1985) *Photochemistry and Photobiology* 41, 209-212.
- Gramlich, V., Herbeck, R., Schlenker, P., & Schmid, E. D. (1978) *J. Raman Spectrosc.* 7, 101-105.
- Gueron, M., Kochoyan, M., & Leroy, J. L. (1986) in *Structure, Dynamics and Function of Biomolecules*, pp. 197-200, Springer-Verlag, Heidelberg.
- Guschlbauer, W. (1980) *Biochimica et Biophysica Acta* 610, 47-55.
- Jia, Y., Kumar, A., & Patel, S. S. (1996) *Journal of Biological Chemistry* 271, 30451-30458.
- Kahn, J. D., Yun, E., & Crothers, D. M. (1994) *Nature* 368, 163-166.
- Lakowicz, J. R. (1991) in *Topics in Fluorescence Spectroscopy, Volume 2: Principles*, pp 432, Plenum Press, New York.
- Lampert, R. A., Chewter, L. A., Phillips, D., O' Connor, D. V., Roberts, A. J., & Meech, S. R. (1983) *Analytical Chemistry* 55, 68-73.
- Lee, C.-H., & Jr., I. T. (1977) *Biochemistry* 16, 5403-5414.
- Marquardt, D. W. (1963) *Journal Society of India Applied Mathematics* 11, 431-441.
- Nordlund, T. M. (1988) *Proceedings of SPIE International Society of Optical Engineers* 909, 35-50.

- Nordlund, T. M., Andersson, S., Nilsson, L., Rigler, R., Graslund, A., & McLaughlin, L. W. (1989) *Biochemistry* 28, 9095-9103.
- Oraevsky, A. A., Sharkov, A. V., & Nikogosyan, D. N. (1981) *Chemical Physics Letters* 83, 276-280.
- Patel, D. J., Kozlowski, S. A., Nordheim, A., & Rich, A. (1982) *Biochemistry* 21, 1413-1417.
- Petersheim, M., & Turner, D. H. (1983) *Biochemistry* 22, 256-263.
- Plavec, J., Fabre-Buet, V., Uteza, V., Grouiller, A., & Chattopadhyaya, J. (1993) *Journal of Biochemical and Biophysical Methods* 26, 317-334.
- Powell, J. T., Richards, E. G., & Gratzer, W. B. (1972) *Biopolymers* 2, 235-250.
- Ramstein, J., & Lavery, R. (1988) *Proceedings of the National Academy of Science of the USA* 85, 7231-7235.
- Stolarski, R., Dudycz, L., & Shugar, D. (1980) *European Journal of Biochemistry* 108, 111-121.
- Stryer, L. (1988) in *Biochemistry*, 3rd ed., pp. 71-116, 649-686. W.H. Freeman and Company, New York.
- Tari, L. W., & Secco, A. S. (1995) *Nucleic Acid Research* 23, 2065-2073.
- Ujvari, A., & Martin, C. T. (1996) *Biochemistry* 35, 14574-14582.
- Ward, D.C., Reich, E., Stryer, L. (1969) *Journal of Biological Chemistry* 244, 1228-1235.
- Wu, P. G., Nordlund, T. M., Gildea, B., & McLaughlin, L. W. (1990) *Biochemistry* 29, 6508-6514.
- Xu, D., Evans, K. O., & Nordlund, T. M. (1994) *Biochemistry* 33, 9592-9599.
- Xu, D.-G. (1996) PhD dissertation in *Physics*, University of Alabama-Birmingham, Birmingham.

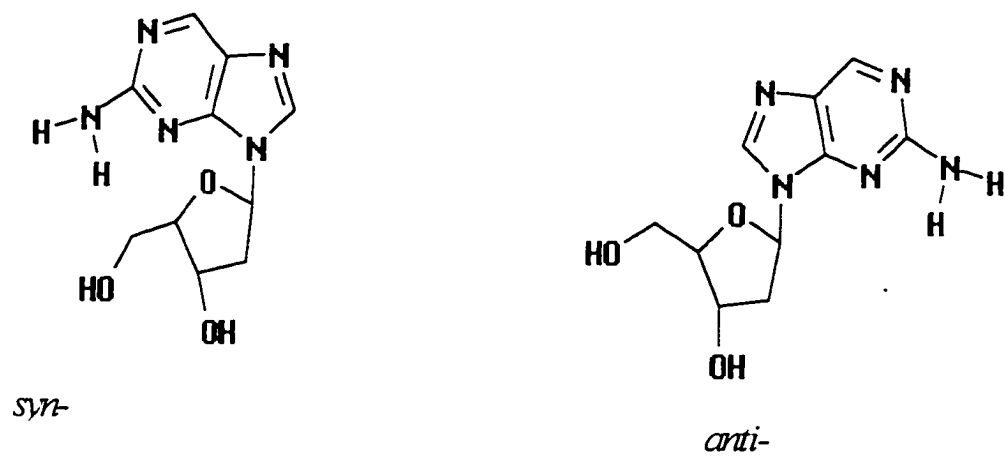


Figure 1: The structural difference between *syn-* and *anti-* conformations of 2AP-dn.

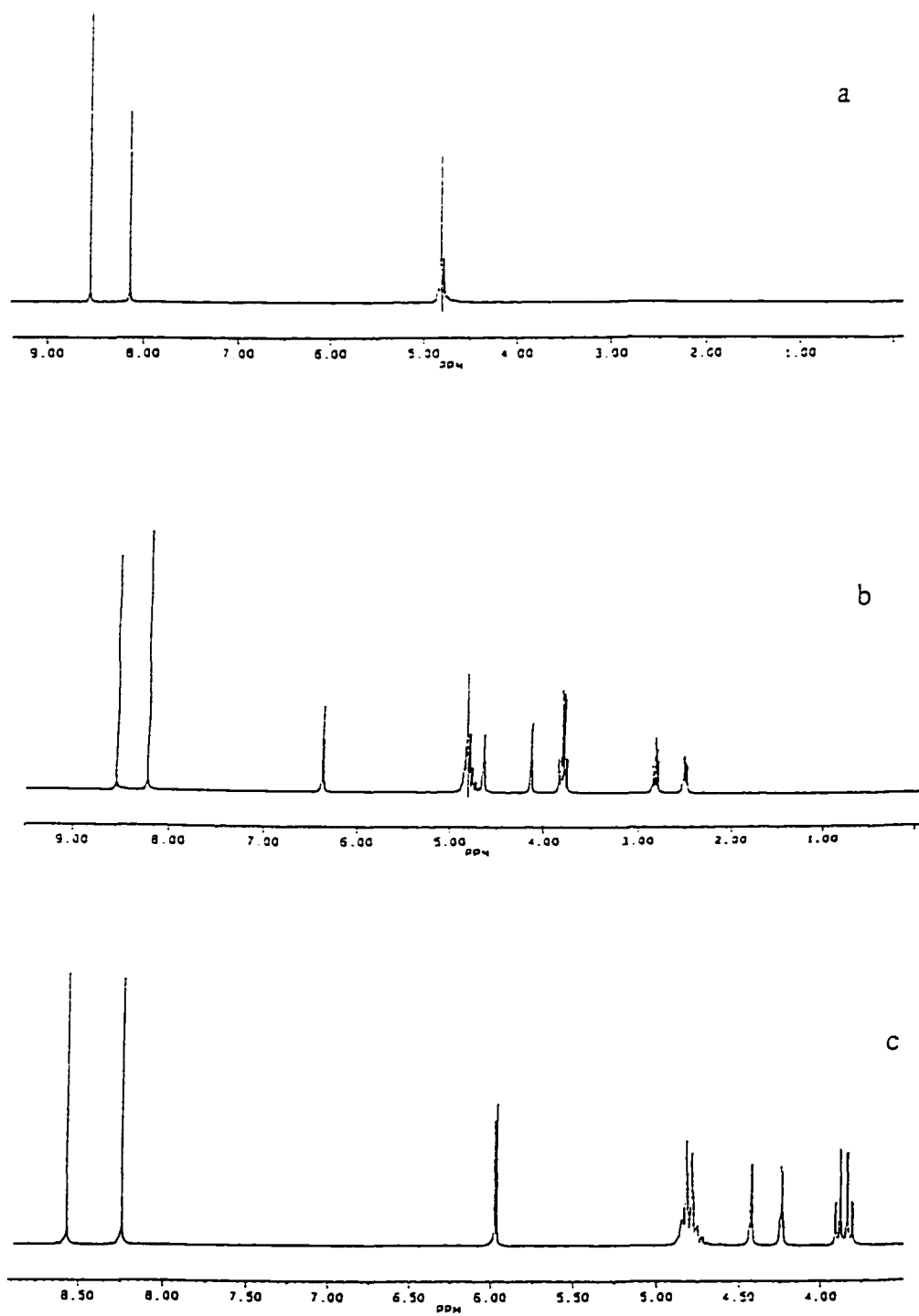


Figure 2: NMR spectra of (a) 2AP, (b) 2AP-dn, and (c) 2AP-rb in D₂O.

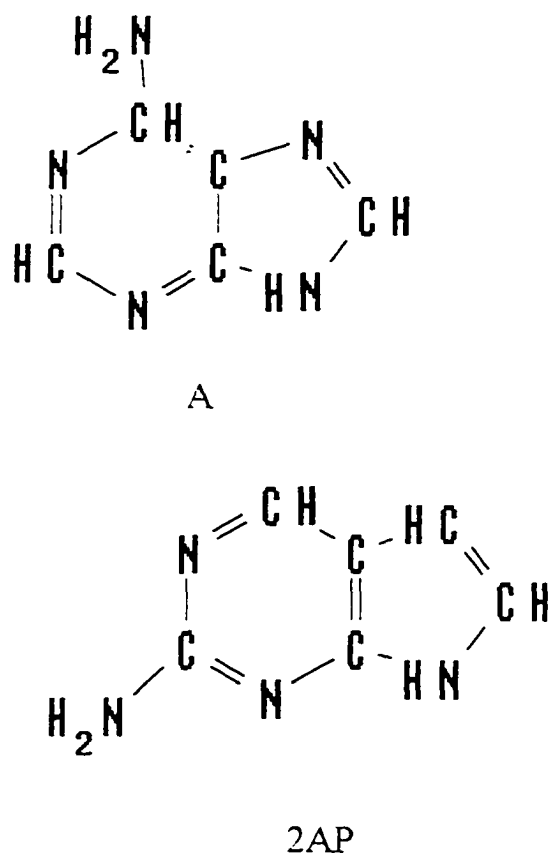


Figure 3: Structural differences between adenine, A, and its fluorescence analog, 2AP.

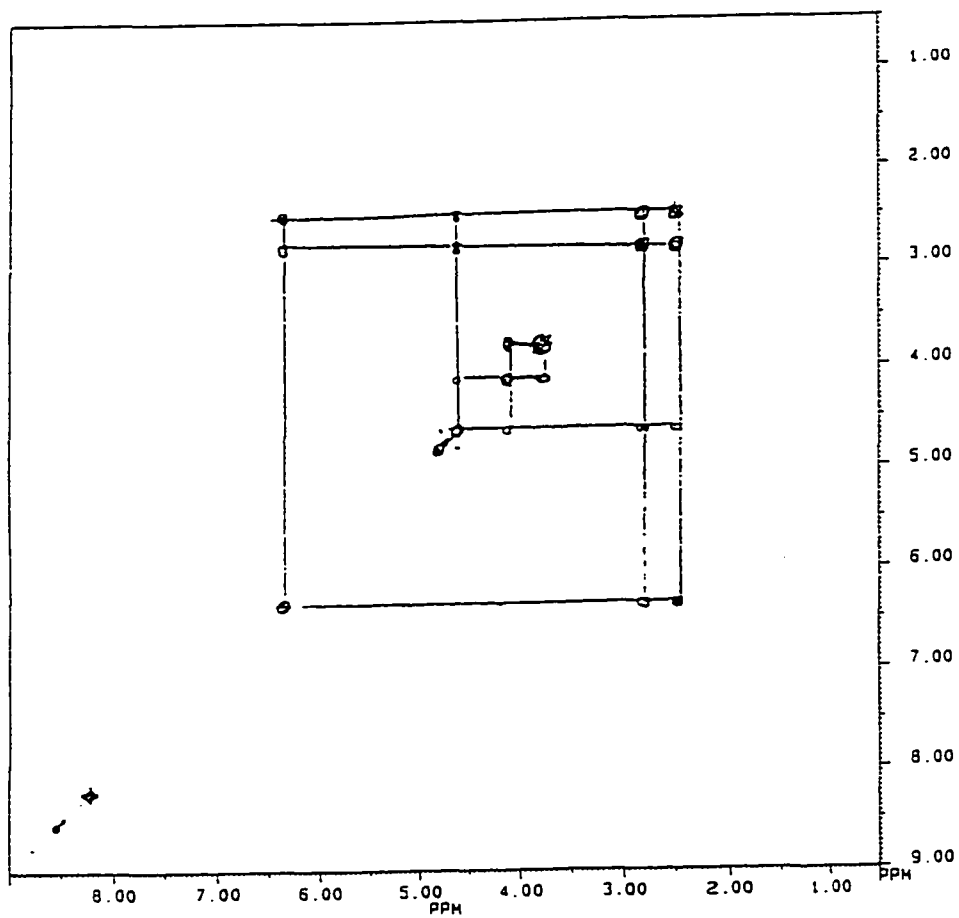


Figure 4: 2D-COSY spectrum of 2AP-dn at room temperature in D_2O .

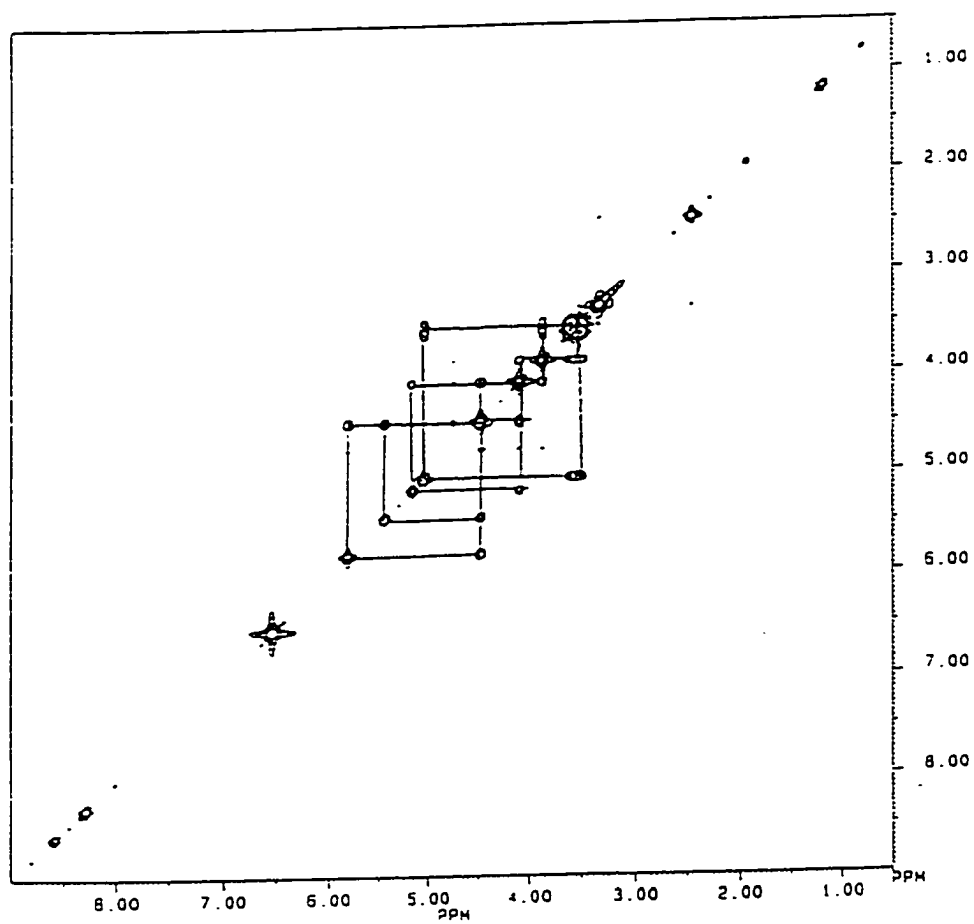


Figure 5: 2D-COSY spectrum of 2AP-rb at room temperature in DMSO-d₆.

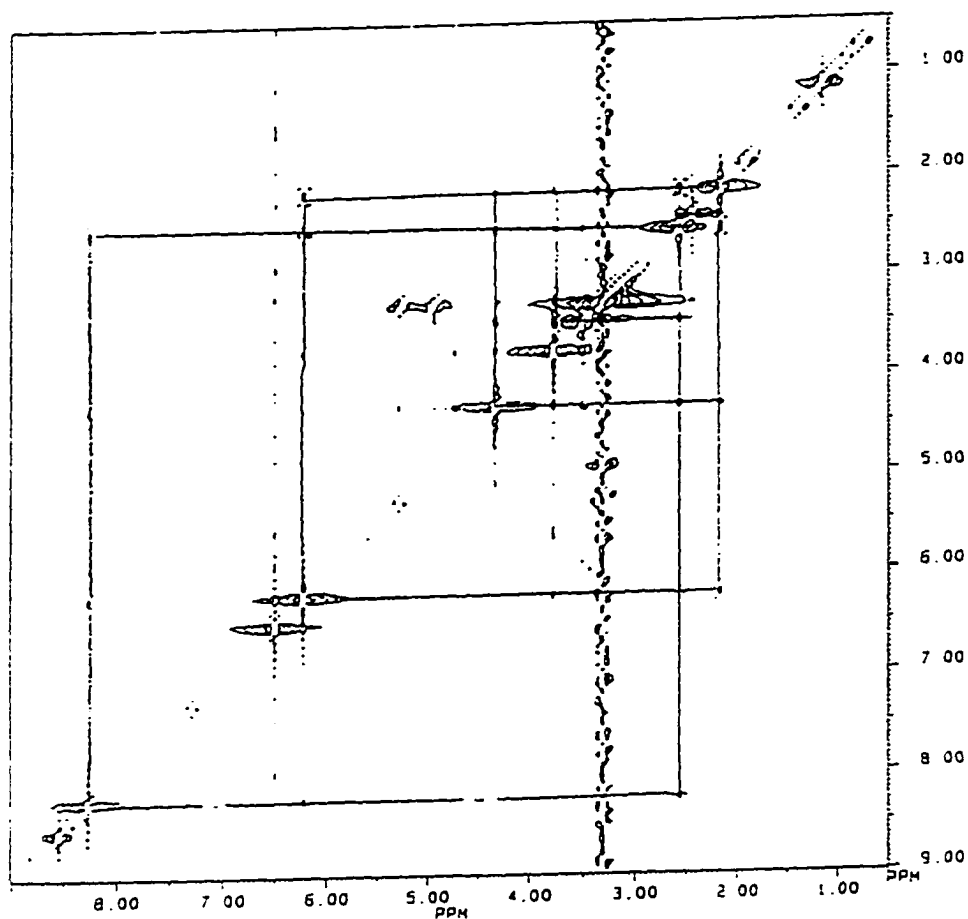


Figure 6: 2D-NOESY spectrum of 2AP-dn at room temperature in DMSO-d₆, 400 ms mixing time.

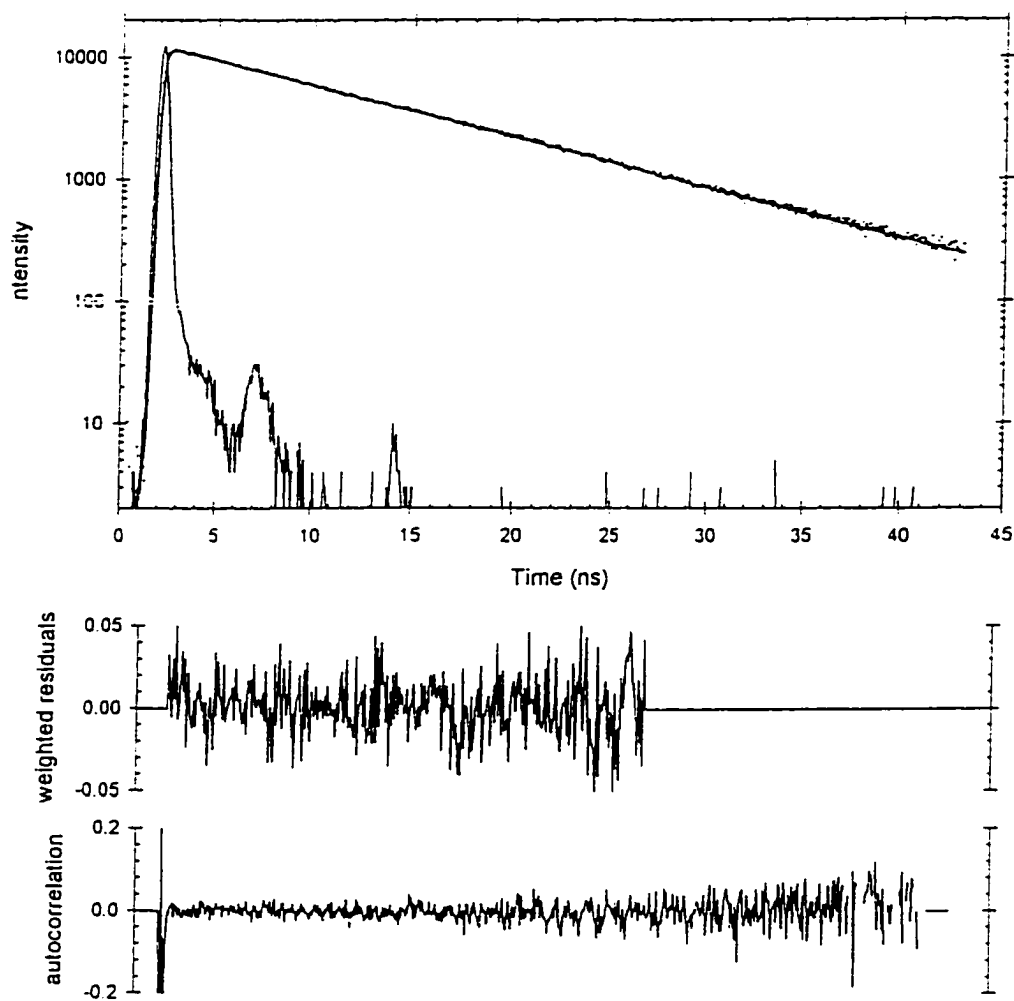


Figure 7: Fluorescence decay curve of 2AP-dn in water (upper) at 22 °C. The sharp-peaked curve is the excitation pulse at 304 nm, the scattered points are the decay data, and the straight line is the fit. The middle and lower plots are those of the autocorrelation and weighted residuals, respectively.

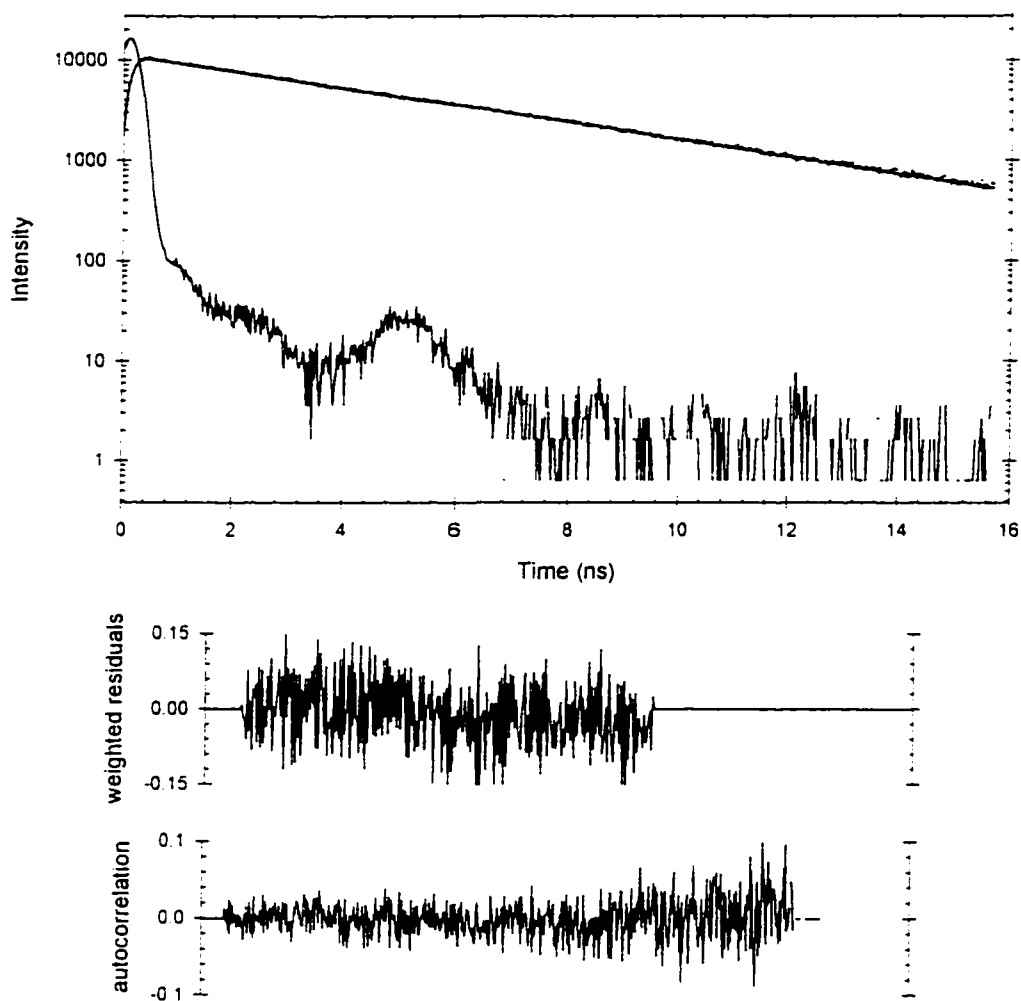


Figure 8: Fluorescence decay curve of 2AP-dn in DMSO (upper) at 22 °C. The sharp-peaked curve is the excitation pulse at 304 nm, the scattered points are the decay data, and the straight line is the single exponential fit. The middle and lower plots are those of the autocorrelation and weighted residuals, respectively.

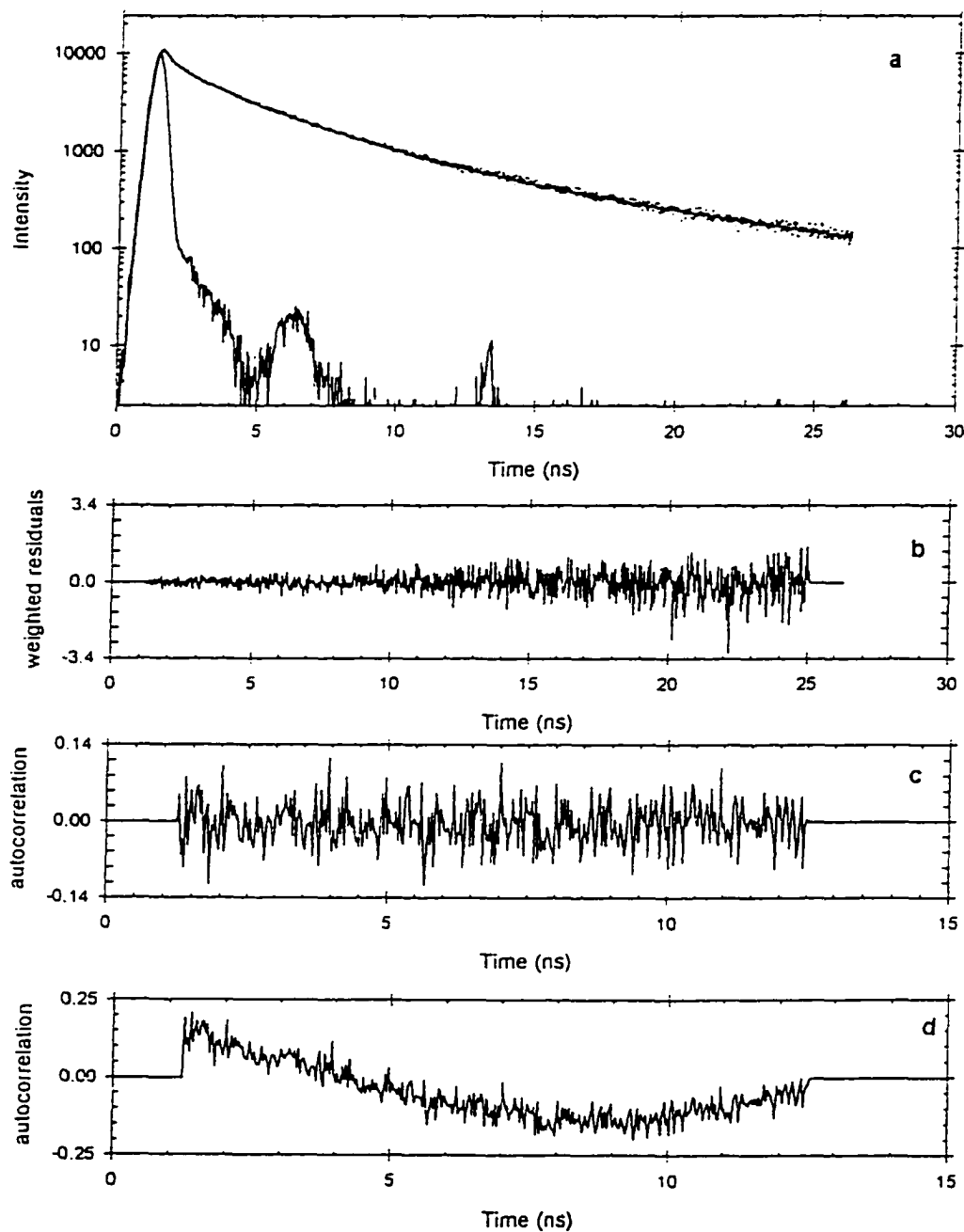


Figure 9: Fluorescence decay curve of 2AP-T (a) in water at 4 °C with (b) weighted residuals and (c) autocorrelation; (d) is the autocorrelation for a double-exponential fit. The sharp-peaked curve is the excitation pulse at 304 nm, the scattered points are the decay data, and the solid line is the three-exponential fit.

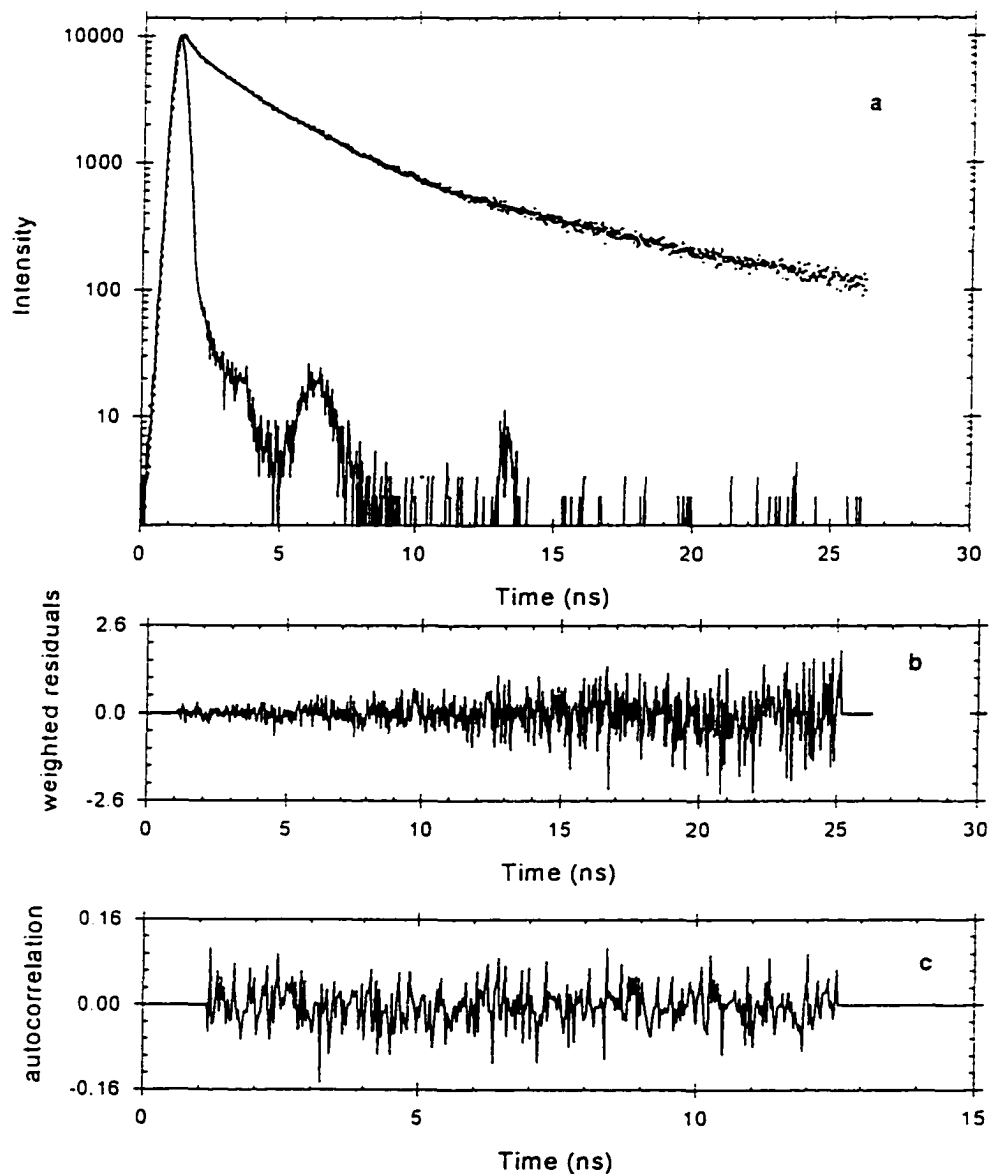


Figure 10. Fluorescence decay curve of 2AP-T (a) in water at 18 °C with (b) weighted residuals and (c) autocorrelation. The sharp-peaked curve is the excitation pulse at 304 nm, the scattered points are the decay data, and the solid line is the three-exponential fit.

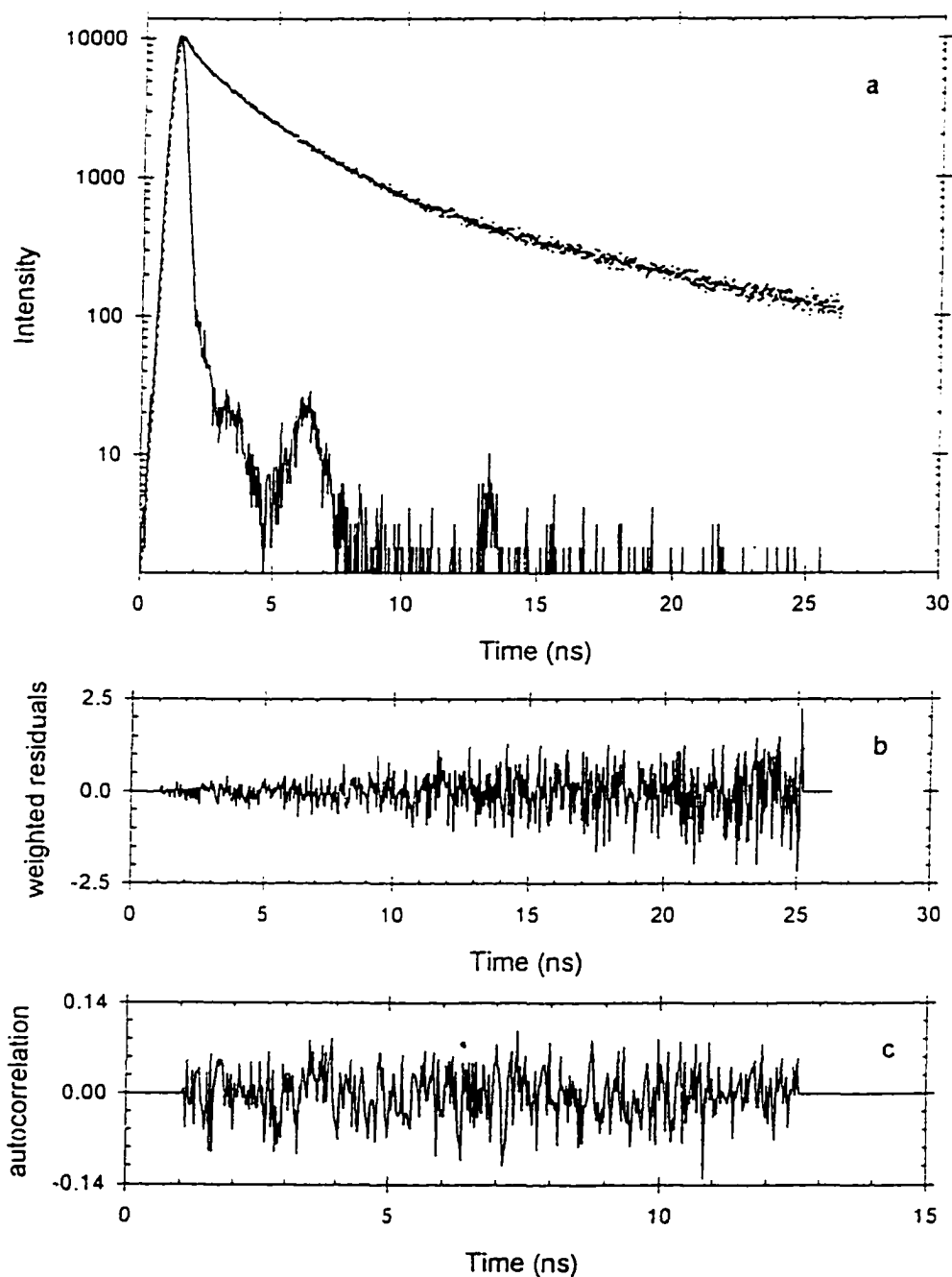


Figure 11: Fluorescence decay curve of 2AP-T (a) in water at 22 °C with (b) weighted residuals and (c) autocorrelation. The sharp-peaked curve is the excitation pulse at 304 nm, the scattered points are the decay data, and the solid line is the three-exponential fit.

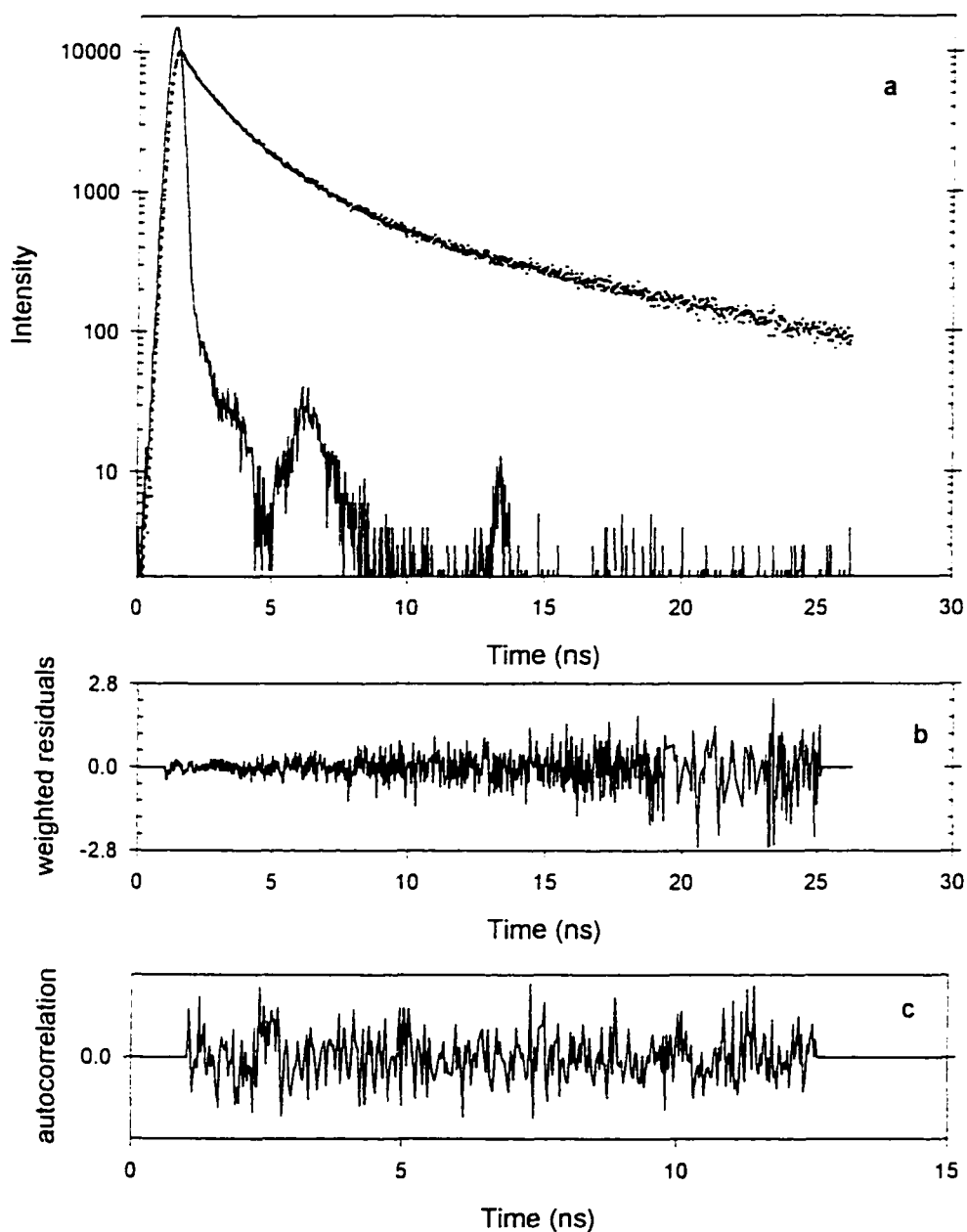


Figure 12: Fluorescence decay curve of 2AP-T (a) in water at 42 °C with (b) weighted residuals and (c) autocorrelation. The sharp-peaked curve is the excitation pulse at 304 nm, the scattered points are the decay data, and the solid line is the three-exponential fit.

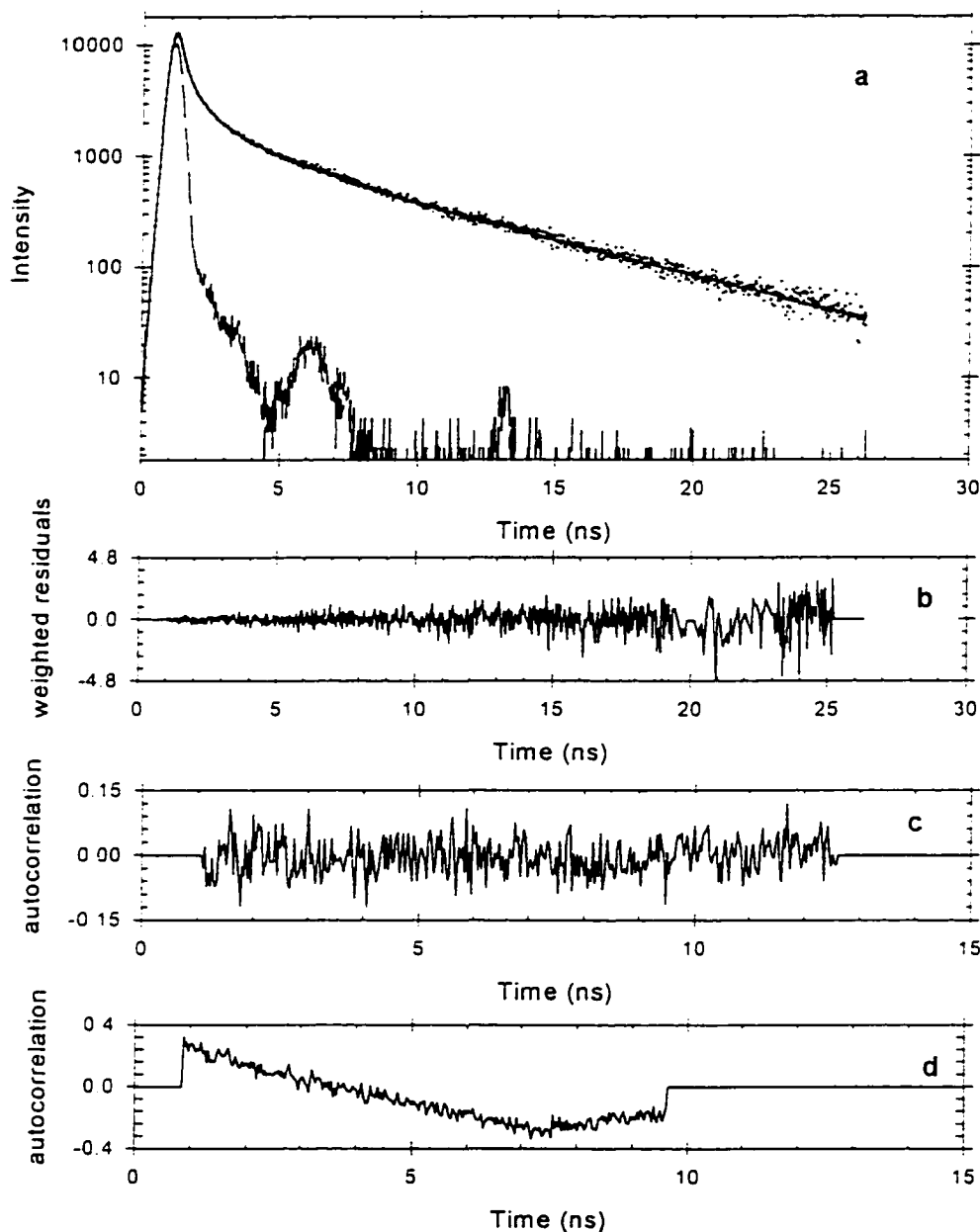


Figure 13: Fluorescence decay curve of A-2AP-T (a) in water at 4 °C with (b) weighted residuals and (c) autocorrelation (for triple-exponential fit); (d) autocorrelation for a double exponential fit. The sharp-peaked curve is the excitation pulse at 304 nm, the time resolved fluorescence of A-2AP-T scattered points are the decay data, and the solid line is the three-exponential fit.

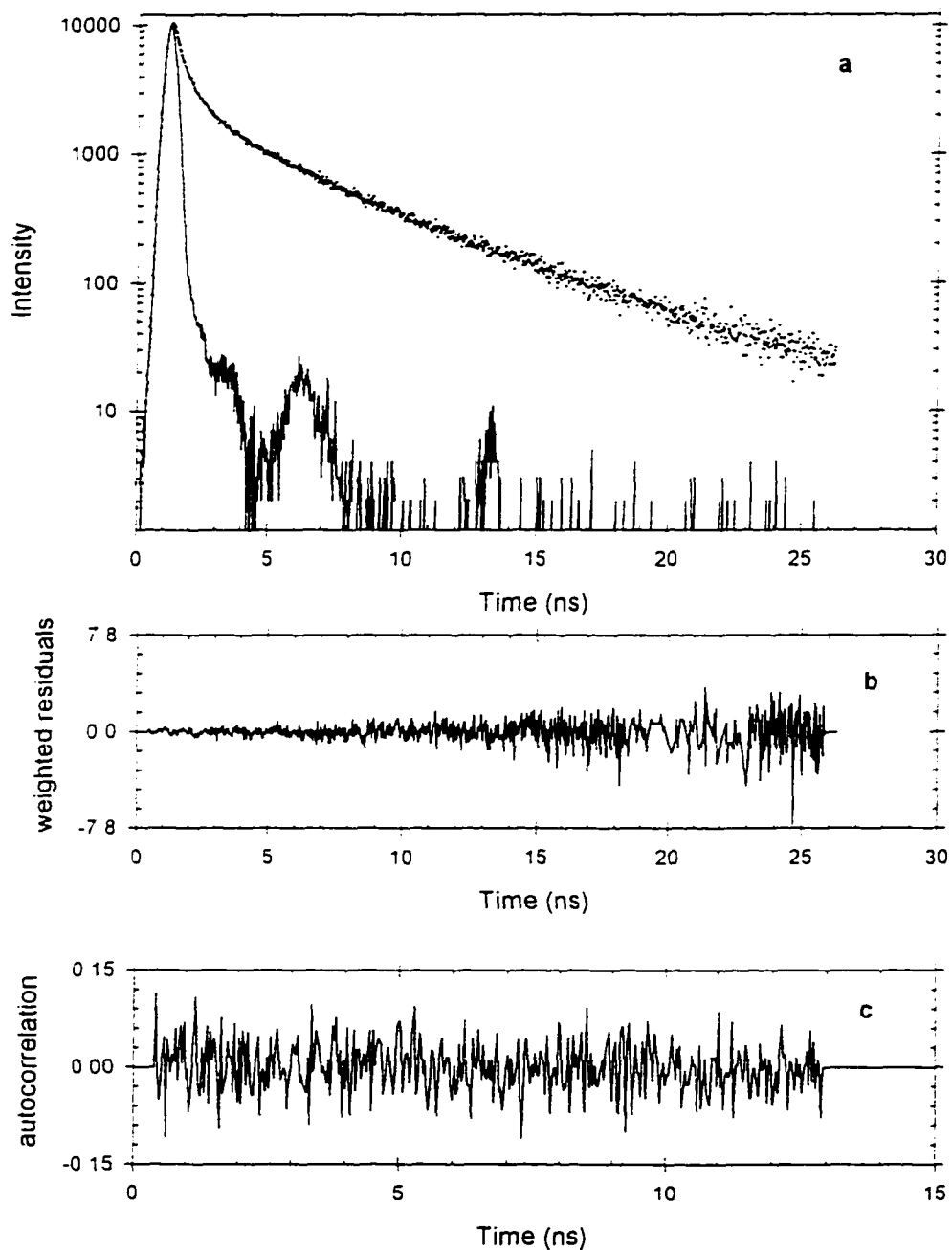


Figure 14: Fluorescence decay curve of A-2AP-T (a) in water at 18 °C with (b) weighted residuals and (c) autocorrelation. The sharp-peaked curve is the excitation pulse at 304 nm, the scattered points are the decay data, and the solid line is the three-exponential fit.

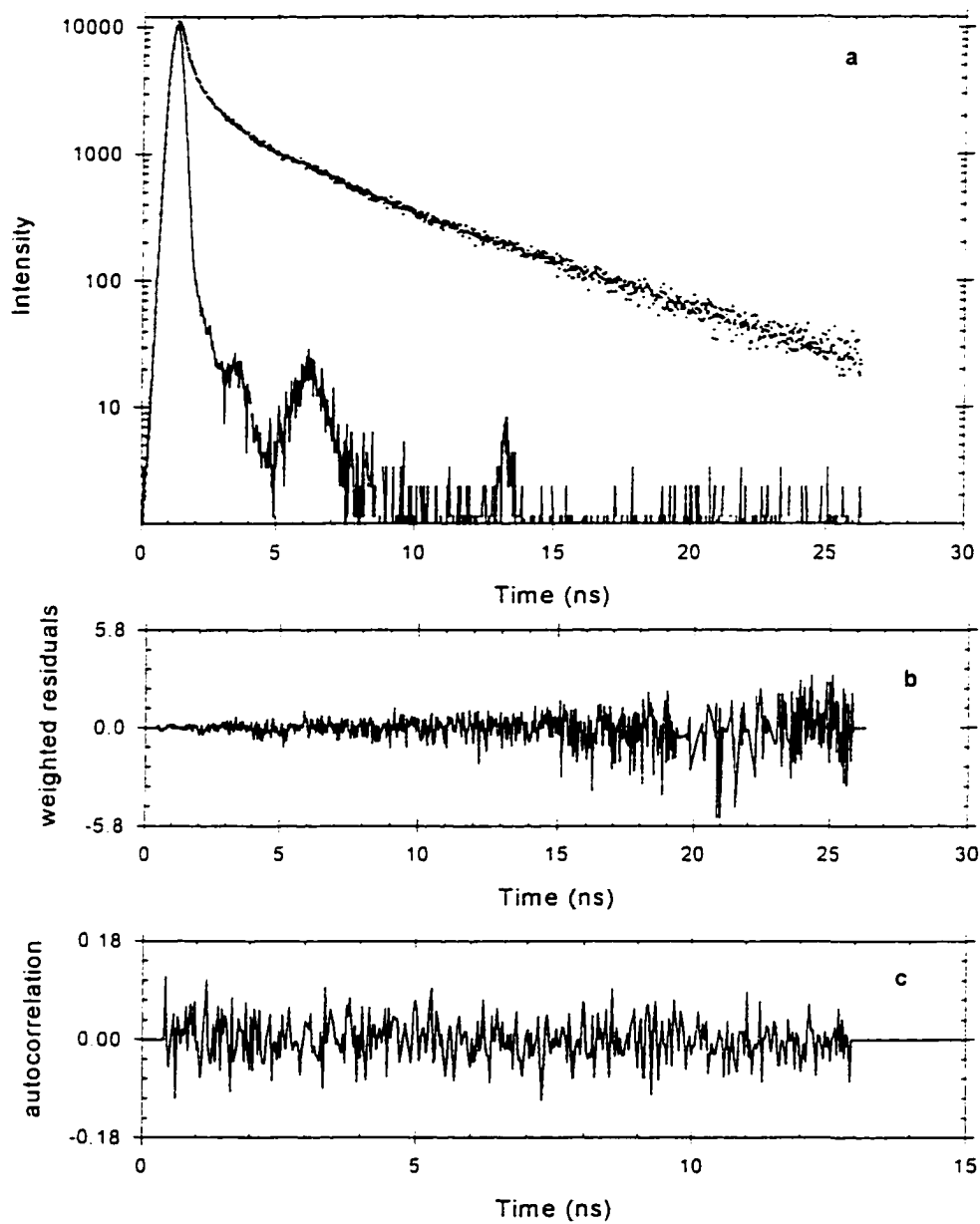


Figure 15: Fluorescence decay curve of A-2AP-T (a) in water at 22 °C with (b) weighted residuals and (c) autocorrelation. The sharp-peaked curve is the excitation pulse at 304 nm, the scattered points are the decay data, and the solid line is the three-exponential fit.

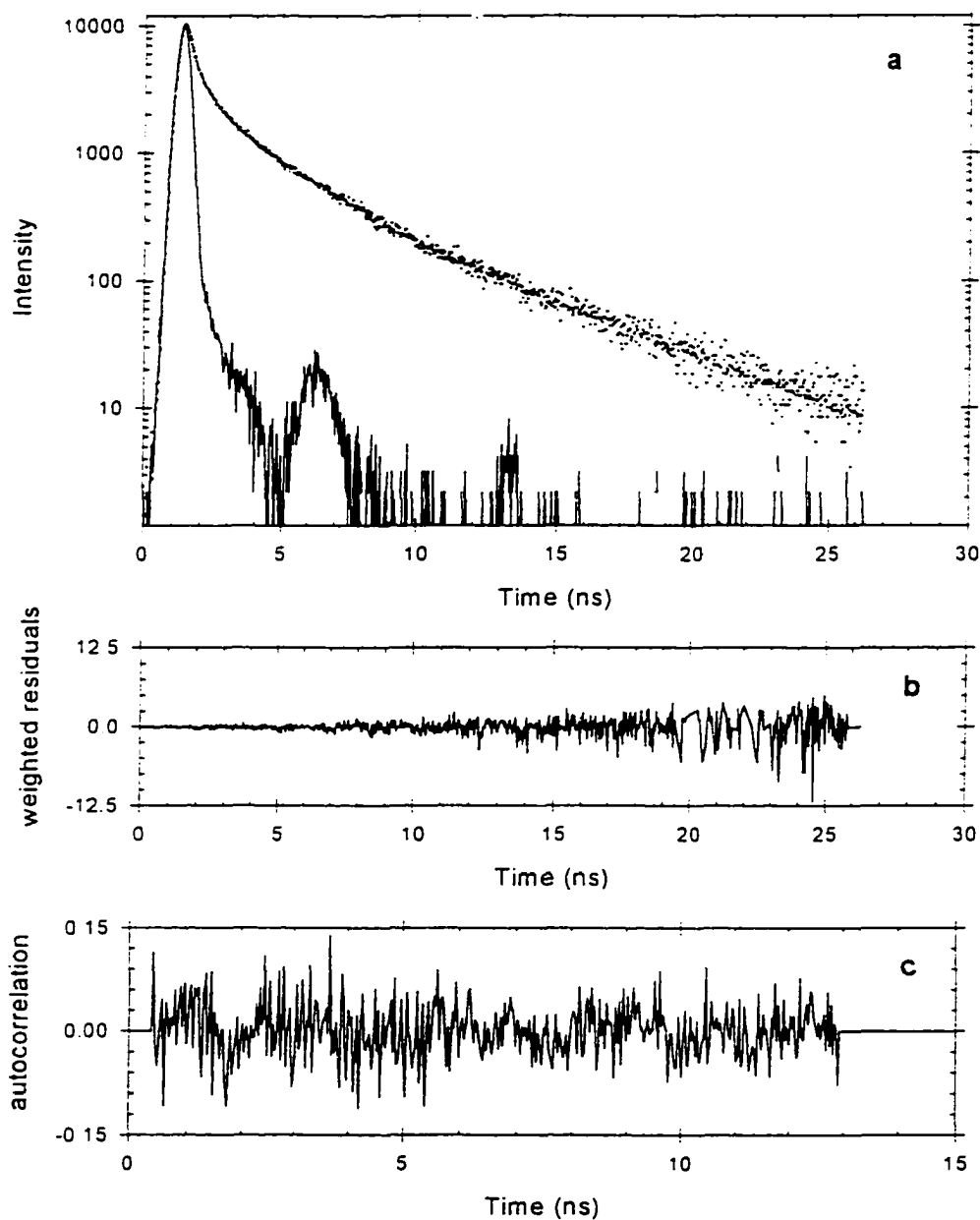


Figure 16: Fluorescence decay curve of A-2AP-T (a) in water at 42 °C with (b) weighted residuals and (c) autocorrelation. The sharp-peaked curve is the excitation pulse at 304 nm, the scattered points are the decay data, and the solid line is the three-exponential fit.

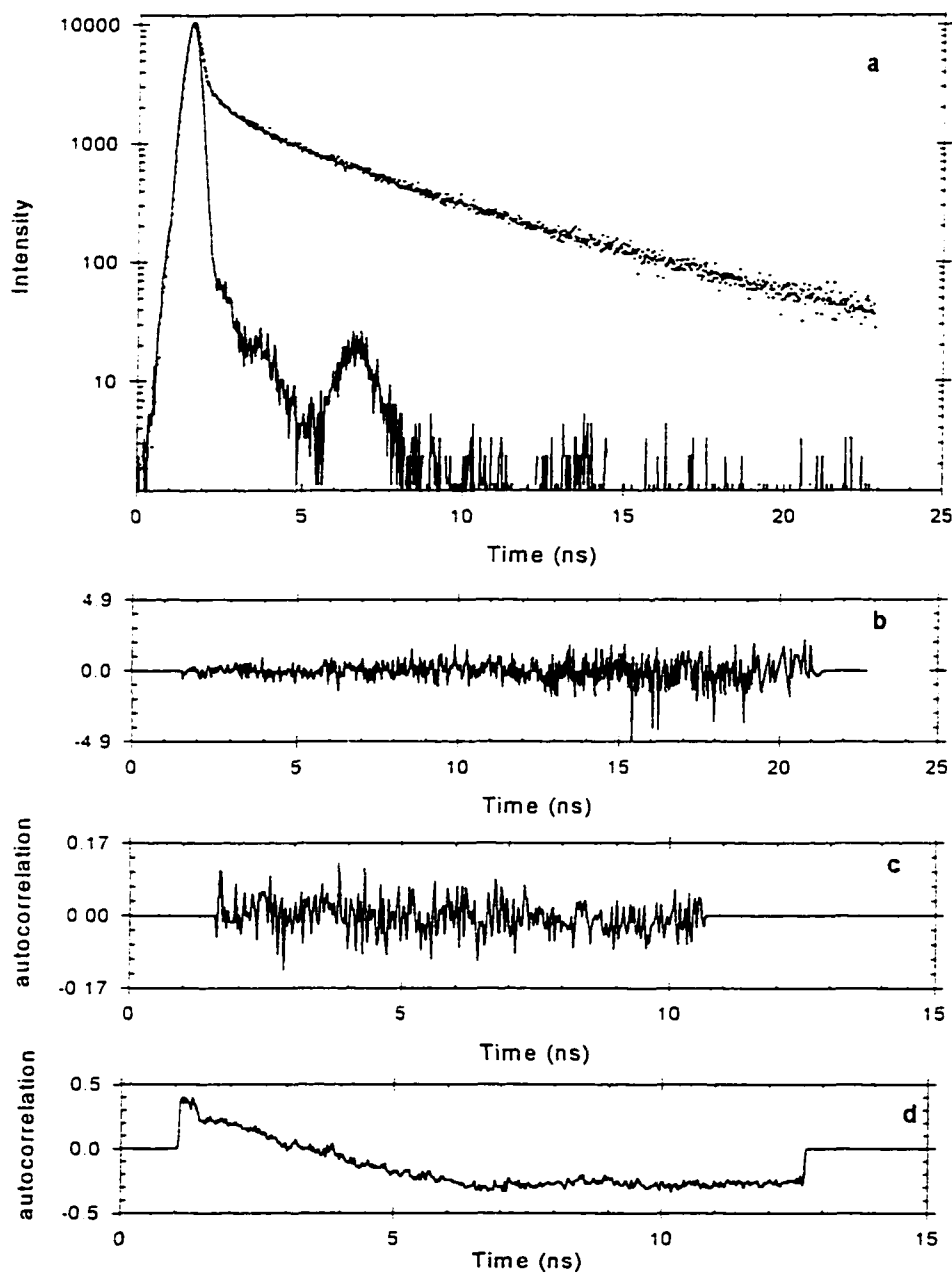


Figure 17: Fluorescence decay curve of G-2AP-C (a) in water at 4 °C with (b) weighted residuals and (c) autocorrelation (for triple-exponential fit); (d) autocorrelation for a double-exponential fit. The sharp-peaked curve is the excitation pulse at 304 nm, the scattered points are the decay data, and the solid line is the three-exponential fit.

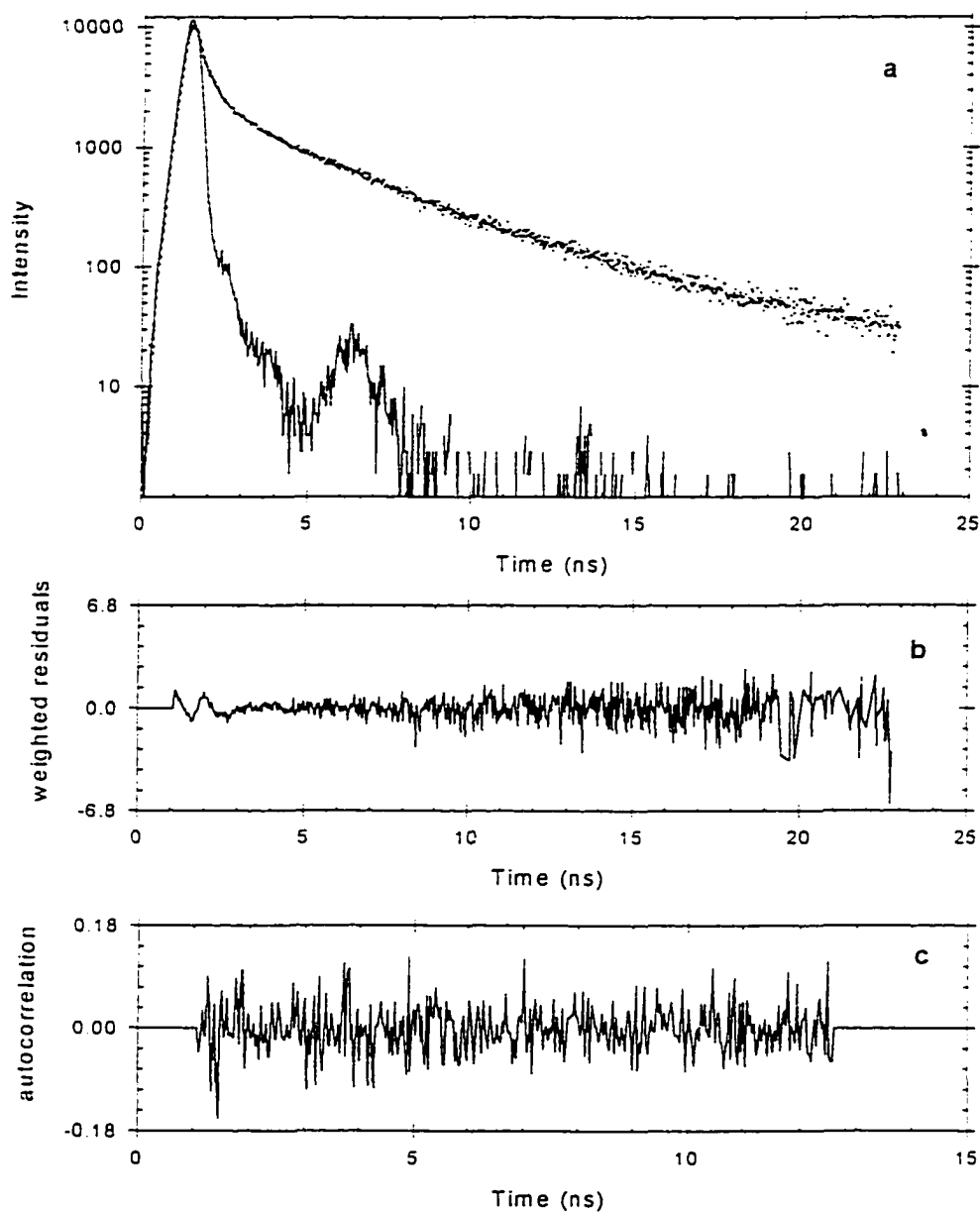


Figure 18. Fluorescence decay curve of G-2AP-C (a) in water at 18 °C with (b) weighted residuals and (c) autocorrelation. The sharp-peaked curve is the excitation pulse at 304 nm, the scattered points are the decay data, and the solid line is the three-exponential fit.

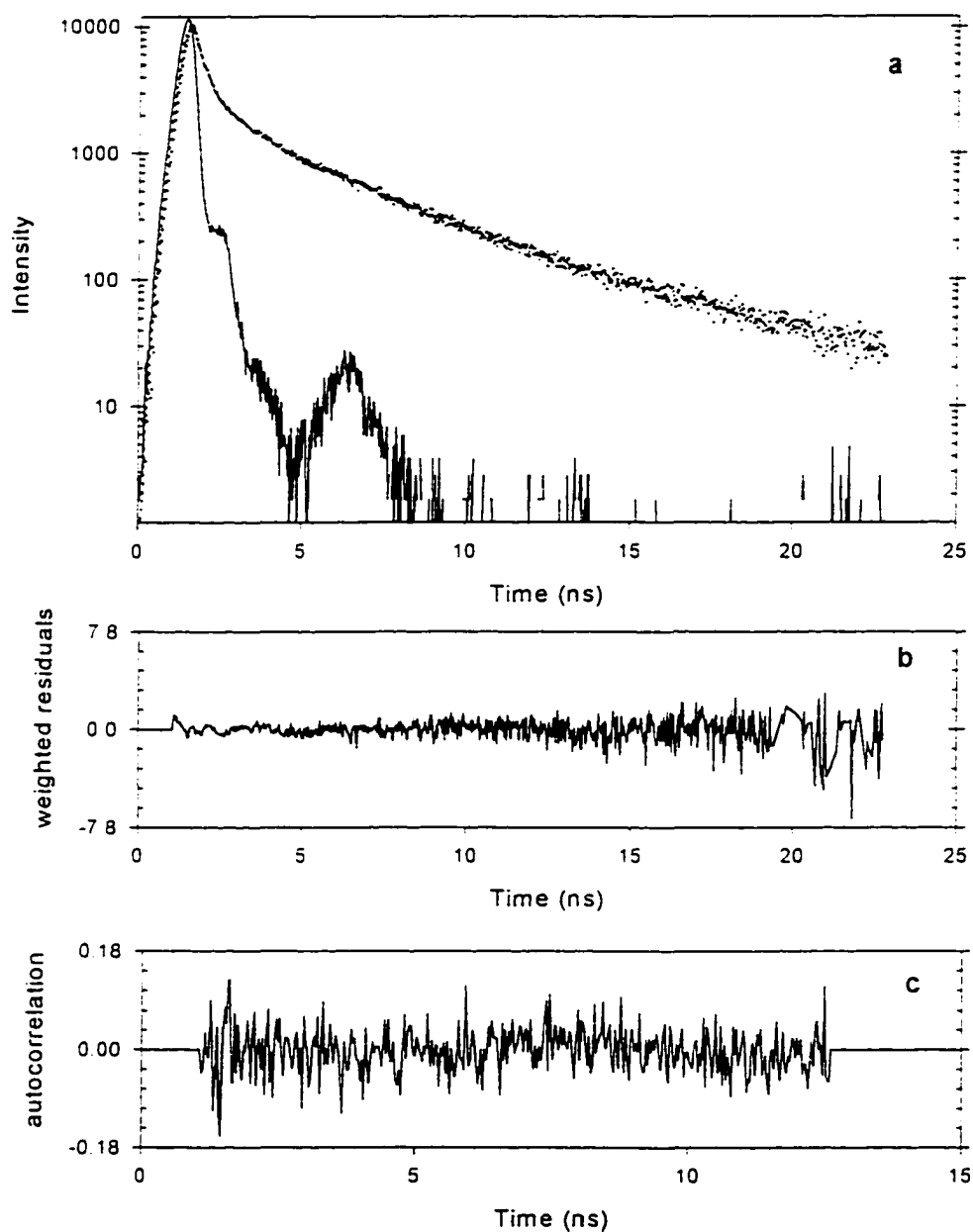


Figure 19: Fluorescence decay curve of G-2AP-C (a) in water at 22 °C with (b) weighted residuals and (c) autocorrelation. The sharp-peaked curve is the excitation pulse at 304 nm, the scattered points are the decay data, and the solid line is the three-exponential fit.

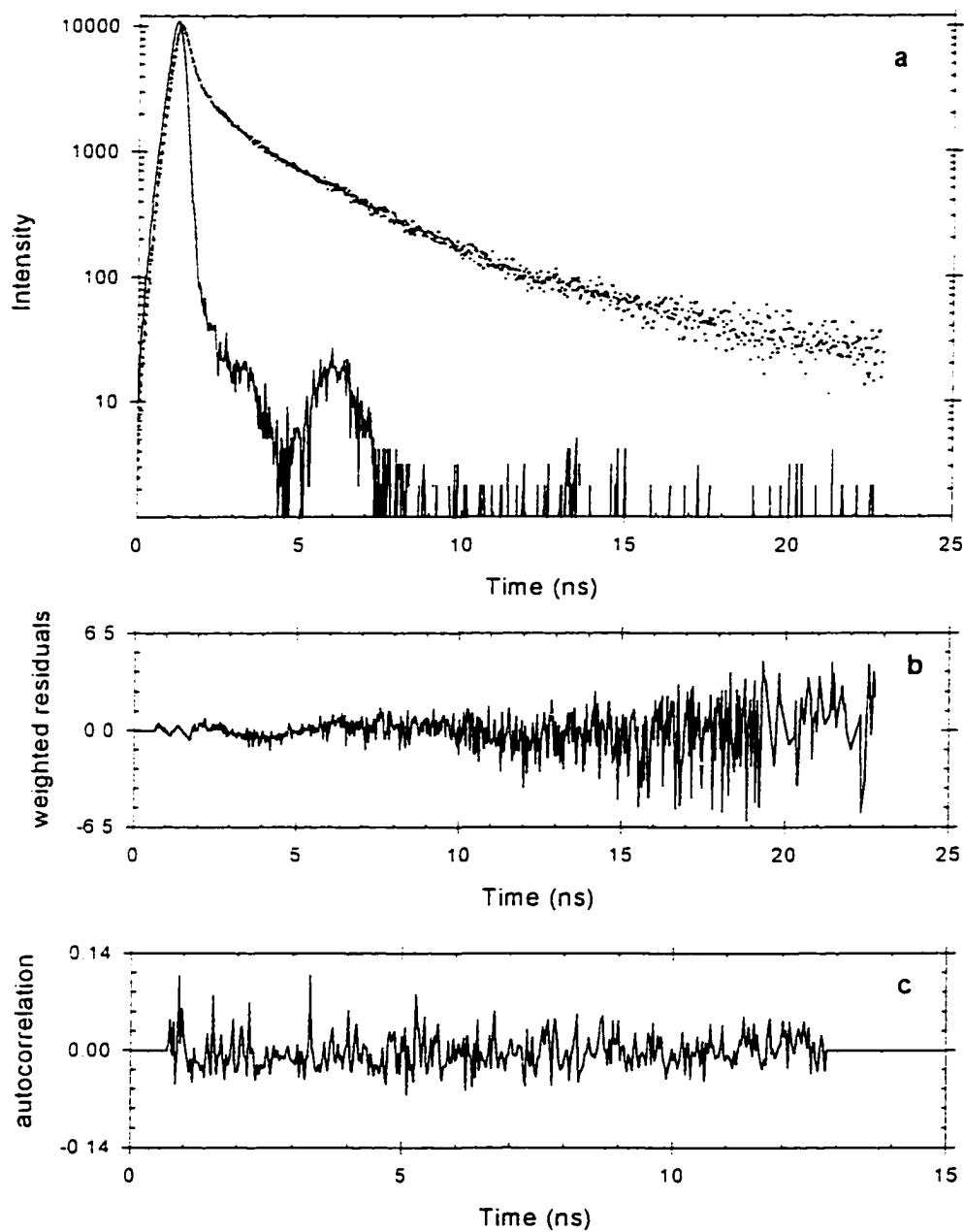


Figure 20: Fluorescence decay curve of G-2AP-C (a) in water at 38 °C with (b) weighted residuals and (c) autocorrelation. The sharp-peaked curve is the excitation pulse at 304 nm, the scattered points are the decay data, and the solid line is the three-exponential fit.

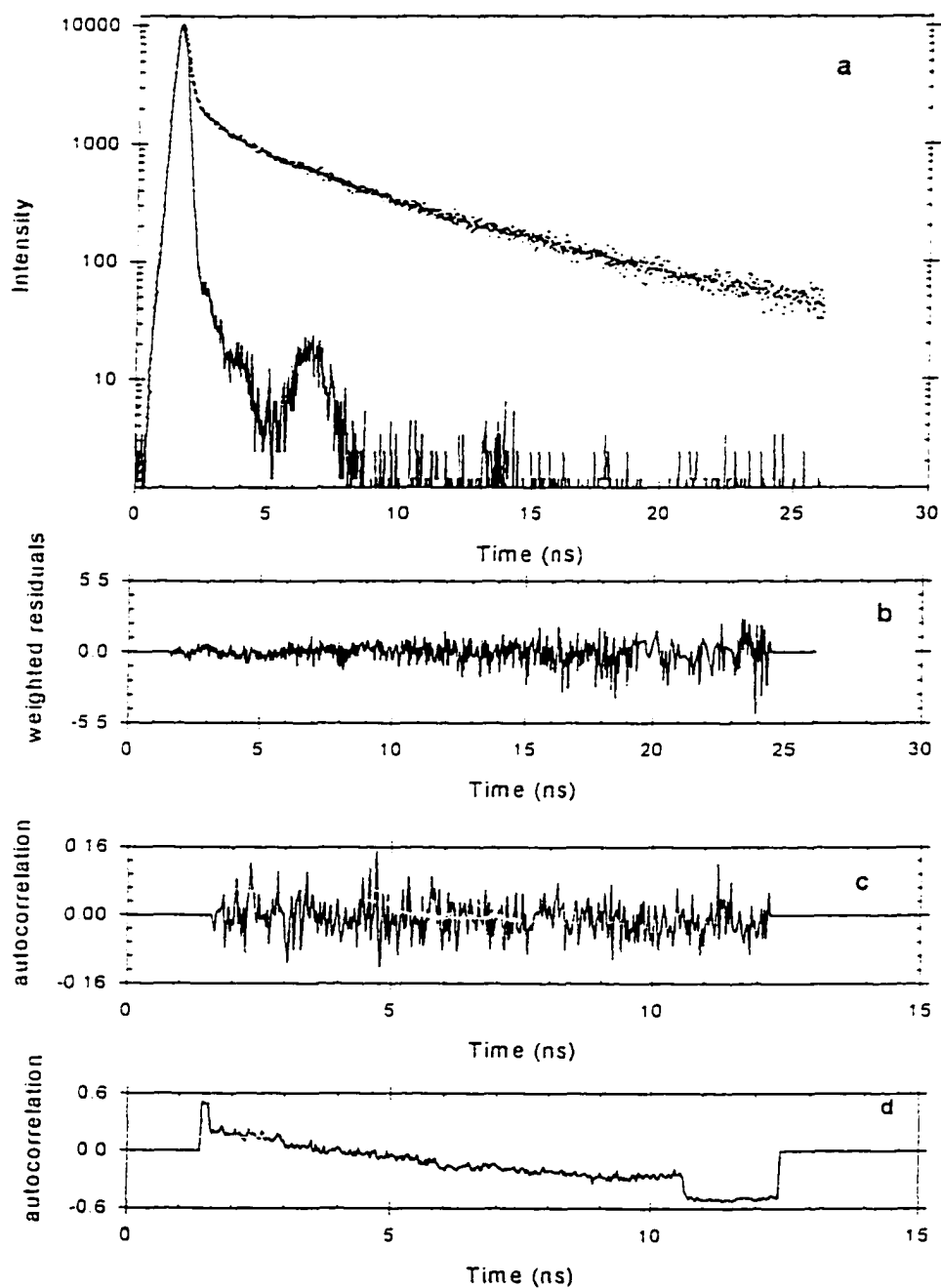


Figure 21: Fluorescence decay curve of C-2AP-G (a) in water at 4 °C with (b) weighted residuals and (c) autocorrelation (for a triple-exponential fit); (d) autocorrelation for a double exponential fit. The sharp-peaked curve is the excitation pulse at 304 nm, the scattered points are the decay data, and the solid line is the three-exponential fit.

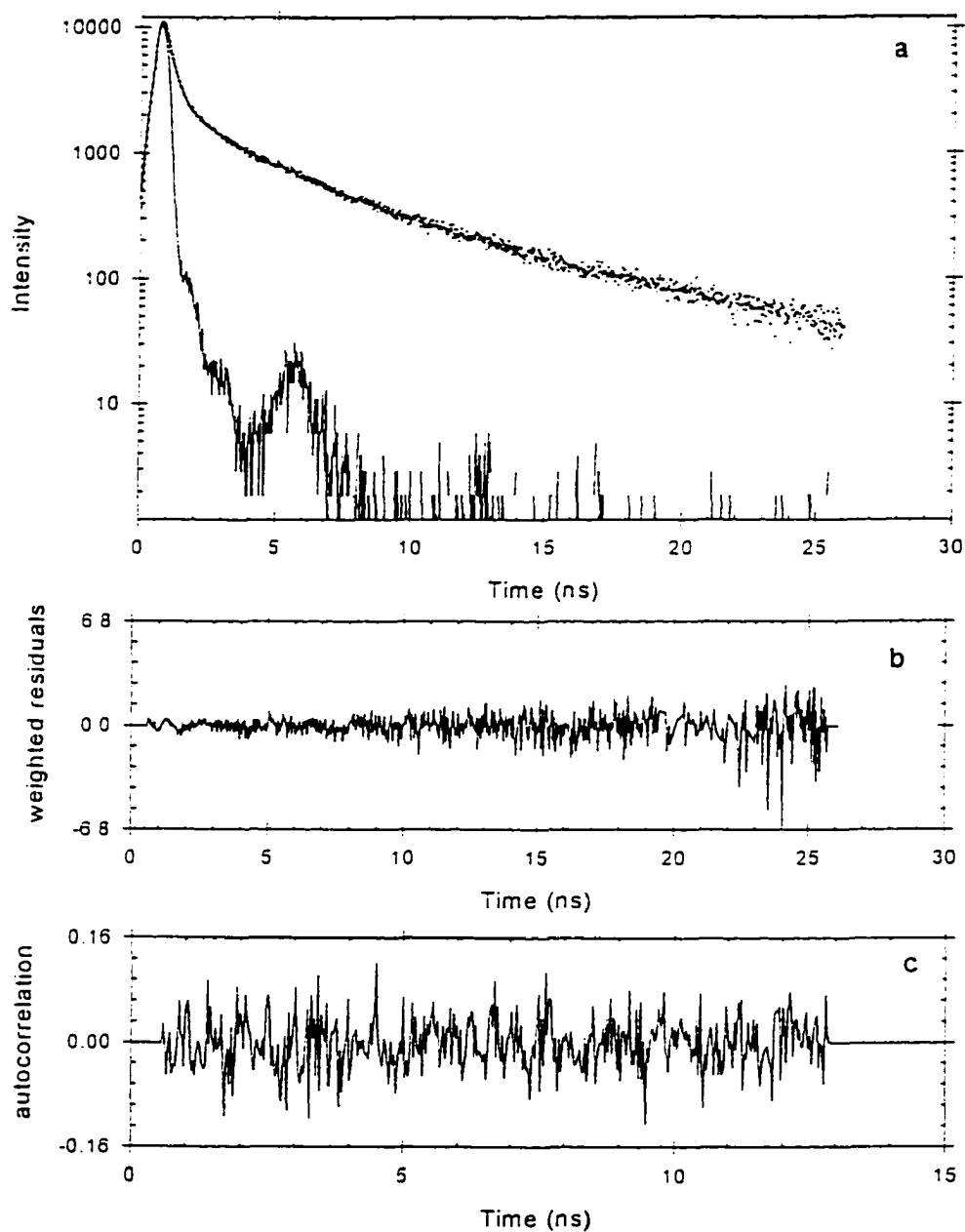


Figure 22. Fluorescence decay curve of C-2AP-G (a) in water at 18 °C with (b) weighted residuals and (c) autocorrelation. The sharp-peaked curve is the excitation pulse at 304 nm, the scattered points are the decay data, and the solid line is the three-exponential fit.

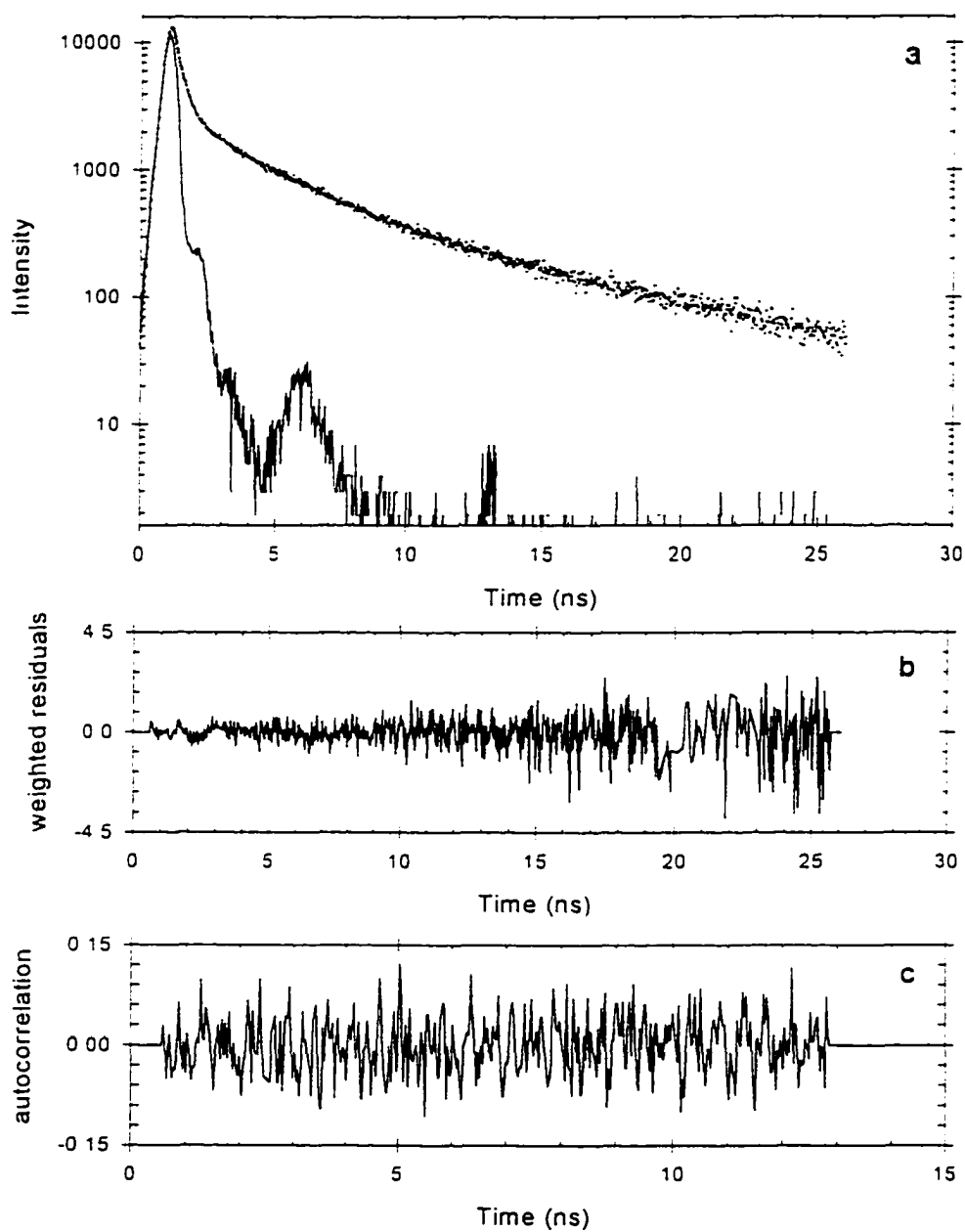


Figure 23: Fluorescence decay curve of C-2AP-G (a) in water at 22 °C with (b) weighted residuals and (c) autocorrelation. The sharp-peaked curve is the excitation pulse at 304 nm, the scattered points are the decay data, and the solid line is the three-exponential fit.

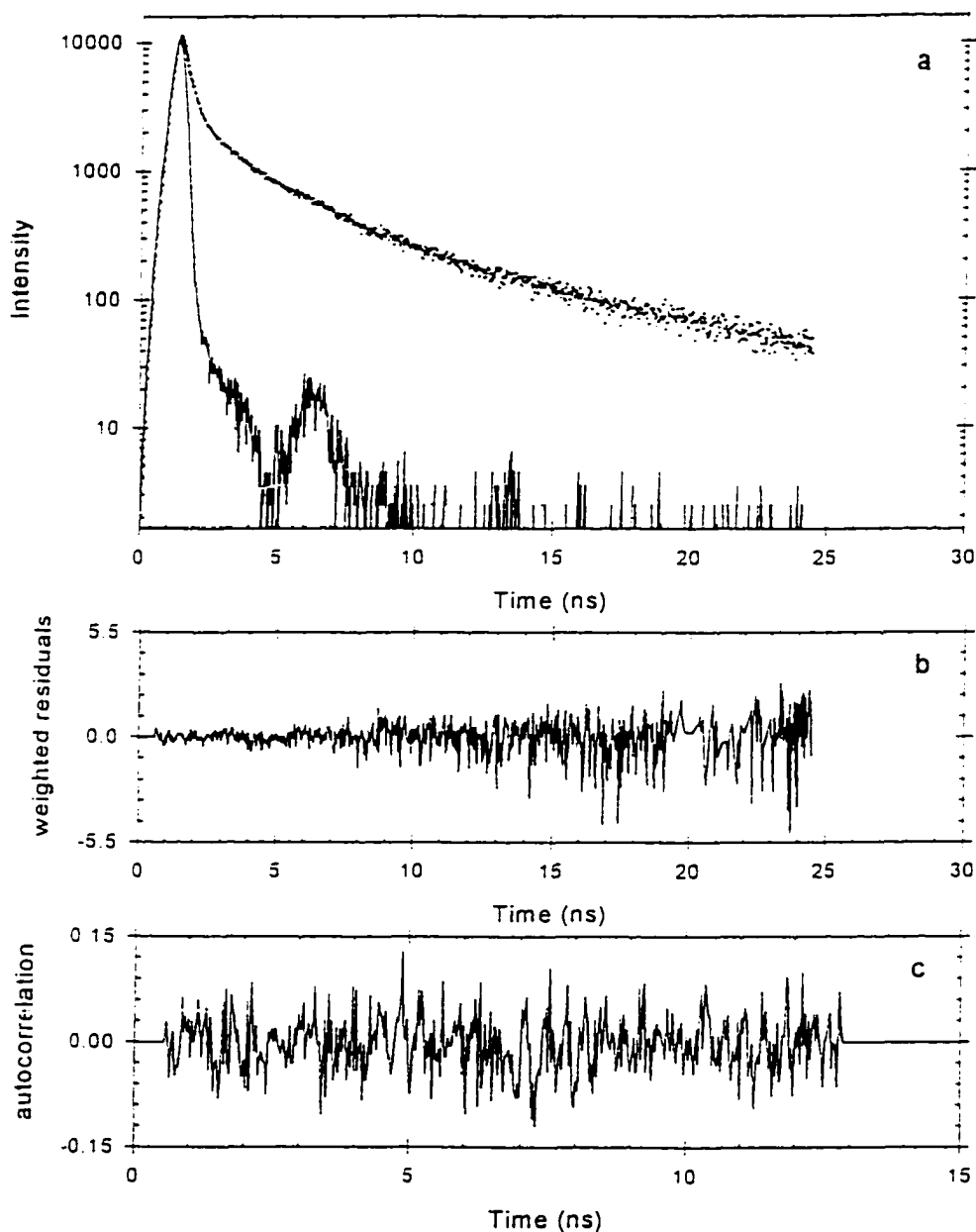


Figure 24: Fluorescence decay curve of C-2AP-G (a) in water at 38 °C with (b) weighted residuals and (c) autocorrelation. The sharp-peaked curve is the excitation pulse at 304 nm, the scattered points are the decay data, and the solid line is the three-exponential fit.

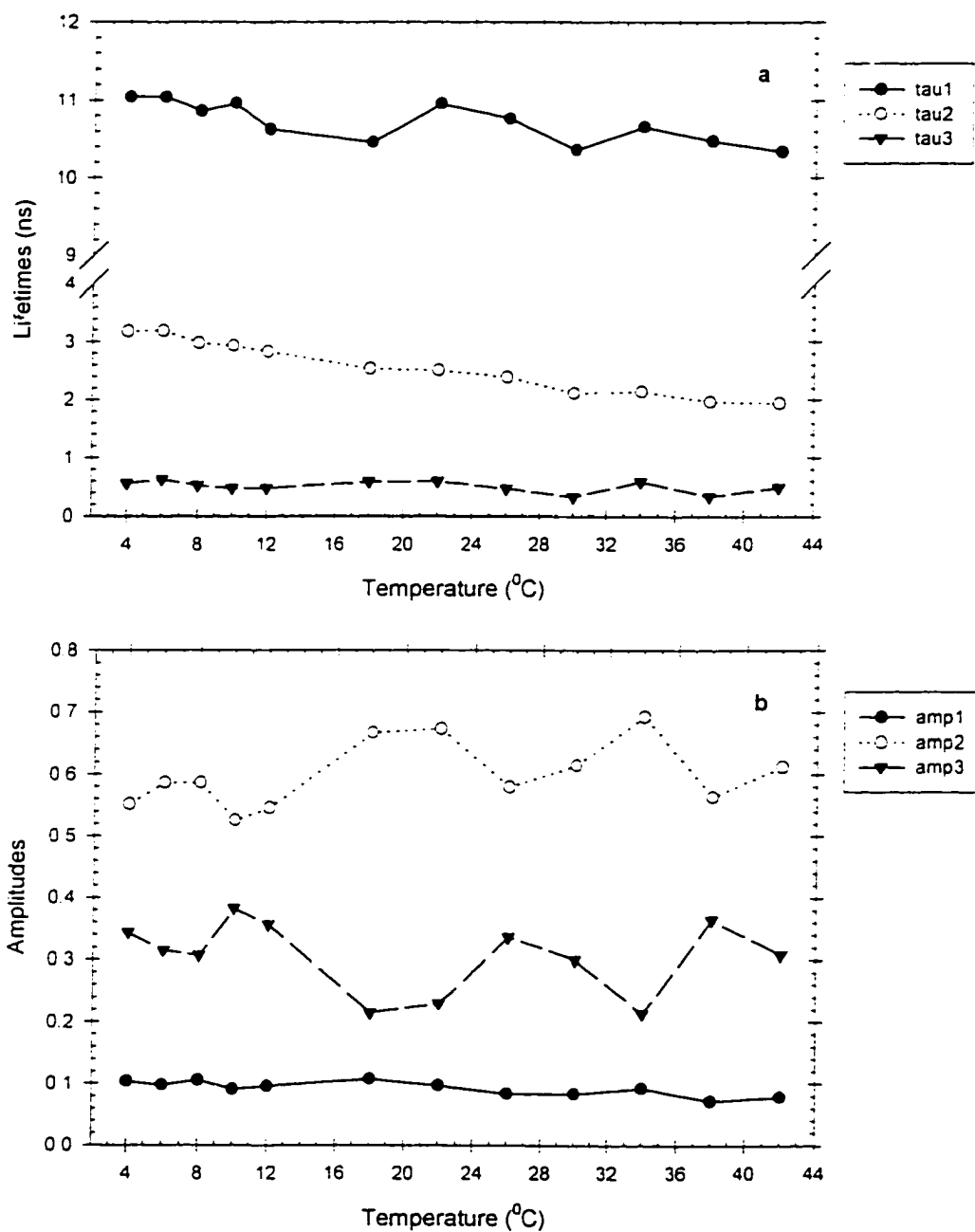


Figure 25: Temperature dependence (4-42 °C) of the fluorescence decay (a) lifetimes and (b) corresponding amplitudes for 2AP-T.

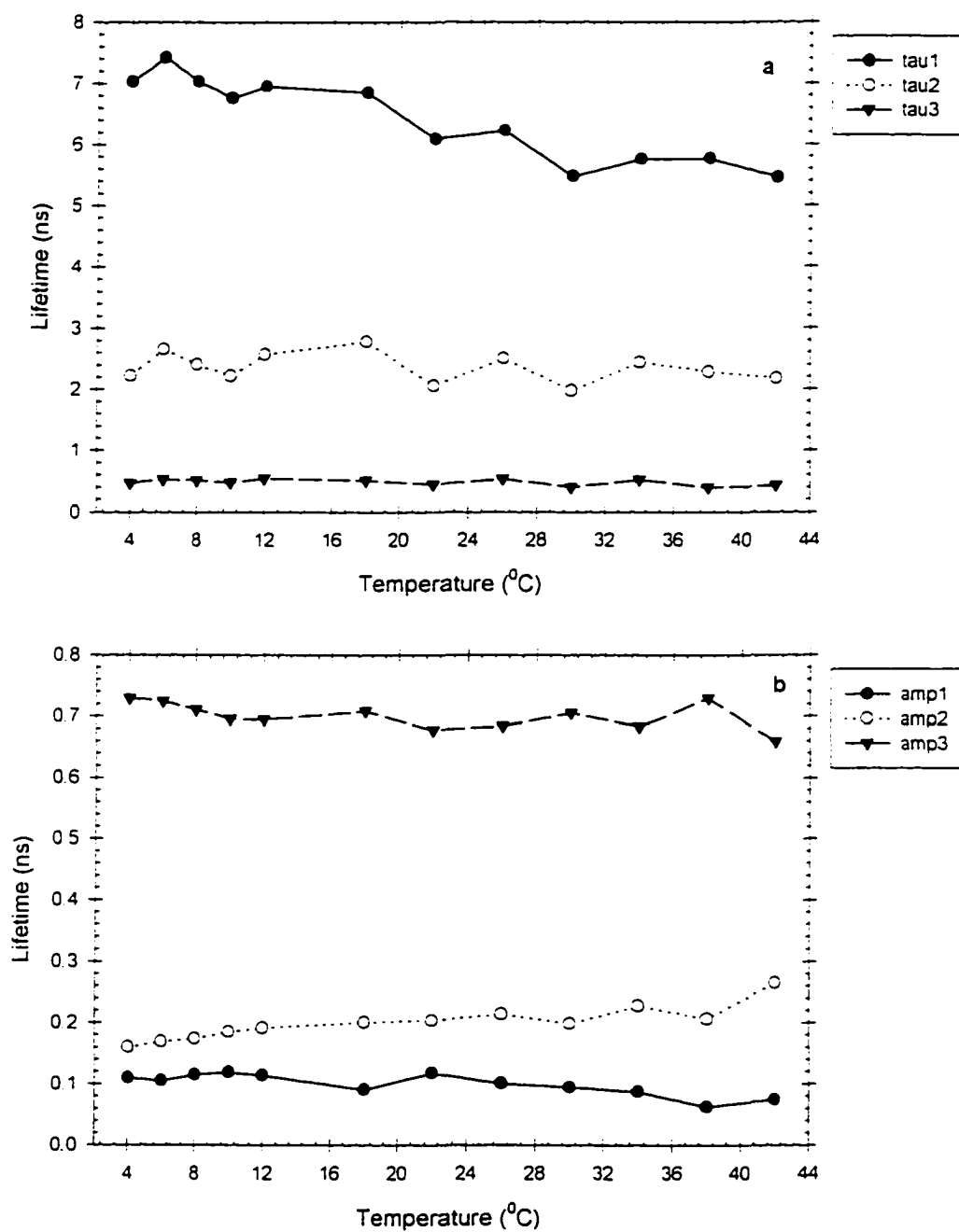


Figure 26: Temperature dependence (4-42 °C) of the fluorescence decay (a) lifetimes and (b) corresponding amplitudes for A-2AP-T.

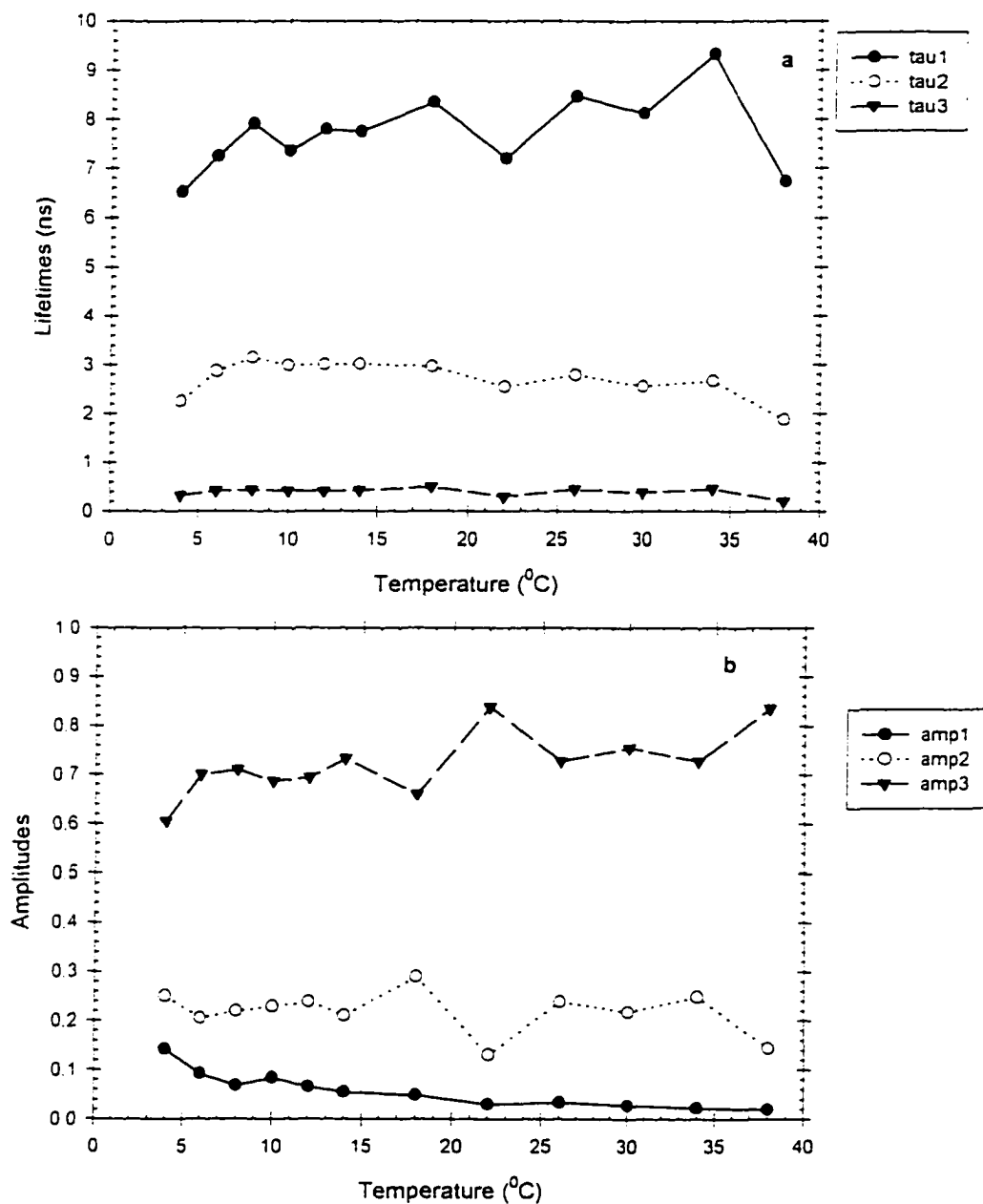


Figure 27: Temperature dependence (4-38 °C) of the fluorescence decay (a) lifetimes and (b) corresponding amplitudes for G-2AP-C.

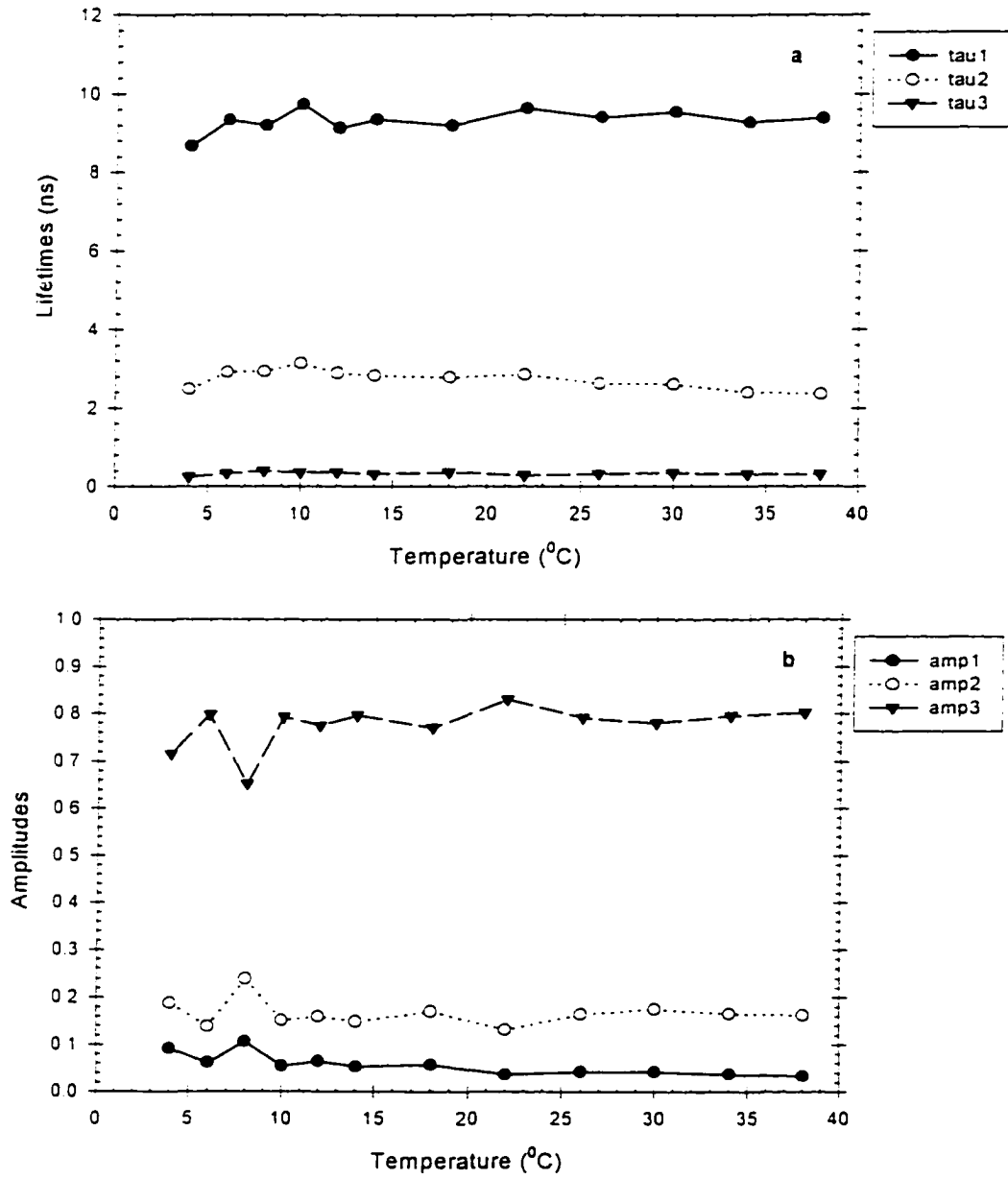


Figure 28: Temperature dependence (4-38 °C) of the fluorescence decay (a) lifetimes and (b) corresponding amplitudes for C-2AP-G.

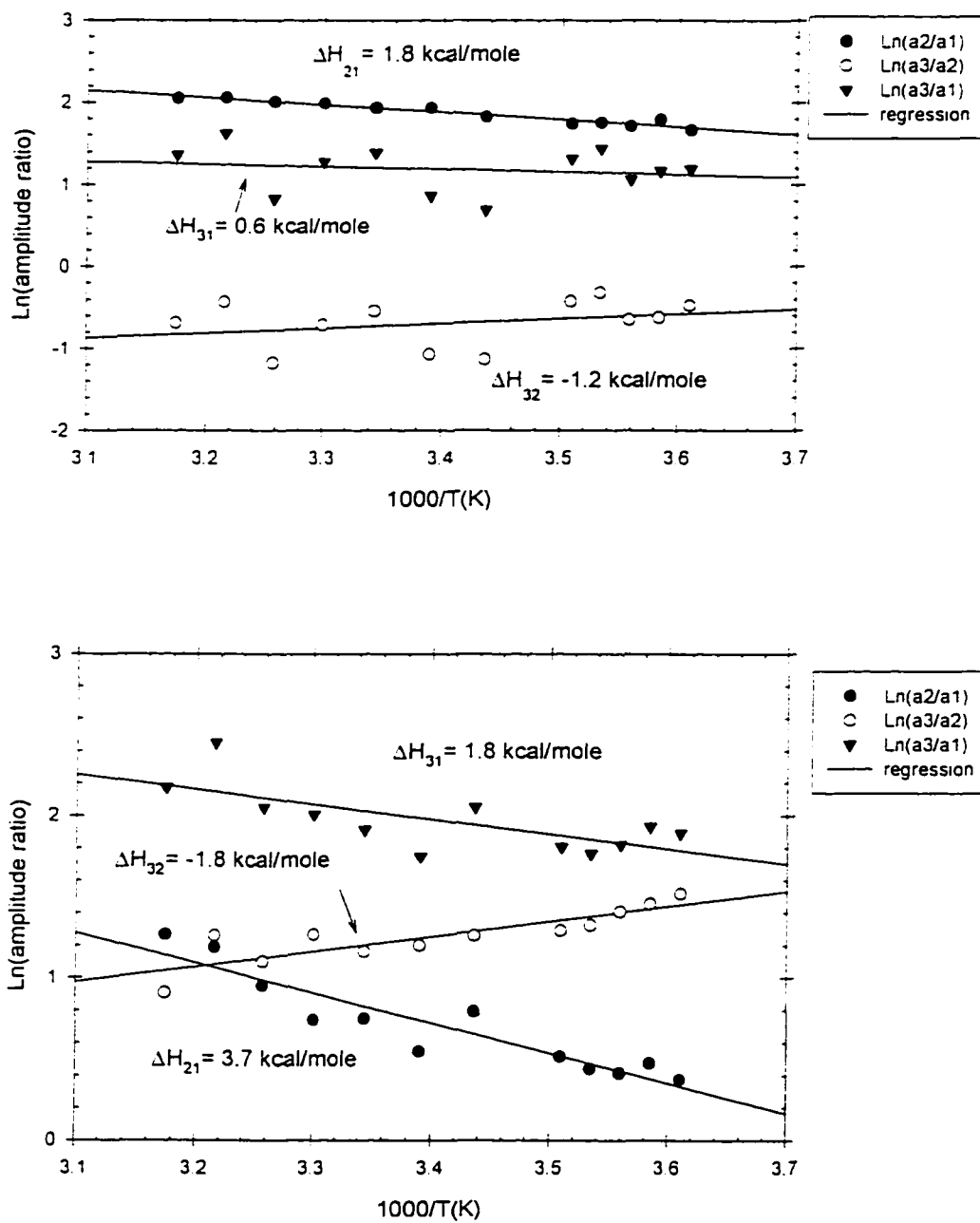


Figure 29: Van't Hoff analysis of fluorescence decay amplitude components for (a) 2AP-T and (b) A-2AP-T.

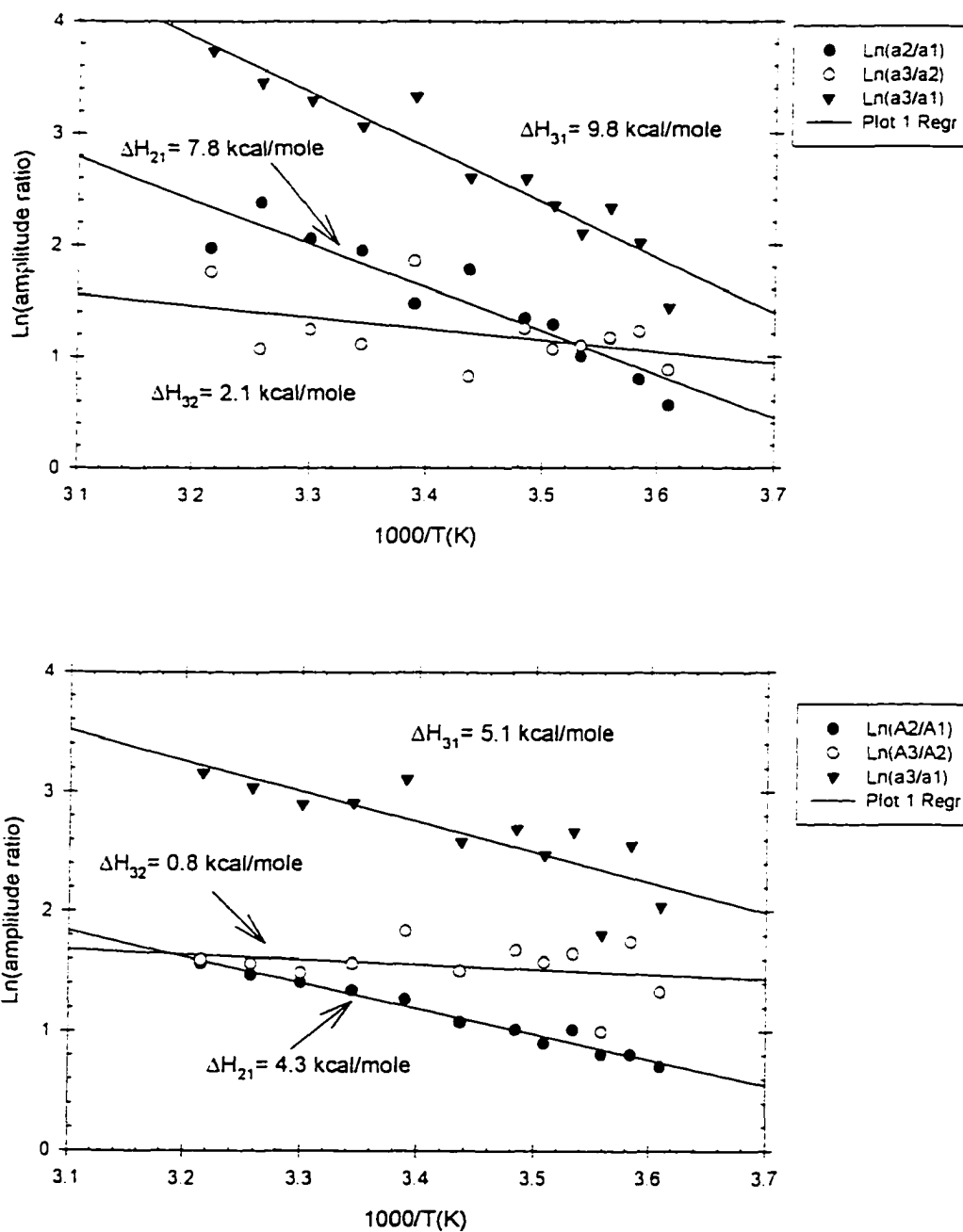


Figure 30: Van't Hoff analysis of fluorescence decay amplitude components for (a) G-2AP-C and (b) C-2AP-G.

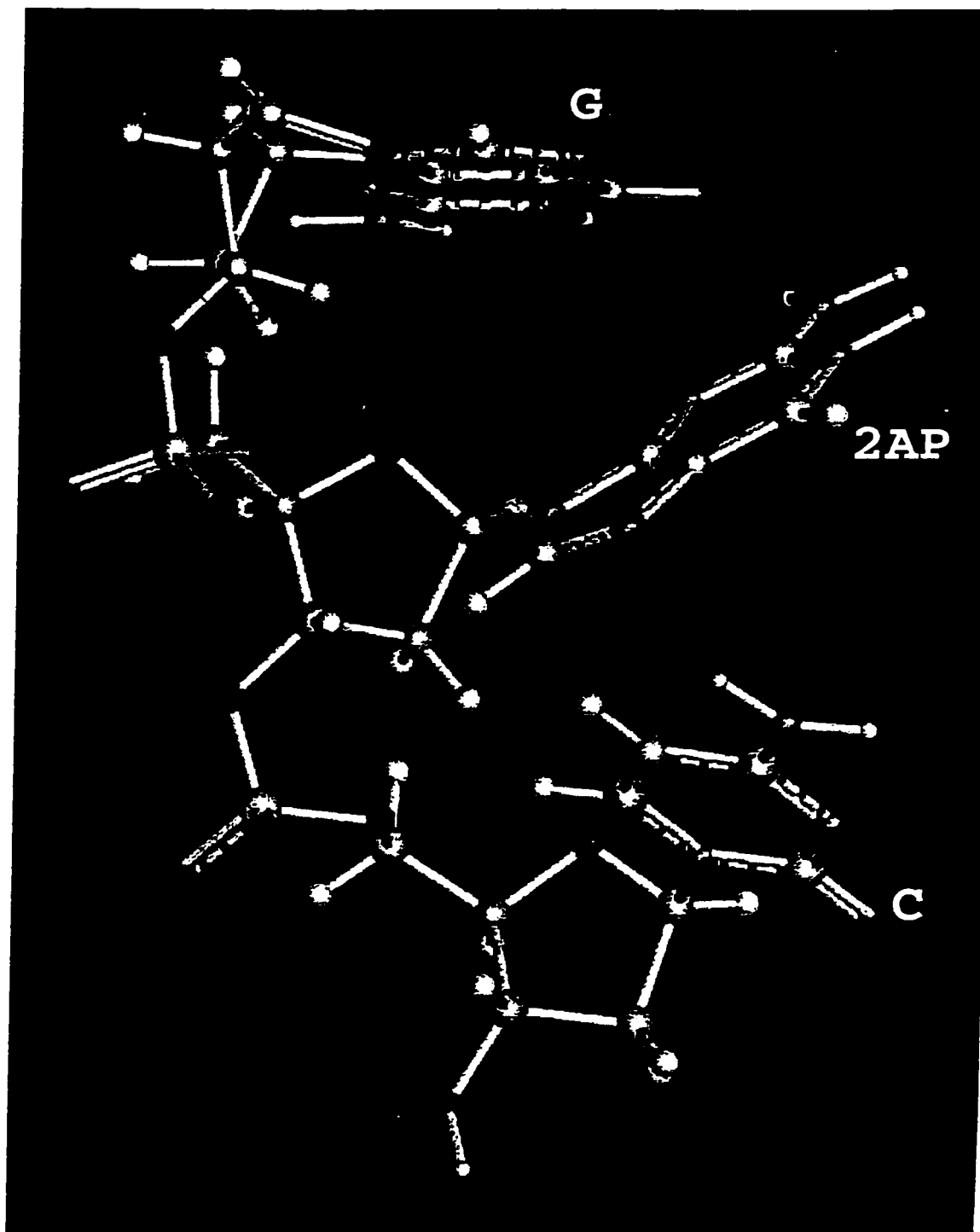


Figure 31: The structure of the trinucleotide G-2AP-C, after energy minimization, showing possible H-bonding between -NH_2 of 2AP and O6 of guanine. H-bonding distance is $\approx 1.6 \text{ \AA}$. This structure was generated using QUANTA program, version 3.1.

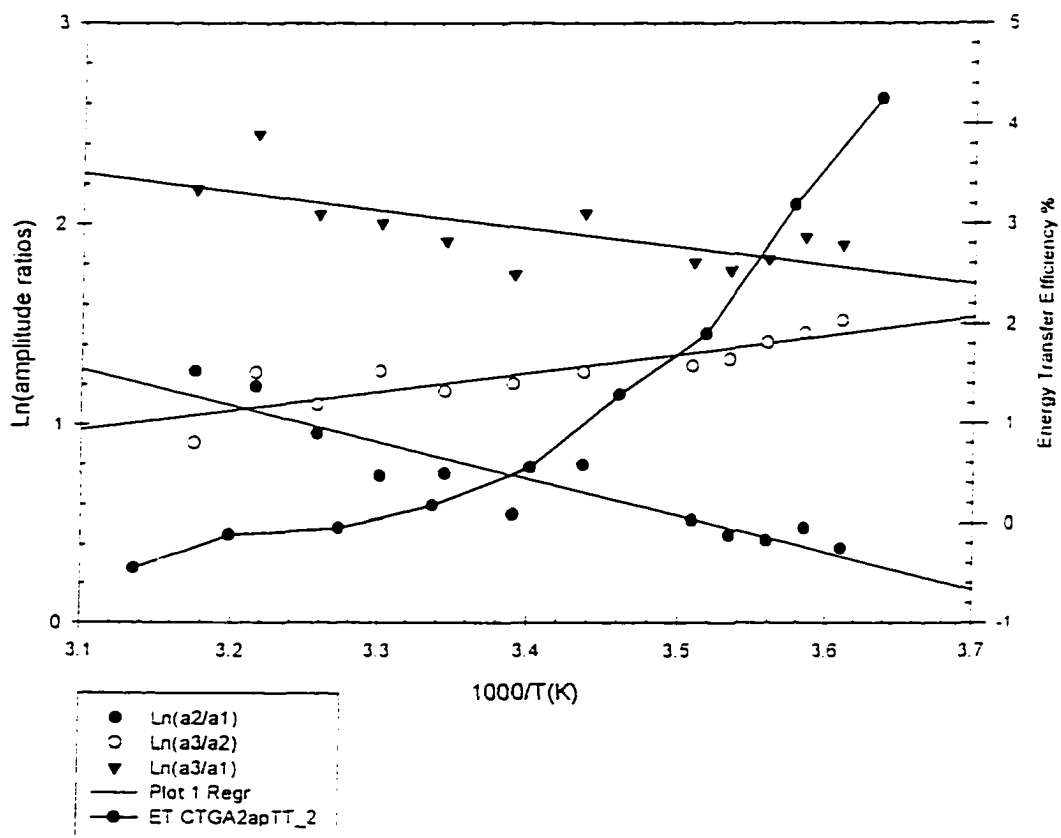


Figure 32: Van't Hoff plot analysis of A-2AP-T trinucleotide compared to the energy transfer efficiency of the CTGAA(2AP)TTCAG decamer.

FOURIER TRANSFORM-INFRARED, INFRARED, AND RAMAN COMPARATIVE
STUDIES OF THE FLUORESCENT MODIFIED DNA BASE 2-AMINOPURINE AND
ITS MONONUCLEOSIDES

by

KERVIN O. EVANS, ANATOLIY KUDRYAVSTEV, LUTHER W. BEEGLE,
THOMAS M. NORDLUND

In preparation for *Journal of Raman Spectroscopy*

Format adapted for dissertation

ABSTRACT

In a continued attempt to develop an optical "guide book" for the modified fluorescent DNA base 2-aminopurine (2AP), we present the laser-Raman and infrared spectra of crystalline 2AP, its mononucleosides 2-aminopurine-2'-deoxyribonucleoside (2AP-dn), and 2-aminopurine ribonucleoside (2AP-rb), and their proposed band assignments. We compared the infrared spectra of 2AP and 2AP-rb to those of their adenine counterparts and to each other (we also compared the Fourier transform infrared spectra to that of the infrared). We also compared the Raman spectra of 2AP to that of adenine and 2AP-rb. Comparison of 2AP and 2AP-rb to adenine and adenosine allowed us to identify some quite distinct vibrational bands associated only with 2AP (and 2AP-rb), in particular the IR band at 2360 (2361 for 2AP-rb) and Raman bands at 428, 494, and four bands in the 1850-1945 cm^{-1} region (492 and 855 cm^{-1} for 2AP-rb; in solution, there was only one band at 862). In spite of large fluorescent background exhibited in the Raman spectra of 2AP nucleosides, it appears that these distinctive bands will be the key to monitoring the vibrational spectroscopy of 2AP.

INTRODUCTION

2-Aminopurine (2AP) has been established, in recent years, as an excellent fluorescent probe of local DNA activities (Allan & Reich, 1996; Bjornson *et al.*, 1996; Bloom *et al.*, 1994; Nordlund *et al.*, 1993; Raney *et al.*, 1994; Xu *et al.*, 1994). However, the fluorescence of 2AP presents somewhat limited information by which to monitor these activities: changes in fluorescence intensity, lifetime decays, or peak positions of

2AP (Evans *et al.*, 1992; Hochstrasser *et al.*, 1994; Xu *et al.*, 1994). Raman spectroscopy, on the other hand, presents a greater amount of information to possibly monitor activities of 2AP using the bands produced by the various vibrational modes of a molecule.

Raman spectroscopy has been used to study biological molecules with great success, including free and complexed nucleic acids and their derivatives (Brahms & Brahms, 1990; Britton *et al.*, 1988; Florian & Leszczynski, 1995; Gfroerer *et al.*, 1991, 1993; Govorun *et al.*, 1991; Katahira *et al.*, 1990; Lamba *et al.*, 1989; Spiro, 1987; Tsuboi *et al.*, 1995). And although infrared presents some of the same information about vibrational band, infrared has been used to complement Raman measurements because some bands that are not Raman active may be infrared active.

In light of the possibility of such a large volume of information being present in the Raman and infrared bands of 2AP (which, as far as we can find, has not been investigated), we attempted to present a second spectroscopic method to monitor 2AP. Therefore, we looked for distinctive vibrational bands of 2AP that may set it apart from the normal DNA bases. In view of this, we present the Raman and infrared spectral bands of crystalline 2AP and its 2'-deoxyribose and ribose nucleosides, and compare the bands of 2AP with those of adenine. At the same time, Fourier transform infrared (FT-IR) spectra are well resolved because of the method used. We, therefore, present a comparison between FT-IR and IR spectra of these samples.

EXPERIMENTAL PROCEDURES

Materials and Methods

2-Aminopurine (2AP) free base, 2-aminopurine ribonucleoside (2AP-rb), adenine, and adenosine were purchased from Sigma Chemical Company and used without further purification. 2-aminopurine-2'-deoxyribonucleoside (2AP-dn) was generously provided by Dr. George W. Koszalka, Burroughs Wellcome Co., Research Triangle Park, NC, and was prepared and analyzed as previously described (Evans *et al.*, 1992).

Raman measurements were done using a 10 mW He-Ne laser as the light source and a CCD-camera for detecting the Raman scattering. Samples in the powder (crystalline) form were placed on a glass slide, and laser light was focused (using a lens with a 10 cm focal length) onto the samples for Raman scattering to be collected. For solution samples, 2AP-dn and 2AP-rb were dissolved in distilled, deionized water at concentrations of ~ 3 mg/ml; samples were placed into a round glass vial for measurements. Some pixels from the CCD-camera showed nonuniformity, so they were eliminated from the data. Data were collected at 5 points. cm^{-1} with a rate of 2 seconds. cm^{-1} and transferred in ASCII format to diskettes.

For the FT-IR and IR samples, approximately 1 mg of each sample was mixed with 100-120 mg of KBr to form a pellet. Sample and KBr mixing were accomplished in an agitator using a polystyrene bead as the mixer (agitation was for about 2 min). Mixtures were then placed into a die-cast for compression into a pellet. Pellet compression was accomplished using a 4-ton jack. Spectra were collected on an Acton

IR absorption spectrometer and a Brinkmann FT-IR spectrometer. All Raman, FT-IR, and IR spectra were transferred in ASCII format to a personal computer for analysis.

RESULTS & DISCUSSIONS

Figure 1 shows the similarities in the IR spectra of adenine and 2AP, especially in the 2300-3500 cm^{-1} region (intensity differences are primarily due to sample amounts of the two, 4-5 mg adenine vs. 1-2 mg 2AP). However, there is an easily noticeable band at approximately 2360 cm^{-1} in the spectra of 2AP that is mostly missing in that of adenine. Also, the spectrum of 2AP separates into three distinct regions (400-900 cm^{-1} , 1100-1800 cm^{-1} , and 2300-3500 cm^{-1}); adenine, on the other hand, is separated into two regions (500-1700 cm^{-1} and 2300-3500 cm^{-1}). Figure 2 shows the IR spectra of 2AP-rb where the band at 2360 cm^{-1} still exists. 2AP-rb, like adenine, is divided into two separate regions. Its bands within 3100-3500 cm^{-1} are quite similar to both adenine and 2AP, with an added band at 3510 cm^{-1} (2AP-dn was not measured due to the short period of spectrometer availability). Figure 3 shows the FT-IR spectra of adenine and 2AP where the spectra are quite similar throughout to their respective FT-IR spectra. The notable exceptions are that bands of adenine at about 1606 and 1665 cm^{-1} are significantly larger than any others of the spectrum and that the 2360 cm^{-1} band is nearly gone from 2AP (possibly due to data average when converted to ASCII format, which may be indicated by the flatness of some peaks). Figure 4 shows the FT-IR spectrum 2AP-rb, where the noticeable difference between it and its IR spectrum is that the band at 2360 cm^{-1} is no longer visible (again, perhaps due to data averaging). Figure 5 shows the Raman spectra

of adenine and 2ap ($188\text{-}2200\text{ cm}^{-1}$) in crystalline form where both have its most pronounced band near 750 cm^{-1} . It is also quite noticeable that spectra of 2AP has a considerable background. Figure 6 shows the spectra of adenine and 2AP from $2380\text{-}3756\text{ cm}^{-1}$, both with their most pronounced bands in the area of $2960\text{-}3200\text{ cm}^{-1}$. Figure 7 shows the Raman scattering from $188\text{-}3756\text{ cm}^{-1}$ for 2AP-rb where the background is so great that a few bands are seen (unfortunately, the background of 2AP-dn was too luminescent for measurements; data not shown).

Table 1 shows the identification of most of the Raman and IR bands of adenine and the relative band-intensities for $200\text{-}1700\text{ cm}^{-1}$. In this region, the most intense band for Raman is at 721 cm^{-1} (in-plane breathing of C-C and C=N), and for IR the strongest band is at 1598 cm^{-1} . We were able to also assign the following vibrational modes of adenine: mild C-C=C bending at 542 cm^{-1} (IR), N-C=C bending at 621 cm^{-1} (mild IR and weak Raman), C-C and C-N in-plane breathing at 720 cm^{-1} (mild IR and very strong Raman), aromatic ring stretching at 795 cm^{-1} (weak IR and very weak Raman), in-plane skeletal mode at 844 cm^{-1} (weak IR and very weak Raman), N9-H out-of-plane bending at 871 cm^{-1} (weak IR), NH₂ rocking at 904 cm^{-1} (mild IR and very weak Raman), N-C=N bending at 939 cm^{-1} (strong IR and weak Raman), N-C-N bending at 1023 (weak IR and very weak Raman), C-N=C bending and stretching at 1124 (mild IR and weak Raman), CH in-plane bending at 1159 (weak IR and very weak Raman), strong IR C6-NH₂ stretching at 1253 , C-N and C=N stretching at 1307 (very strong IR and weak Raman) and 1332 (strong IR and very strong Raman), mild and weak C-H out-of-plane bending (IR and Raman, respectively) at 1368 , strong and very weak N=CH bending (IR and

Table 1. Raman and infrared absorption band assignments for crystalline adenine 200-1700 cm^{-1} .

solid sample				mode assignments ^h
IR		Raman		
$\nu(\text{cm}^{-1})$	I_{rel}	$\nu(\text{cm}^{-1})$	I_{rel}	
		236	vw	
		326	m	
		533	w	
542	m			C-C=C bending
		556	vw	
622	m	620	w	N-C=C bending
642	m			
723	m	721	vs ^d	C-C, C-N in-plane breathing
797	w	794	vw	aromatic ring stretching
848	w	840	vw	in-plane skeletal mode
871	w			N9-H out-of-plane bending
912	m	896	vw	NH ₂ rocking
939	s	938	w	N-C=N bending
1023	w	1022	vw	N-C-N bending
1125	m	1123	w	C2-N1=C6 bending, C5-N7=C8 stretching
1156	w	1162	vw	CH bending in-plane
1253	s			C-NH ₂ stretching
1309	vs	1306	w	C-N, C=N stretching
1334	s	1331	vs	C-N, C=N stretching
1367	m	1370	w	C8-H, C2-H out-of-plane bending
1419	s	1418	vw	N=CH bending
1450	m			imidazole ring stretching
1469	w			
		1482	m	C6-H deformation
1508	w			C-N9-H bending
1598	vs ^d	1596	vw	
1607	vs	1612	vw	C=N, C=C stretching
1665	vs			NH ₂ scissors
1678	vs	1677	vw	
2600	s	2594	vw	
		2636	vw	
		2664	vw	
2691	s	2692	vw	
		2742	vw	
2792	vs	2784	vw	C-H stretching
		2912	vw	
2950	s			
2983	vs			N9-H stretching

Table 1. (continued)

solid sample				mode assignments ^b
IR		Raman		
$\nu(\text{cm}^{-1})$	I_{ref}	$\nu(\text{cm}^{-1})$	I_{ref}	
		3035	s	
3051	vs ^a			
		3116	vs ^a	NH ₂ anti-symmetric stretching
3161	vs			
3201	s			
3210	s			
3285	vs			
3297	vs	3295	w	NH ₂ symmetric stretching
3309	vs			NH ₂ symmetric stretching
3344				
3354	s	3358	vw	

^a Intensity taken as reference intensity.

^b Assignments based on guidelines in Carey (1982), Fadini & Schnepel (1989), Lin-Vien *et al.* (1991) and comparisons of adenine assignments Mathlouthi *et al.* (1984).

Note. vs - very strong, s - strong, m - mild, w - weak, vw - very weak.

Raman, respectively) at 1418, mild imidazole ring stretching at 1450 (IR), mild C6-H Raman deformation at 1481, weak C-N9-H IR bending at 1508, C=N and C=C stretching at 1609 (very strong IR and very weak Raman), and very strong NH₂ scissors bending at 1665 in the IR. We also assigned C-H stretching at 2788 cm⁻¹ (very strong IR and very weak Raman), very strong N9-H stretching in the IR at 2983, very strong NH₂ anti-symmetric stretching in Raman at 3116, and NH₂ symmetric stretching at 3296 (very strong IR and weak Raman) and 3309 (very strong IR).

In comparison, the assignments for 2AP are similar to those of adenine, where slight shifts in the bands, missing bands, and changes in relative intensities are the differences between 2AP and adenine. In Table 2, we assigned the following modes with the aide of the structure of 2AP (Figure 8): C-C=C bending at 536 cm⁻¹ (weak in both IR

Table 2. Raman and infrared absorption band assignments of crystalline 2AP 200-1800 cm^{-1} .

solid sample				mode assignments ^b
IR		Raman		
$\nu(\text{cm}^{-1})$	I_{rel}	$\nu(\text{cm}^{-1})$	I_{rel}	
		371	w	
		428	w	
445	w			
494	w	494	w	
504	w			
533	w	538	w	C-C=C bending
543	w			
616	m			
631	m	639	w	N-C=C bending
668	m			
744	w			
787	m	792	vs ^d	aromatic ring stretching
799	m			aromatic ring stretching
844	m	840	w	in-plane skeletal mode
872	m			N9-H out-of-plane bending
		896	w	NH ₂ rocking
934	m	930	m	
954	m			N-C=N bending
965	m	968	w	
		1125	w	C2-N1=C6 bending, C5-N7=C8 stretching
1142	m			
1169	w	1170	w	CH in-plane bending
1207	m	1200	w	
1250	s	1255	m	C-NH ₂ stretching
1284	vs	1285	s	
1310	m	1302	s	C-N, C=N stretching
1360	m	1360	m	C8-H, C6-H out-of-plane bending
1402	vs ^d	1402	m	
1428	vs	1425	w	N=CH bending
1452	s			imidazole bending
1491	s	1485	w	C2-H deformation
1511	s	1517	m	C-N9-H bending
1582	vs	1587	w	
1618	vs			C-N, C=C stretching
1649	vs	1639	w	NH ₂ scissors
		1856	w	
		1890	w	
1934	w	1935	w	

Table 2. (continued).

solid sample				mode assignments ^b
IR		Raman		
$\nu(\text{cm}^{-1})$	I_{rel}	$\nu(\text{cm}^{-1})$	I_{rel}	
		1943	w	
2342	s			
2361	s			
2565	s			
2636	s			
2703	s			
2743	s			
2815	s	2819	vw	C-H stretching
		2910	vw	
2929	m			
3011	s	3008	s	N9-H stretching
3024	s	3018	s	
		3036	s	
		3077	vs ^a	
3094	s	3103	s	NH ₂ anti-symmetric stretching
		3153	s	
3184	vs ^a			
		3311	vw	NH ₂ symmetric stretching
3327	s			NH ₂ symmetric stretching
		3379	m	
		3522	m	
		3543	s	

^a Taken as the reference intensity.

^b Assignments based on guidelines in Carey (1982), Fadini & Schnepel (1989), Lin-Vien *et al.* (1991) and comparisons of adenine assignments Mathlouthi *et al.* (1984).

Note. vs - very strong, s - strong, m - mild, w - weak, vw - very weak.

and Raman: mild Raman for adenine). N-C=C bending at 635 (mild IR and weak Raman), aromatic ring stretching at 789 (mild in IR and very strong Raman) and 799 (mild IR, doublet of 789), in-plane skeletal mode at 842 (mild IR and weak Raman), N9-H out-of-plane bending at 872 (mild IR), NH₂ rocking at 896 (weak Raman), N-C=N bending at 954 (mild IR), C-N=C bending and stretching at 1125 (weak Raman), CH in-

plane bending at 1169 (weak IR and Raman bands), C-NH₂ stretching at 1252 (strong IR and mild Raman), C-N and C=N stretching at 1306 (mild IR and strong Raman), C-H out-of-plane bending at 1360 (mild IR and Raman), N=CH bending at 1427 (very strong IR and mild Raman), imidazole bending at 1452 (strong IR), C-N9-H bending at 1514 (strong IR and mild Raman), NH₂ scissors at 1644 (very strong IR and weak Raman), C-H stretching at 2815 (strong IR and very weak Raman). In Table 3, we assigned N9-H stretching at 3009 (strong IR and Raman), NH₂ anti-symmetric stretching at 3099 (strong IR and Raman), and NH₂ symmetric stretching at 3310 (very weak Raman), and 3327 (very strong IR).

As Tables 3 and 4 show, the bands for 2AP-rb (structure in Figure 9) are listed according to those previously assigned to 2AP and those assigned to the ribose ring (Mathlouthi & Seuvre, 1983). As indicated, most of the ribose ring vibrational modes are within the 880-1100 cm⁻¹ range, which agrees with the findings of others (Mathlouthi & Seuvre, 1983). We, however, were able to assign only a few (due to large background) of the IR vibrational modes: O-C1'-H1' bending at 653 cm⁻¹, C-C-H stretching at 940, C-O-H bending at 1047, N9-C1'-H1' (connective bond between 2AP and ribose ring; see Figure 9) bending at 1062, CH₂ bending at 1329, C-H stretching at 2859, and CH₂ stretching at 2897.

Upon comparison to one another, it is clear that a few of the IR and Raman bands are distinctive to 2AP and not adenine. For instance, there are two IR and two Raman bands in the 400-505 cm⁻¹ region (445, 494 cm⁻¹ and 428, 494 cm⁻¹, respectively) that belong only to 2AP. At the same time, aromatic ring stretching is strongest for 2AP at

Table 3. Raman and infrared absorption band assignments of crystalline 2AP-rb.

solid sample				mode assignments ^b
IR		Raman		
$\nu(\text{cm}^{-1})$	I_{rel}	$\nu(\text{cm}^{-1})$	I_{rel}	
410	w			
436	vw			2AP
452	vw			2AP
		492	w	2AP
		536	w	2AP
576	w			
617	w	627	w	2AP
634	m			2AP
653	w			R. O-C1'-H1' bending
668	w			2AP
748	w			2AP
796	w	788	vs ^a	2AP
		855	w	
881	w			2AP
895	vw			R
940	vw			2AP
989	w			R. C-C-H stretching
1047	w			R. C-OH bending
1062	m			R. N9-C1'-H1' bending
1083	w			R
1103	vs			2AP
1117	m			2AP
1138	w			2AP
1199	w			2AP
1224	m			2AP
1246	vw			2AP
1275	w			R
1294	m	1292	m	2AP
		1329	s	R. CH ₂ bending
1350	w			2AP
1368	w			2AP
1390	w			R
1399	w			2AP
1435	vs			2AP
1479	m			2AP
1521	m	1513	m	2AP

Table 3. (continued).

solid sample				mode assignments ^b
IR		Raman		
$\nu(\text{cm}^{-1})$	I_{rel}	$\nu(\text{cm}^{-1})$	I_{rel}	
1586	vs ^a			2AP
1614	vs	1617	m	2AP
1646	vs			2AP

^a Taken as the reference intensity.

^b Assignments based on comparisons of 2AP and ribose assignments Mathlouthi & Seuvre (1983).

Note. vs, very strong; s, strong; m, mild; w, weak; vw, very weak; R, ribose ring; 2AP, 2-aminopurine

792 cm^{-1} in the Raman spectra. In the 1850-1950 cm^{-1} region, there are four Raman bands (1856, 1889, 1935, and 1943) and one IR band (1934) that are present in only 2AP, whereas, there are two strong vibrational modes exhibited by 2AP in the IR region 2340-2360 cm^{-1} (2342 and 2361) that are not seen with adenine.

With the attachment of ribose to 2AP (2AP-rb), these distinctive bands change somewhat. In the 400-505 cm^{-1} region, only three distinct bands remain: two IR band (410 and 452) and one Raman (492). There are two new distinct bands in the 850-900 cm^{-1} , one IR (895) and one Raman (855). The IR spectrum of 2AP-rb also exhibit further distinction in the 1700-1790 cm^{-1} range with 2 bands (1700 and 1782), and in the 2725-2900 cm^{-1} with three (2725, 2764, and 2891). Also, the most intense band for 2AP-rb is at 1586 cm^{-1} for the IR spectrum (not at 1402 as for 2AP), and at 788 for the Raman (792 for 2AP). Compared to adenosine (Mathlouthi *et al.*, 1984), the distinguishing IR bands for 2AP-rb become 410, 436, 452, 576, 618, 1274, 1700, 1782, 2341, 2360, 2764, 2891, 3191, 3225, and 3478.

Table 4. Raman and Infrared Absorption Band Assignments of 2AP-rb 2000-3800 cm^{-1} .

solid sample				mode assignments ^b
IR		Raman		
$\nu(\text{cm}^{-1})$	I_{ref}	$\nu(\text{cm}^{-1})$	I_{ref}	
1700	w			
1782	vw			
2341	vw			2AP
2360	w			2AP
2725	w			
2764	w			
2859	w			R. CH stretching
2891	w	2897	m	R. CH ₂ stretching
2936	m	2926	vs	2AP
		2948	vs ^a	
3191	vs			2AP. IR only
3225	vs			
3331	vs ^a			2AP. IR only
3478	vs			

^a Taken as the reference intensity.

^b Assignments based on comparisons of 2AP and ribose assignments Mathlouthi & Seuvre (1983).

Note: vs, very strong; s, strong; m, mild; w, weak; vw, very weak; 2AP, 2-aminopuine; R, ribose.

When comparing IR to FT-IR bands of each sample (adenine, 2AP, and 2AP-rb), it is clear that all bands are not consistent between the two methods. As Table 5 shows, the bands that distinguish 2AP and 2AP-rb from adenine and adenosine are fewer in FT-IR bands. For 2AP, those bands that are not in the FT-IR are 494, 1935, and 2342. For 2AP-rb, FT-IR bands at 576, 1700, 1782, and 2725 are missing; however, the 576 band is replaced by one at 505. Bands such as this that appear in FT-IR spectra but not in IR may be explained by IR emission by the sample that is received and modulated by the

Table 5. Comparison of IR and FT-IR bands of crystalline adenine, 2AP, and 2AP-rb.

Adenine		2AP		2AP-rb	
IR	FT-IR	IR	FT-IR	IR	FT-IR
				410	407
		445	443	436	
				452	451
		494			
		504	503		505
		533			
542	542	543	542		
				576	
622	621	616	615	617	617
		631	633	634	634
642	646			653	652
		668	667	668	
	692		694		698
723	723				
		744	742	748	748
		787			
797	796	799	798	796	795
848	847	844	843		
871		872	868		
				881	881
				895	953
912	912				
939	939	934	935	940	
		954	953	989	989
		965	968		
1023	1022				
				1047	
				1062	1063
				1083	1084
				1103	1104
				1117	
1125	1124		1126		
		1142	1142	1138	1138
1156	1153				
		1169		1199	1198
		1207	1201		
				1224	1223
1253	1254	1250	1250	1246	1246

Table 5. (continued).

Adenine		2AP		2AP-rb	
IR	FT-IR	IR	FT-IR	IR	FT-IR
				1275	1275
		1284	1284		
				1294	1294
1309	1308	1310	1306		
1334	1333				
		1360	1362	1350	1348
1367	1365			1368	1369
				1390	1390
		1402	1402	1399	1398
1419	1419				
		1428	1427	1435	1435
1450	1450	1452	1452	1479	1479
1469					
		1491	1487		
1508	1504	1511	1510		
				1521	1520
		1582	1581	1586	1587
1598					
1607	1604				
		1618	1620	1614	1614
		1649	1649	1646	1645
1665	1670	1934			
1678					
				1700	1699
				1782	1782
		2342		2341	
		2361	2364	2360	
		2565			
2600	2600				
			2636		
2691	2690				
				2725	
2792	2800			2764	
			2814		
				2859	
				2891	2891
			2922		
				2936	2935
2950					

Table 5. (continued).

Adenine		2AP		2AP-rb	
IR	FT-IR	IR	FT-IR	IR	FT-IR
2983	2980		3026		
3051			3095		
	3122				
3161					
			3180		
3201				3191	
3210					
				3225	3224
3285					
3297					
3309	3305				
			3327	3331	3329
3344					
3354					
			3377		
				3478	3479

interferometer and sent back to the sample. However, it is not clear what causes IR bands to not appear in FT-IR spectra.

From the solution samples of 2AP-dn and 2AP-rb, we were able to obtain only a few Raman bands because fluorescence continued to provide a large background in region of 200-2300 cm^{-1} , just as was the case for crystalline samples: water vibrations are the only discernible modes over the fluorescent background in the area of 2400-3800 cm^{-1} (Figure 10, 11, and 12). As Table 6 shows, we were able to assign the vibrational modes for 2AP-dn and 2AP-rb in solution to bands that 2AP and ribose exhibited. The two exceptions are the 862 cm^{-1} band (distinction band) for vertically polarization of 2AP-rb, and the bands for 2AP-dn and 2AP-rb near 1620 cm^{-1} . Because of the broadness

Table 6. Raman band assignments for 2AP-dn and 2AP-rb in solution.

	Raman solution samples				mode assignments ^a
	2AP-dn		2AP-rb		
vertically polarized ^b	$\nu(\text{cm}^{-1})$	I_{ref}	$\nu(\text{cm}^{-1})$	I_{ref}	
	801	s	794.21	vs	2AP
			861.51	m	
			1298.34	vs	2AP
	1333	m	1339.11	vs ^c	R. CH ₂ wagging
	1517	s	1515.04	vs	2AP
	1628	vs ^c	1622.04	vs	H ₂ O bending
horizontally polarized ^b	^d		799	vs	2AP
			1275	w	2AP
			1298	m	2AP
			1339	m	R. CH ₂ wagging
			1517	m	2AP
			1625	vs ^c	H ₂ O bending

^a Assignments based on previous assignments of 2AP and ribose (Mathlouthi & Seuvre, 1983).

^b Horizontal and vertical polarization were used in this case because only the asymmetric stretching of H₂O was exhibited in the spectra of 2AP-dn.

^c Intensity used as reference.

^d Background fluorescence too large to distinguish any actual peak.

Note: vs. very strong; s. strong; m. mild; w. weak; vw. very weak; 2AP, 2-aminopuine; R. ribose.

of this band and the fact that hydrogen bonding is known to cause a shift to lower frequencies (Lin-Vien *et al.*, 1991), we assigned this band to water where it hydrogen bonds to 2AP (Evans *et al.*, 1992).

CONCLUSIONS

From our FT-IR, IR, and Raman spectroscopic studies, we have been able to assign most of the vibrational bands that 2AP, 2AP-dn, and 2AP-rb exhibit. From these vibrational spectra we have shown that the small structural change in adenine, where the NH_2 is moved from the 6-position to the 2-position to create 2AP, produces considerably different vibrational bands between adenine and 2AP. For instance, IR absorption of 2AP exhibits distinct vibrational bands at 445, 494, 1935, 2342, and 2361 cm^{-1} . In the case of 2AP-rb, the distinct IR vibrational bands are at 410, 436, 452, 575, 618, 895, 1274, 1700, 1782, 2341, 2360, 2725, 2764, 2891, 3191, 3225, and 3478 cm^{-1} , the most distinctive being 2360. When FT-IR was used, the distinctive vibrational bands were reduced, but still numerous. With Raman, these distinctions were further reduced to a few bands, two bands in the 420-500 cm^{-1} region and four in 1850-1945 cm^{-1} region for 2AP: the bands are only at 492 and 855 for crystalline 2AP-rb, and 862 for 2AP-rb in solution. With such bands being distinctive to 2AP, it is our contention that vibrational spectroscopy will prove to be another excellent monitor of 2AP independent of other nucleic acids.

REFERENCES

- Allan, B. W., & Reich, N. O. (1996) *Biochemistry* 35, 14757-14762.
- Bjornson, K. P., Moore, K. J., & Lohman, T. M. (1996) *Biochemistry* 35, 2268-22682.
- Bloom, L. B., Otto, M. R., Eritja, R., Reha-Grantz, L. J., Goodman, M. F., & Beechem, J. M. (1994) *Biochemistry* 33, 7576-7586.
- Brahms, S., & Brahms, J. G. (1990) *Nucleic Acids Res.* 18, 1559-1564.

- Britton, K. A., Dalterio, R. A., Nelson, W. H., Britt, D., & Sperry, J. F. (1988) *Appl. Spectrosc.* 42, 782-788.
- Carey, P. R. (1982) in *Biochemical Applications of Raman and Resonance Raman Spectroscopies*, pp 1-70, 184-207, Academic Press, New York.
- Evans, K., Xu, D.-G., Kim, Y.-S., & Nordlund, T. M. (1992) *Journal of Fluorescence* 2, 209-216.
- Fadini, A., & Schnepel, F.-M. (1989) in *Vibrational Spectroscopy: Methods and Applications*, pp 1-205, John Wiley & Sons, New York.
- Florian, J., & Leszczynski, J. (1995) *Int. J. Quantum Chem., Quantum Biol. Symp.* 22, 207-225.
- Gfroerer, A., Schnetter, M. E., Wolfrum, J., & Greulich, K. O. (1991) *Ber. Bunsen-Ges. Phys. Chem.* 95, 824-833.
- Gfroerer, A., Schnetter, M. E., Wolfrum, J., & Greulich, K. O. (1993) *Ber. Bunsen-Ges. Phys. Chem.* 97, 155-162.
- Govorun, D. N., Mishchuk, Y. R., & Zheltovskii, N. V. (1991) *Biopolim. Kletka* 7, 55-62.
- Hochstrasser, R. A., Carver, T. E., Sowers, L. C., & Millar, D. P. (1994) *Biochemistry* 33, 11971-11979.
- Katahira, M., Lee, S. J., Kobayashi, Y., Sugeta, H., Kyogoku, Y., Iwai, S., Ohtsuka, E., Benevides, J. M., & Thomas, G. J., Jr. (1990) *J. Am. Chem. Soc.* 112, 4508-4512.
- Lamba, O. P., Wang, A. H. J., & Thomas, G. J., Jr. (1989) *Biopolymers* 28, 667-678.
- Lin-Vien, D., Colthup, N. B., Fateley, W. G., & Grasselli, J. G. (1991) in *The Handbook of Infrared and Raman Characteristic Frequencies of Organic Molecules*, pp 1-503, Academic Press, Inc., Boston, MA.
- Mathlouthi, M., & Seuvre, A. M. (1983) *Carbohydrate Research* 122, 31-47.
- Mathlouthi, M., Seuvre, A. M., & Koenig, J. L. (1984) *Carbohydr. Res.* 131, 1-15.
- Nordlund, T. M., Xu, D., & Evans, K. O. (1993) *Biochemistry* 32, 12090-12095.
- Raney, K. D., Sowers, L. C., Millar, D. P., & Benkovic, S. J. (1994) *Proceedings of the National Academy of Science of the USA* 91, 6644-6648.

Spiro, T. G. (1987) *Biological Applications of Raman Spectroscopy, V. 1: Raman Spectra and the Conformations of Biological Macromolecules*, pp 81-134. John Wiley & Sons, New York.

Tsuboi, M., Ueda, T., Ushizawa, K., & Nagashima, N. (1995) *J. Raman Spectrosc.* 26, 745-749.

Xu, D., Evans, K. O., & Nordlund, T. M. (1994) *Biochemistry* 33, 9592-9599.

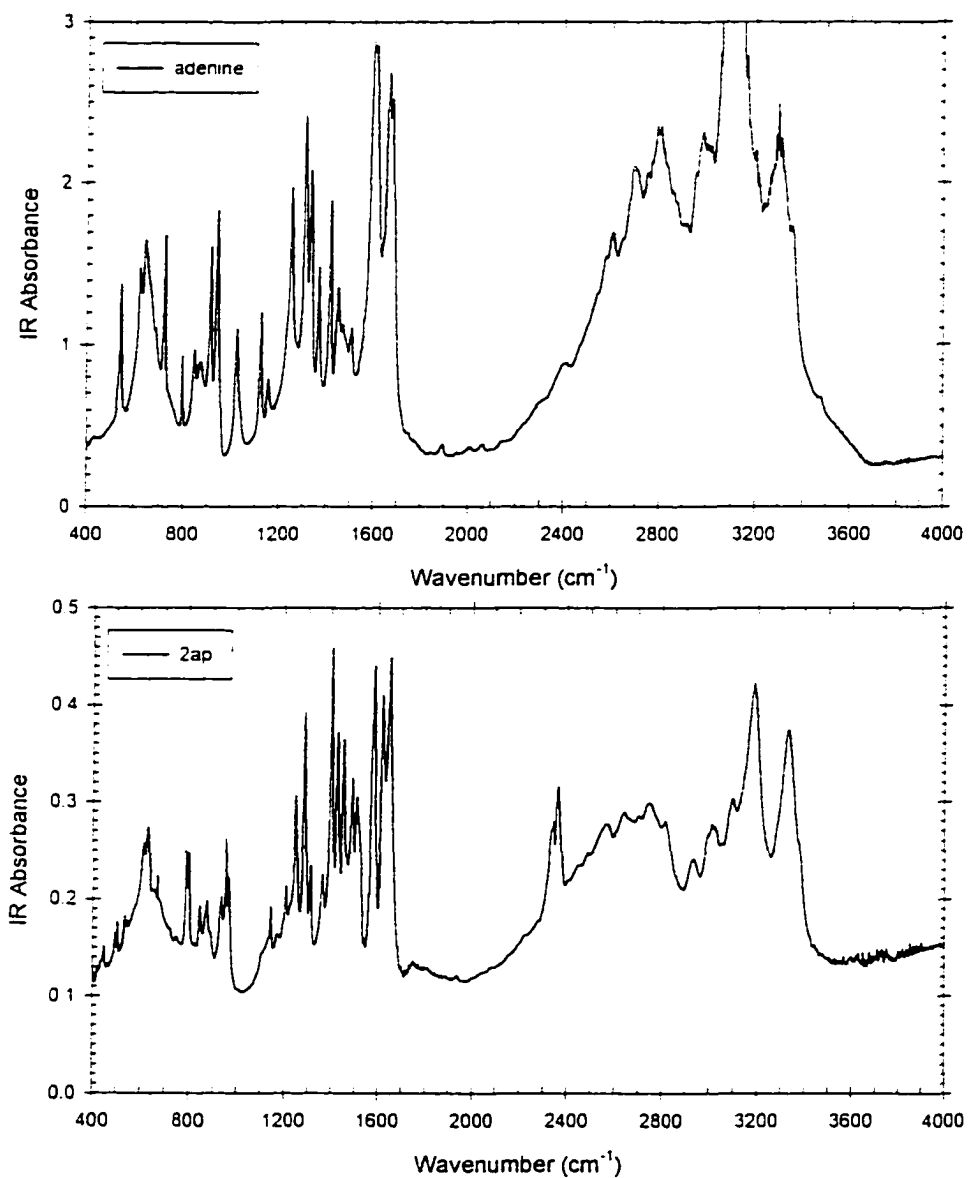


Figure 1: IR spectra of crystalline adenine (upper) and 2AP (lower). Samples were mixed with 100-120 mg of KBr to form a pellet for spectral measurements.

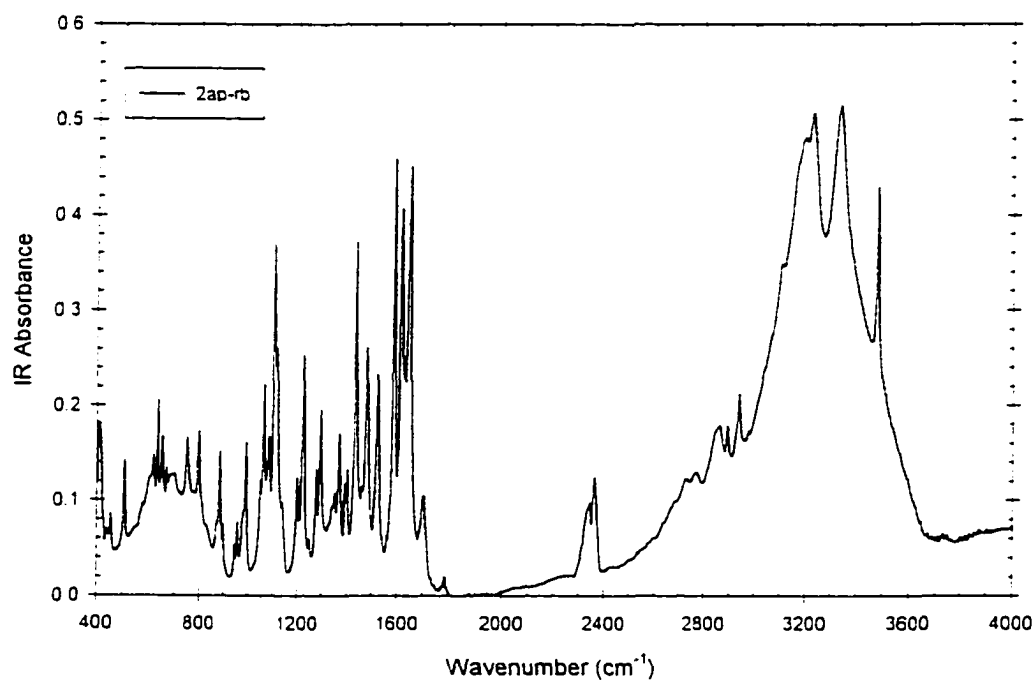


Figure 2: IR spectra of crystalline 2AP-rb. Samples were mixed with 100-120 mg of KBr to form a pellet for spectral measurements.

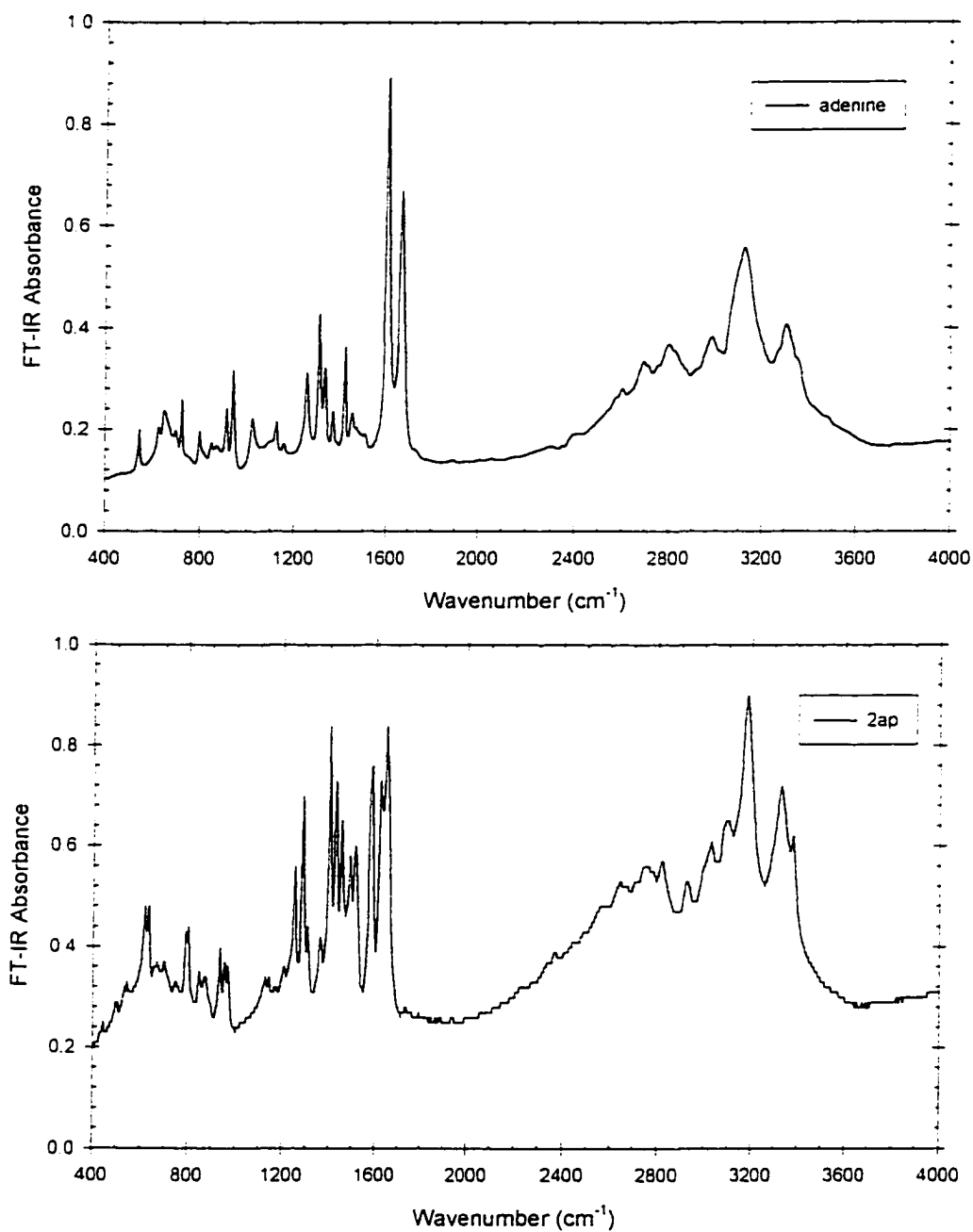


Figure 3: FT-IR spectra of crystalline adenine and 2AP.

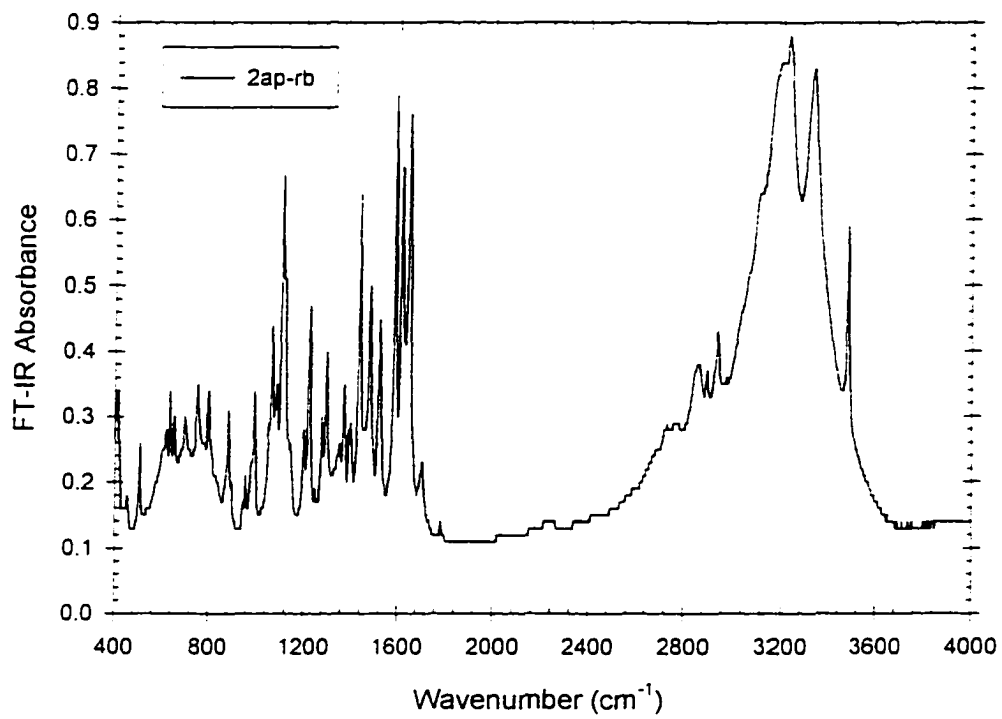


Figure 4: FT-IR spectra of crystalline adenosine and 2AP-rb.

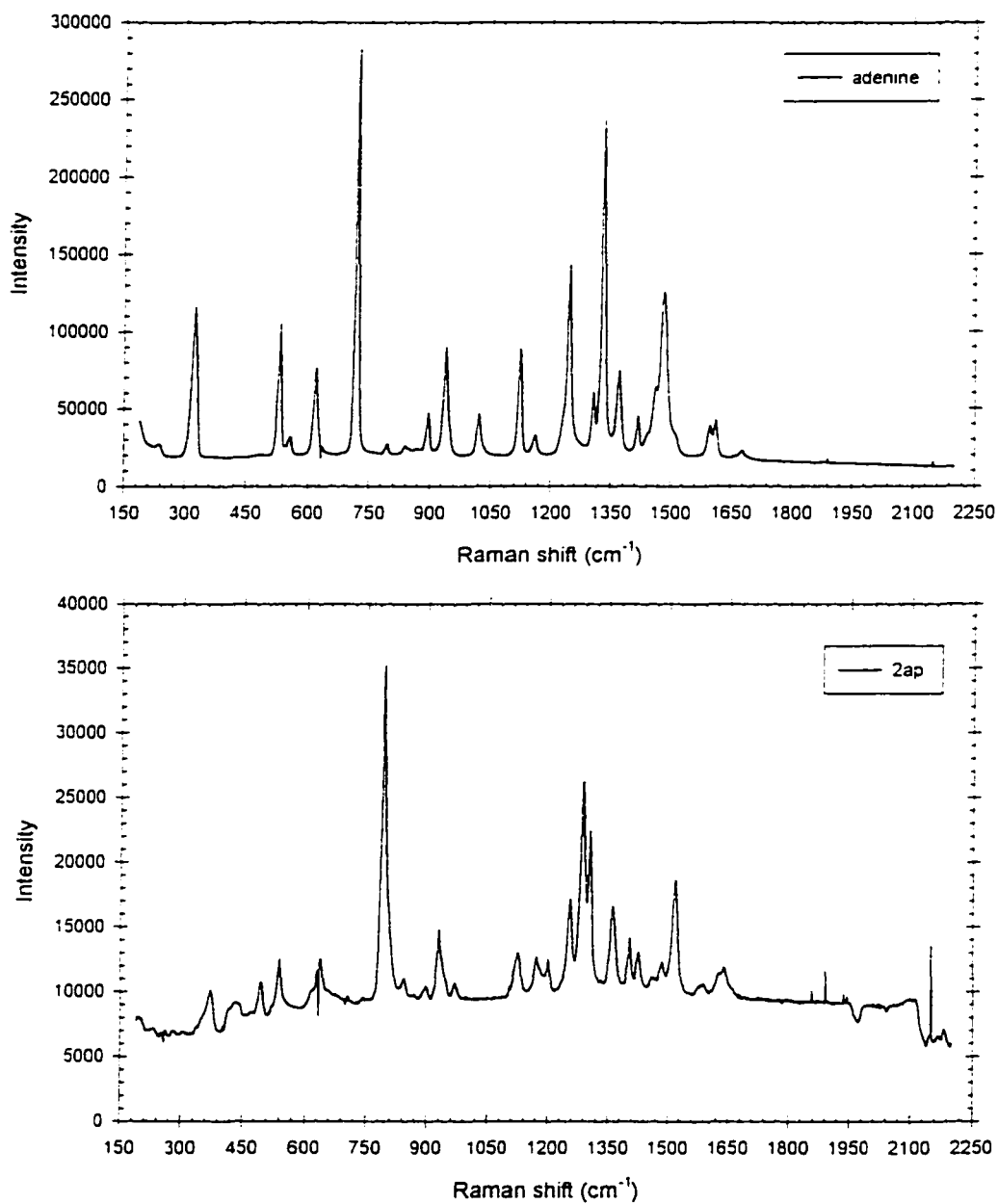


Figure 5: Laser-Raman spectra (188-2200 cm⁻¹) of crystalline adenine (upper) and 2AP (lower) free bases.

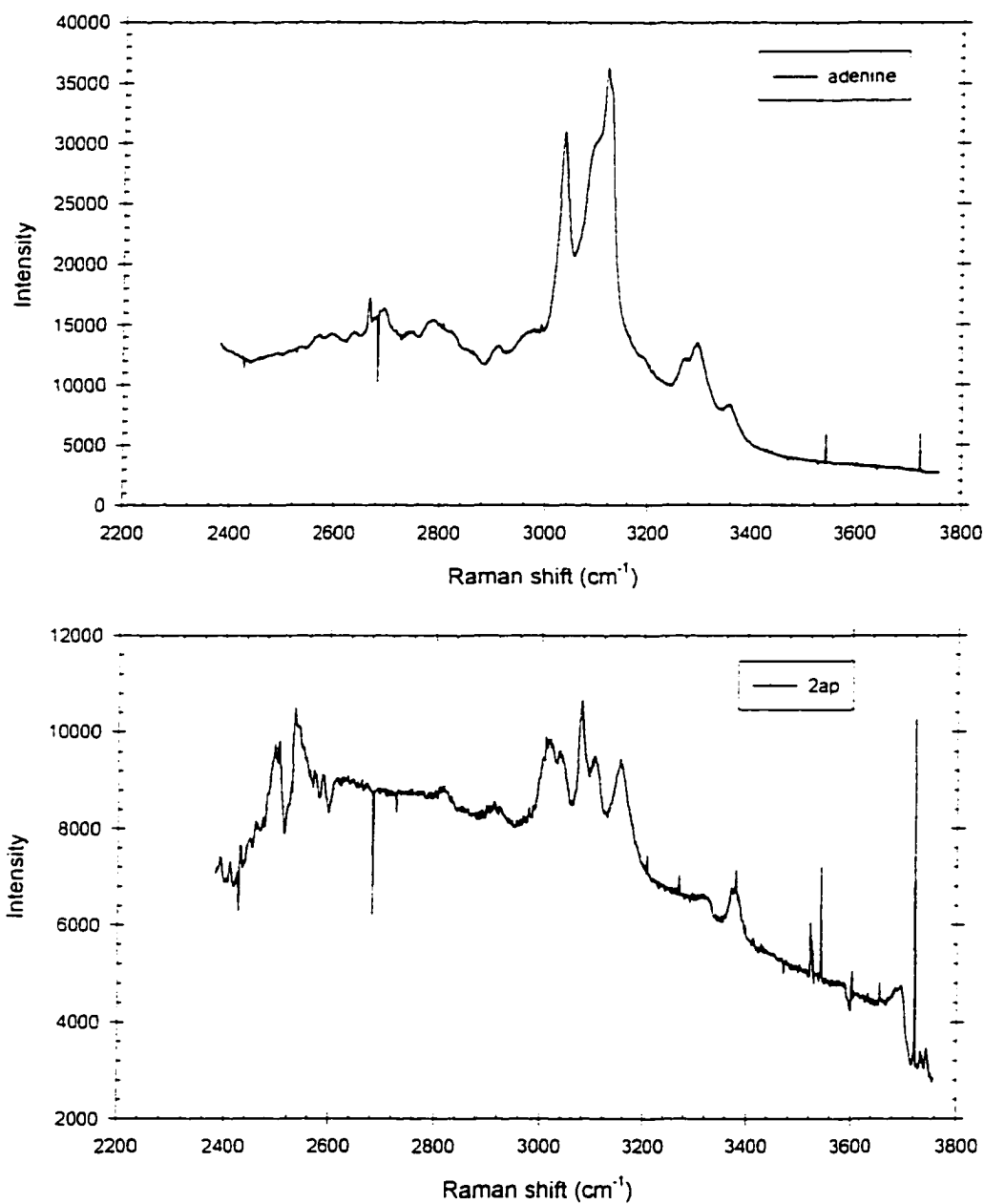


Figure 6: Laser-Raman spectra ($2380\text{-}3800\text{ cm}^{-1}$) of crystalline adenine (upper) and 2AP (lower) free bases.

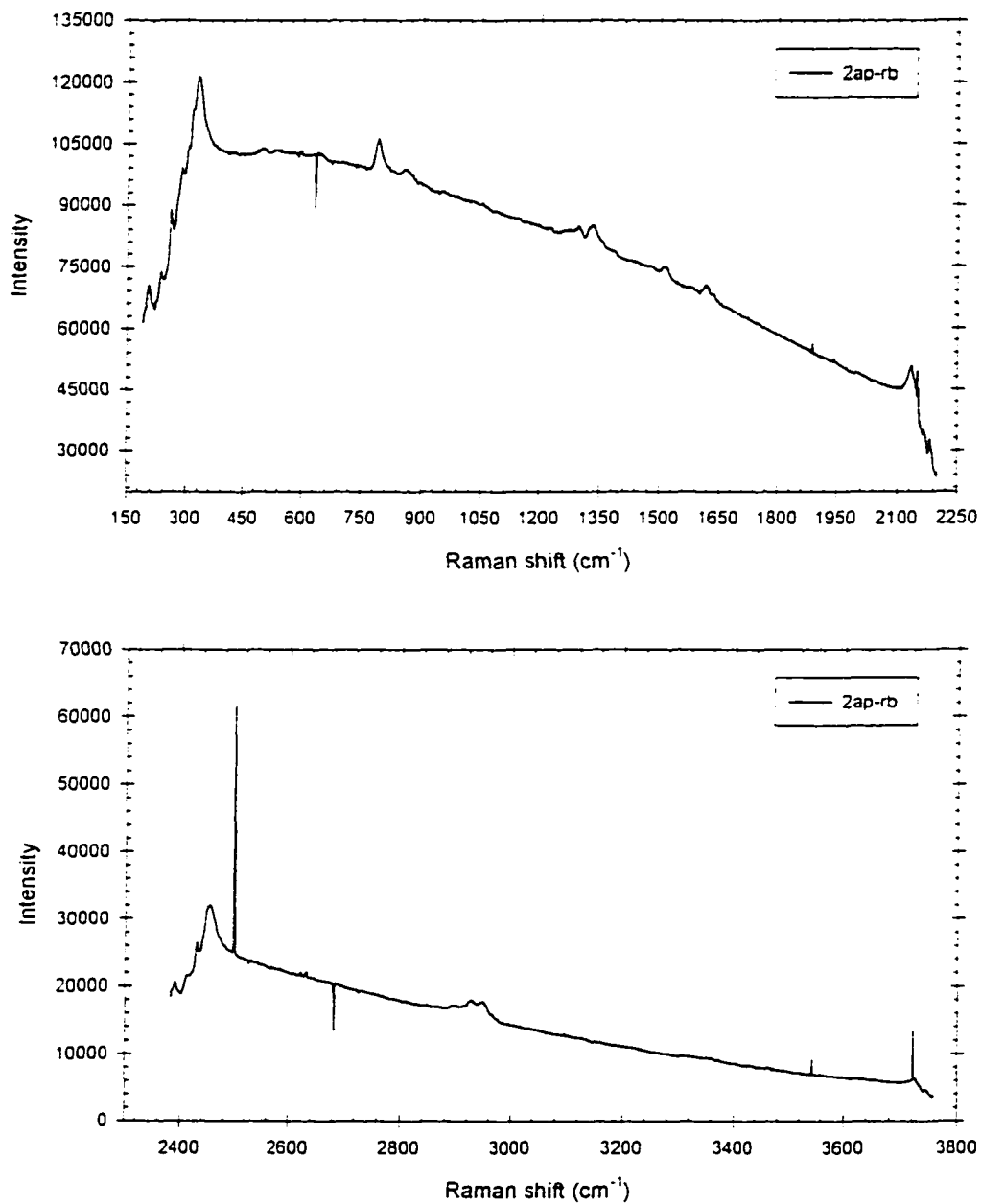


Figure 7: Laser-Raman spectra of crystalline 2AP-rb, 188-2200 cm⁻¹ (upper) and 2300-3800 cm⁻¹ (lower).

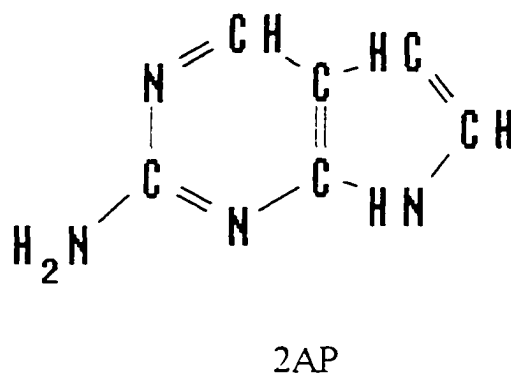
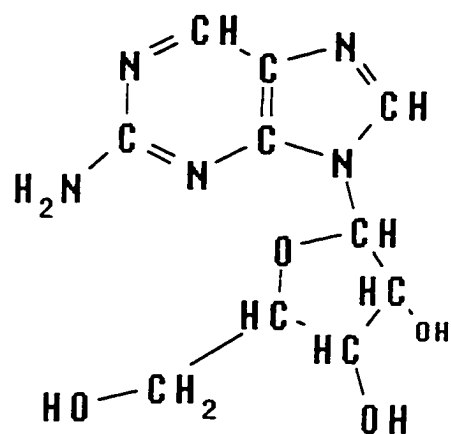


Figure 8: Molecular structure of 2AP used to assign vibrational modes.



2AP-rb

Figure 9: Molecular structure of 2AP-rb.

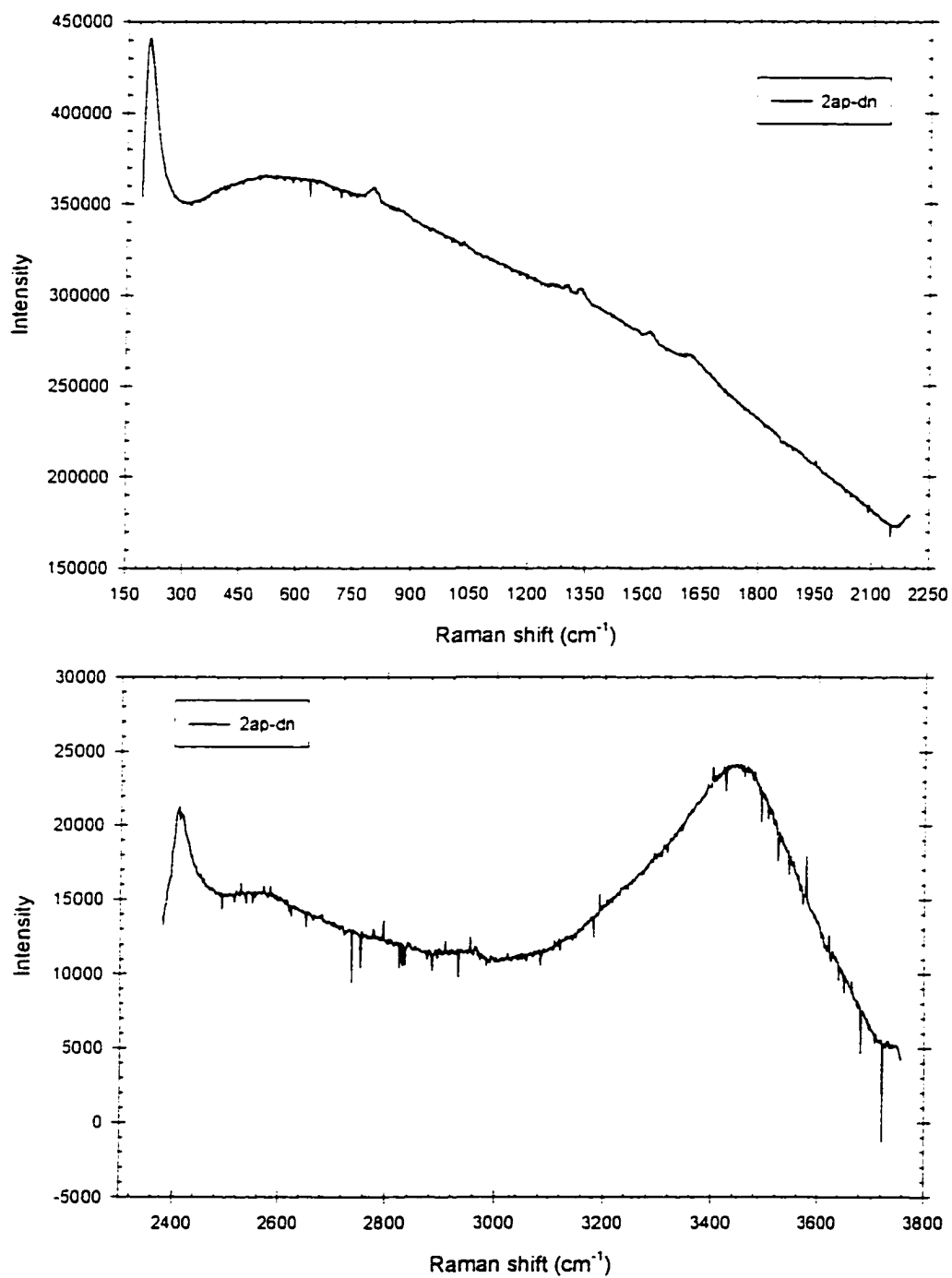


Figure 10: Vertically polarized Raman spectra of 2AP-dn in solution, 200-2300 cm⁻¹ (upper), 2400-3800 cm⁻¹ (lower).

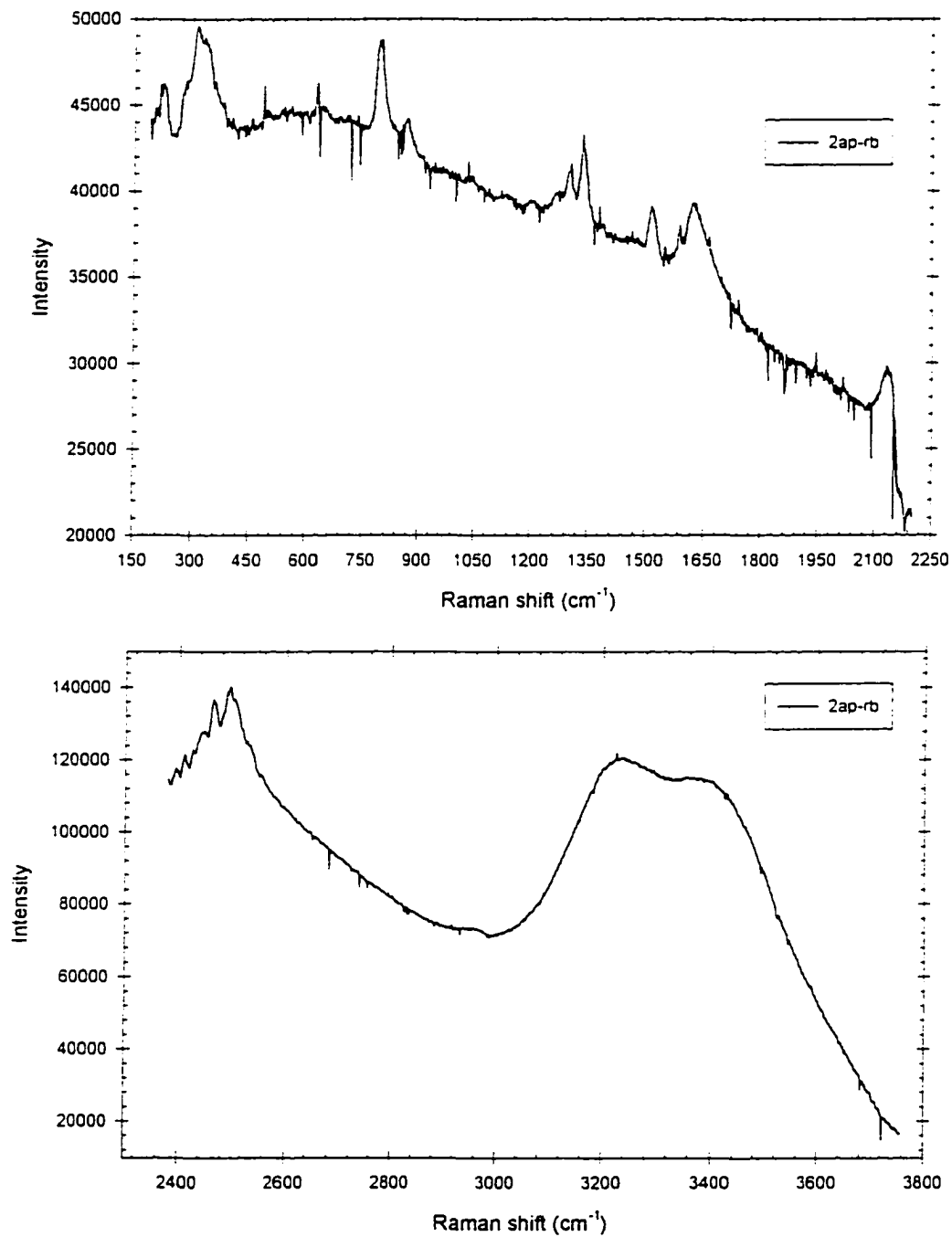


Figure 11: Vertically polarized Raman spectra of 2AP-rb in solution, 200-2300 cm⁻¹ (upper), 2400-3800 cm⁻¹ (lower).

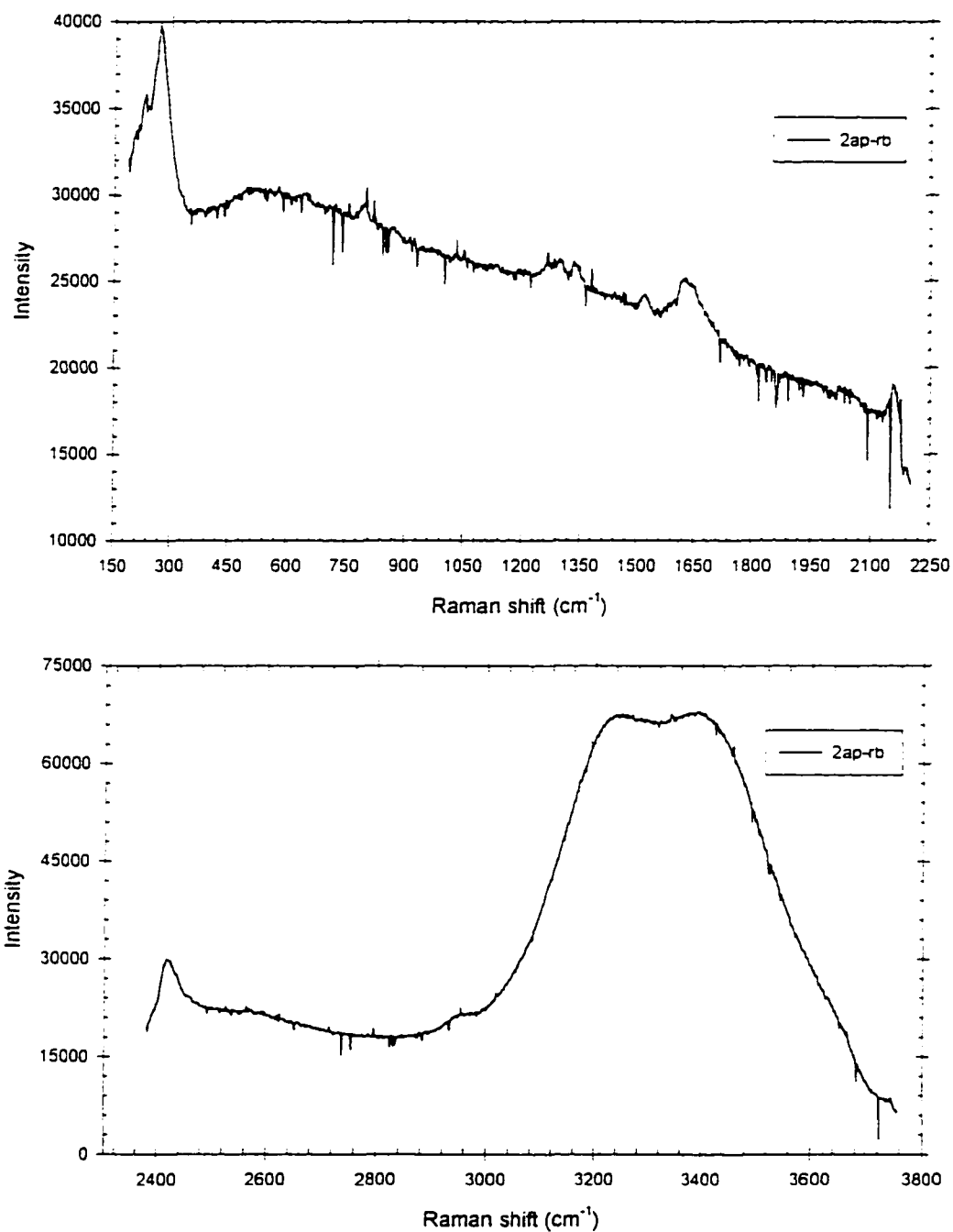


Figure 12: Horizontally polarized Raman spectra of 2AP-rb in solution, 200-2300 cm⁻¹ (upper), 2400-3800 cm⁻¹ (lower).

GENERAL CONCLUSIONS

The overall goal of this study was to try to characterize the spectroscopic measurements of 2AP in terms of specific structures. In the first paper of this dissertation, we studied the time-resolved fluorescence of 2AP as a free base, mononucleoside (2AP-dn), and as part of short oligonucleotides (2AP-T, A-2AP-T, G-2AP-C and C-2AP-G). We were able to show that the fluorescence lifetime of the free base and mononucleoside are single exponential. This characterizes one state in solution. However, NMR measurements indicated two structural states (*syn* and *anti* conformations) for 2AP-dn (in DMSO). Once another base was attached to 2AP, the fluorescence lifetime became triple exponential, suggesting three independent states. We characterized these states as fully stacked, partially stacked, and unstacked, with enthalpy differences in good agreement with other findings of stacking enthalpies for nucleotide.

We found stacking to have a minimum effect on the fluorescence lifetime when only one base was attached to 2AP (thymine in the 3'-position). Upon the addition of adenine in the 5'-position, the fluorescence lifetime of 2AP was significantly reduced, suggesting strong stacking interaction between adenine and 2AP. When guanine and cytosine both were inserted as the two neighboring bases (either at the 5'- or 3'-position) the fluorescence lifetime of 2AP was only slightly reduced from the free base. This further implies that adenine has the strongest stacking effect on the fluorescence of 2AP. However, enthalpy differences are greater between the fully stacked and unstacked states

of 2AP when guanine and cytosine are both the neighboring bases, the largest enthalpic change occurring when guanine is in the 5'-position and cytosine is in the 3'-position. We believe that this can be explained by possible H-bonding between the O6 of guanine and the NH₂ of 2AP.

Our goal in the second paper was to identify distinguishing vibrational bands of 2AP that allowed independent monitoring of 2AP using IR and Raman spectroscopy. From those studies, we found that the subtle physical change in adenine that creates 2AP (moving NH₂ from the 6-position for adenine to the 2-position to get 2AP) not only creates a more highly fluorescent species (the fluorescence of 2AP is 1000 times longer than that of adenine), but also creates a considerably different set of vibrational bands between the two (although the region where the bands appear is about the same, 400-1800 cm⁻¹ and 2300-3500 cm⁻¹ for both adenine and 2AP). Of this different set of vibrational bands, those for 2AP at 445, 494, 1935, 2342, and 2361 cm⁻¹ and those for 2AP-rb at 410, 436, 452, 575, 618, 895, 1274, 1700, 1782, 2341, 2360, 2725, 2764, 3191, 3225, and 3478 cm⁻¹ in the IR may prove useful in independently monitoring the 2AP; using FT-IR reduced these bands such that those at 494, 1935, and 2342 cm⁻¹ were missing for 2AP and those at 576, 1700, 1782, and 2725 cm⁻¹ were missing for 2AP-rb. Using Raman spectroscopy, we found bands that distinguish 2AP from adenine to be in the 420-500 and 1850-1945 cm⁻¹ regions; distinctive bands for 2AP-rb were at 492 and 855 cm⁻¹ (only 862 in solution). These distinguishing vibrational characteristics of 2AP may prove to be an excellent aid in monitoring 2AP through another optical spectroscopic method.

GENERAL LIST OF REFERENCES

- Alpert, N. L., Keiser, W. E., & Szymanski, H. A. (1970) in *IR: Theory and Practice of Infrared Spectroscopy*, 2nd ed., pp 99-103. Plenum Press, New York.
- Baker, B. M., Vanderkooi, J., & Kallenbach, N. R. (1978) *Biopolymers* 17, 1361-1372.
- Ballini, J.-P., Daniels, M., & Vigny, P. (1988) *European Biophysical Journal* 16, 131-142.
- Bertini, I., Molinari, H., & Niccolai, N. (1991) in *NMR and Biomolecular Structure*, pp 1-60, 113-140. VCH Verlagsgesellschaft Publishers, New York.
- Bloom, L. B., Otto, M. R., Beechem, J. M., & Goodman, M. F. (1993) *Biochemistry* 32, 11247-11258.
- Breslauer, K. J., & Sturtevant, J. M. (1977) *Biophysical Chemistry* 7, 205-209.
- Cantor, C. R., & Schimmel, P. R. (1980) in *Biophysical Chemistry, part II: Techniques for the Study of Biological Structure and Function, Vol. II*, pp 433-538. W.H. Freeman and Company, San Francisco.
- Chan, S. S., Austin, R. H., Mukerji, I., & Spiro, T. G. (1997) *Biophysical Journal* 72, 1512-1520.
- Chan, S. S., Breslauer, K. J., Hogan, M. E., Kessler, D. J., & Austin, R. H. (1990) *Biochemistry* 29, 6161-6171.
- Chen, Y. Z., Feng, Y., & Prohofsky, E. W. (1991a) *Biopolymers* 31, 139-148.
- Chen, Y. Z., Zuang, W., & Prohofsky, E. W. (1991b) *Biopolymers* 31, 1273-1281.
- Colthup, N. B., Daly, L. H., & Wiberley, S. E. (1964) in *Introduction to Infrared and Raman Spectroscopy*, pp 1-484, Academic Press, New York.
- Evans, K., Xu, D.-G., Kim, Y.-S., & Nordlund, T. M. (1992) *Journal of Fluorescence* 2, 209-216.

- Evans, K. O. (1996). MS thesis in *Physics*, University of Alabama-Birmingham, Birmingham.
- Frederick, C. A., Grable, J., Melia, M., Samadzi, C., & Jen-Jacobson, L. (1984) *Nature* 309, 327-331.
- Friebolin, H. (1991) in *Basic One- and Two-Dimensional NMR Spectroscopy*, pp 1-384, VCH Verlagsgesellschaft, Weinheim, Federal Republic of Germany.
- Gardiner, D. J., & Graves, P. R. (1989) in *Practical Raman Spectroscopy*, pp 1-53, Springer-Verlag, Berlin.
- Georghiou, S., Nordlund, T. M., & Saim, A. M. (1985) *Photochemistry and Photobiology* 41, 209-212.
- Graslund, A., Claesens, F., McLaughlin, L. W., Lycksell, P. O., Larson, U., & Rigler, R. (1987) in *Structure, Dynamics and Function of Biomolecules*, pp 201-207, Springer-Verlag, Berlin.
- Gueron, M., Eisinger, J., & Lamola, A. A. (1974) in *Basic Principles in Nucleic Acid Chemistry, Vol. 1*, pp 311-398, Academic Press, New York.
- Gueron, M., Kochoyan, M., & Leroy, J. L. (1986) in *Structure, Dynamics and Function of Biomolecules*, pp 197-200, Springer-Verlag, Heidelberg.
- Hager, P. W., Reich, N. O., Day, J. P., Coche, T. G., & Boyer, H. W. (1990) *Journal of Biological Chemistry* 265, 21520-21526.
- Hogan, M. E., & Austin, R. H. (1987) *Nature* 329, 263-266.
- Kahn, J. D., Yun, E., & Crothers, D. M. (1994) *Nature* 368, 163-166.
- Kim, Y., Grable, J. C., Love, R., Greene, P. J., & Rosenberg, J. M. (1990) *Science* 249, 1307-1309.
- Lakowicz, J. R. (1983) in *Principles of Fluorescence Spectroscopy*, pp 1-496, Plenum Press, New York.
- Lakowicz, J. R. (1991) in *Topics in Fluorescence Spectroscopy*, pp 1-432, Plenum Press, New York.
- Lee, C.-H., & Tinoco, I. (1977) *Biochemistry* 16, 5403-5414.
- Lycksell, P. O., Graslund, A., Claesens, F., McLaughlin, L. W., & Larson, U. (1987) *Nucleic Acids Research* 15, 9011-9025.

- Macomber, R. S. (1988) in *NMR Spectroscopy: Basic Principles and Applications*, pp 1-209, Harcourt Brace Jovanovich, San Diego, New York, London.
- McClarlin, J. A., Frederick, C. A., Wang, B. C., Greene, P., Boyer, H. W., Grable, J., & Rosenberg, J. M. (1986) *Science* 234, 1526-1541.
- McLaughlin, L. W., Benseler, F., Graser, E., Piel, N., & Scholtissek, S. (1987) *Biochemistry* 26, 7238-7245.
- Millar, D. P., & Sowers, L. C. (1990) in *Proceedings of SPIE International Conference of Optical Engineers 1204*, 656-662.
- Nordlund, T. M. (1988) in *Proceedings of SPIE International Society of Optical Engineers 909*, 35-50.
- Nordlund, T. M., Anderson, S., Nilsson, L., Rigler, R., & Graslund, A. (1989) *Biochemistry* 28, 9095-9103.
- Powell, J. T., Richards, E. G., & Gratzel, W. B. (1972) *Biopolymers* 2, 235-250.
- Ramstein, J., & Lavery, R. (1988) *Proceedings of the National Academy of Science of the USA* 85, 7231-7235.
- Raney, K. D., Sowers, L. C., Millar, D. P., & Benkovic, S. J. (1994) *Proceedings of the National Academy of Science of the USA* 91, 6644-6648.
- Rigler, R., & Claesens, F. (1986) in *Structure and Dynamics of RNA*, pp 45-54, Plenum Press, New York.
- Robinson, C. R., & Sligar, S. G. (1994) *Biochemistry* 33, 3787-3793.
- Ronen, A. (1979) *Mutation Research* 75, 1-47.
- Sarma, R. H. (1980) in *Nucleic Acid Geometry and Dynamics*, pp 429, Pergamon Press, New York.
- Spiro, T. G. (1987) in *Biological Applications of Raman Spectroscopy, V. 1: Raman Spectra and the Conformations of Biological Macromolecules*, pp 81-134, John Wiley & Sons, New York.
- Stewart, J. E. (1970) in *Infrared Spectroscopy: Experimental Methods and Techniques*, pp 1-26, Marcel Dekker, Inc., New York.
- Stryer, L. (1988) in *Biochemistry*, 3rd ed., pp 71-116, 649-686, W.H. Freeman and Company, New York.

- Tari, L. W., & Secco, A. S. (1995) *Nucleic Acid Research* 23, 2065-2073.
- Voet, D., & Voet, J. G. (1988) in *Biochemistry*, 2nd ed., pp 848-913. John Wiley & Sons, Inc., New York.
- Ward, D. C., Reich, E., & Stryer, L. (1969) *Journal of Biological Chemistry* 244, 1228-1235.
- Westhof, E., & Moras, D. (1987) in *Structure, Dynamics and Function of Biomolecules* (Ehrenberg, A., Ed.) pp 208-11. Springer-Verlag, Heidelberg.
- Xu, D.-G. (1996) PhD dissertation in *Physics*, University of Alabama-Birmingham, Birmingham.

APPENDIX A
TIME-RESOLVED FLUORESCENCE OF 2AP-T

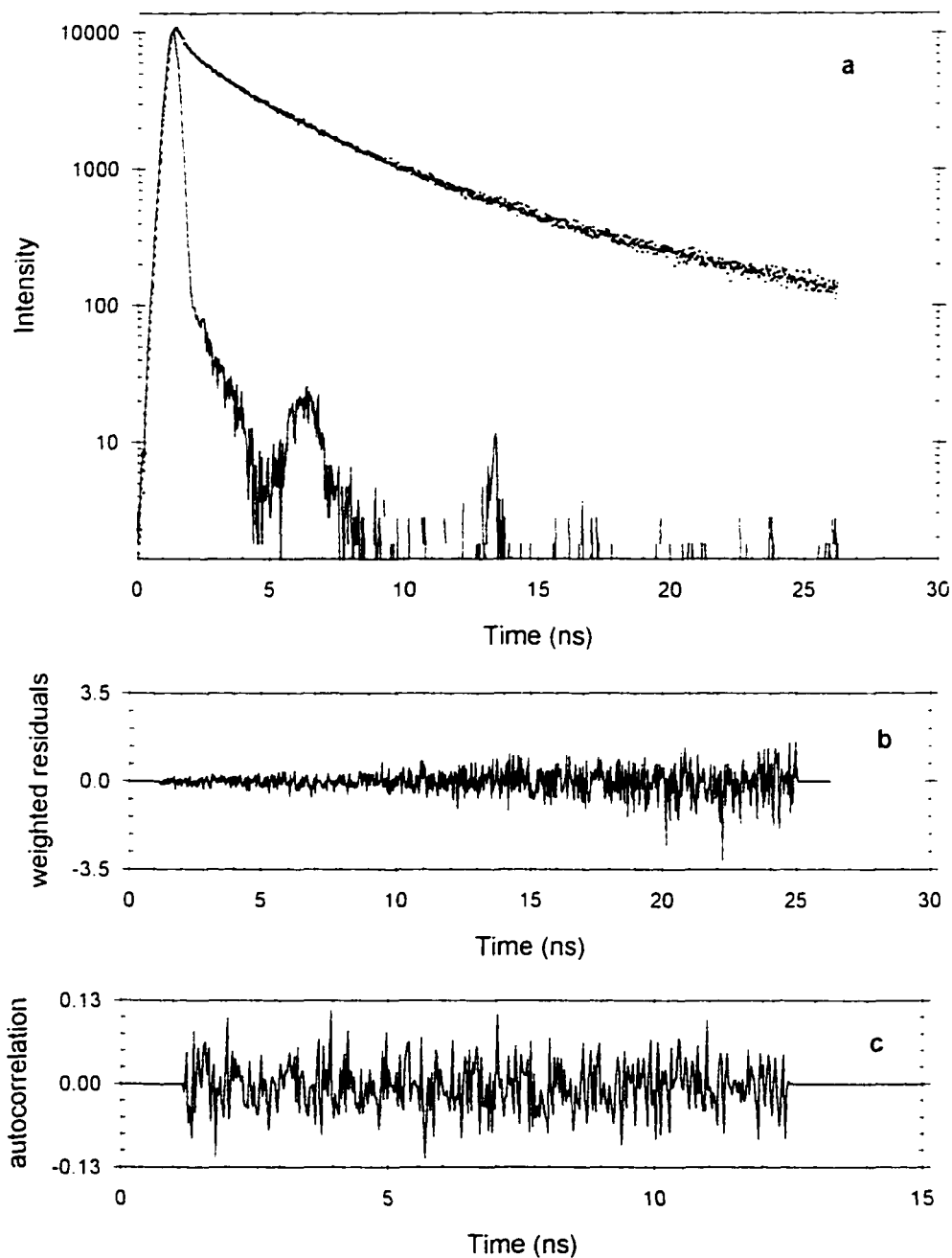


Figure A1: Fluorescence decay curve of 2AP-T (a) in water at 6 °C with (b) weighted residuals and (c) autocorrelation. The sharp-peaked curve is the excitation pulse at 304 nm, the scattered points are the decay data, and the solid line is the three-exponential fit.

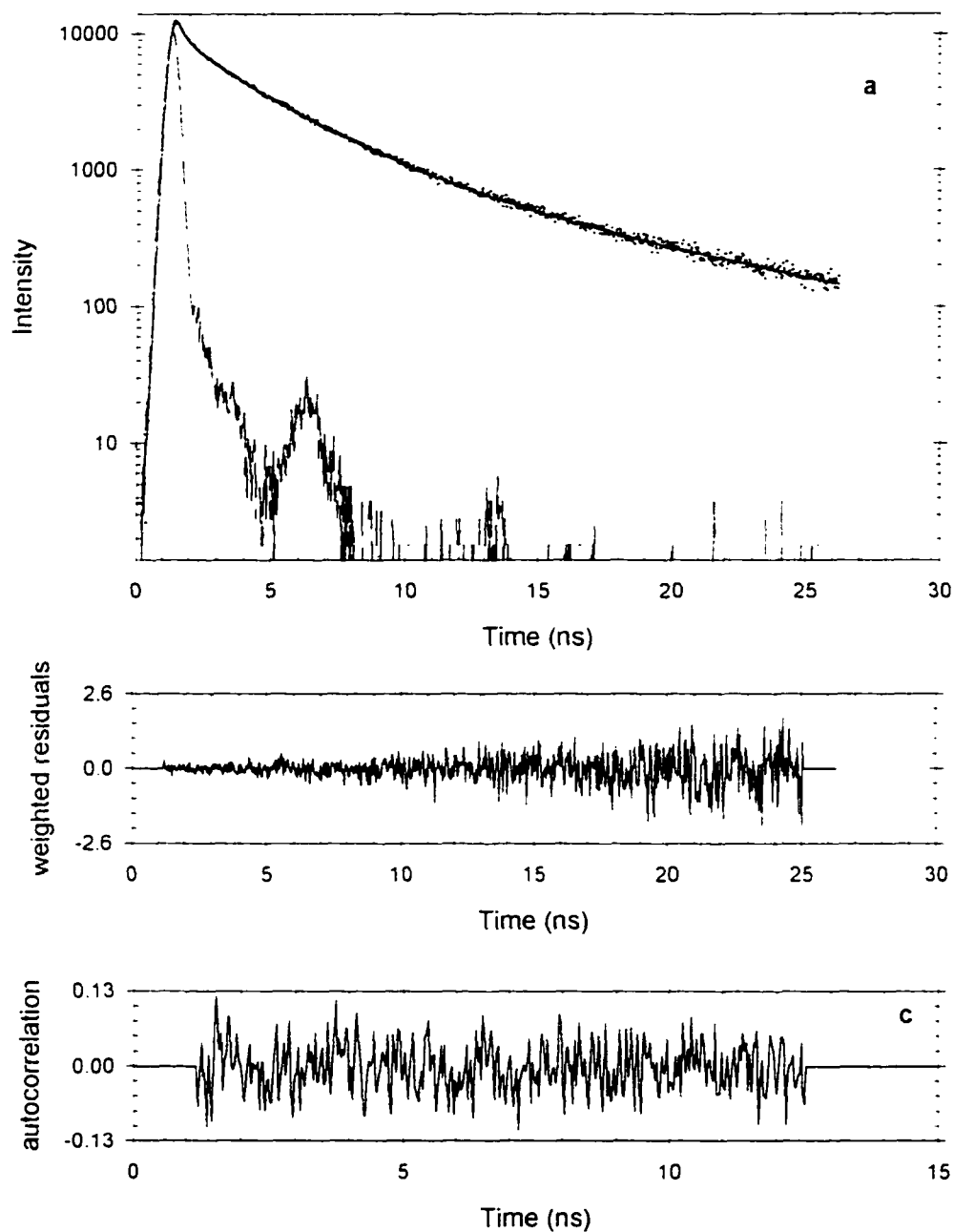


Figure A2: Fluorescence decay curve of 2AP-T (a) in water at 8 °C with (b) weighted residuals and (c) autocorrelation. The sharp-peaked curve is the excitation pulse at 304 nm, the scattered points are the decay data, and the solid line is the three-exponential fit.

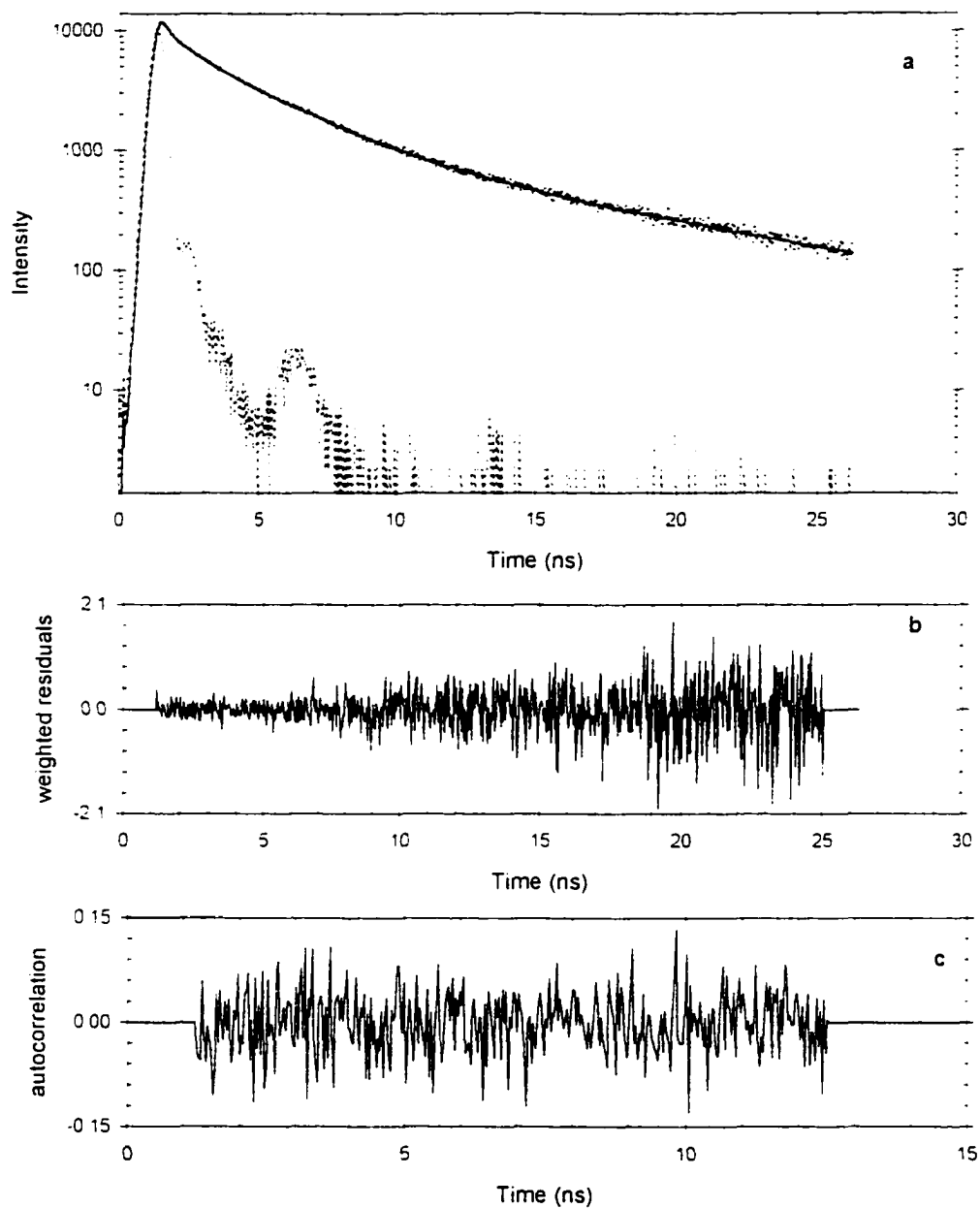


Figure A3: Fluorescence decay curve of 2AP-T (a) in water at 10 °C with (b) weighted residuals and (c) autocorrelation. The sharp-peaked curve is the excitation pulse at 304 nm, the scattered points are the decay data, and the solid line is the three-exponential fit.

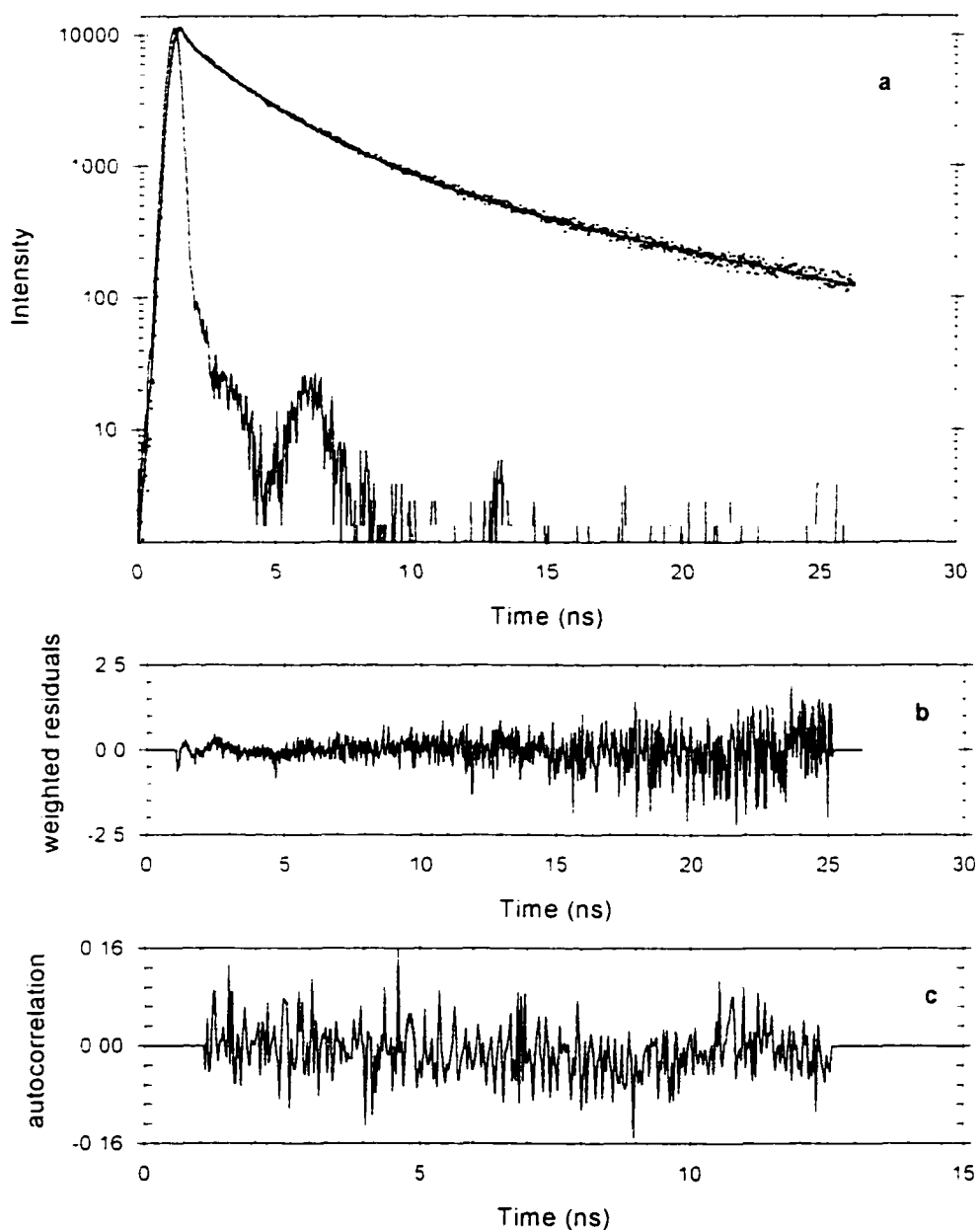


Figure A4: Fluorescence decay curve of 2AP-T (a) in water at 14 °C with (b) weighted residuals and (c) autocorrelation. The sharp-peaked curve is the excitation pulse at 304 nm, the scattered points are the decay data, and the solid line is the three-exponential fit.

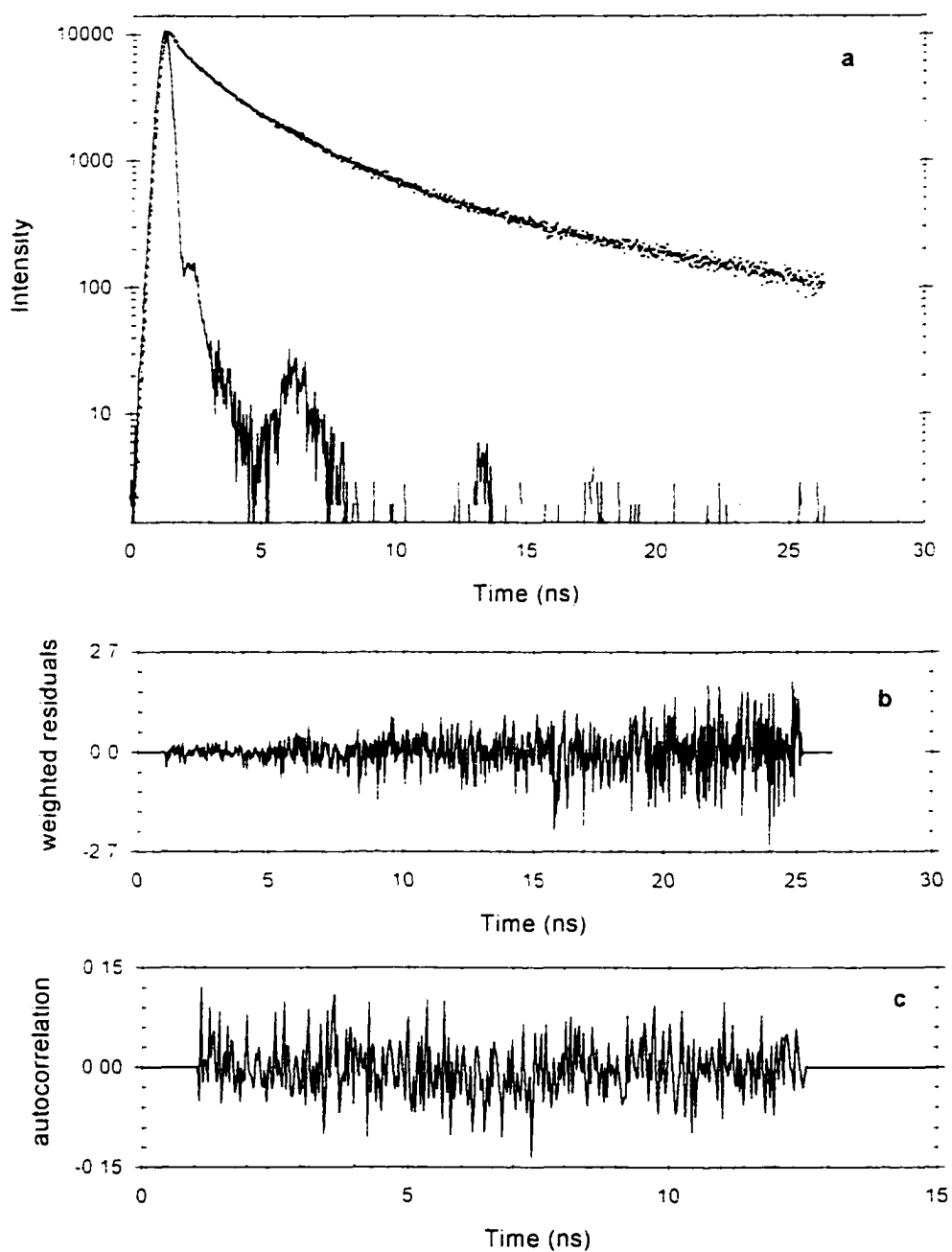


Figure A5: Fluorescence decay curve of 2AP-T (a) in water at 26 °C with (b) weighted residuals and (c) autocorrelation. The sharp-peaked curve is the excitation pulse at 304 nm. the scattered points are the decay data, and the solid line is the three-exponential fit.

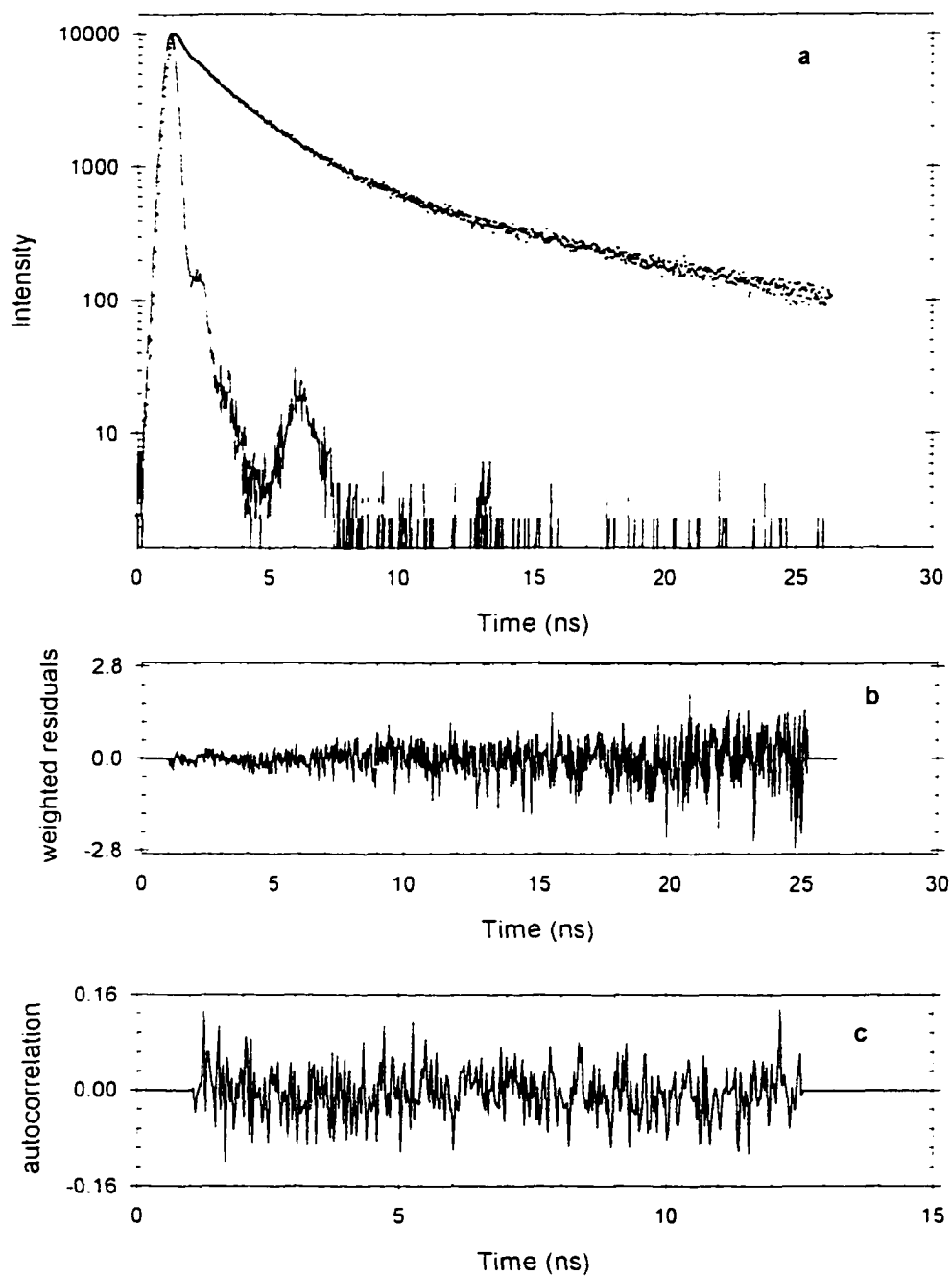


Figure A6: Fluorescence decay curve of 2AP-T (a) in water at 30 °C with (b) weighted residuals and (c) autocorrelation. The sharp-peaked curve is the excitation pulse at 304 nm, the scattered points are the decay data, and the solid line is the three-exponential fit.

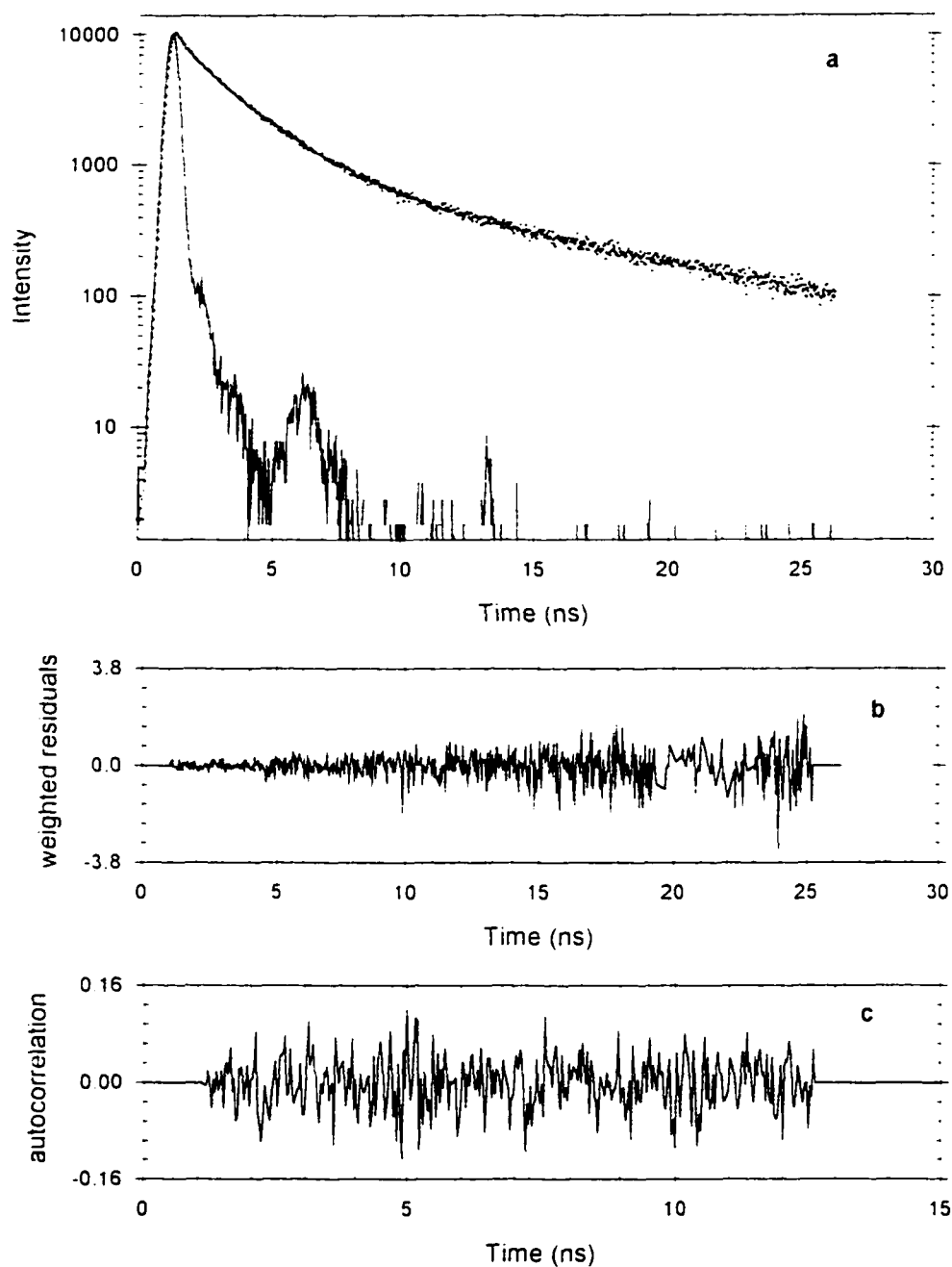


Figure A7: Fluorescence decay curve of 2AP-T (a) in water at 34 °C with (b) weighted residuals and (c) autocorrelation. The sharp-peaked curve is the excitation pulse at 304 nm, the scattered points are the decay data, and the solid line is the three-exponential fit.

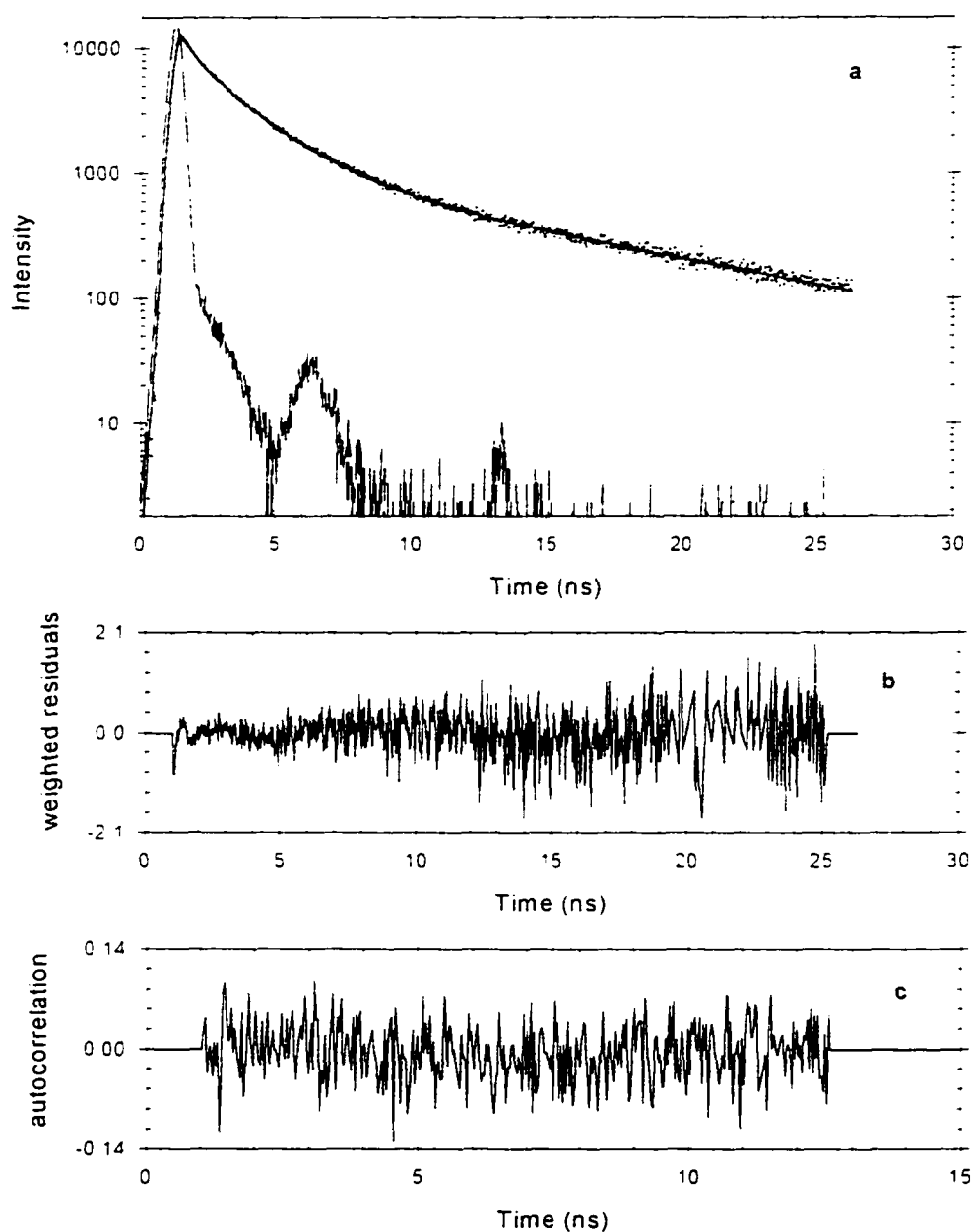


Figure A8: Fluorescence decay curve of 2AP-T (a) in water at 38 °C with (b) weighted residuals and (c) autocorrelation. The sharp-peaked curve is the excitation pulse at 304 nm, the scattered points are the decay data, and the solid line is the three-exponential fit.

APPENDIX B

TIME-RESOLVED FLUORESCENCE OF A-2AP-T

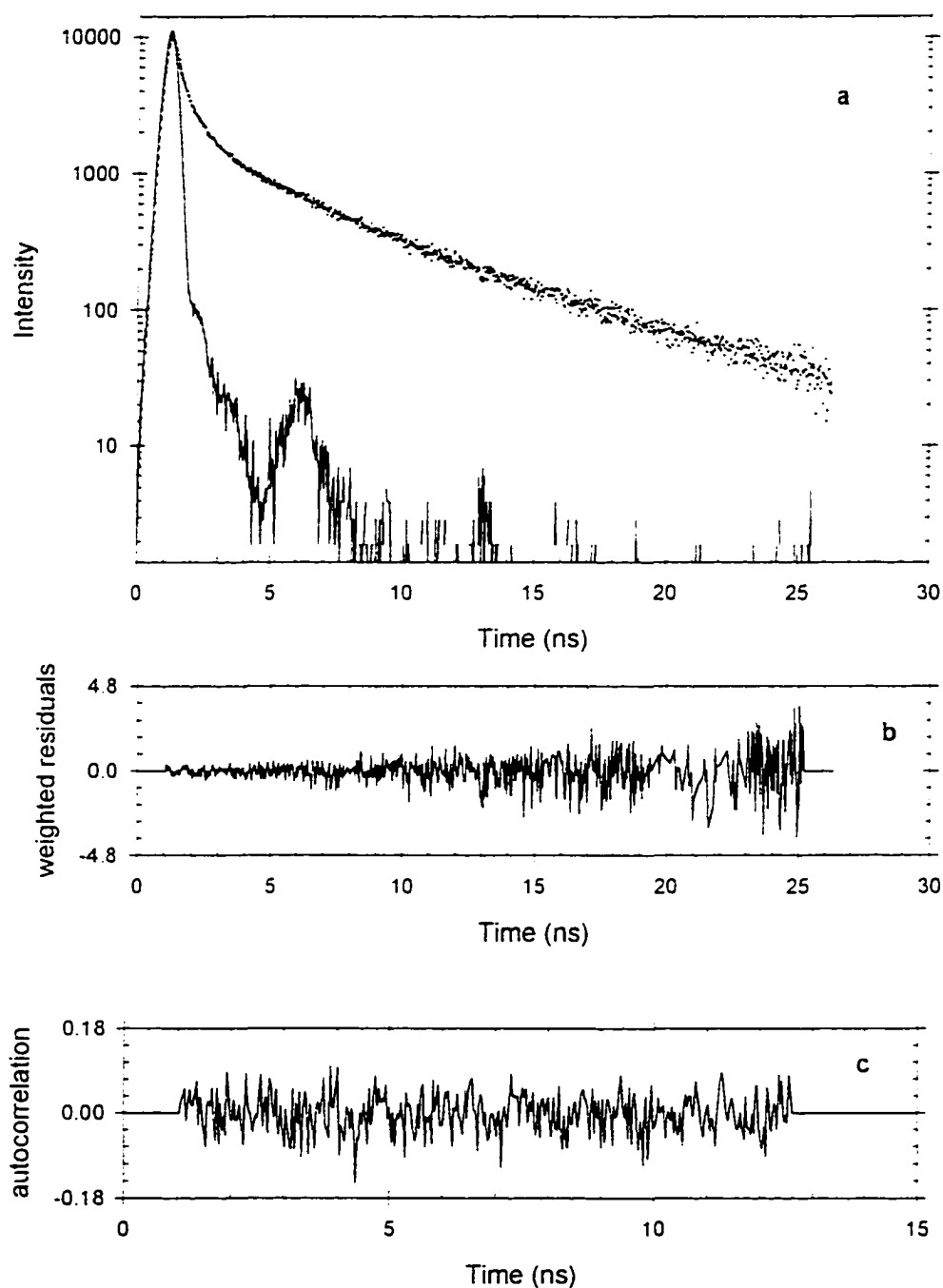


Figure B1: Fluorescence decay curve of A-2AP-T (a) in water at 6 °C with (b) weighted residuals and (c) autocorrelation. The sharp-peaked curve is the excitation pulse at 304 nm, the scattered points are the decay data, and the solid line is the three-exponential fit.

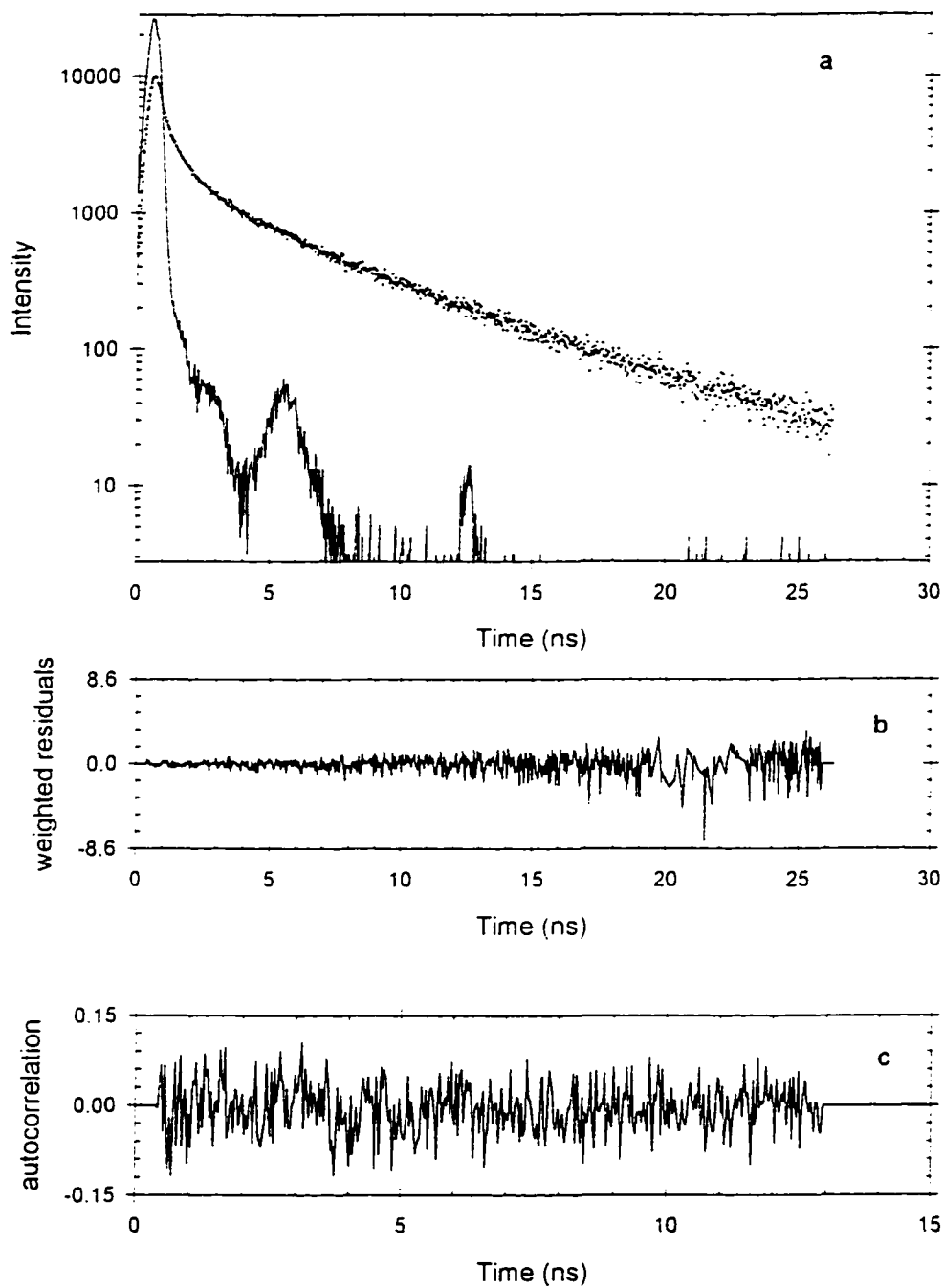


Figure B2: Fluorescence decay curve of A-2AP-T (a) in water at 8 °C with (b) weighted residuals and (c) autocorrelation. The sharp-peaked curve is the excitation pulse at 304 nm, the scattered points are the decay data, and the solid line is the three-exponential fit.

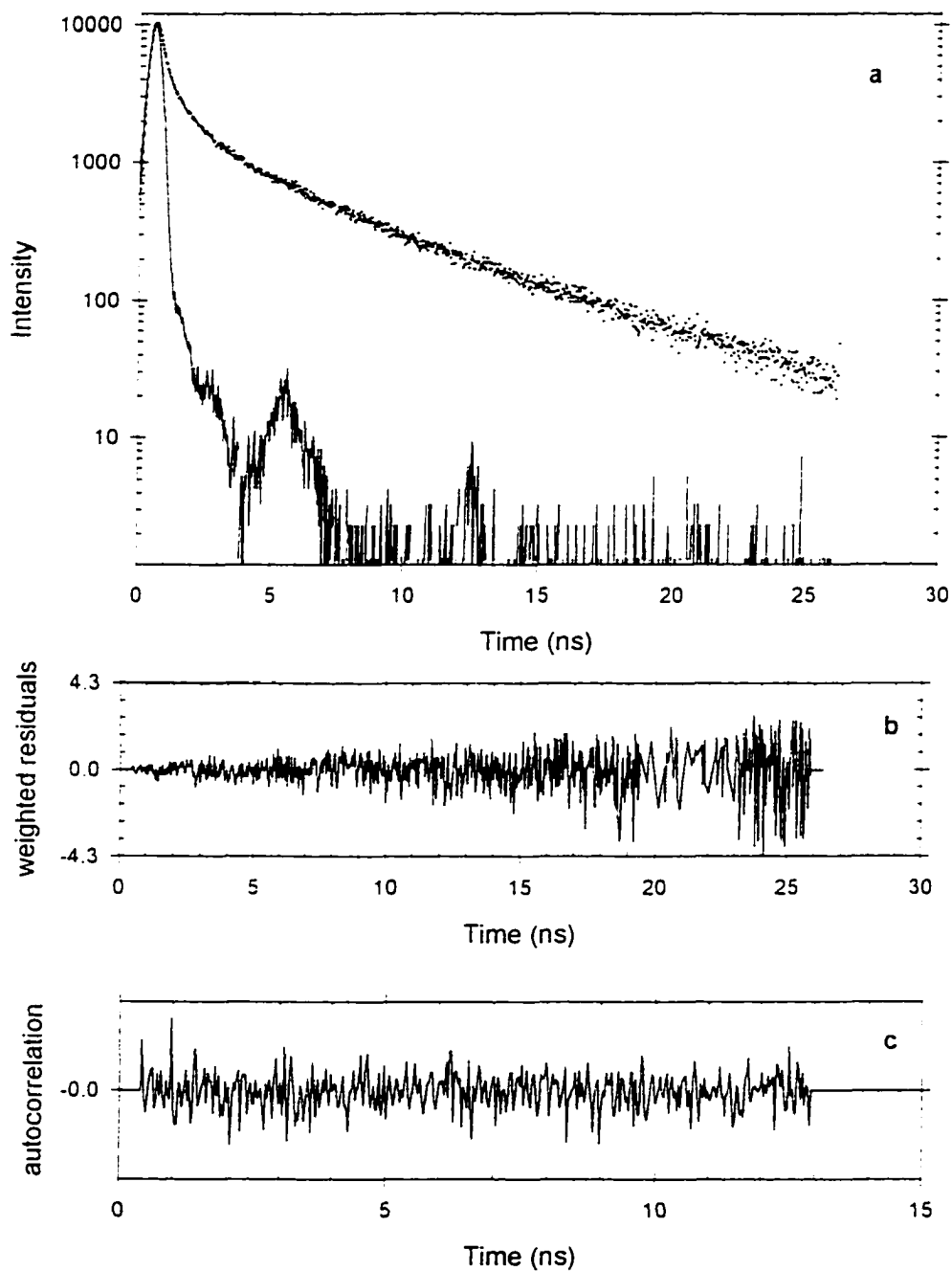


Figure B3: Fluorescence decay curve of A-2AP-T (a) in water at 10 °C with (b) weighted residuals and (c) autocorrelation. The sharp-peaked curve is the excitation pulse at 304 nm, the scattered points are the decay data, and the solid line is the three-exponential fit.

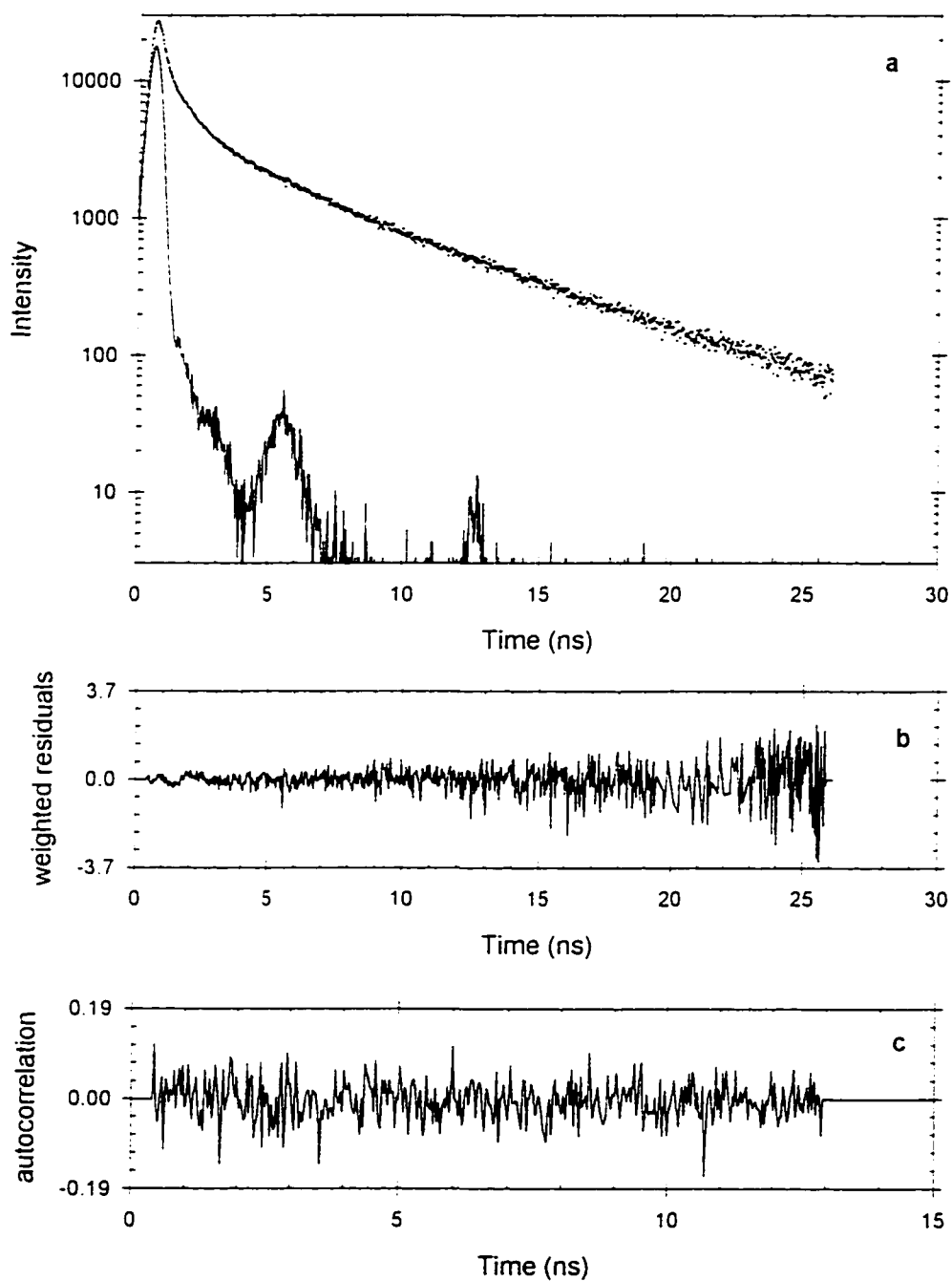


Figure B4: Fluorescence decay curve of A-2AP-T (a) in water at 12 °C with (b) weighted residuals and (c) autocorrelation. The sharp-peaked curve is the excitation pulse at 304 nm, the scattered points are the decay data, and the solid line is the three-exponential fit.

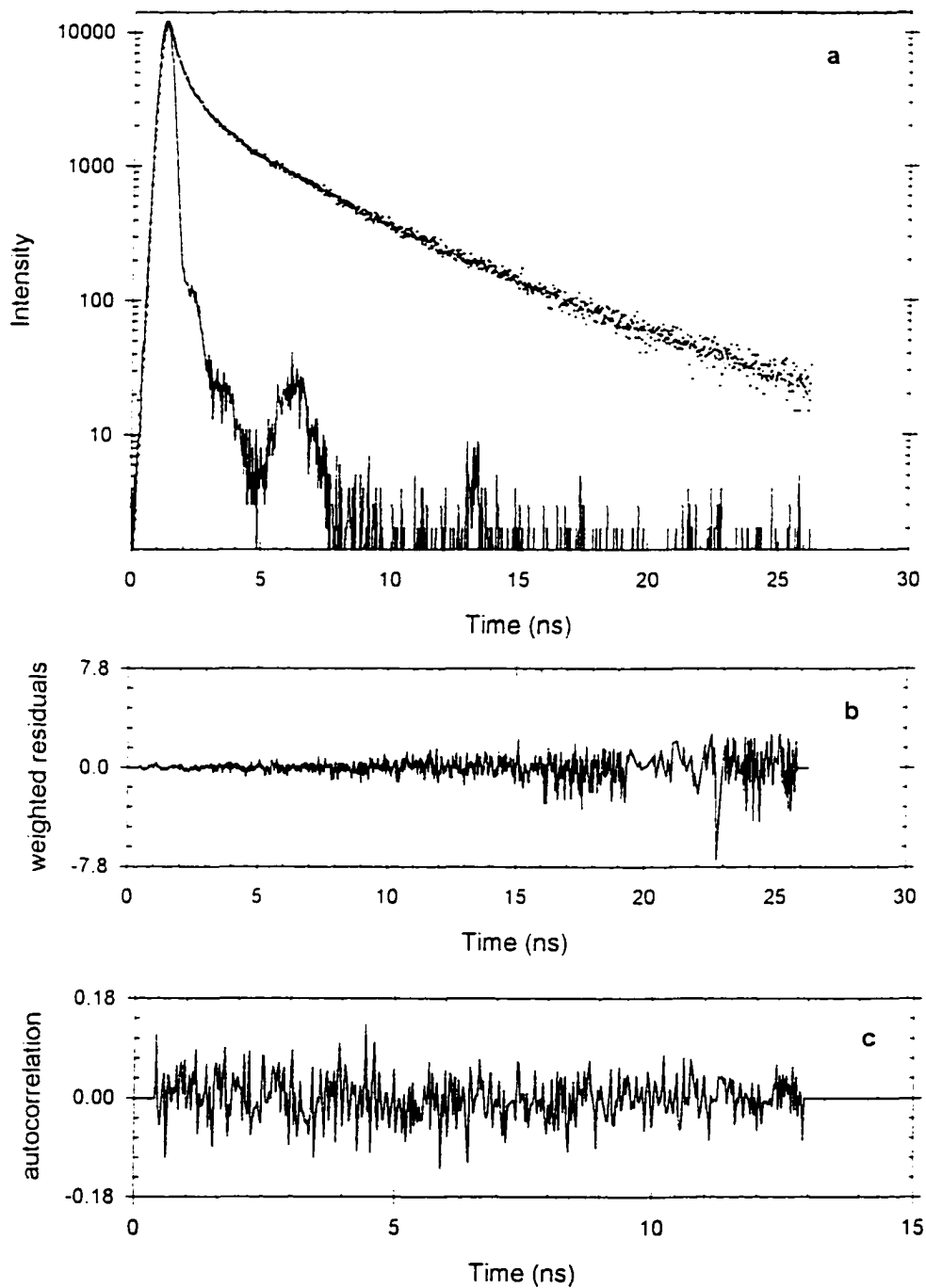


Figure B5: Fluorescence decay curve of A-2AP-T (a) in water at 26 °C with (b) weighted residuals and (c) autocorrelation. The sharp-peaked curve is the excitation pulse at 304 nm, the scattered points are the decay data, and the solid line is the three-exponential fit.

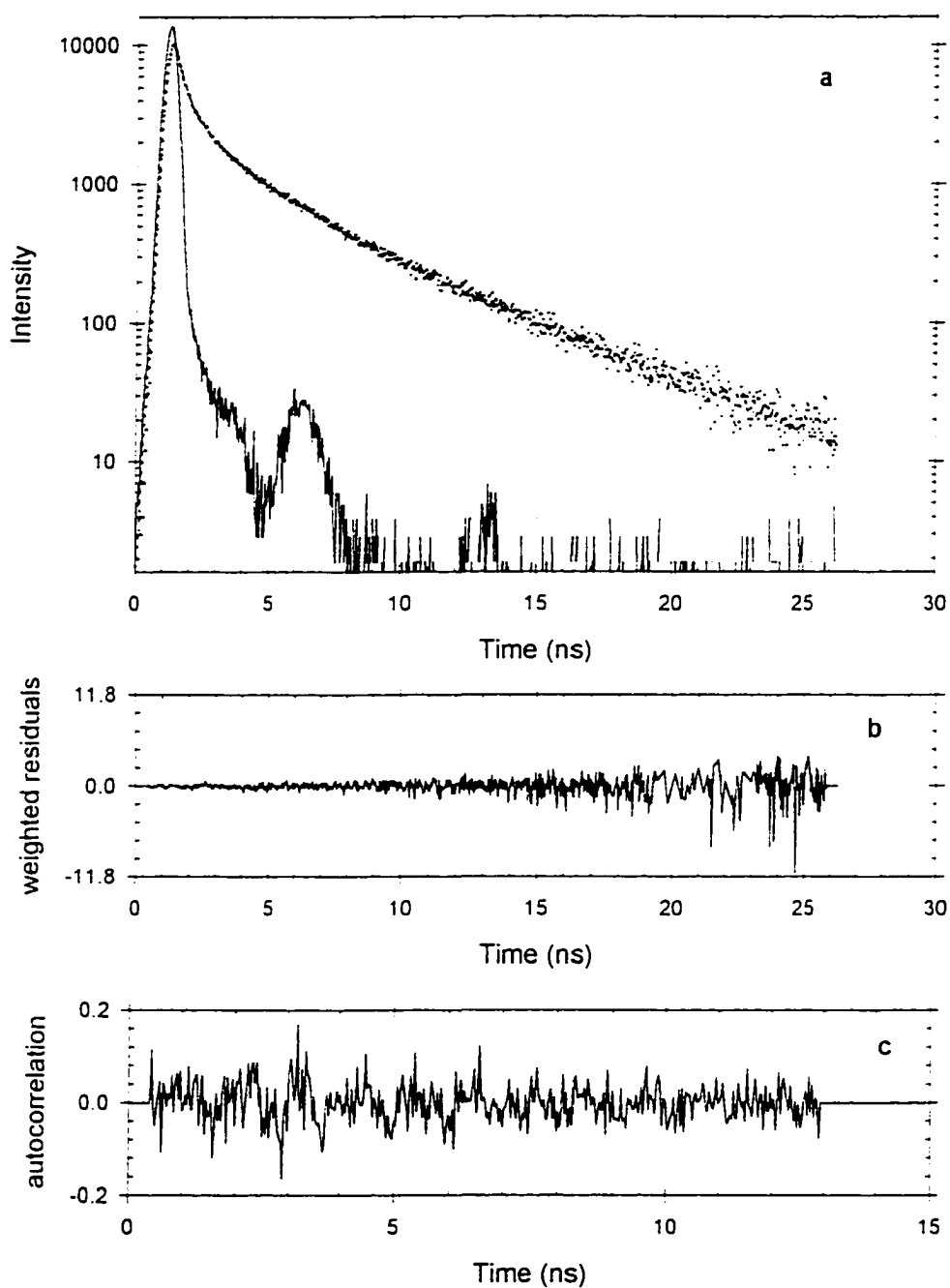


Figure B6: Fluorescence decay curve of A-2AP-T (a) in water at 30 °C with (b) weighted residuals and (c) autocorrelation. The sharp-peaked curve is the excitation pulse at 304 nm, the scattered points are the decay data, and the solid line is the three-exponential fit.

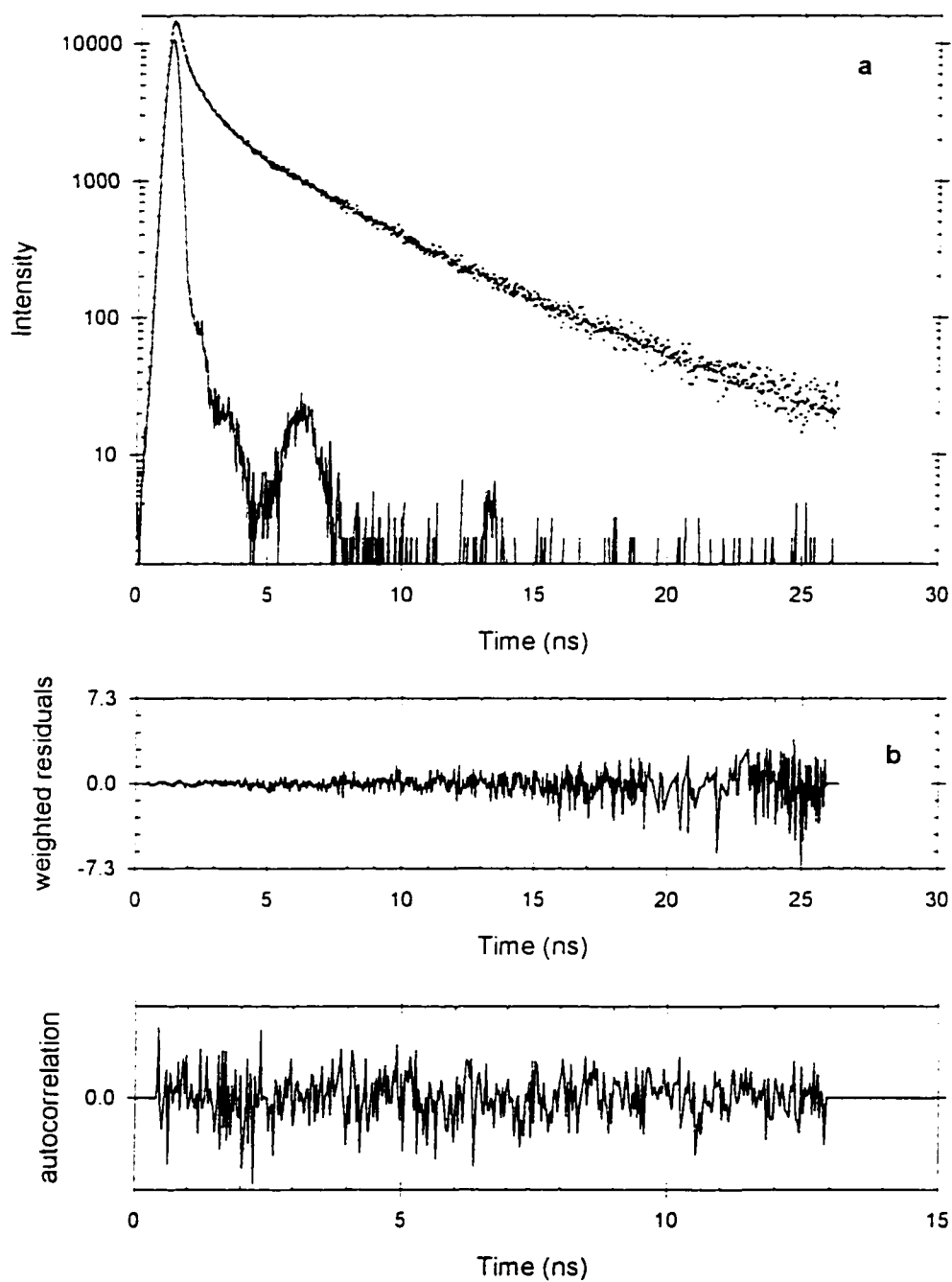


Figure B7: Fluorescence decay curve of A-2AP-T (a) in water at 34 °C with (b) weighted residuals and (c) autocorrelation. The sharp-peaked curve is the excitation pulse at 304 nm, the scattered points are the decay data, and the solid line is the three-exponential fit.

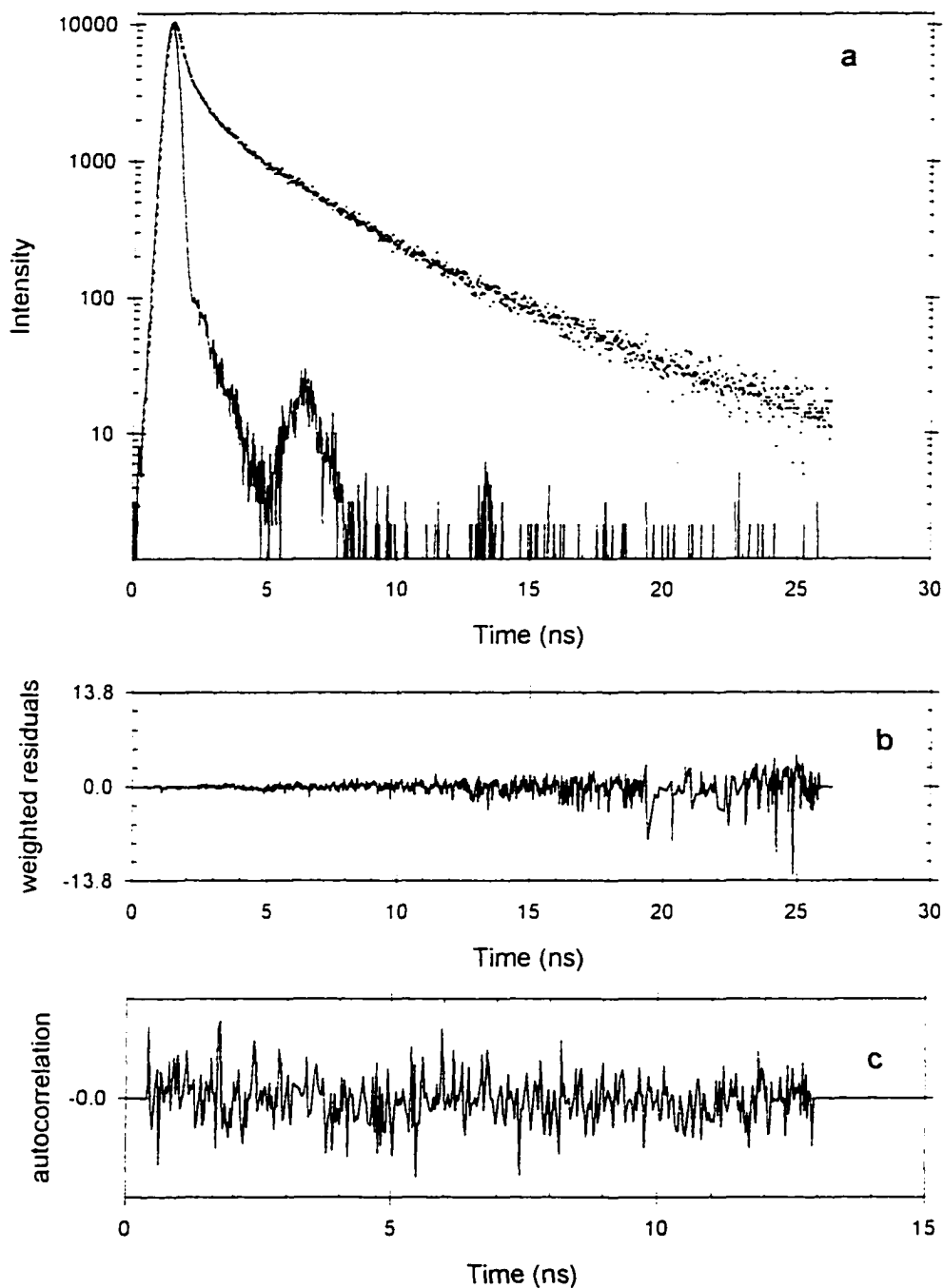


Figure B8: Fluorescence decay curve of A-2AP-T (a) in water at 38 °C with (b) weighted residuals and (c) autocorrelation. The sharp-peaked curve is the excitation pulse at 304 nm, the scattered points are the decay data, and the solid line is the three-exponential fit.

APPENDIX C

TIME-RESOLVED FLUORESCENCE OF G-2AP-C

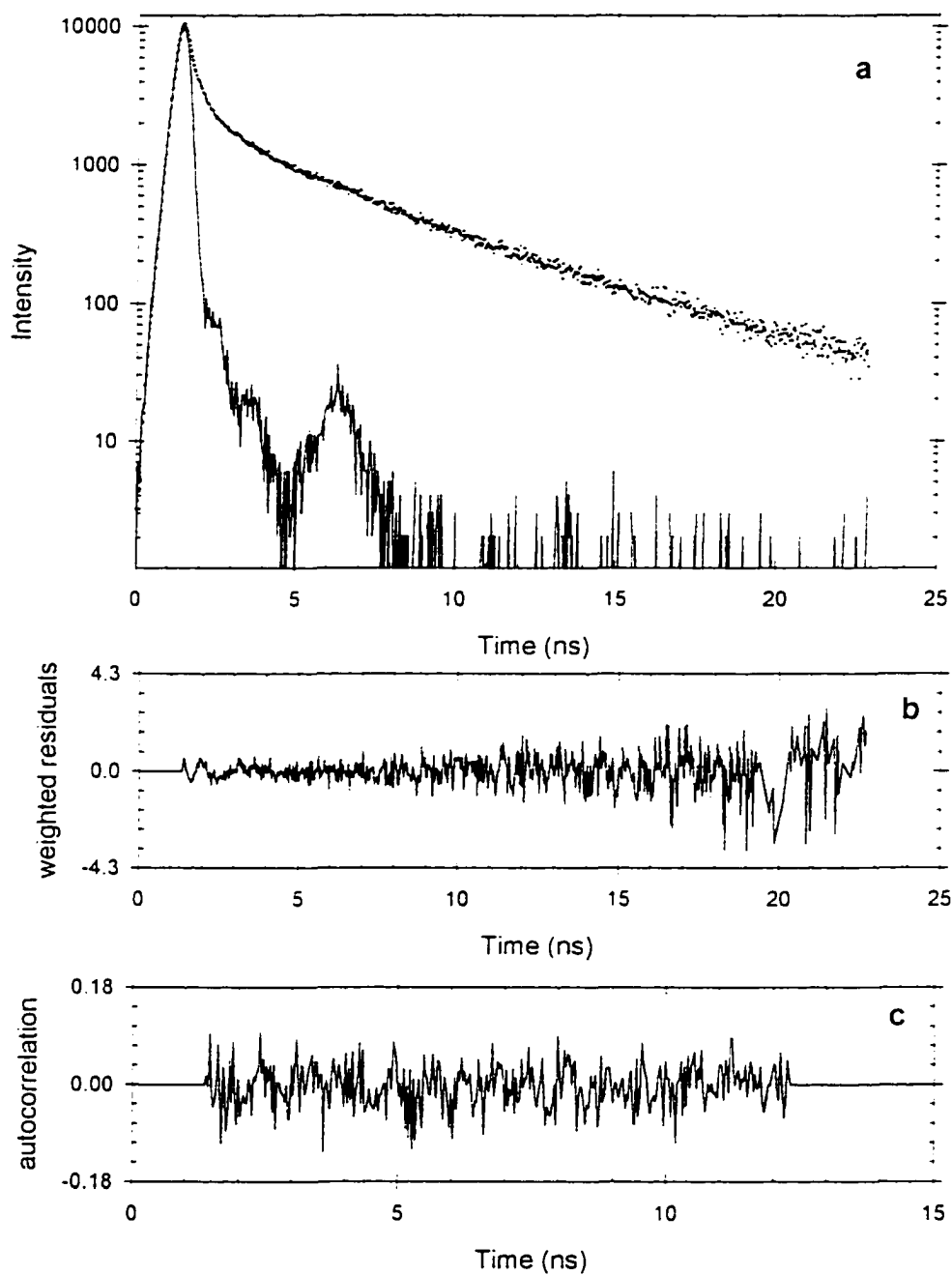


Figure C1: Fluorescence decay curve of G-2AP-C (a) in water at 6 °C with (b) weighted residuals and (c) autocorrelation. The sharp-peaked curve is the excitation pulse at 304 nm, the scattered points are the decay data, and the solid line is the three-exponential fit.

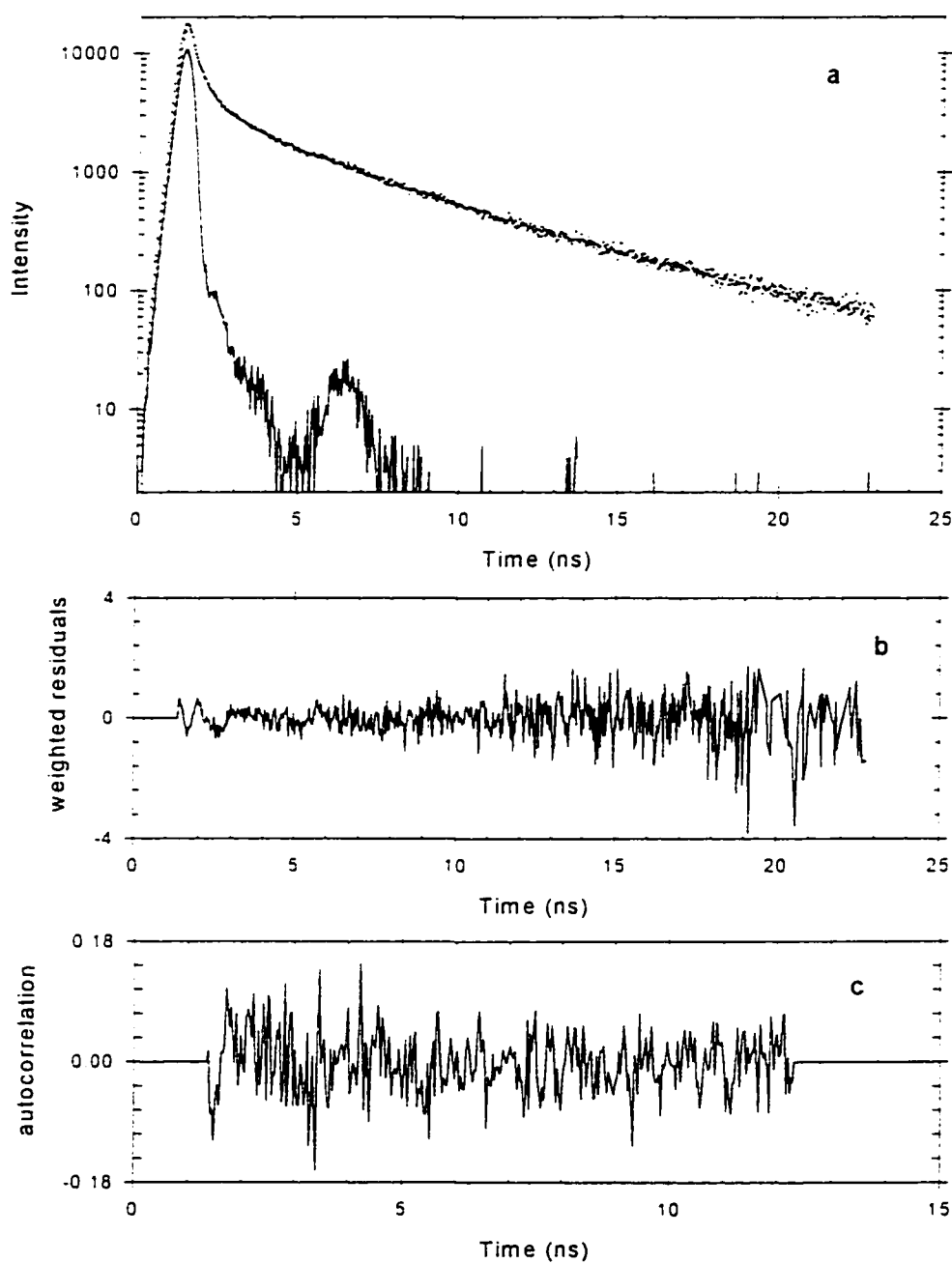


Figure C2: Fluorescence decay curve of G-2AP-C (a) in water at 8 °C with (b) weighted residuals and (c) autocorrelation. The sharp-peaked curve is the excitation pulse at 304 nm, the scattered points are the decay data, and the solid line is the three-exponential fit.

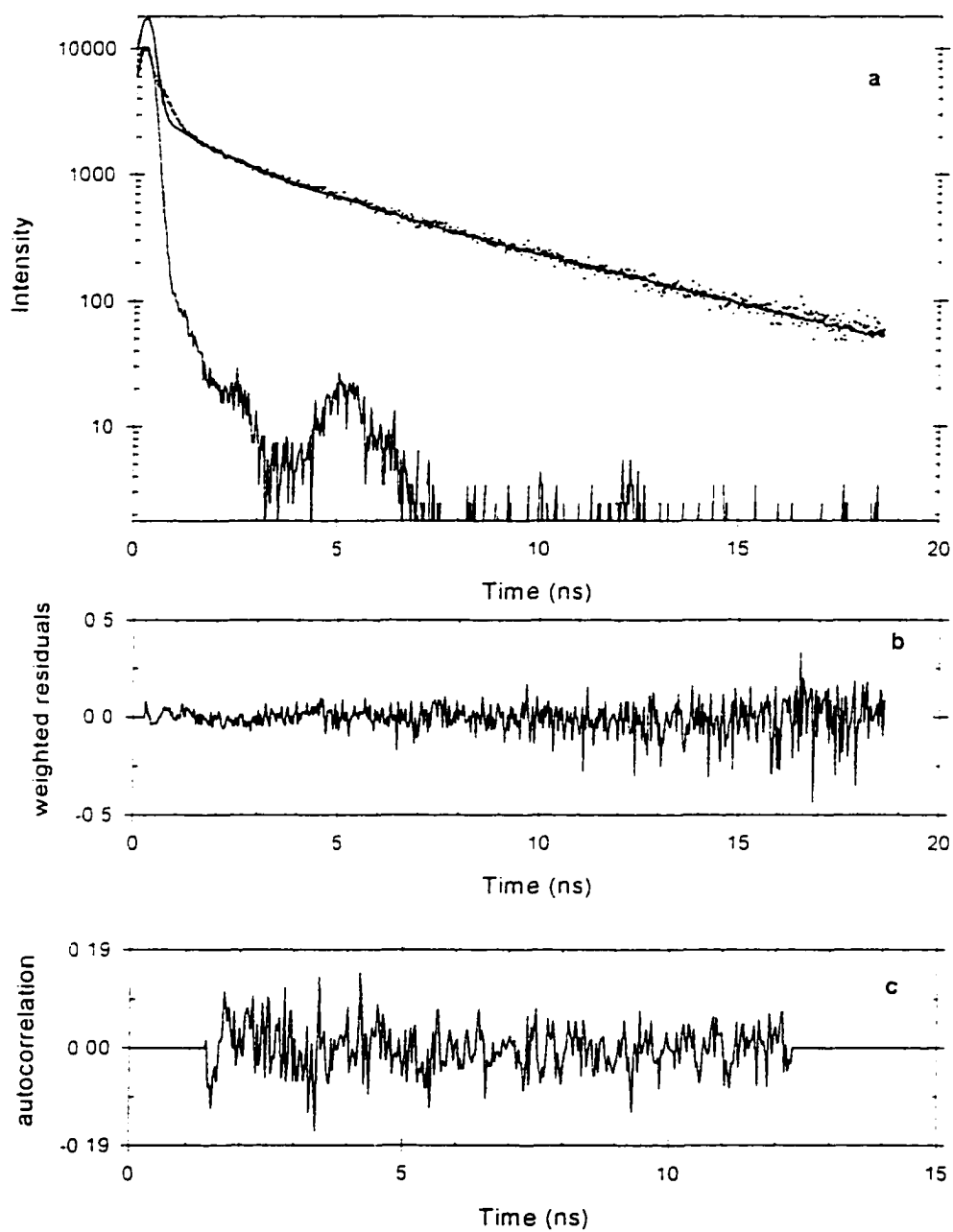


Figure C3: Fluorescence decay curve of G-2AP-C (a) in water at 10 °C with (b) weighted residuals and (c) autocorrelation. The sharp-peaked curve is the excitation pulse at 304 nm, the scattered points are the decay data, and the solid line is the three-exponential fit.

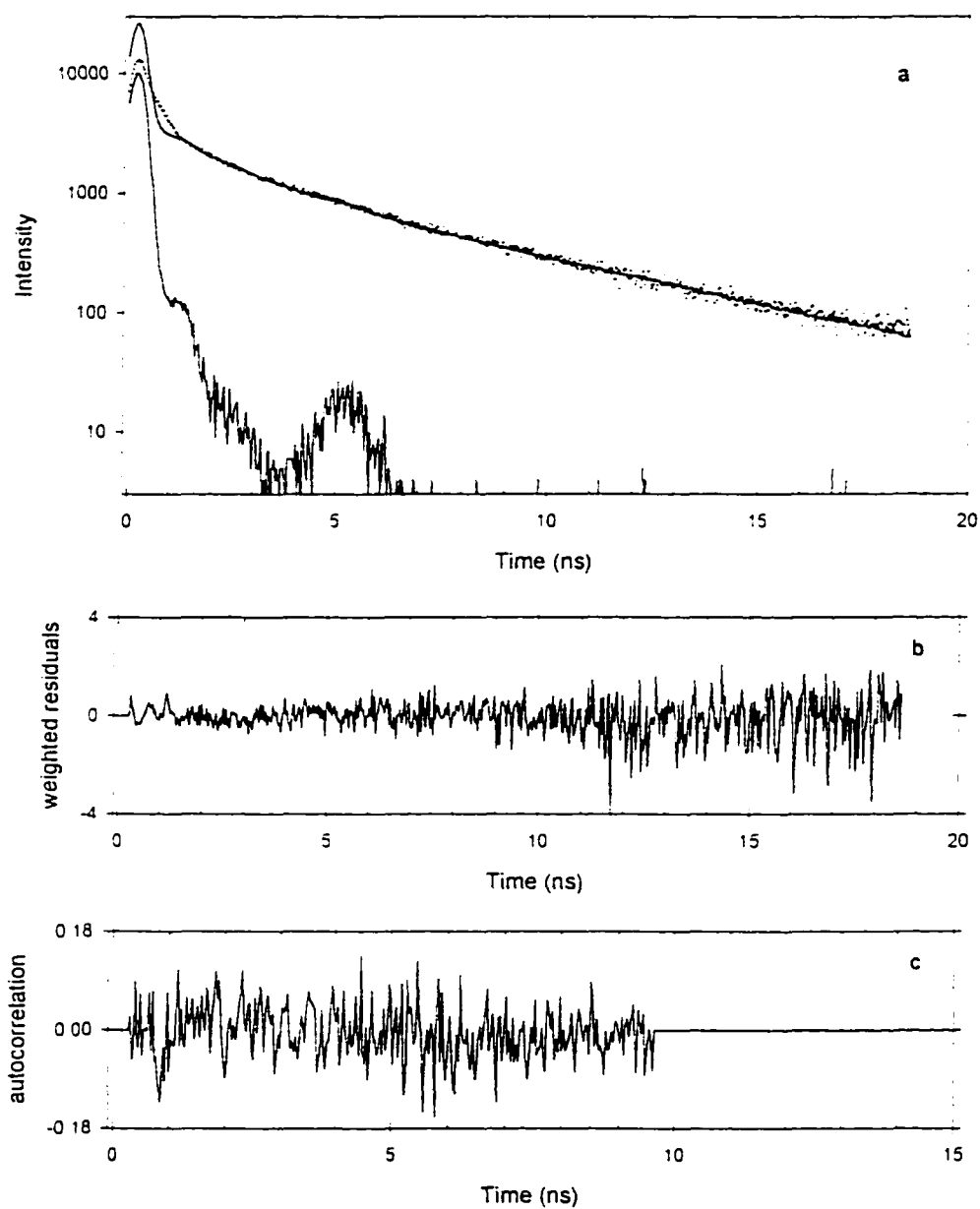


Figure C4: Fluorescence decay curve of G-2AP-C (a) in water at 12 °C with (b) weighted residuals and (c) autocorrelation. The sharp-peaked curve is the excitation pulse at 304 nm, the scattered points are the decay data, and the solid line is the three-exponential fit.

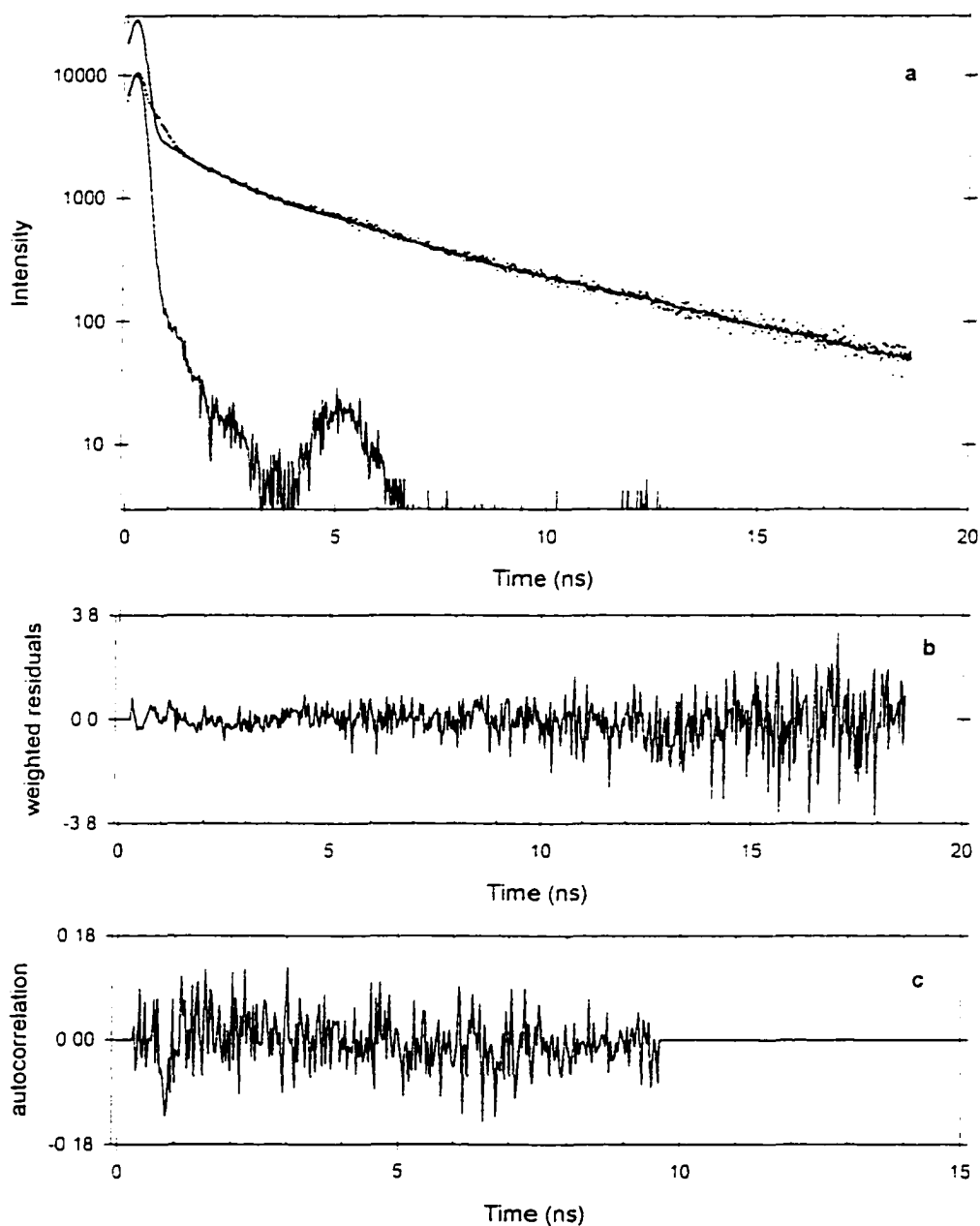


Figure C5: Fluorescence decay curve of G-2AP-C (a) in water at 14 °C with (b) weighted residuals and (c) autocorrelation. The sharp-peaked curve is the excitation pulse at 304 nm, the scattered points are the decay data, and the solid line is the three-exponential fit.

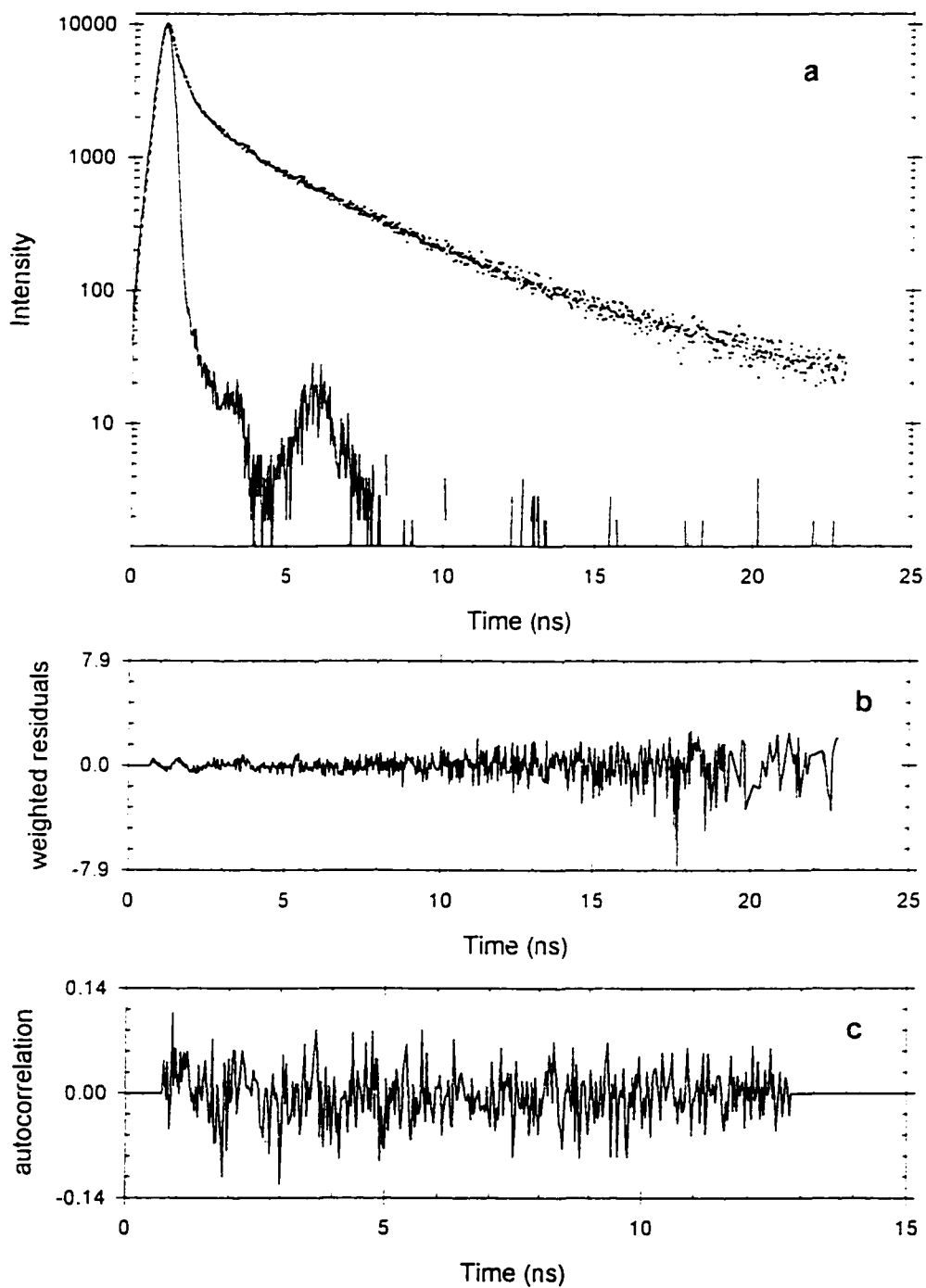


Figure C6: Fluorescence decay curve of G-2AP-C (a) in water at 26 °C with (b) weighted residuals and (c) autocorrelation. The sharp-peaked curve is the excitation pulse at 304 nm, the scattered points are the decay data, and the solid line is the three-exponential fit.

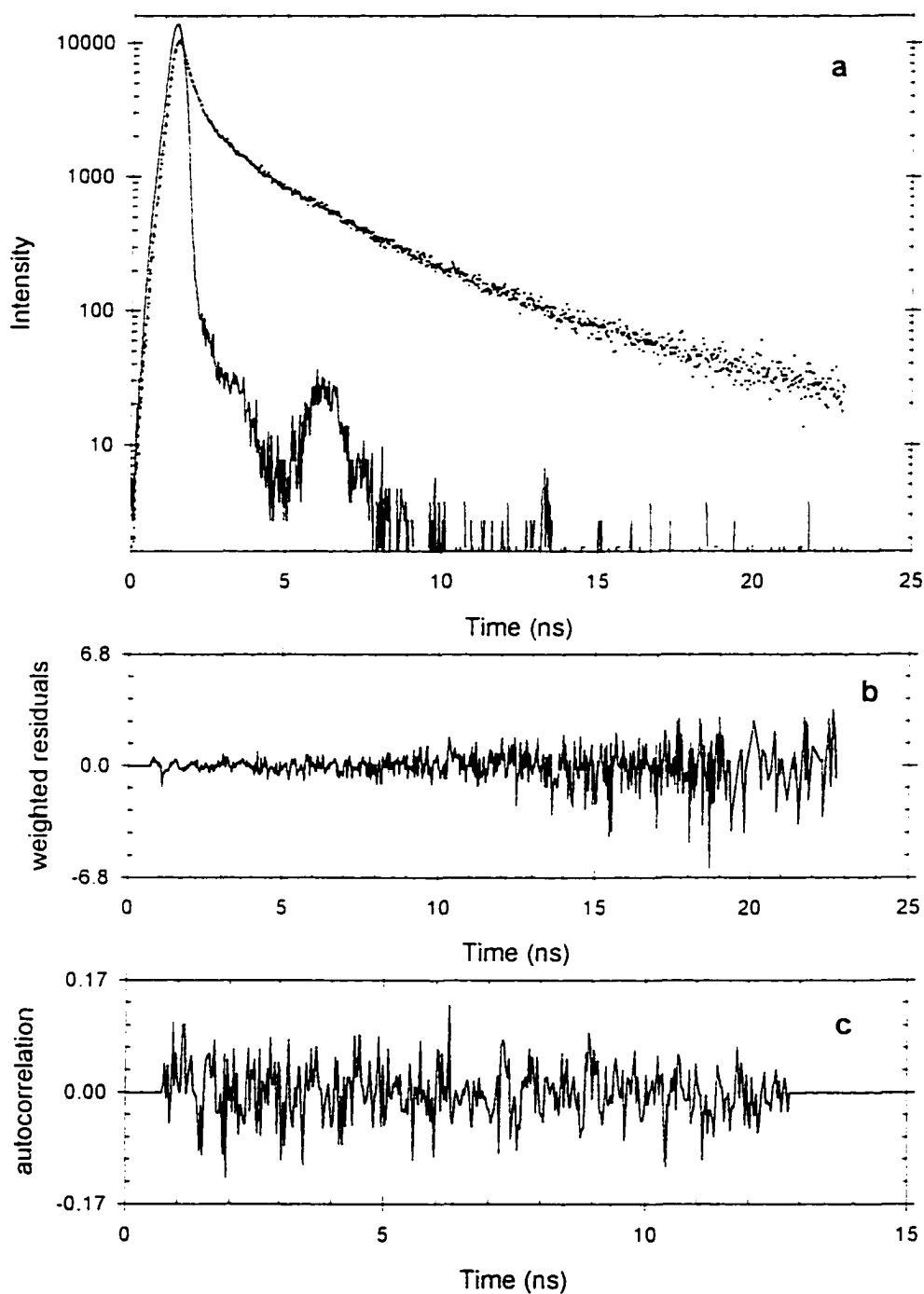


Figure C7: Fluorescence decay curve of G-2AP-C (a) in water at 30 °C with (b) weighted residuals and (c) autocorrelation. The sharp-peaked curve is the excitation pulse at 304 nm, the scattered points are the decay data, and the solid line is the three-exponential fit.

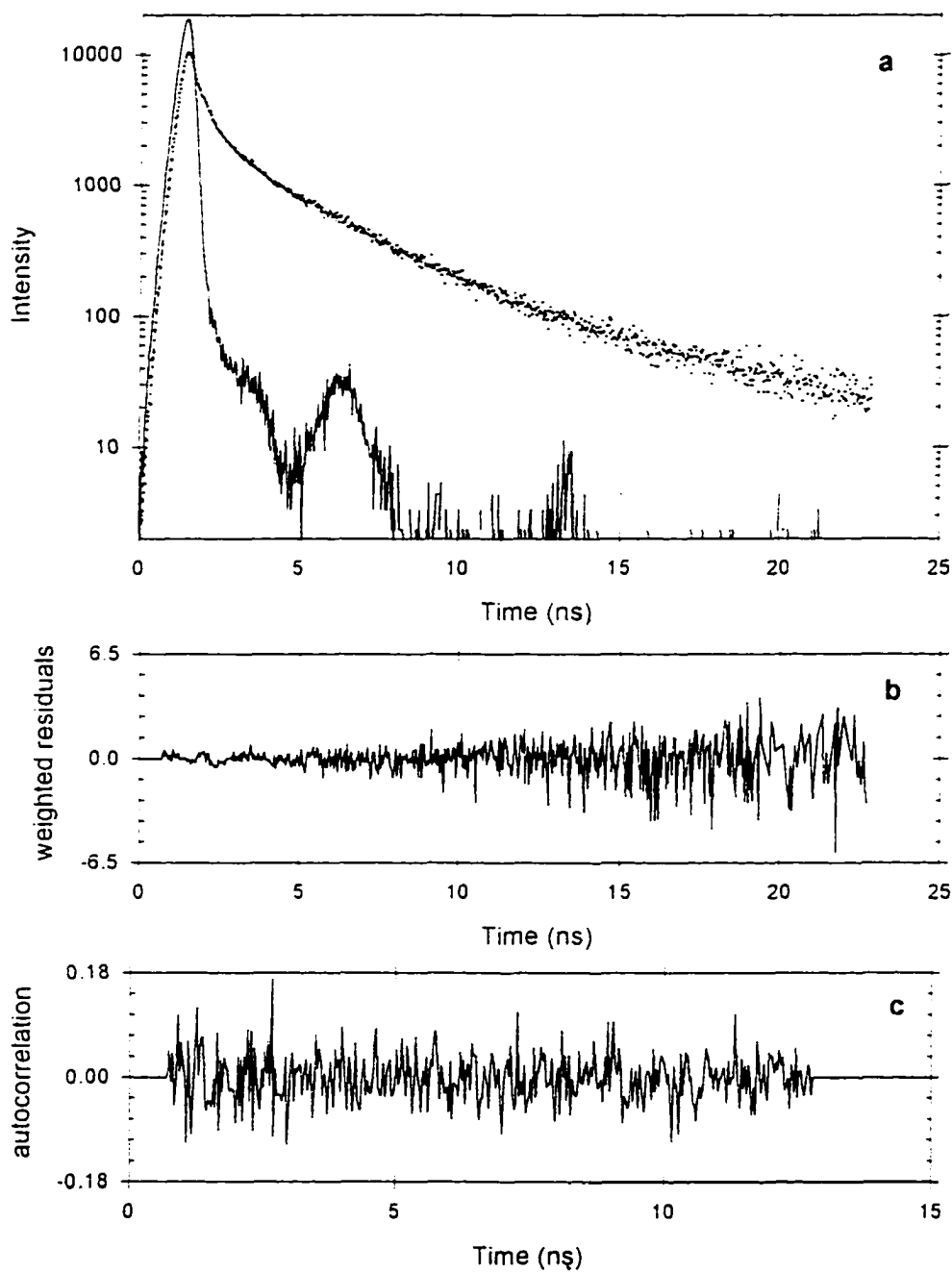


Figure C8: Fluorescence decay curve of G-2AP-C (a) in water at 34 °C with (b) weighted residuals and (c) autocorrelation. The sharp-peaked curve is the excitation pulse at 304 nm, the scattered points are the decay data, and the solid line is the three-exponential fit.

APPENDIX D

TIME-RESOLVED FLUORESCENCE OF C-2AP-G

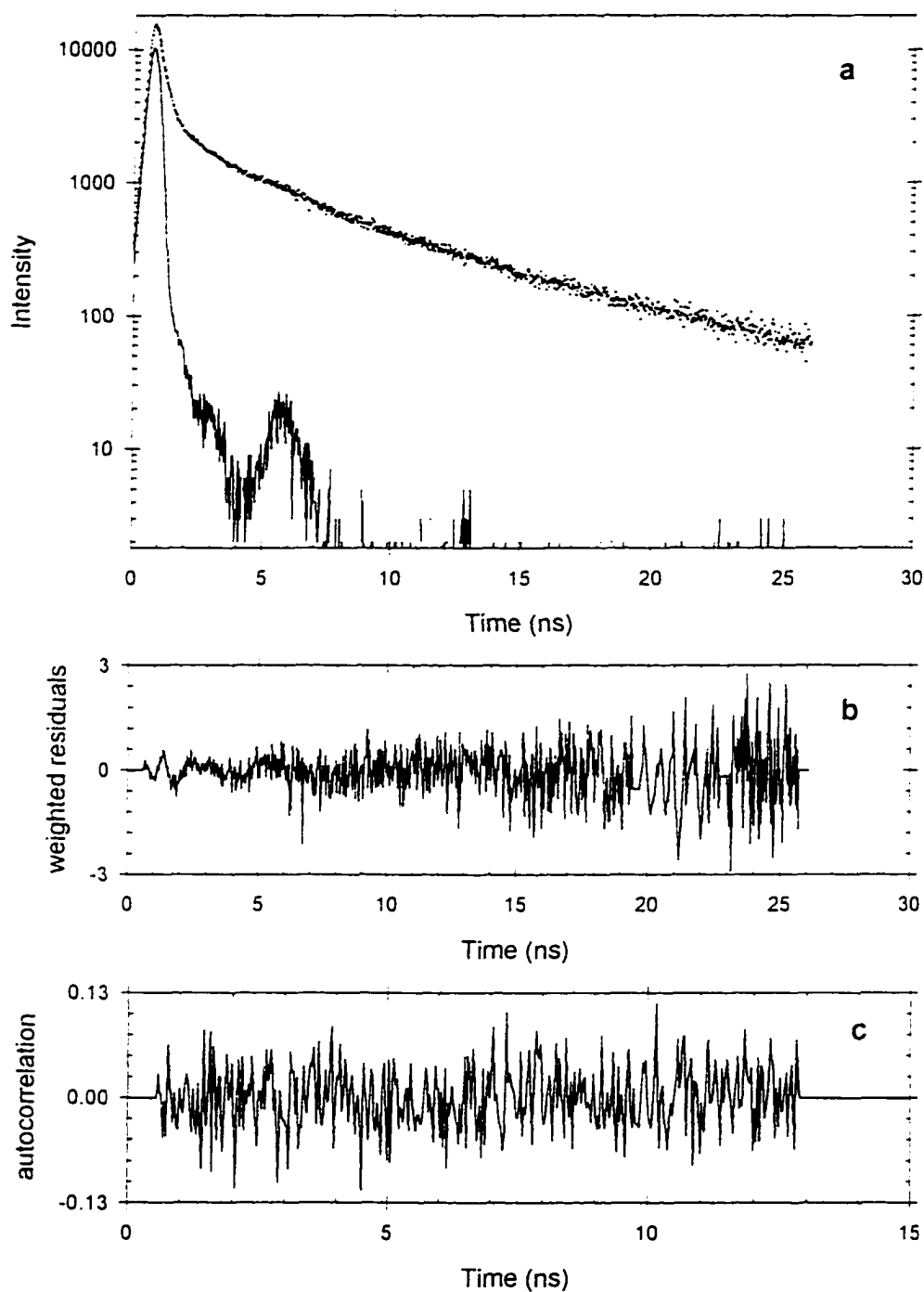


Figure D1: Fluorescence decay curve of C-2AP-G (a) in water at 6 °C with (b) weighted residuals and (c) autocorrelation. The sharp-peaked curve is the excitation pulse at 304 nm, the scattered points are the decay data, and the solid line is the three-exponential fit.

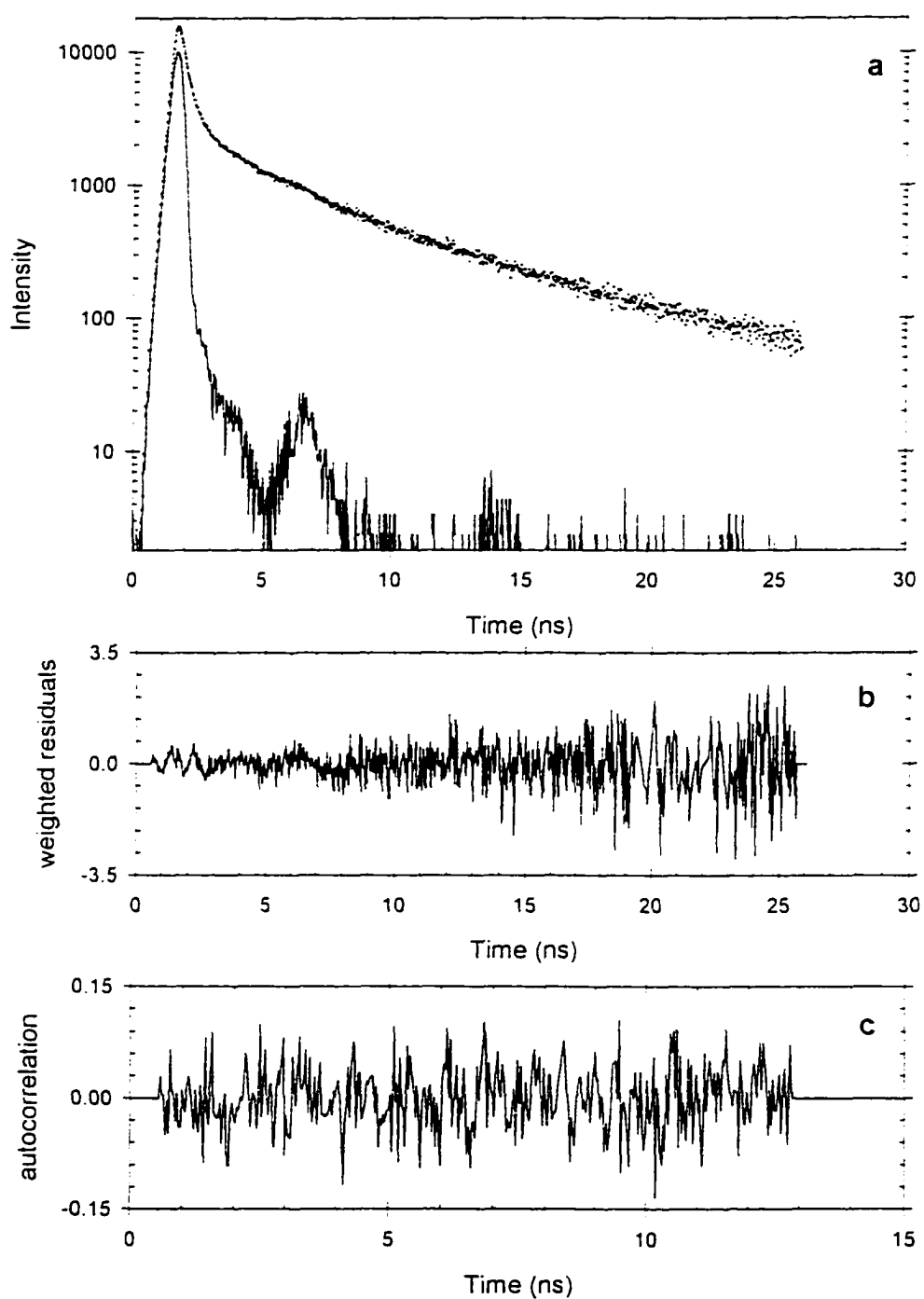


Figure D2: Fluorescence decay curve of C-2AP-G (a) in water at 8 °C with (b) weighted residuals and (c) autocorrelation. The sharp-peaked curve is the excitation pulse at 304 nm, the scattered points are the decay data, and the solid line is the three-exponential fit.

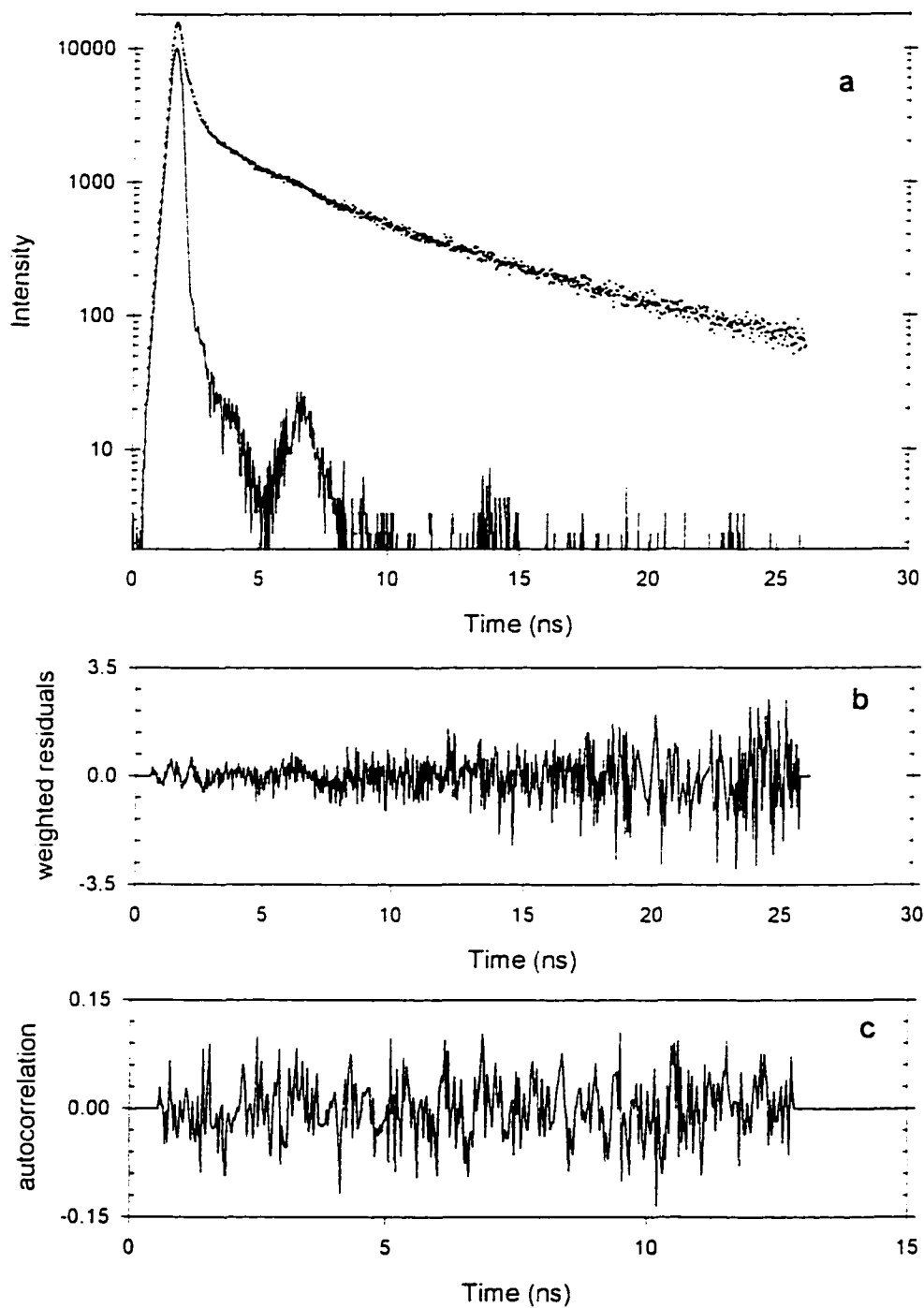


Figure D3: Fluorescence decay curve of C-2AP-G (a) in water at 10 °C with (b) weighted residuals and (c) autocorrelation. The sharp-peaked curve is the excitation pulse at 304 nm, the scattered points are the decay data, and the solid line is the three-exponential fit.

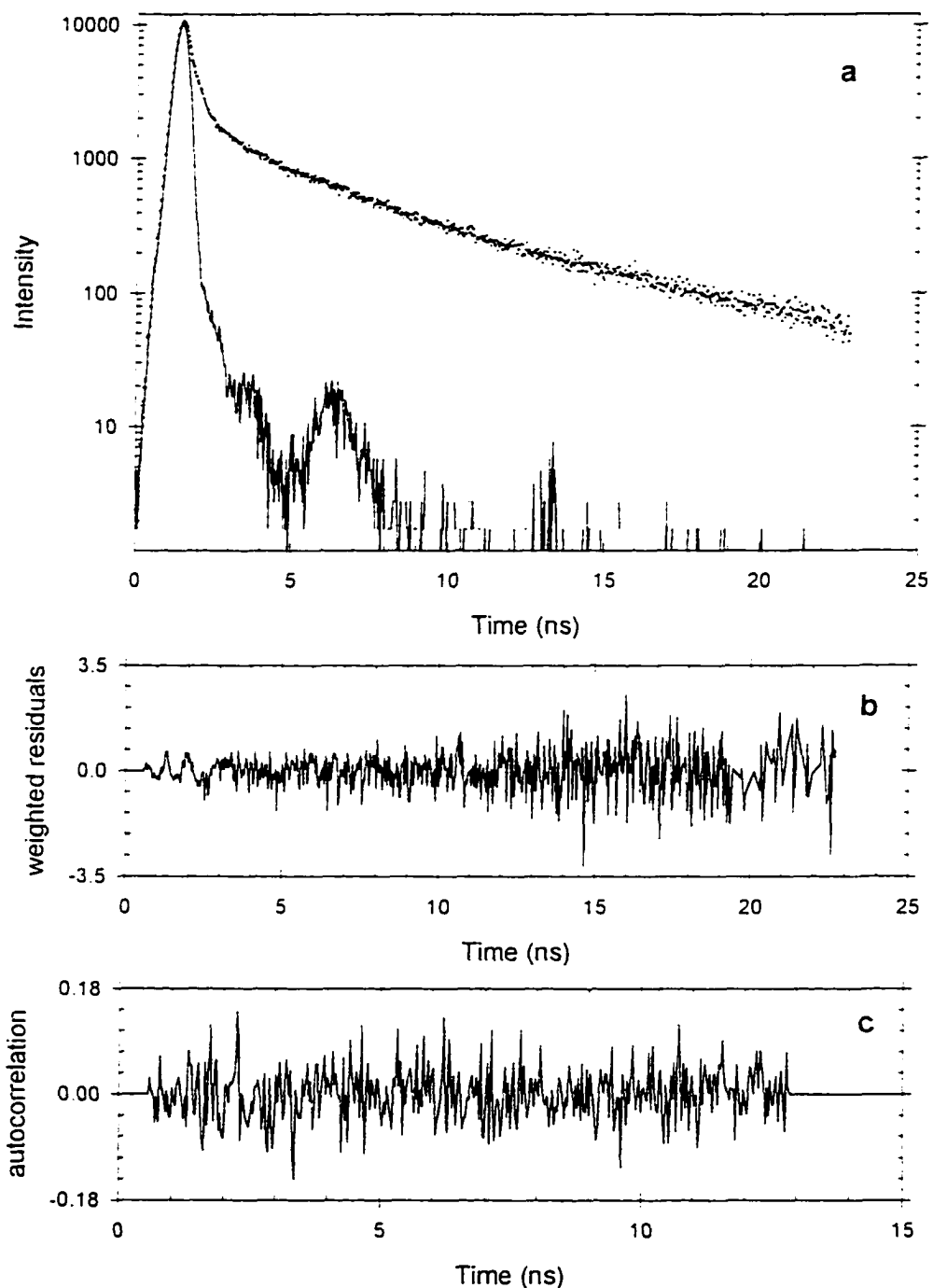


Figure D4: Fluorescence decay curve of C-2AP-G (a) in water at 12 °C with (b) weighted residuals and (c) autocorrelation. The sharp-peaked curve is the excitation pulse at 304 nm, the scattered points are the decay data, and the solid line is the three-exponential fit.

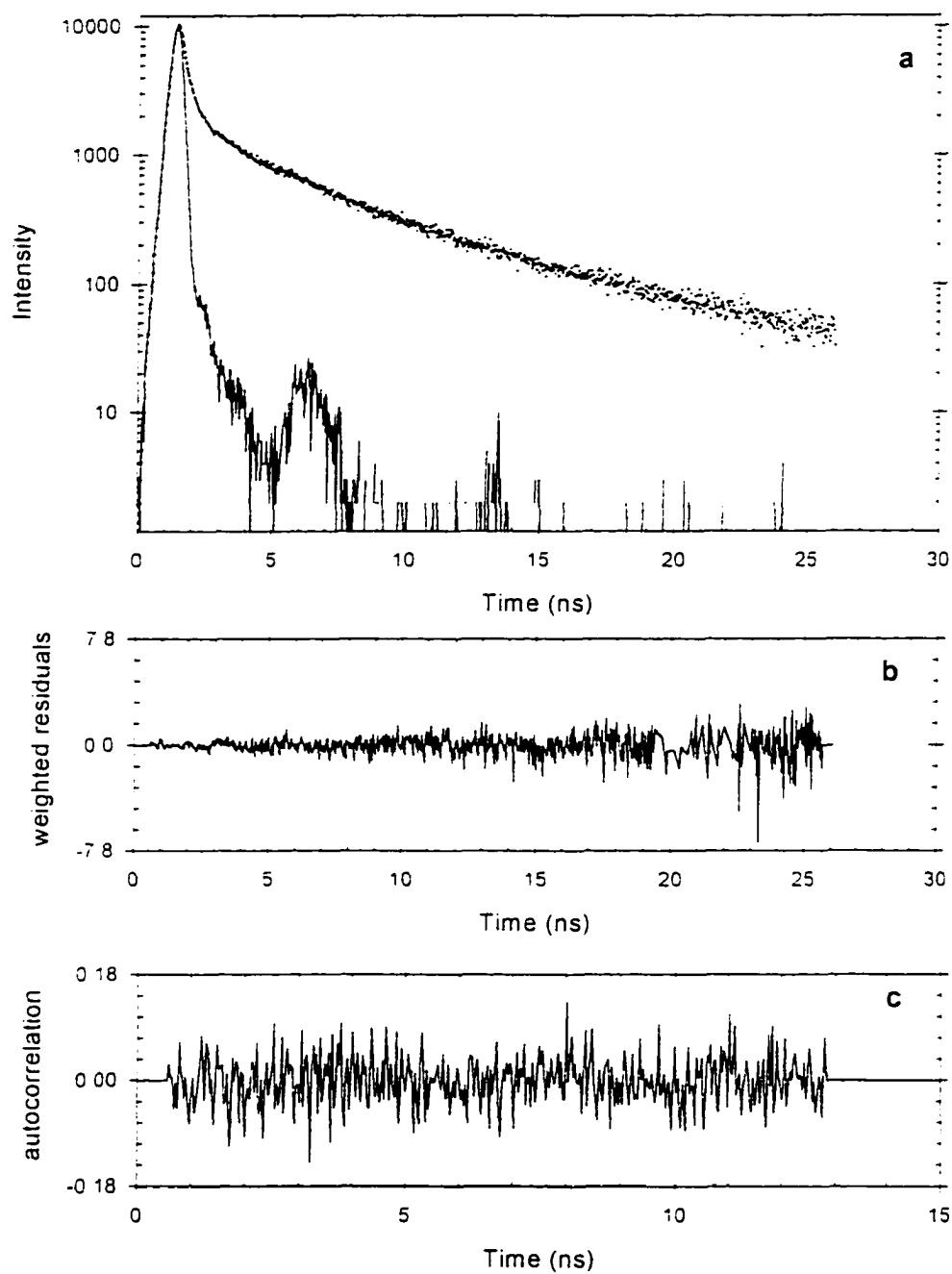


Figure D5: Fluorescence decay curve of C-2AP-G (a) in water at 14 °C with (b) weighted residuals and (c) autocorrelation. The sharp-peaked curve is the excitation pulse at 304 nm, the scattered points are the decay data, and the solid line is the three-exponential fit.

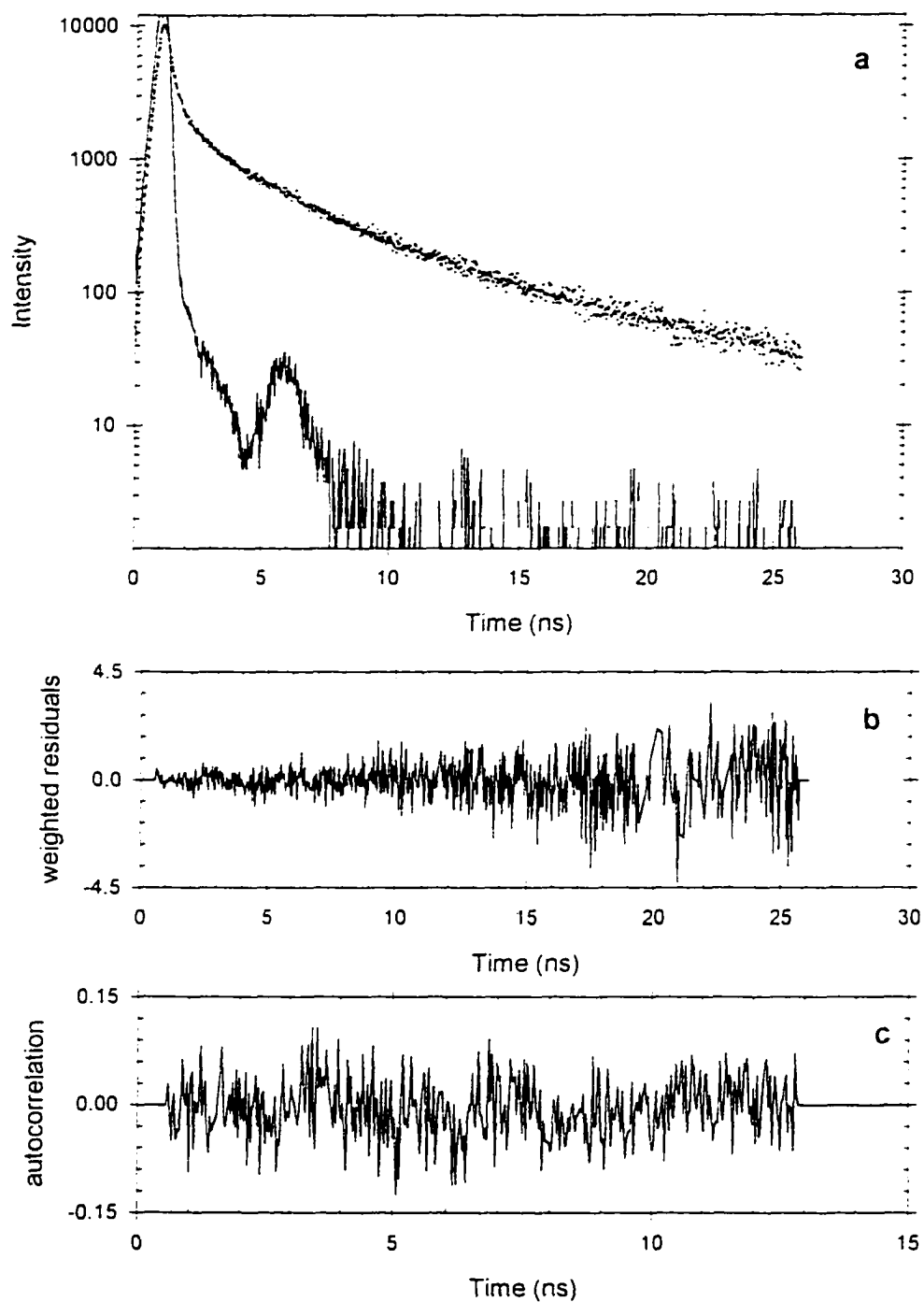


Figure D6: Fluorescence decay curve of C-2AP-G (a) in water at 26 °C with (b) weighted residuals and (c) autocorrelation. The sharp-peaked curve is the excitation pulse at 304 nm, the scattered points are the decay data, and the solid line is the three-exponential fit.

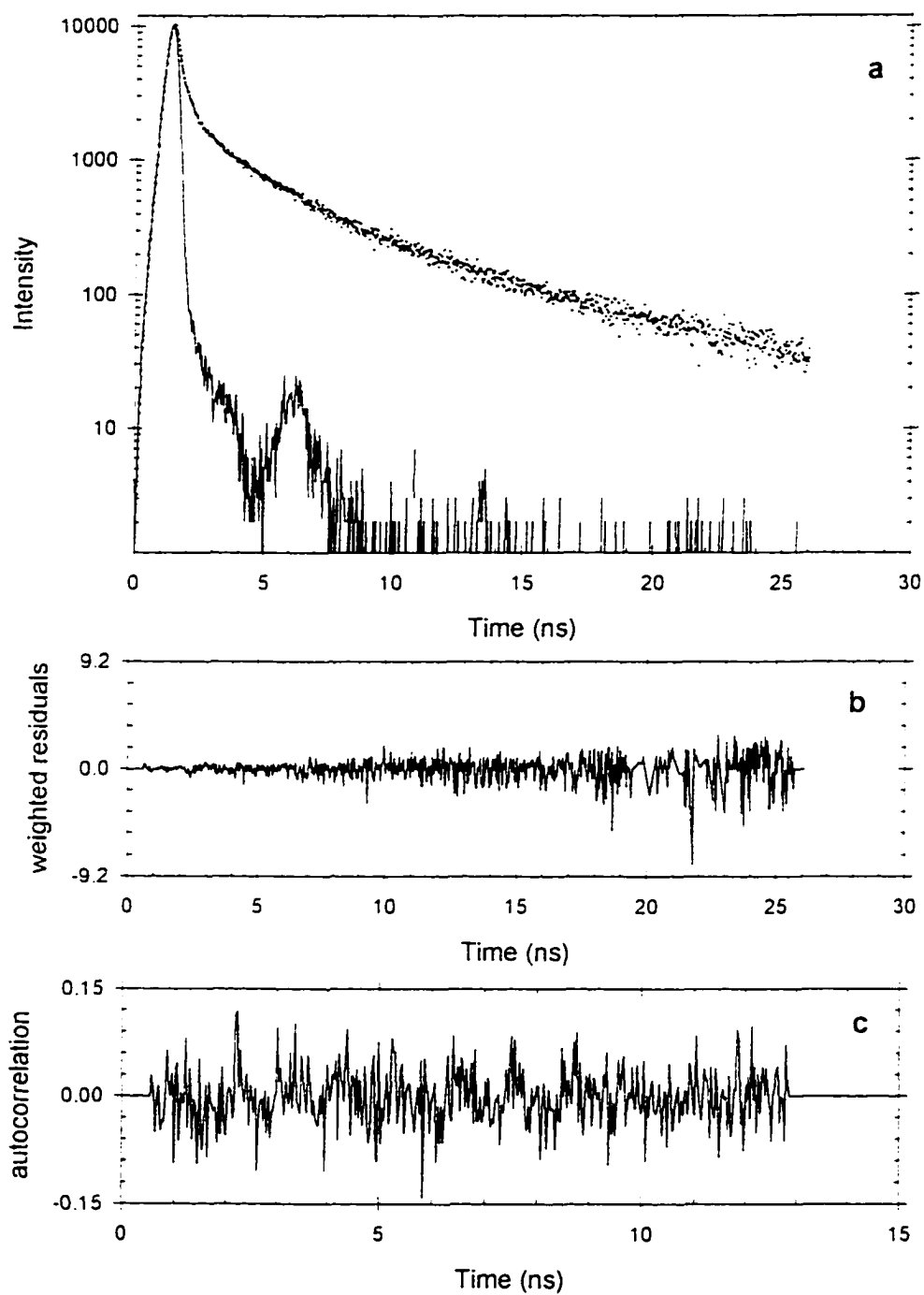


Figure D7: Fluorescence decay curve of C-2AP-G (a) in water at 30 °C with (b) weighted residuals and (c) autocorrelation. The sharp-peaked curve is the excitation pulse at 304 nm, the scattered points are the decay data, and the solid line is the three-exponential fit.

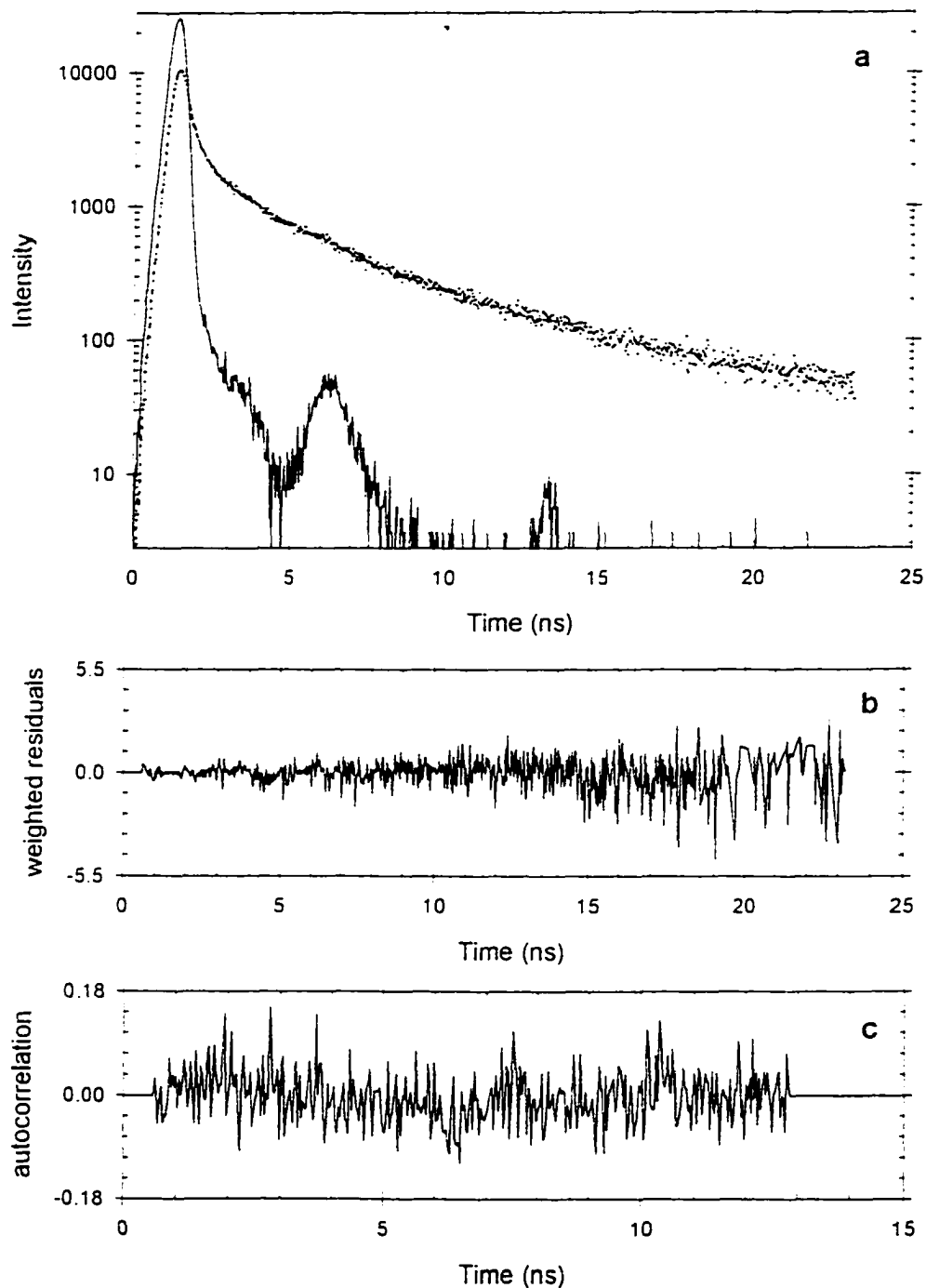


Figure D8: Fluorescence decay curve of C-2AP-G (a) in water at 34 °C with (b) weighted residuals and (c) autocorrelation. The sharp-peaked curve is the excitation pulse at 304 nm, the scattered points are the decay data, and the solid line is the three-exponential fit.

**GRADUATE SCHOOL
UNIVERSITY OF ALABAMA AT BIRMINGHAM
DISSERTATION APPROVAL FORM
DOCTOR OF PHILOSOPHY**

Name of Candidate Kervin O. Evans

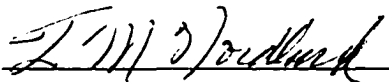
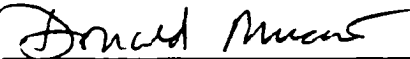
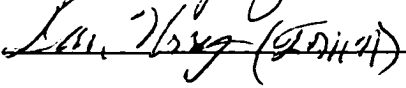
Major Subject Physics

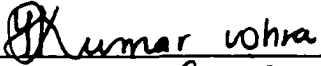
Title of Dissertation Dynamic Characterization of 2-Aminopurine in Oligonucleotides

Using Fluorescence, Magnetic Resonance, and Raman Spectroscopies

I certify that I have read this document and examined the student regarding its content. In my opinion, this dissertation conforms to acceptable standards of scholarly presentation and is adequate in scope and quality, and the attainments of this student are such that he may be recommended for the degree of Doctor of Philosophy.

Dissertation Committee:

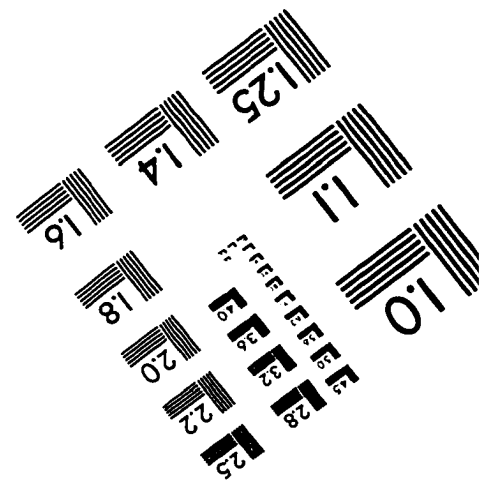
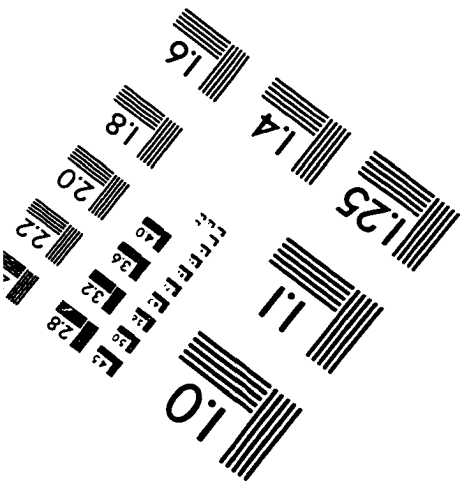
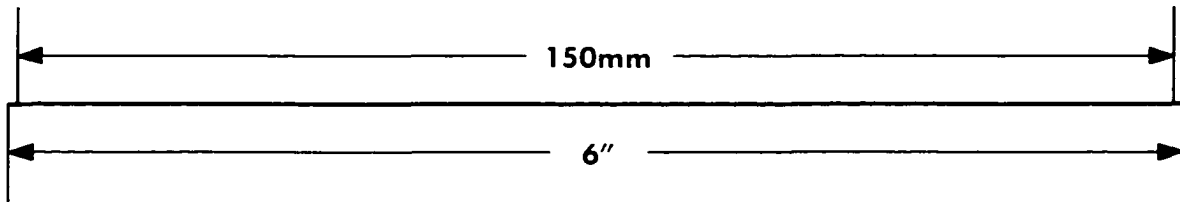
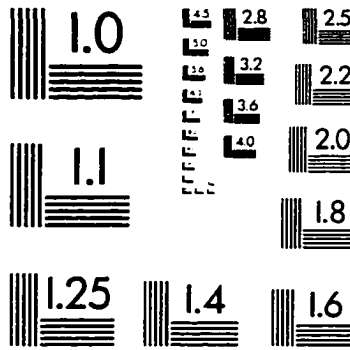
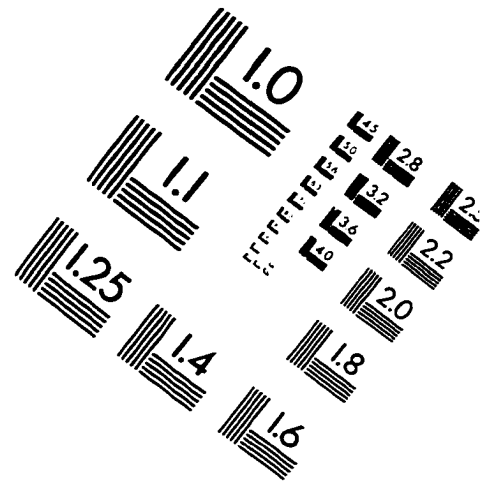
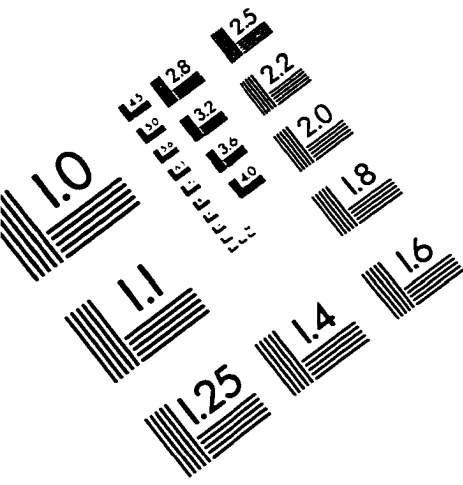
Name	Signature
<u>Thomas Nordlund, Ph.D.</u> , Chair	<u></u>
<u>Donald Muccio, Ph.D.</u>	<u></u>
<u>Edward Wills, Ph.D.</u>	<u></u>
<u>John Young, Ph.D.</u>	<u></u>
<u>Dan Urry, Ph.D.</u>	<u></u>

Director of Graduate Program 

Dean, UAB Graduate School 

Date 4/29/98

IMAGE EVALUATION TEST TARGET (QA-3)



APPLIED IMAGE, Inc
 1653 East Main Street
 Rochester, NY 14609 USA
 Phone: 716/482-0300
 Fax: 716/288-5989

© 1993, Applied Image, Inc., All Rights Reserved